The endothelial-specific highly expressed long non-coding RNA *LINC00607* governs the endothelial phenotype

Dissertation

zur Erlangung des Doktorgrades

der Naturwissenschaften

vorgelegt beim

Fachbereich Biochemie, Chemie und Pharmazie

der Johann Wolfgang Goethe-Universität

in Frankfurt am Main

von

Frederike Margarete Boos

aus Andernach

Frankfurt am Main, 2023

(D30)

vom Fachbereich Biochemie, Chemie und Pharmazie (FB14) der
Johann Wolfgang Goethe-Universität als Dissertation angenommen.

Dekan: Prof. Dr. Clemens Glaubitz

Gutachter: Prof. Dr. Dieter Steinhilber
Prof. Dr. Ralf P. Brandes

Datum der Disputation:

Contents

1 Introduction

1.1 Long non-coding RNAs

Despite the fact that only 3% of the human genome gives rise to protein-coding transcripts, there are many more short- and long non-coding transcripts being generated (**Figure 1**)[1,2]. For a long time, these non-coding genes were considered non-functional "Junk RNA", but over the last two decades, it has become evident that especially long non-coding RNAs (lncRNAs) are physiologically relevant and have many different important functions[3]. Until now, there are approximately two thousand publications reporting on lncRNA functions[4,5].

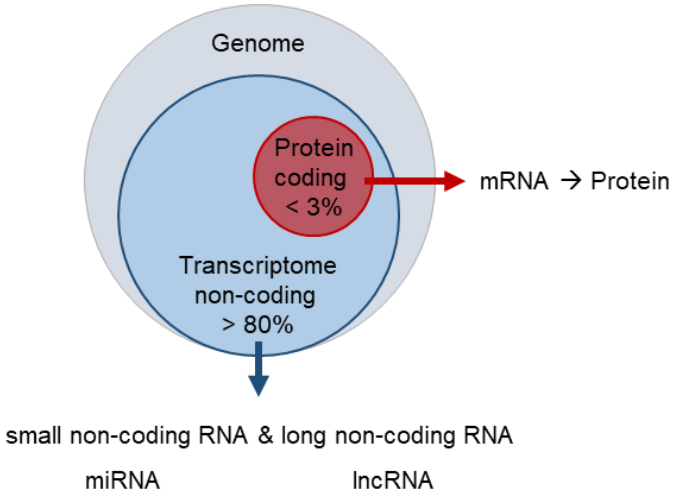

Figure 1 Proportion of coding and non-coding transcripts generated from the human genome
Approximately 3% of the transcripts generated from the human genome have protein-coding potential and over 80% give rise to non-coding RNAs. This includes small and long non-coding RNAs. Figure adapted from Uchida & Dimmeler (2015)[2].

1.1.1 Classification of lncRNAs

By definition, lncRNAs lack apparent protein-coding potential and are longer than 200 nucleotides (nt). The length distinguishes lncRNAs from e.g. shorter non-coding RNAs like micro RNAs (miRNA), transfer RNAs (tRNA) and small nuclear RNAs (snRNAs)[3]. As the majority of lncRNAs are often multi-exonic and transcribed by RNA Polymerase II (RNA Pol II), they share many properties with messenger RNAs (mRNAs). These features include 7-methyl guanosine (m^7G) at their 5′ ends, polyadenylated 3′ ends and alternative splicing[4–6]. In addition to the definition by length, there is no fixed classification and nomenclature[3,5]. However, a proposed classification into lncRNA biotypes can be made with respect to the closest protein-coding gene[7].

The first distinction among lncRNAs is made between genic and intergenic lncRNAs, which either share the genomic locus with a protein-coding gene or are encoded in an intergenic region of the genome. A lncRNA gene can be oriented in sense and antisense to the DNA strand encoding for the neighboring gene and, if a lncRNA shares the locus with another gene, it can be intronically or exonically located (**Figure 2A**).

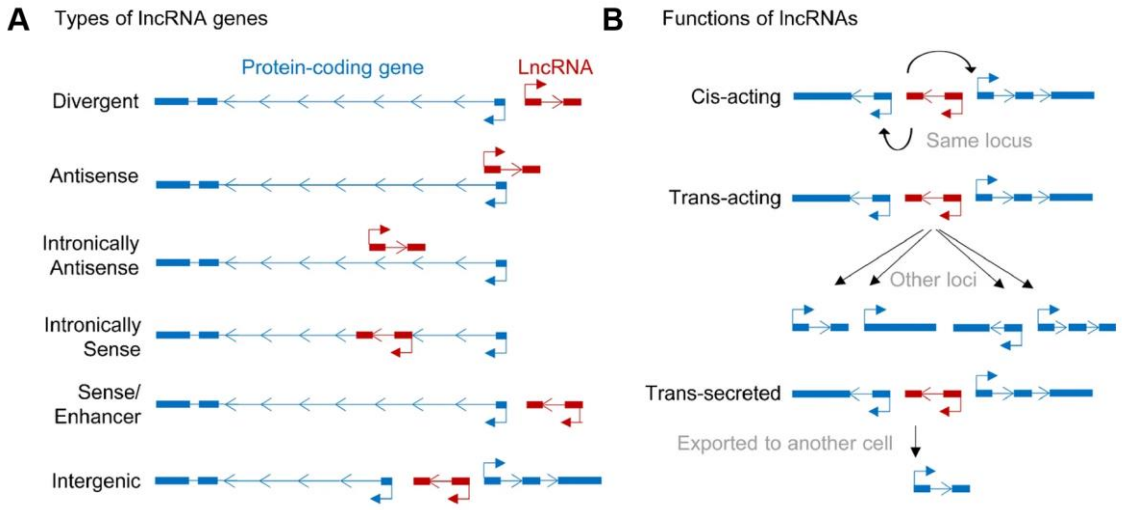

Figure 2 Biotypes and functions of lncRNA genes
A LncRNAs are classified into different biotypes based on their genomic location relative to other protein-coding genes. **B** Based on the distance to genes affected by a lncRNA, lncRNAs can act in *cis* or *trans* or are trans-secreted to other cells. Figure adapted from Oo *et al.* (2022)[3].

Another classification of lncRNAs is based on their mode of action. LncRNAs affecting genes within their immediate genomic location are called *cis*-acting, whereas lncRNAs affecting genes distant to their location or on other chromosomes are called *trans*-acting lncRNAs (**Figure 2B**). Additionally, lncRNAs can be secreted after transcription to impact on surrounding cells or other cell types. As such, *trans*-secreted lncRNAs can be used as clinical markers for example in the plasma or serum of patients (**Figure 2B**)[3,8]. Another level of complexity and functional specification is added to lncRNAs through the folding into distinct secondary and tertiary structures[9].

1.1.2 Conservation of lncRNAs

Most lncRNAs are less well conserved across species than mRNAs[5,10]. Additionally, the number of lncRNAs seems to increase during animal evolution, with one-third of lncRNAs emerging in the primate lineage[7,11,12]. It is most likely that the larger number of lncRNAs is not resulting from higher complexity in organisms but is

caused by increased fractions of genome being derived from repetitive elements, like *Alu* elements, a primate specific transposable element (TE)[13]. In fact, the majority of lncRNA genes contain at least one TE[14]. TEs can give rise to alternative promoters and may also be functional elements in the lncRNA itself[15]. Additionally, the fact that the human and primate genomes are subjected to extensive sequencing might also result in a high identification rate of lncRNAs as compared to other species[5]. The low level of conservation observed across species poses significant difficulties when studying the clinical and therapeutic relevance of human lncRNAs.

1.1.3 LncRNAs have numerous functions in the nucleus and cytoplasm

LncRNAs have been reported to be involved in essentially all stages of genome organization, gene expression and cell structure development and maintenance[5,14]. This is achieved by lncRNAs through interaction with proteins, DNA and RNA (**Figure 3**)[4,16].

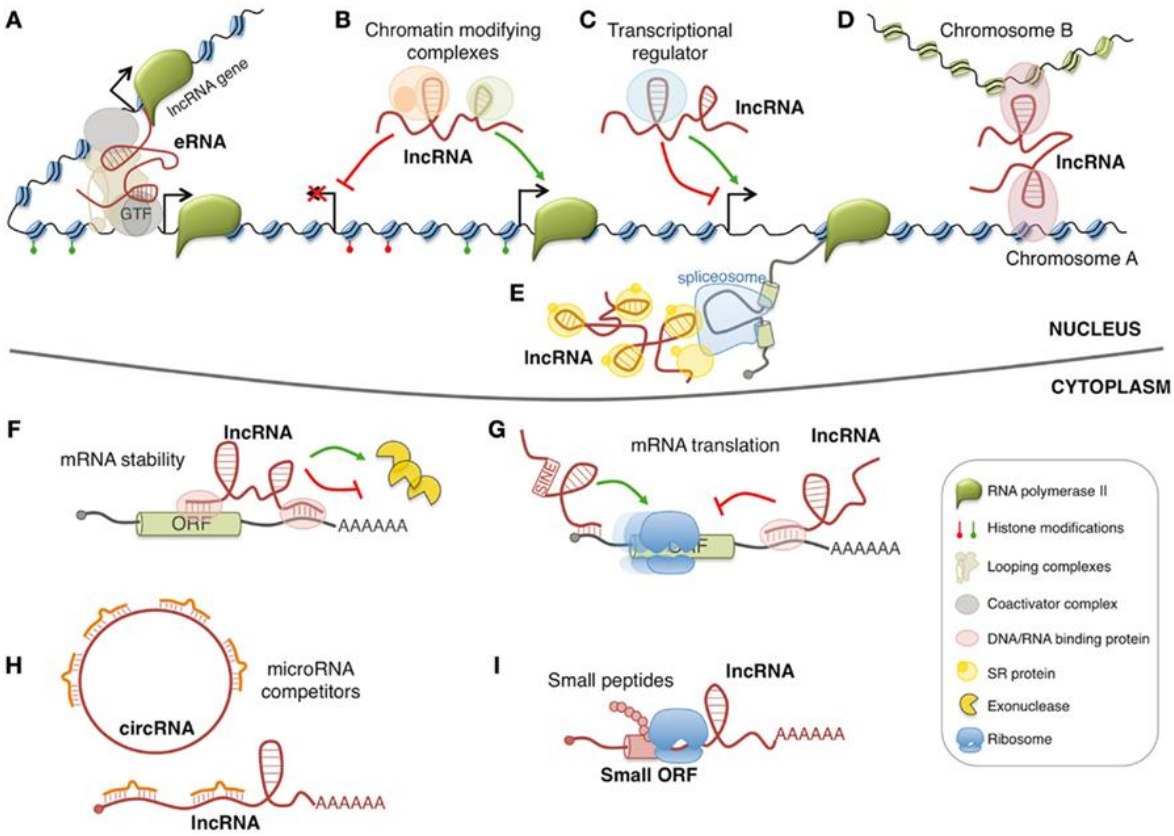

Figure 3 Diversity of lncRNA function in the nucleus and cytoplasm
LncRNA functions in the nucleus: **A** LncRNAs can act as enhancer RNAs. GTF: general transcription factor. **B&C** They influence activity of chromatin remodeling complexes (B) and transcription factors (C). **D** LncRNAs can influence chromosomal conformation and interactions. **E** They are also involved in splicing control of other RNAs (SR: splicing regulator). LncRNA functions in the cytoplasm: **F&G** LncRNAs can alter mRNA stability (F) and translation (ORF: open reading frame) (G). **H** They can act as miRNA sponges like circular RNAs (circRNA). **I** Micro-peptides translated from lncRNAs can also exert cytosolic functions. Figure adapted from Morlando *et al.* (2015)[16].

In the nucleus, lncRNAs regulate transcription in multiple ways, e.g. through activity as enhancer RNAs (eRNA), recruitment of chromatin remodelling complexes, by facilitating or inhibiting transcription factor binding or by changing the spatial conformation of chromatin (**Figure 3A-D**). Additionally, lncRNAs are known to participate in and modulate mRNA splicing (**Figure 3E**). In the cytoplasm, lncRNA function ranges from controlling mRNA stability and translation to being miRNA sponges (**Figure 3F-H**). Finally, some lncRNAs, despite having a low coding potential, can give rise to micropeptides, which in turn have specific molecular functions[4,17].

1.2 Regulation of chromatin remodelling and gene transcription by lncRNAs

Many lncRNAs participate in chromatin remodelling and transcriptional regulation[4]. Chromatin refers to the assembly of DNA, histone proteins, and other proteins that form the chromosomes[18]. Chromatin is the condensed and stable configuration of packaged and structured DNA that can fit within the limited confines of the eukaryotic cell nucleus. Chromatin is built of many nucleosomes, each consisting of 147 nt of DNA wrapped around an octamer of four core histones[19]. Nucleosomes can be altered by changing its position on the DNA, its composition or structure [20,21]. The most described mechanism is the chemical modification of histone tails, resulting in modulation of its affinity to and thus interaction with DNA and other proteins[22,23]. Modifications of histone tails can include lysine and arginine methylation, lysine acetylation, serine and threonine phosphorylation, ADP-ribosylation, ubiquitination, SUMOylation and others[24,25]. These modifications and especially their position on histones impact on gene expression. LncRNAs participate in the process of histone modification changes[25].

An example of a lncRNA mediating histone modification changes is *X-inactive specific transcript* (*XIST*). In females, *XIST* recruits the Polycomb Repressive Complex 2 (PRC2) through binding to the subunit Enhancer Of Zeste 2 Polycomb Repressive Complex 2 Subunit (EZH2), to one of the X chromosomes to initiate X chromosome inactivation[26–28]. PRC2 catalyzes the tri-methylation on lysine 27 on histone 3 (H3K27me3), which is needed for transcriptional silencing[29]. Another example is the lncRNA *trans-spliced rhabdomyosarcoma 2 associated transcript* (*tsRMST*), which functions to inhibit lineage differentiation in human embryonic stem

cells. In pluripotent cells, *tsRMST* interacts with NANOG homeobox (NANOG) and the PRC2 complex, resulting in their binding to inactive genes like GATA Binding Protein 6 (GATA6) and Paired Box 6 (PAX6). Conversely, in differentiating cells, the absence of *tsRMST* causes the displacement of PRC2, leading to the activation of lineage-specific genes[30].

There are many more lncRNAs described to specifically target PRC1 and PRC2 to chromatin sites, both in *cis* and *trans*. Another example is *Antisense Non-coding RNA in the INK4 Locus* (*ANRIL*), which was shown to silence the *INK4b/ARF/INK4a* locus by recruiting the PRC2 complex in *cis*[31], as well as acting as a scaffold for the PRC1 and PRC2 complexes to *trans*-regulate expression of pro-atherogenic gene networks[32]. These examples may give rise to the question whether PRC addressing of chromatin is dependent on lncRNAs[33].

1.2.1 Functions of chromatin remodeling complexes

Another way by which lncRNAs influence chromatin structure and transcription is through interaction with chromatin remodeling complexes (CRCs). These multi-protein complexes contribute to the dynamic accessibility of DNA, which is important to facilitate transcription through binding of activating or repressive transcription factors (**Figure 4A**)[34].

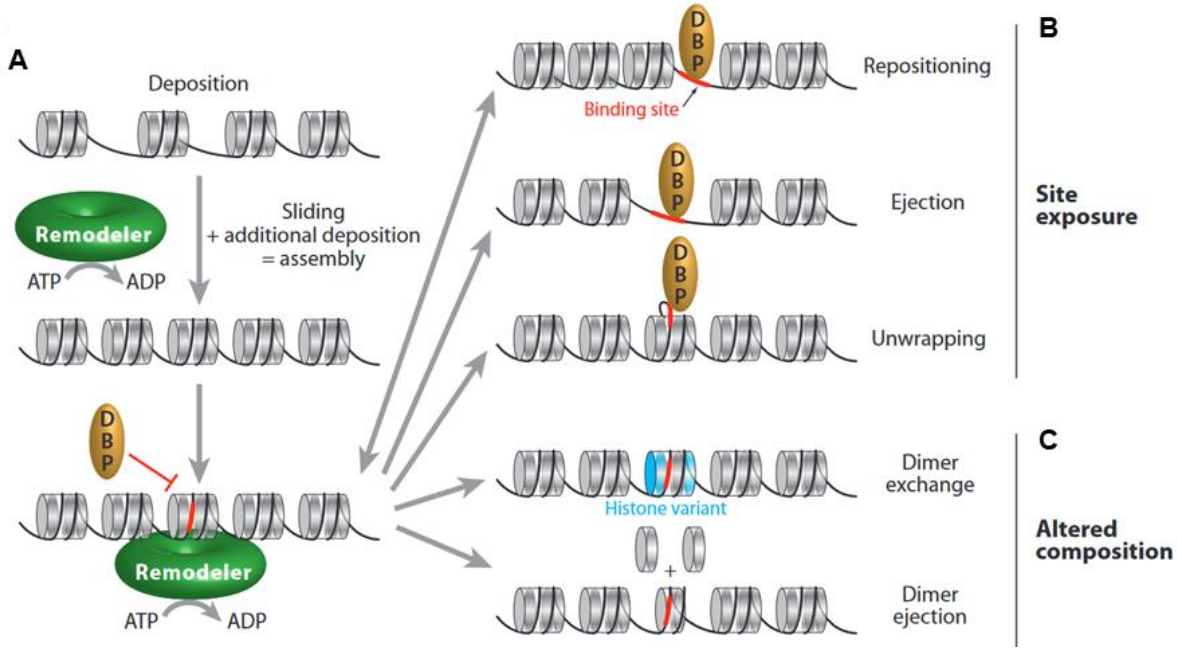

Figure 4 Different functions of chromatin remodelling factors
A Decreasing DNA accessibility by deposition and sliding of histones by CRCs. DBP: DNA binding protein. **B** DNA site exposure by repositioning and ejection of histone octamer and DNA unwrapping. **C** Altered histone composition by dimer exchange or ejection. Figure adapted from Clapier and Cairns (2009)[35].

CRCs often alter chromatin accessibility in an ATP-dependent manner through sliding or removal of nucleosomes or changing histone composition through ejection or removal of histone dimers (**Figure 4B&C**)[36]. The four classes of CRCs are the "chromodomain helicase DNA-binding" (CHD), the "imitation switch" (ISWI), the "inositol requiring 80" (INO80) and the "switch/sucrose non-fermentable" (SWI/SNF) families[35].

These complex families can be grouped by distinct functions: CHD and ISWI are mainly described in nucleosome assembly by spacing out histones, whereas INO80 performs nucleosome editing through histone dimer exchanges (**Figure 5A&B**). The SWI/SNF complex on the other hand can directly alter DNA accessibility by repositioning or ejecting histones and histone dimers (**Figure 5C**)[37].

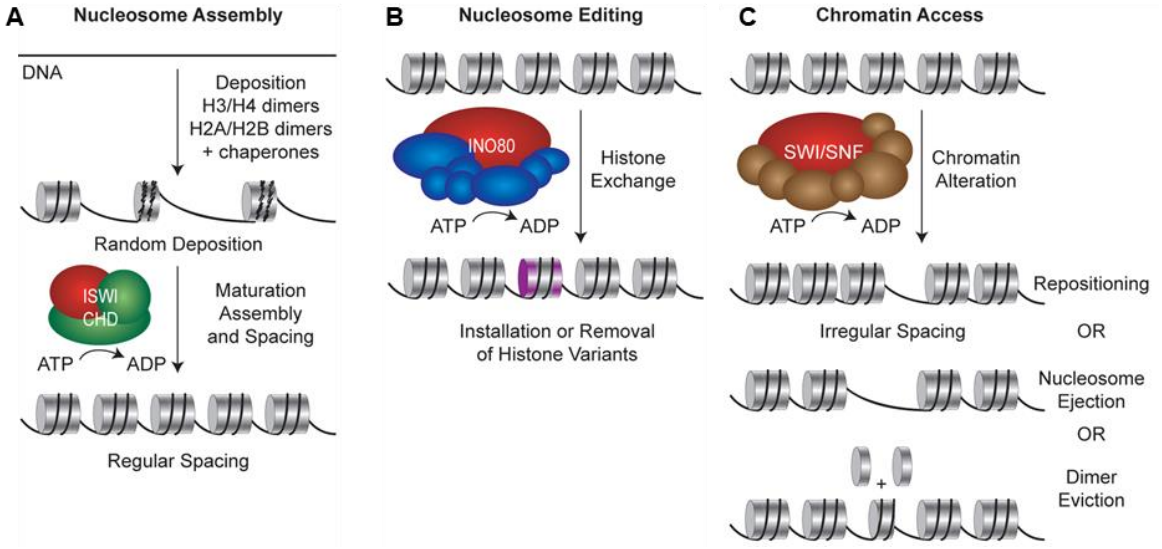

Figure 5 Different functions of the chromatin remodelling complex families
A-C ISWI and CHD are involved in nucleosome assembly (A), INO80 in nucleosome composition editing (B) and SWI/SNF alters chromatin accessibility by repositioning or sliding of histones (C). Figure adapted from Clapier *et al*. (2017)[37].

While the various functions of the distinct chromatin remodeling complexes are vital to cellular activity, SWI/SNF remains the most significant in terms of direct control over transcription[37].

1.2.2 The SWI/SNF chromatin remodeling complex

The human SWI/SNF complex is composed of 11-15 subunits. The complex composition depends on the cell type and the cellular environment and phenotypic specification but always requires four core-subunits for correct function (BRG1 or hBRM, BAF155, BAF170 and BAF47)[36,38]. The mutually exclusive catalytic ATPase core subunits of the SWI/SNF complex are Brahma-Related Gene 1 (BRG1, also

known as SMARCA4 (SWI/SNF Related, Matrix Associated, Actin Dependent Regulator Of Chromatin, Subfamily A, Member 4)) and human Brahma (hBRM)[39]. The SWI/SNF complex is highly important for genomic stability, DNA repair and transcription regulation during development of the cardiovascular and nervous system[39–41]. This is also illustrated by the high degree of complex conservation from yeast and drosophila to mammals[42–44]. Moreover, many mutations of complex members are associated with different diseases and developmental disorders. In particular, approximately 20% of all cancers carry a mutation within SWI/SNF[40,41,45–49]. Interestingly, it has been reported that SWI/SNF, which is dependent on BRG1, has antagonistic functions to the PRC1 and PRC2 complexes[46,50]. In contrast to the transcriptional repression carried out by PRC1 and PRC2, the SWI/SNF complex is important in transcriptional activation and enhancer activation through nucleosome sliding around enhancer sites and recruitment of transcription factors and RNA Pol II (**Figure 6A**)[51–53].

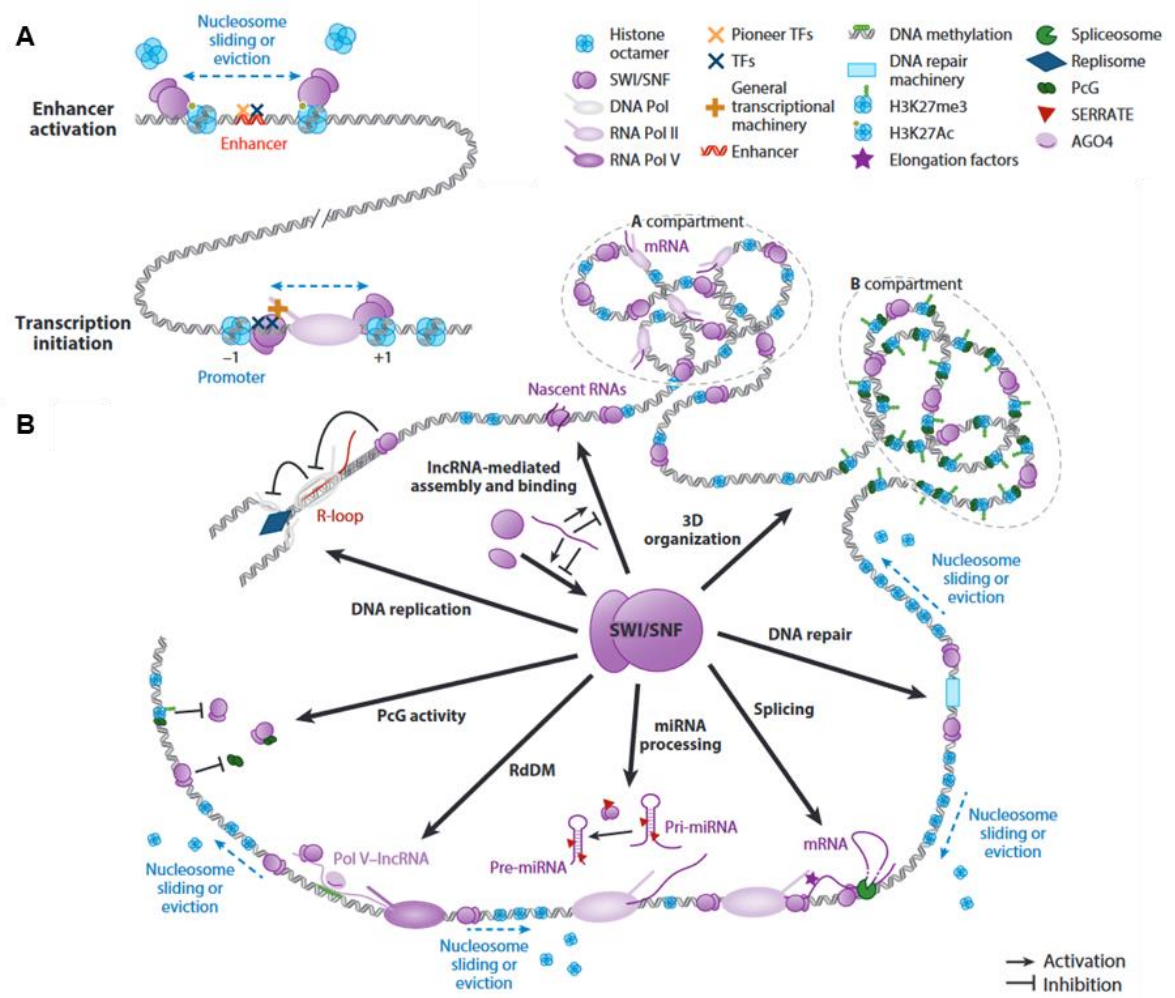

Figure 6 Summary of known SWI/SNF complex activities

Different functions are attributed to the SWI/SNF complex: **A** Direct regulation of gene transcription by increasing enhancer accessibility and recruitment of transcription factors and RNA Pol II. **B** Additional functions include lncRNA mediated complex assembly and functional modulation, DNA replication, inhibition of Polycomb group activity (PcG), modulation of RNA-dependent DNA methylation (RdDM), miRNA processing, splicing regulation, initiation of DNA repair and orchestration of 3D chromatin organization. SERRATE: RNA processing protein. Figure adapted from Bieluszewski *et al.* (2023)[53].

Additionally, SWI/SNF is involved in DNA replication, modulation of RNA-dependent DNA methylation, miRNA processing, splicing regulation, initiation of DNA repair and orchestration of 3D chromatin organization (**Figure 6B**)[54–56]. These reported functions can be enhanced or inhibited by lncRNAs, especially in a cell type specific manner, which is the subject of the next chapter.

1.2.3 The influence of lncRNAs on BRG1 and the SWI/SNF chromatin remodeling complex

The functional integrity of the SWI/SNF complex is highly dependent on BRG1, which is its core catalytic subunits. Homozygous BRG1 knock-out during preimplantation leads to embryonic lethality in mice[57]. Generally, BRG1 is important in development and cellular homeostasis. BRG1 is also a *bona fide* tumor suppressor and its loss leads in most cases to impaired cell cycle control, reduced DNA repair mechanisms, enhanced cell proliferation, decreased recognition by the immune system and other tumor-driving mechanisms[58]. BRG1 can act either as part of the SWI/SNF complex, as a single protein or together with the three other “core” subunits of SWI/SNF[59]. Therefore, BRG1 activity modulation by lncRNAs can have a strong impact on the function and the phenotype of a cell. Conversely, it is considered that lncRNAs may add a cell-type specific guidance for the SWI/SNF complex and BRG1 to certain regions on the DNA.

In fact, BRG1 has already been reported to be influenced by a number of lncRNAs: The lncRNA *MANTIS* for example, secures the ATPase activity of BRG1 by stabilizing the interaction between BRG1 and the SWI/SNF core subunit BAF155, in human umbilical vein endothelial cells (HUVECs)[60]. Additionally, under laminar flow conditions or statin treatment of HUVECs, *MANTIS* acts in a vascular-protective manner by preventing BRG1 recruitment to the Intercellular Adhesion Molecule 1 (ICAM-1) locus. This reduces the ICAM-1-mediated monocyte adhesion to HUVECs and the inflammatory stress response in endothelial cells (ECs)[61]. The lncRNA *Nuclear Paraspeckle Assembly Transcript 1* (*NEAT1*) binds and recruits BRG1 to paraspeckles and nuclear stress bodies[62]. Moreover, *NEAT1* guides BRG1 to the promoter of *Growth Arrest And DNA Damage Inducible Alpha (GADD45A)* leading

to the alteration of histone modifications (H3K27me3 and H3K4me3), which adjusts GADD45A-dependent G2/M cell cycle progression in gastric cancer. As a consequence, tumorigenesis is accelerated, which subsequently drives tumor progression[63]. Another example of a lncRNA affecting the function of BRG1 in cancer is *Urothelial Carcinoma Associated 1* (*UCA1*). In bladder cancer *UCA1* interacts with BRG1 and impairs its ATPase activity. It also prevents BRG1 binding to the p21 promoter, which leads to accelerated disease progression[64]. An ultraconserved lncRNA modulating BRG1 activity during embryonic mouse forebrain development is *Evf2*. Early in life, BRG1 facilitates transcription of Dlx1, which in turn initiates expression of Dlx5*,* Dlx6 and *Evf2*. Through a negative feedback loop, *Evf2* represses BRG1 activity and transcription of *Dlx5*, *Dlx6.* Disordered expression of *Evf2* can therefore result in severe neurological developmental disorders[65].

1.3 Alternative splicing

BRG1 has also been reported to be involved in alternative splicing (AS)[56]. AS is a crucial step in the maturation of mRNA and facilitates protein diversity, a process which is thought to contribute to adaptation to the microenvironment[66,67]. AS occurs in different ways, including intron inclusion, exon skipping, mutually exclusive exons and alternative 5' and 3' splice sites, resulting in different protein isoforms derived from a single gene[68]. Aberrant AS is implicated in the pathogenesis of various diseases and conversely, splicing is essential to maintain the cellular homeostasis.

The basis of splicing is a two-step reaction, by which an intron is removed from the precursor messenger RNA (pre-mRNA) and two neighboring exons are joined to form the mature mRNA (**Figure 7A**)[69]. The information on the site of splicing is encoded in short sequences within the intron, in form of a 5′ splice site (ss), a 3′ss and a branch site (**Figure 7A&B**). In metazoans, the branch site is usually located 19-40 nt upstream of the 3′ss and is followed by a polypyrimidine tract (Y(n), **Figure 7B**). The removal of an intron is carried out by two consecutive transesterification reactions[70]. This reaction is facilitated by the spliceosome executing a complex reaction cycle (**Figure 7C**)[71].

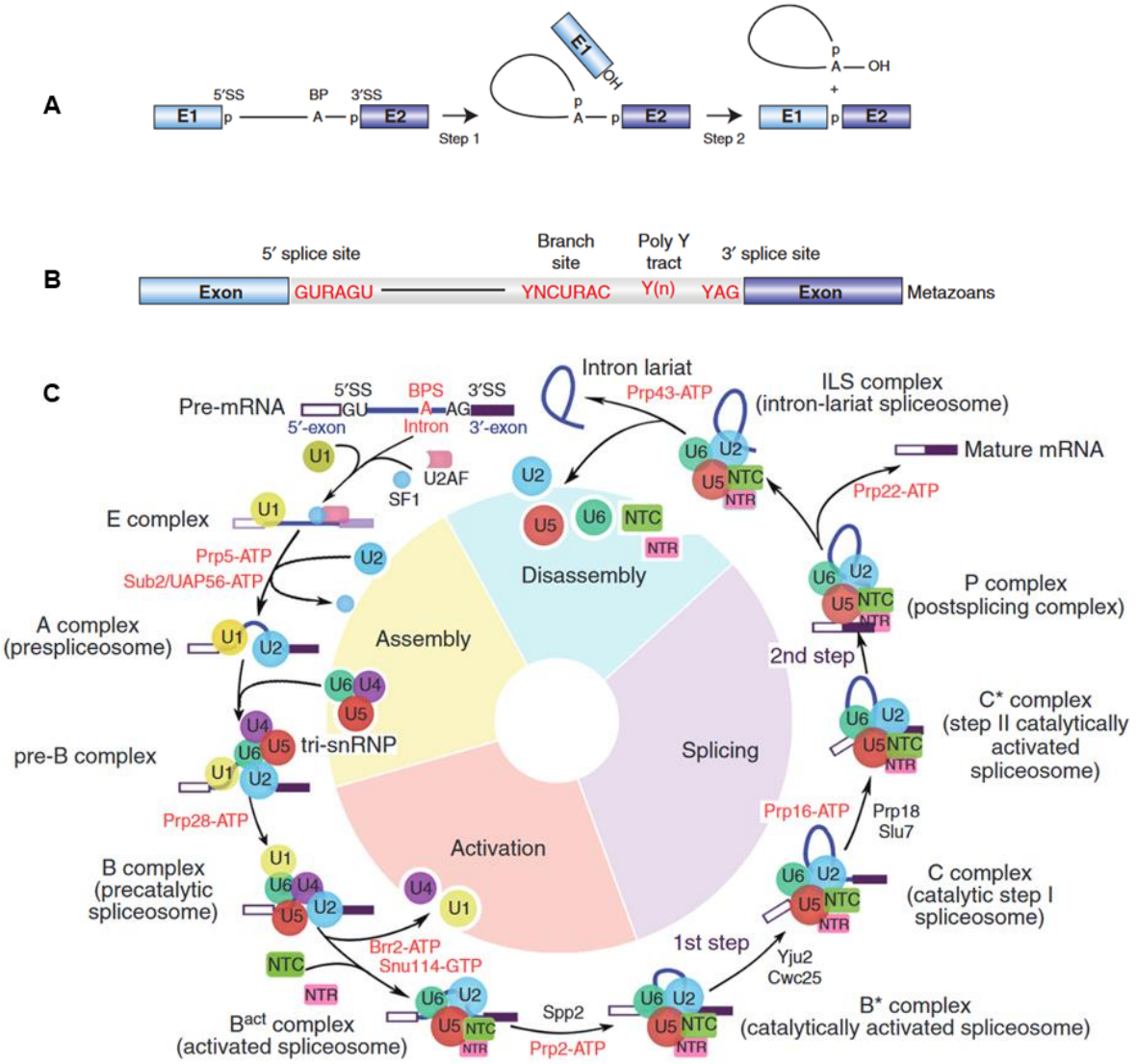

Figure 7 Schematic overview of the pre-mRNA splicing cycle
A Intron removal from precursor messenger RNA (pre-mRNA) by the dual reaction of phosphoryl transfer: branching and exon-ligation. **B** Characteristics of human introns: the highly conserved 5′ and 3′ splice sites (5′ss and 3′ss) and the internal branch point (BP). **C** Overview of the pre-mRNA splicing cycle. The phases of the cycle are assembly and activation of the spliceosome, followed by the splicing reaction and the disassembly of the spliceosome. Within these phases the spliceosomal complex passes through multiple steps with each step requiring a different complex composition, with the pre-B complex being the first complete one of the cycle. Figures adapted form Will & Luhrmann (2011)[69] and Yan *et al*. (2019)[71].

The components of the spliceosome include uridine-rich small nuclear ribonucleoproteins (U1, U2, U4, U5, and U6 snRNPs), splicing factors, RNA-dependent ATPase/helicases, the NineTeen complex (NTC), the NTC-related complex (NTR) and other proteins[71,72]. The spliceosome passes through a sequence of 8 steps in which each step comprises a uniquely composed spliceosome (**Figure 7C**)[71]. Exon recognition and splicing initiation occur during the pre-B, B and activated B (B^{act}) complex[71,73]. After assembly, the pre-catalytic spliceosome (B complex) becomes catalytically activated and facilitates branching.

This is followed by the formation of the catalytic spliceosome (C complex), which ligates the exons (**Figure 7C**)[71]. Finally, the spliced and mature mRNA is released from the post-catalytic spliceosome (P complex), which is disassembled and its components are being recycled (**Figure 7C**). Despite the high degree of flexibility in complex composition, based on its fundamental importance and paradigmatic function, almost the complete structure and composition of the spliceosomal complexes have been described to near-atomic resolution[74]. The spliceosome, which assembles in close proximity to RNA Pol II, processes nascent RNA simultaneously to its transcription[75]. Interestingly, BRG1 and the SWI/SNF complex have recently been discovered to be involved in the early stages of pre-mRNA recognition and formation of the pre-B complex by recruitment of the U2 snRNP[56,76]. This implies that changes in the function of BRG1 also impact on splicing.

1.3.1 LncRNAs are subjects and mediators of AS

LncRNAs add another layer of complexity to the highly orchestrated splicing process. Alternative splicing of mRNAs and lncRNAs may lead to the creation of alternative lncRNA transcripts which differentially regulated cellular pathways, which might contribute to diseases like cancer or cardiovascular diseases[77,78]. Conversely, lncRNAs can modulate splicing of pre-mRNA in different ways as illustrated in **Figure 8**.

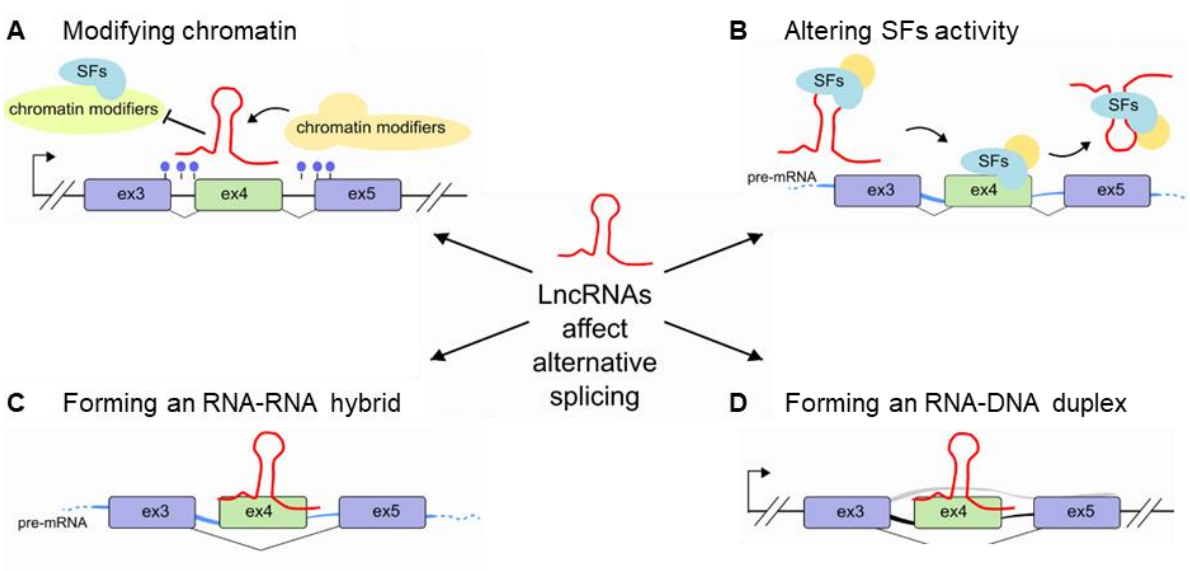

Figure 8 LncRNAs can affect splicing in different ways
LncRNAs (red) are able to adjust AS. **A&B** This is carried out by interaction with chromatin modifying proteins (A) or by altering splicing factor activity (B). **C&D** Additional influence can be exerted by the lncRNA forming an RNA-RNA hybrid with pre mRNA (C) or forming a RNA-DNA duplex with the gene being transcribed (D). Figure adapted from Pisignano & Ladomery (2021)[79].

Alterations in histone modifications in proximity to exon splice sites, by lncRNA-mediated recruitment of a CRC, can alter AS (**Figure 8A**)[79]. The lncRNA *asFGFR2* affects histone methylation of certain exons of the fibroblast growth factor receptor 2 (FGFR2) by recruitment of the PRC members EZH2 and SUZ12, in epithelial cells. This results in abundant H3K27 tri-methylation and prevents the chromatin-splicing adaptor complex MRG15–PTB1 from binding to these exons, which are then excluded. This generates an epithelial-specific FGFR2 isoform[80].

LncRNAs can also influence the activity of a splicing factor (SF, **Figure 8B**) or alter its access to the DNA or pre-mRNA by blocking or opening relevant sites through direct binding (**Figure 8C&D**)[79]. Direct binding to DNA or RNA is mostly carried out by a *cis*-acting, antisense lncRNA binding to the pre-mRNA of its host gene[78]. An example of a lncRNA influencing splicing of its host genes pre-mRNA is the nuclear lncRNA *Fas-antisense* (*Saf)*. *Saf* interacts with the Fas receptor pre-mRNA and the human splicing factor 45 (SPF45) leading to the exclusion of exon 6 and subsequently to the generation of the soluble isoform of the Fas receptor. This alternative isoform is protective against FasL induced apoptosis[81]. In contrast, the lncRNA *MALAT1* has been shown to regulate the function of the serine/arginine splicing factors by controlling their level of phosphorylation[82]. Given the complexity of splicing and the fact the contribution of lncRNAs to this process has just recently been recognized, there still appears to be a large room for mechanistic discoveries on lncRNA-dependent splicing control.

1.4 Physiology of the endothelium

The endothelium is built of a monolayer of endothelial cells (ECs). It serves as a semi-permeable barrier separating the vessel wall form circulating blood and lymph. Among its various functions, the endothelium actively regulates vascular homeostasis and vascular tone. The endothelium is crucial for adequate adaptation to a broad spectrum of physiological and pathological stimuli. Among them are cytokines, released during inflammation, the blood flow (laminar/turbulent flow), cues from cellular adhesion, oxidative stress, and metabolic cues (**Figure 9**)[83].

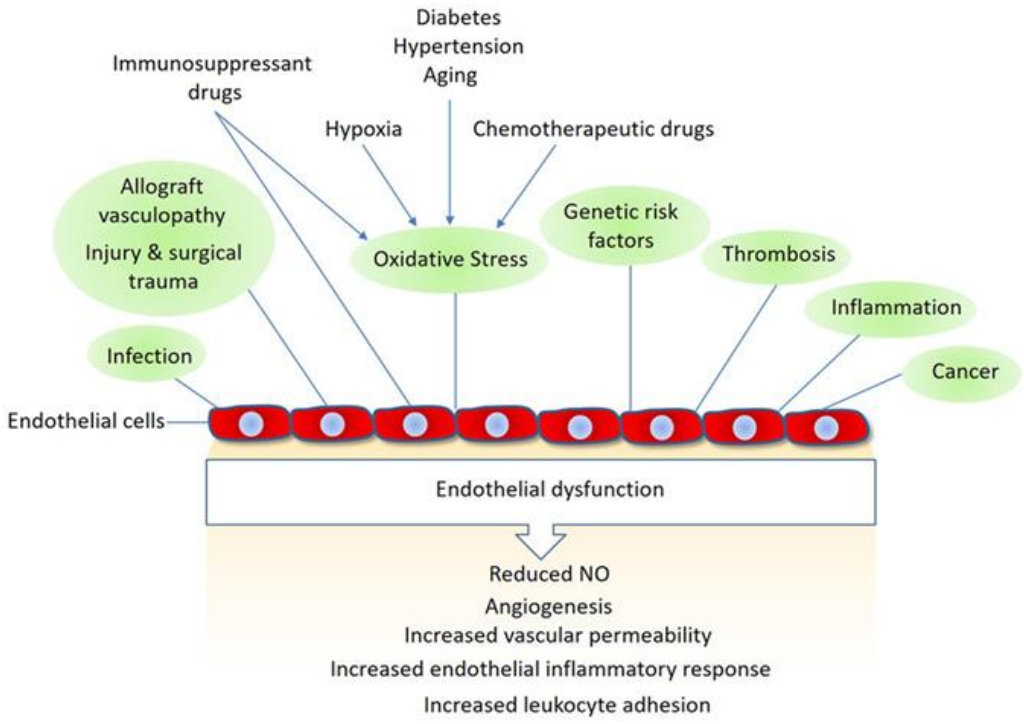

Figure 9 Key factors triggering endothelial dysfunction
Factors (green) that trigger endothelial dysfunction, which can manifest as reduced production of nitric oxide (NO), angiogenesis, increased vascular permeability and others. Figure adapted from Rahimi (2017)[84].

Gene transcription control, as a response to these stimuli, is executed by transcription factors. The endothelium itself, however, is also defined by a certain set of (endothelial-) specific transcription factors (TFs). These are isoforms within the Sox, Kruppel-like, Forkhead, Erythroblast Transformation Specific (ETS) and GATA families[85]. Among them, the ETS TF family is one of the most prominent protein families, with a TF recognition motif present in virtually every gene promoter of endothelial signature genes[85,86]. The ETS TF family has numerous members, which execute individual functions. ERG (ETS Transcription Factor ERG) is the most prominent ETS family member, with high expression in mature human ECs[87]. Among the gene programs activated by ERG are blood vessel morphogenesis and angiogenesis in response to Vascular Endothelial Growth Factor (VEGF) stimulation[88]. ERG carries out both repressive and activating function to regulate gene expression in response to different endothelial stimuli[88]. These functions are executed by binding to its DNA recognition motif with the consensus sequence: 5′-RSA**GGAA**G-3′ [89].

An altered gene transcription control in response to stimuli can lead to endothelial dysfunction, which can be the underlying cause to a vast number of cardiovascular diseases (CVDs, **Figure 9**)[90]. Endothelial dysfunction is characterized by a reduced

availability of nitric oxide, impaired angiogenesis and increased leucocyte adhesion, vascular inflammatory activation and increased vascular permeability (**Figure 9**)[84]. In addition to the transcription control by TFs, several lncRNAs have been described to regulate endothelial specific gene programs.

1.4.1 Angiogenesis

One of the main functions of the vascular system is to ensure sufficient oxygen supply for all tissues and organs. As the diffusion rate of oxygen is limited to a distance of approximately 200 µm[91], cells with a greater distance to the nearest vessel will become hypoxic and experience a lack of nutrient supply. In order to prevent necrosis, cells adapt their metabolism and release pro-angiogenic signalling molecules[92]. This process is initiated in large parts by the stabilization of the TFs hypoxia-inducible factor 1/2α (HIF1α and HIF2α, **Figure 10**)[93].

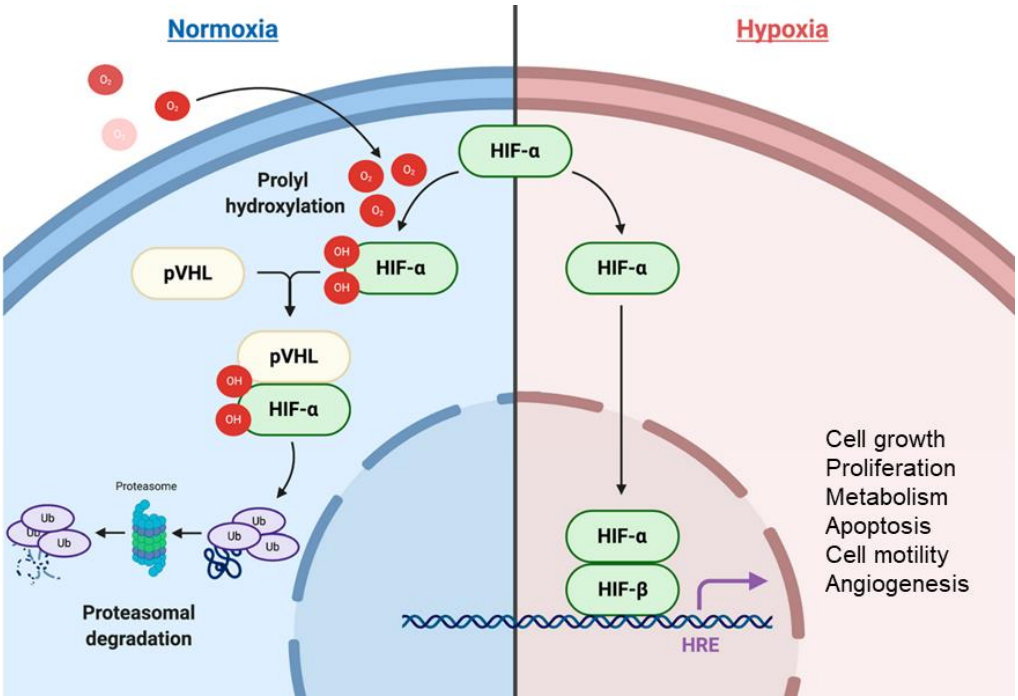

Figure 10 Signalling pathway of the Hypoxia Inducible Factor (HIF)
Under normoxic conditions, HIF1α and the Von Hippel-Lindau (pVHL) are ubiquitinated (Ub) and proteasomally degraded. In hypoxia, HIFα is stabilized, translocates into the nucleus and initiates transcription of its target genes. These are involved in altering the metabolism towards glycolysis, activating cell growth and initiating proliferation, cell motility and angiogenesis. Figure adapted from Vito *et al*. (2020)[93].

Besides switching of the metabolism to glycolysis and other hypoxia responses, an important consequence of hypoxia is induction of angiogenesis. Angiogenesis, the formation of new vessels by sprouting from a pre-existing vascular network, is important not only as a response to hypoxia but also, during development and wound healing[90]. Importantly, angiogenesis is also required for cancer progression,

as the growing tumor depends on an increasing blood supply[94] and during macular degeneration[95,96].

Angiogenesis is a strictly ordered process which results in the development of new functional vessels. Among the many factors promoting angiogenesis, VEGF is certainly the most prominent and studied one. In response to a VEGF-A gradient, the extracellular matrix surrounding the ECs is broken down due to the release of proteases from the endothelium. Subsequently, certain ECs, called tip cells, migrate towards the gradient of VEGF-A. Following these tip cells are proliferating ECs, called stalk cells. The angiogenic sprouts then form a lumen and branches, connect with other vessels and mature (**Figure 11**)[97].

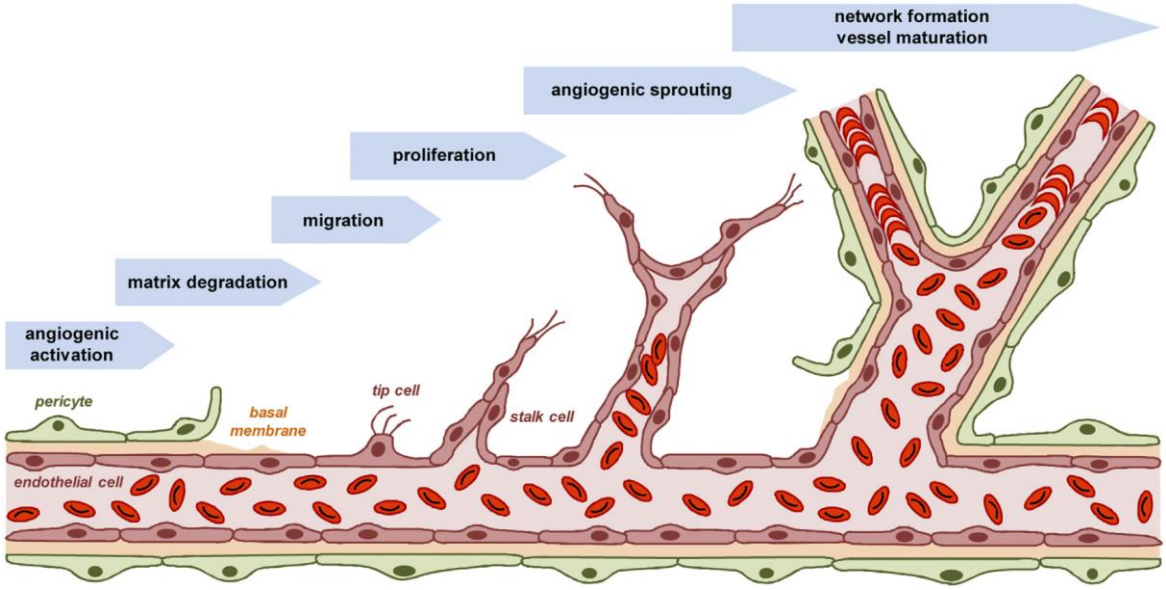

Figure 11 Angiogenesis progression in response to VEGF or hypoxia
Sequential steps of angiogenesis: After angiogenesis activation by growth factors like VEGF-A, the basal membrane is degraded by matrix metalloproteinases (MMPs). Following this, the endothelial tip cell migrates towards the signalling gradient and is followed by proliferating stalk cells, together forming an endothelial sprout. After forming a lumen, the sprout branches, connects with other vessels and matures. Figure adapted from Laschke *et al*. (2022)[97].

1.4.2 VEGF signalling as a key mediator of angiogenesis

Many signalling molecules and proteins promote and initiate the so-called angiogenic switch, including the VEGF-VEGFRs, Delta-Notch and the angiopoietin-Tie system[97,98]. The most prominent, however, is the VEGF system of Vascular Endothelial Growth Factors (VEGF-A/-B/-C/-D/-E) and Vascular Endothelial Growth Factor Receptors (VEGFR1-3) (**Figure 12**)[84,98]. In hypoxic cells, like epithelial cells, myocytes, macrophages and ECs, the HIF TFs actively increase VEGF expression further driving the progression of hypoxia-induced angiogenesis. The VEGF

receptors belong to the class of receptor tyrosine kinases consisting of a cytoplasmic tyrosine kinase and an extracellular ligand-binding domain that contains seven immunoglobulin (Ig)-like domains connected by a transmembrane segment[84]. The different VEGF isoforms acting as ligands are capable to bind to the VEGF receptors, initiating different endothelial responses. Alternative splicing of VEGF or the VEGF receptors modulate VEGF signalling. There are both, pro- and anti-angiogenic isoforms of VEGF, e.g. VEGF-A_{xxx} and VEGF-A_{xxx}b, where xxx indicate the length of VEGF in number of amino acids[99]. A similar situation exists for the VEGF receptors. For VEGF-Receptor 1, also called FLT1, a membrane-bound and soluble receptor isoform (sFLT1) exist, and sFLT1 therefore acts as a decoy receptor[100,101]. Other alternatively spliced molecules impacting on the VEGF signalling are HIF1α[102] as well as the KDR (VEGF-Receptor 2) co-receptors NRP1 and NRP2[100].

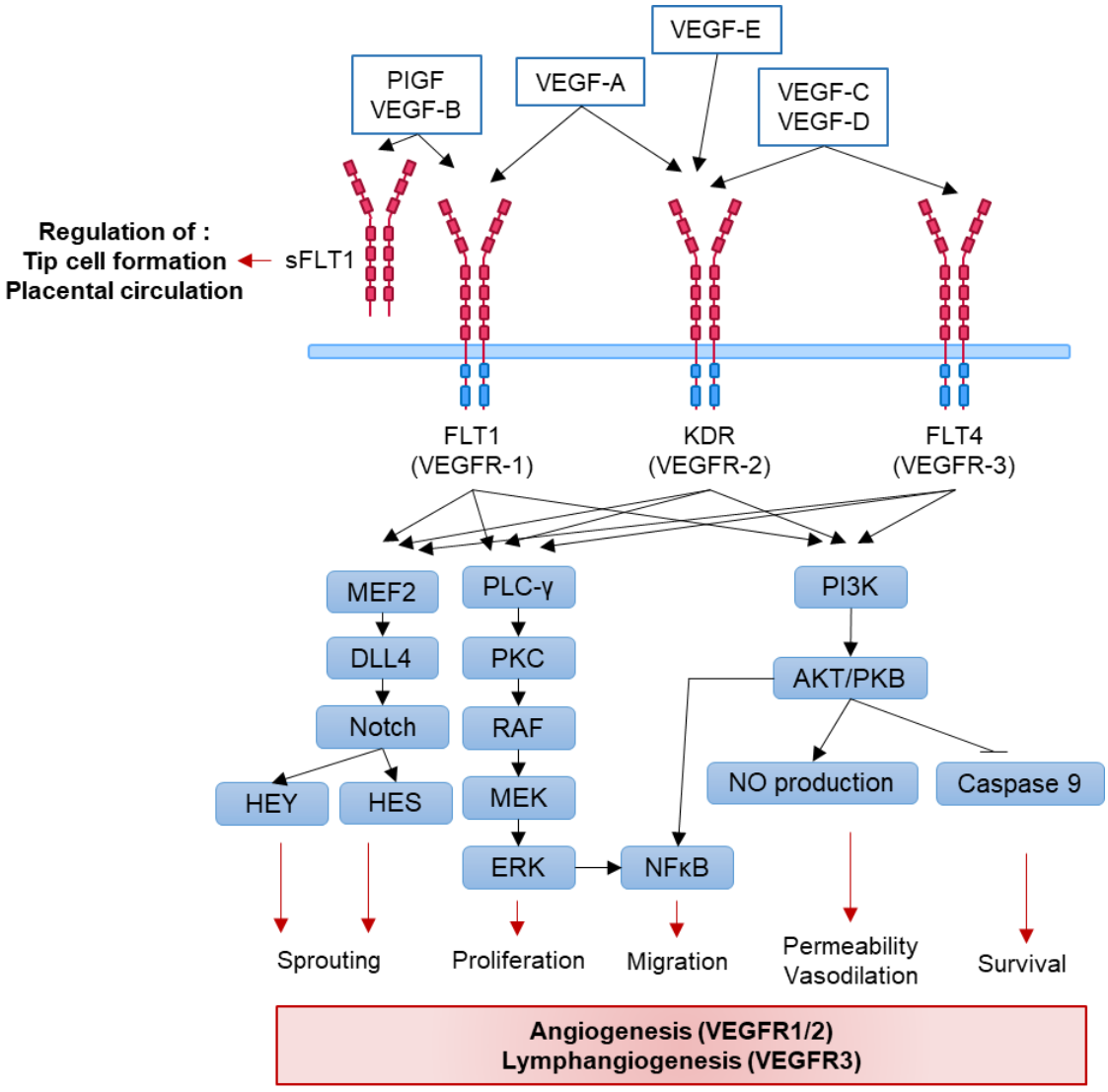

Figure 12 VEGF receptors, their ligands and mode of action

VEGF-A can bind the VEGF receptors FLT1 (VEGFR1) and KDR (VEGFR2) leading to induction of angiogenesis and vasculogenesis related gene programs. VEGF-E is a KDR-specific ligand, whereas VEGF-C and VEGF-D can bind KDR and FLT4 (VEGFR3). FLT4 orchestrates lymphangiogenesis. sFLT1 is the soluble, anti-angiogenic AS variant of FLT1. sFLT1 binds Placental Growth Factor (PIGF) and VEGF-A and is involved in tip cell formation and regulation of the placental circulation. Downstream signalling of all VEGF receptors include Notch-, MAPK-, PI3K-, AKT- and NFκB signalling. Figure adapted from Falk *et al.* (2010)[103]; Shibuya *et al*. (2011)[98], Tsuji-Tamura and Ogawa (2018)[104] and Bui & Hong (2020)[105].

Angiogenesis is most frequently induced by VEGF-A activating VEGFR1 (Fms Related Receptor Tyrosine Kinase 1, FLT1) and VEGFR2 (Kinase Insert Domain Receptor, KDR). Binding of the ligand to the VEGF receptors triggers the downstream signalling, among them the PI3K-, AKT-, MAPK- and NFκB-cascades (**Figure 12**)[103,105]. These pathways are interconnected and all contribute to the angiogenic programs. By activation of Notch signalling the expression of the TFs HEY1 (Hes Related Family BHLH Transcription Factor With YRPW Motif 1) and HES (Hes Family BHLH Transcription Factor) is induced, which contributes to the sprouting phenotype of EC[104]. The Mitogen-activated protein kinase (MAPK) cascade facilitates EC proliferation. Nuclear factor-kappaB (NFκB) enables endothelial migration by inducing the expression of extracellular matrix degrading proteins, the matrix metalloproteinases[106]. Besides other functions, phosphatidylinositol-3 kinase (PI3K)/protein kinase B (AKT) activates NFκB, which increases NO production to allow for a permeable and dilated endothelium and inhibits Caspase 9 to promote cell survival[107]. These and other VEGF receptor downstream signalling events enable angiogenesis.

As for many other processes in ECs, lncRNAs also contribute to the correct orchestration of angiogenesis-associated gene programs, as detailed in the following chapter.

1.4.3 LncRNAs in the endothelium

The role of lncRNAs in the cardiovascular system and the endothelium is highly diverse and has been subject to substantial research over the last decade. This has led to the identification of lncRNAs as clinically relevant biomarkers and as co-regulatory molecules[108]. Examples for cardiovascular lncRNAs as biomarker are the lncRNA *ANRIL* as a biomarker for atherosclerosis[32] or *MIAT* and *HOTAIR* for myocardial infarction[109,110] or *LIPCAR* for heart failure[111]. Additionally, many lncRNAs have been shown to be protective against CVD progression or, if altered in their expression to be drivers of disease progression[108]. Among them is the lncRNA *H19*, which is cardio-protective by indirect suppression of pro-hypertrophic

nuclear factor of activated T cells (NFAT) expression through interaction with the PRC2 subunit EZH2. In failing hearts, *H19* has been shown to be strongly downregulated, further promoting disease progression[112]. Another example of CV disease-relevant lncRNAs is *MALAT1* that safeguards EC homeostasis by an anti-migratory and anti-angiogenic mode of action[113]. In addition to the previously described lncRNA *MANTIS*, the endothelial lncRNA *STEEL* (*spliced-transcript endothelial-enriched lncRNA*) regulates expression of the local blood flow mediator endothelial nitric oxide synthase (eNOS) and the sheer-stress sensing molecule Krupple-like factor 2 (KLF2)[114]. By forming a ribonucleoprotein complex with poly(ADP-ribose) polymerase 1 (PARP1), STEEL affects the position- and shear-dependent angiogenic response within the vascular tree[114].

These few examples demonstrate the potential that lncRNAs have for cardiovascular research.

2 Aim

LncRNAs, a recently appreciated class of RNAs with diverse regulatory functions, modulate chromatin composition and gene expression to impact on cellular phenotype during development and homeostasis. Given the critical role of the vascular endothelium in maintaining vascular homeostasis and its association with cardiovascular diseases, extensive research has been conducted to better understand the molecular basis of normal endothelial function and endothelial dysfunction. The contribution of endothelial lncRNAs to those conditions, however, is largely undefined. LncRNAs have the potential to serve as biomarkers and therapeutic targets in CVD, making them an exciting and significant group of molecules worth investigating.

Accordingly, the aim of this study was the identification and functional characterization of endothelial lncRNAs. On this basis, *LINC00607* was identified to be highly expressed and endothelial-specific with potential clinical significance. On this basis, the first aim of this thesis was the identification of the physiological importance of *LINC00607* in endothelial cells by combining loss of function approaches with physiological assays. As a second aim, I intend to extend the knowledge on *LINC00607* to its molecular function, by leveraging advanced high-throughput sequencing technologies combined with computational methodologies, such as a splicing analysis. This information and these results should aid in clarifying the function of *LINC00607* and its relevance in cardiovascular diseases.

Interestingly the characterization of *LINC00607* revealed two molecular functions for endothelial cells: epigenetic regulation of chromatin accessibility and alternative splicing.

3 Materials and methods

3.1 Materials

3.1.1 Chemicals

Table 1. List of Chemicals

Chemicals	Catalogue No.	Company
2-Acrylamido-2-methylpropane sulfonic acid (AMPS)	A0838,9010	Applichem, Darmstadt
Acriflavine	A8126	Sigma-Aldrich, Taufkirchen
Acrylamide solution, 37.5:1	10688.03	Serva, Heidelberg
Agar	A5306	AppliChem, Darmstadt
Agarose	BS20.46	Bio&Sell, Feucht
Ampicillin sodium salt	A9518	Sigma-Aldrich, Taufkirchen
AMPure XP beads	A63881	Beckman Coulter, Brea (USA)
Aquatex Mounting medium	1.08562	Merck, Darmstadt
BioMag®Plus Concanavalin A (ConA) beads	86057	Polysciences, Hirschberg an der Bergstraße
BSA	8076.3	Roth, Karlsruhe
Braunol	3864219	Braun, Melsungen
Casyton	2501037	Roche, Basel
Chloroform	32211	Sigma-Aldrich, Taufkirchen
CUTANA™ pAG-MNase	15-1016	EpiCypher, Inc., Durham (USA)
D(+)-Sucrose	A3935	AppliChem, Darmstadt
DAPI	D9542	Sigma-Aldrich, Taufkirchen
Deoxyribose nucleotides (dNTPs)	BIO-39026	Bioline, Memphis (USA)
Dichloromethane (DCM)	270997	Sigma-Aldrich, Taufkirchen
Dibenzyl ether (DBE)	108014	Sigma-Aldrich, Taufkirchen

Dimethyl sulfoxide (DMSO)	D2650	Sigma-Aldrich, Taufkirchen
Dithiothreitol (DTT)	P/N Y00147	Invitrogen, Carlsbad (USA)
DMOG	400091	Merck, Darmstadt
DNase I, RNase-free	M6101	Promega, Madison (USA)
DNase/RNase free water	10977035	Invitrogen, Carlsbad (USA)
Doxorubicin	324380	Sigma-Aldrich, Taufkirchen
Dulbecco`s Phosphate Buffered Saline (DPBS)	14190-094	Gibco, Thermo Fisher Scientific, Schwerte
Dynabeads Protein A	10001D	Life technologies, Carlsbad (USA)
Ethylene diamine tetraacetic acid (EDTA)	A1103,0250	Applichem, Darmstadt
Ethylene glycol tetraacetic acid (EGTA)	A0878,0100	Applichem, Darmstadt
EtOH absolute	24102-2.5L-R	Sigma-Aldrich, Taufkirchen
Fibrinogen	356009	Corning, Corning (USA)
Fetal calf serum (FCS)	S0113	Biochrom, Berlin
Formaldehyde 37%	A0877,0250	Applichem, Darmstadt
Formamide	A0937,1000	Applichem, Darmstadt
Gelatin	356009	Corning, Corning (USA)
GeneTrans Transfection Reagents	0203B	MoBiTec, Goettingen
Glycine	3908.3	Roth, Karlsruhe
Glycogen	R0561	Thermo Fisher Scientific, Schwerte
Hanks' balanced salts (HBSS)	A3140,5000	Applichem, Darmstadt
Hydrochloric acid (HCl)	P074.3	Roth, Karlsruhe
HEPES (N-2-Hydroxyethylpiperazin-N'-2-ethansulfonic acid)	9105.3	Roth, Karlsruhe
Hygromycin	30-240-CR	Corning, Corning (USA)
IL-1 beta, recombinant human	200-01B	PeproTech, Thermo Fisher Scientific, Schwerte
Incucyte® Nuclight Rapid Red Dye	4717	Essen Bioscience, Ann Arbour (USA)

Incucyte® Annexin Green Dye	4642	Essen Bioscience, Ann Arbour (USA)
Isoflurane	B506	Abbvie, North Chicago (USA)
Isopropyl alcohol	W292907	Sigma-Aldrich, Taufkirchen
iTaq™ Universal SYBR® Green Supermix	10000068167	Bio-Rad, Munich
Ketamine (Ketaset)	07506004	Zoetis, Parsippany-Troy Hills Township (USA)
L-Glutamine (100x)	25030	Gibco, Thermo Fisher Scientific, Schwerte
Loading Dye, 6x	R0611	Life technologies, Carlsbad (USA)
Methanol	32213-2.5 mL	Sigma-Aldrich, Taufkirchen
Methocel	SM0512	Sigma-Aldrich, Taufkirchen
MyOne Streptavidin C1 beads	65001	Gibco, Thermo Fisher Scientific, Schwerte
Nonidet (NP-40)	74385	Sigma-Aldrich, Taufkirchen
Okadaic acid (OA)	A2200,0025	Applichem, Darmstadt
Orthovanadate (OV)	A2196,0005	Applichem, Darmstadt
Paraformaldehyde (PFA)	16005-1KG-R	Sigma-Aldrich, Taufkirchen
PCR Mastermix	K0171	Thermo Fisher Scientific, Schwerte
Polyethylenamine (PEI)	408727	Sigma-Aldrich, Taufkirchen
Phenylmethanesulfonylfluoride (PMSF)	P7626-5G	Sigma-Aldrich, Taufkirchen
Penicillin/Streptomycin (100x)	30-002-CI	Corning, Manassas (USA)
Precision Plus Protein All Blue Standard	161-0374	Bio-Rad, Munich
Protein-inhibitor mix (PIM)	4693132001	Sigma-Aldrich, Taufkirchen

Propranolol hydrochloride	P0884	Sigma-Aldrich, Taufkirchen
Puromycin Dihydrochlorid	0240.4	Roth, Karlsruhe
Polybrene Infection/Transfection Reagent	TR-1003-G	Millipore, Burlington (USA)
Potassium chloride (KCl)	6781	Roth, Karlsruhe
Proteinase K	kcH-507-100	Diagenode, Liege (Belgium)
QIAzol lysis reagent	79306	Qiagen, Hilden
Random Primers	C118A	Promega, Madison (USA)
Reverse Transcriptase Superscript III	18080-085	Life technologies, Carlsbad (USA)
RNaseA	EN0531	Thermo Fisher Scientific, Schwerte
RNAlater RNA Stabilization Sol.	AM7020	Thermo Fisher Scientific, Schwerte
Roti-Block	A151.1	Roth, Karlsruhe
Roti-Quant	K015.2	Roth, Karlsruhe
Roti-Gel Stain, Ethidium bromide	3865.1	Roth, Karlsruhe
Sodium acetate	S8750	Sigma-Aldrich, Taufkirchen
Sodium bicarbonate (NaHCO3)	S5761-500	Sigma-Aldrich, Taufkirchen
Sodium chloride (NaCl)	31434-5KG-R	Sigma-Aldrich, Taufkirchen
Sodium citrate	3580.1	Roth, Karlsruhe
Sodium dodecyl sulfate (SDS)	CN30.3	Roth, Karlsruhe
Sodium deoxycholate	D6750	Sigma-Aldrich, Taufkirchen
Sodium hydroxide (NaOH)	30620	Sigma-Aldrich, Taufkirchen
SuperaseIN	AM2694	Life technologies, Carlsbad (USA)
Tetrahydrofuran	186562	Sigma-Aldrich, Taufkirchen
Tetramethylethylenediamine (TEMED)	A1148,0100	Applichem, Darmstadt

TGFβ2	100-35B	Peprotech, Schwerte
Thymidine	T9250	Sigma-Aldrich, Taufkirchen
TRIS	AE15.3	Roth, Karlsruhe
Triton X-100	3051.3	Roth, Karlsruhe
Trypan Blue solution	93595-50mL	Sigma-Aldrich, Taufkirchen
Trypsin-EDTA	T3924-100mL	Sigma-Aldrich, Taufkirchen
Tween-20	P 1379-500mL	Sigma-Aldrich, Taufkirchen
VEGF-A (165), recombinant human	293-VE-010	R&D, Minneapolis (USA)
Xylazine (Rompun 2%)	14840	Bayer, Wuppertal

3.1.2 Consumables

Table 2. List of Consumables

Material	**Catalogue No.**	**Company**
AriaMx Low Profile Strip Tubes	401493	Agilent Technologies, Waldbronn
High profile strip PCR Tubes	I 1402-3500	Starlab, Hamburg
35mm cell culture plate	353001	BD Bioscience, Franklin Lakes (USA)
60mm cell culture plate	83.3901	Starlab, Hamburg
100mm cell culture plate	83.3902	Starlab, Hamburg
12-well cell culture plate	83.3921.005	Starlab, Hamburg
48-well cell culture plate	677180	Greiner, Kremsmünster
96-well cell culture plate	655180	Greiner, Kremsmünster
96-well ImageLock cell culture plate	4379	Essen Bioscience
Ibidi µ-Slide 8 well	80826	Ibidi, Gräfelfing
Test and centrifugal tubes (15 mL, 50 mL)	62515028, 62526028	Starlab, Hamburg
Nitrocellulose Transfer Membrane PROTRan BA 85	260201196	NeoLab, Heidelberg
Whatman Paper / Gel-Blotting-Paper	GB58	A. Hartenstein, Würzburg

3.1.3 Equipment

Table 3. List of Equipment

Equipment	Model	Company
Autoclave	3150 ELV	Tuttnauer, Beit Shemesh (Israel)
Neo 5.5 (3-tap) sCOMs Camera	Mod. No.: DC-152q-C00-FI	Andor Technology Ltd, Belfast (UK)
Cell Counter	Casy	Schärfe System, Reutlingen
Centrifuge	5415 R (F45-24-11)	Eppendorf, Hamburg
	Micro Star 17R (75003424)	VWR, Darmstadt
	Heraeus Megafuge 16 (75003629)	Thermo Fisher Scientific, Schwerte
	Sorvall RC 6+ (F13-14x50cy or F10-6x500y)	Thermo Fisher Scientific, Schwerte
Cryostat	HM550	Thermo Fisher Scientific, Schwerte
Freezer	HERAfreeze basic (-80 °C)	Heraeus Instruments, Hanau
	Freezer 150°C	Ewald Innovationstechnik, Rodenberg
Gel documentation system	Intas Gel-Stick Imager	Royal Biotech, Frankfurt/Main
Heating block	Thermomixer compact	Eppendorf, Hamburg
HybEZ Oven	HybEZ Oven	Advanced Cell Diagnostics, Newark
Incucyte Woundmaker	96-pin Tool	Essen Bioscience, Dümmer
Incubator	Hera Cell 150i CO2 Incubator	Thermo Fisher Scientific, Schwerte
	IL 23	VWR, Darmstadt
	SciTive Workstation - hypoxia	Baker Ruskinn, I&L Biosystems, Königswinter
	Incucyte S3 Live Cell Analysis System	Essen Bioscience, Dümmer
Infrared scanner	Odyssey	LI-COR Biosciences, Bad Homburg
Magnetic stirrers	Heidolph MR Hei-Mix L	NeoLab, Heidelberg
Microplate Reader	Infinite 200 PRO	Tecan, Männedorf

Microscope	Laser Scanning Microscope LSM800	Zeiss, Göttingen
	Evos XL Core	Thermo Fisher Scientific, Schwerte
	Light sheet microscope, UltraMicroscope II	Lavision Biotech, Bielefeld
pH meter	PP-50	Sartorius, Göttingen
PCR device	Eppendorf Mastercycler Gradient	Eppendorf AG, Hamburg
Pipette	0.1 - 2.5 µL 1 - 10 µL 2 - 20 µL 20 - 200 µL 100 - 1000 µL	Eppendorf, Hamburg
Power supply	CS - 300V	Roth, Karlsruhe
	PowerPac HC	Bio-Rad, München
qPCR device	AriaMx Real-Time PCR	Agilent Technologies, Waldbronn
Rotor	Stuart SB3	Stuart, Staffordshire (UK)
Scale	Analytical Balance	Sartorius, Göttingen
	MC1	Sartorius, Göttingen
Shaker	GFL-3013	Thermo Fisher Scientific, Schwerte
	MaxQ 4000 Benchtop Orbital	Thermo Fisher Scientific, Schwerte
Spectrophotometer	NanoDrop® ND-1000	Nanodrop Technologie, Rockland (USA)
Sterile bench	Laminarflow HB 2448	Heraeus Instruments, Hanau
	Herasafe HS 12	Heraeus Instruments, Hanau
Transfection system	Neon	Thermo Fisher Scientific, Schwerte
UV irradiation system	BIO-LINK, BLX-254	Vilber, Eberhardzell
Vortex mixer	Vortex Genie 2	Scientific Industries, New York (USA)
Water purification system	Milli-Q Q-POD	Millipore, Billerica (USA)

Western blot chambers	1658004	Biorad, München

3.1.4 Buffers and solutions

Table 4. Recipes for buffers and solutions

Buffer	Recipe
1x Wash buffer (Western blot)	0.3% Tween-20 50 mM Tris/HCl, pH 7.5 150 mM NaCl ddH_2O
1x Transfer buffer (Western blot)	25 mM Tris/HCl 190 mM Glycine 20% Methanol ddH_2O
1x Running buffer (Western blot)	25 mM Tris/HCl 190 mM Glycine 0.1% SDS ddH_2O
1x Sample buffer (Western blot)	125.3 mM Tris/HCl, pH 6.8 17% Glycerol 4% SDS 40 mM DTT 0.004% Bromophenol blue ddH_2O
Hanks' buffer	4 mM Na_2CO_3 in Hanks' salt
Covaris Fixing Buffer (ChIP)	450 µL 10x Fixing Buffer (A) to 5 mL ddH_2O
Covaris Lysis buffer (ChIP)	200 µL 5x Lysis Buffer (B) 10 µL 100x Protease Inhibitor to 1 mL ddH_2O
Covaris Shearing buffer (ChIP)	200 µL 10x Shearing Buffer (D3) 20 µL 100x Protease Inhibitor to 2 mL ddH_2O
Covaris Wash buffer (ChIP)	100 µL 10x Wash Buffer (C) 10 µL 100x Protease Inhibitor to 1 mL ddH_2O

Dilution buffer (ChIP)	20 mM Tris/HCl pH 7.4 100 mM NaCl 2 mM EDTA pH 8.0 0.5% Triton X-100 400 nM PMSF 25 nM PIM ddH_2O
6 x DNA loading dye	10 mM Tris/HCl pH 7.6 60% v/v glycerol 0.03% w/v bromphenol blue 0.03% w/v xylene cyanol 60 mM EDTA ddH_2O
Buffer A (cytoplasmic lysis)	10 mM Hepes pH 7.9 10 mM KCl 0.1 mM EDTA 0.1 mM EGTA Protease inhibitors (PIM, PMSF, DTT) ddH_2O
Buffer C1 (nuclear lysis)	20 mM Hepes pH 7.9 0.4 M NaCl 1 mM EDTA 1 mM EGTA Protease inhibitors (PIM, PMSF, DTT) ddH_2O
Buffer C2 (C1 dilution buffer)	20 mM Hepes pH 7.9 1 mM EDTA 1 mM EGTA Protease inhibitors (PIM, PMSF, DTT) ddH_2O
Buffer C3	20 mM Hepes pH 7.9 0.2 M NaCl 1 mM EDTA 1 mM EGTA Protease inhibitors (PIM, PMSF, DTT) ddH_2O
Hybridisation Buffer (RNA-FISH)	10% Dextran Sulfate

	1 µL/mL SuperaseIN
	0.02% RNase-free BSA
	400 µg *E. Coli* tRNA
	50% formamide
	2XSSC
	ddH_2O
3 x Laemmli buffer	11.28 mM Tris/HCl pH 6.8
	25.5% glycerol
	6% SDS
	60 mM DTT
	0.04% bromphenol blue
	ddH_2O
Methocel	6 g methocel
	500 mL EBM
Antibody RIP lysis buffer	50 mM Tris/HCl pH 7.4
	100 mM NaCl
	1% NP-40
	0.1% SDS
	0.5% Sodium deoxycholate
	protease inhibitors (PIM, PMSF, DTT)
	ddH_2O
Antibody RIP wash buffer (high salt)	50 mM Tris/HCl pH 7.4
	1 M NaCl
	1 mM EDTA
	0.1% SDS
	0.5% Sodium deoxycholate
	1% NP-40
	ddH_2O
Antibody RIP Buffer PNK wash	350 mM Tris/HCl pH 6.5
	50 mM $MgCl_2$
	5 mM DTT
	ddH_2O
RIP RNaseA digestion Buffer	20 mM Tris/HCl
	EDTA pH 8.0
	10 mg/mL RNase A
	ddH_2O
20x SSC (RNA-FISH)	3 M NaCl

	300 mM Trisodium Citrate ddH_2O
TE buffer pH 8.0 (ChIP)	10 mM Tris/HCl pH 8.0 1 mM EDTA ddH_2O
RIPA Lysis Buffer	1X TBS 1% Desoxycholat 1% Triton 0.1% SDS protease inhibitors (PIM, PMSF, OV, OA) ddH_2O
Lysis Buffer (genomic DNA)	0.1 M Tris/HCl pH 8.5 0.5 M NaCl 0.2% SDS 0.05 M EDTA 22.2 mg/mL Proteinase K ddH_2O
3x Laemmli Sample Buffer	6% SDS. 30% glycerol. 0.3% bromphenol blue. 0.150 mM Tris/HCl, pH 6.8 300 mM DTT
2YT bacteria growth medium	16 g/L Tryptone 10 g/L Yeast Extract 5 g/L NaCl ddH_2O

3.1.5 Human eukaryotic cells

Table 5. Origin of cells and description

Cells	Description	Origin
HUVEC	human umbilical vein endothelial cells	Promocell, Heidelberg Batches: 405Z013, 408Z014, 416Z042
HEK293	human embryonic kidney cell line	ATCC, Manassas (USA)
LentiX HEK293T	HEK293 transformed with adenovirus type 5 DNA	Takara, Kusatsu (Japan)

3.1.6 Cell culture media

Table 6. Media used for cultivation of eukaryotic cells

Medium	Supplements	Company
Endothelial Basal Medium (EBM)	Glutamine	Pelo Biotech, Planegg
Enhanced Endothelial Cell Growth Medium (EGM)	Glutamine bFGF hEGF VEGF 8% fetal calf serum 50 U/mL penicillin 50 µg/mL streptomycin	Pelo Biotech, Planegg
EndMT Differentiation Medium (DM)	EBM Glutamine 8% fetal calf serum 50 U/mL penicillin 50 µg/mL streptomycin 10 ng/mL TGFβ2 1 ng/mL IL-1β	Pelo Biotech, Planegg
Minimal Essential Medium (MEM)	8% fetal calf serum 0.1% Gentamycine 1% Sodium pyruvate 1% non-essential amino acids	Thermo Fisher Scientific, Schwerte
Trypsion solution (10X)	-	Sigma Aldrich, Taufkirchen

3.1.7 Synthetic oligonucleotides

Table 7. Primer sequences for qPCR (E = exon, alt = alternative)

Gene	Species	Forward Primer (5´-3´)	Reverse Primer (5´-3´)
β-Actin	*Human*	TGACAGGATGCAGAAGGAGA	GCTGGAAGGTGGACAGTGAG
LINC00607	*Human*	CCACCACCACCATTACTTTC	AGGCTCTGTATTCCCAACTG
CNN1	*Human*	CATCGGCAACTTCATCAAGG	CCTGCAGCCCAATGATGTTC
TAGLN	*Human*	TTCTGAGCAAGCTGGTGAAC	AGTTGGGATCTCCACGGTAG
COL1A1	*Human*	TGCTGGTGCTCCTGGTACTC	GGGACCACGTTCACCACTTG
PECAM1	*Human*	GCGGTATTCAAAGACAACCC	ATCACCTTCACCCTCAGAAC
BRG1	*Human*	TCGCCAAGATCCGTTGGAAG	GCCACATAGTGCGTGTTGAG
TGFβ2	*Human*	GAGCTATATCAGATTCTCAAGTC	GCCATCAATACCTGCAAATCTTG

RSPO3	*Human*	TGTGCAACATGCTCAGATTACA	TGCTTCATGCCAATTCTTTCCA
VWF	*Human*	CCTTGACCTCGGACCCTTATG	GATGCCCGTTCACACCACT
DLL4	*Human*	CAGCACTCCCTGGCAATGTA	CACAGTAGGTGCCCGTGAAT
GUCY1A1	*Human*	AGAGCTGGATGTCTACAAGG	CGCTATCTGAACAGCATGAG
mFLT1 E13-E15	*Human*	AAATGCCGACGGAAGGAGAG	GTGGCTTTGCAGTGATAGAC
mFLT1 E13-E14	*Human*	AAATGCCGACGGAAGGAGAG	AGGTTTCGCAGGAGGTATGG
sFLT1 E13-altE15	*Human*	GCAAGATTCAGGCACCTATG	TGACGATGGTGACGTTGATG
sFLT1 E14-altE15	*Human*	CAGCAGTTCCACCACTTTAG	TGACGATGGTGACGTTGATG
LINC00607 mf	*Macaca fascicularis*	CTGCAGTCACCGCATACCC	TGGCTCTGCTGCTGGAGTAG
GAPDH_mf	*Macaca fascicularis*	TGCACCACCAACTGCTTAGC	GGCGTGGACTGTGGTCATGAG

Table 8. CRISPR/Cas9 guide RNA (gRNA) oligonucleotides

Gene	Forward Primer (5´-3´)	Reverse Primer (5´-3´)
*LINC00607*_A	CACCGCATGTGCCCCCTTTGTTGA	AAACTTCAACAAAGGGGGCACATGC
*LINC00607*_B	CACCGCAGTGTGTCATGTTATCTTG	AAACCAAGATAACATGACACACTGC
BRG1	CACCGCATGCTCAGACCACCCAG	AAACCTGGGTGGCTCTGAGCATGC
Non-target control (NTC)	CACCGTTCCGGGCTAACAAGTCCT	AAACAGGACTTGTTAGCCCGGAAC

Table 9. Primer sequences for genomic DNA amplification

Gene	Forward Primer (5´-3´)	Reverse Primer (5´-3´)
LINC00607	CTTCAGCCCACTGAGTCTTG	GAGGAACCAGCCAGAATAGC
GAPDH	TGGTGTCAGGTTATGCTGGGCCAG	GTGGGATGGGAGGGTGCTGAACAC

Table 10. Primer sequences used in the splicing analysis of the endothelial predominant *LINC00607* transcript (ex: exon; annot: annotated)

No.	Description	Orientation	Primer (5´-3´)
1	*LINC00607ex1-2*	forward	GGTGATTCCAGCAGGCTGAG
2	*LINC00607ex1-2*	reverse	TCTCAGCCTGCTGGAATCAC
3	*LINC00607ex2-3*	forward	ACAGCGTCTGAGGGTCATTG
4	*LINC00607ex2-3*	reverse	TCAGACGCTGTAGGAAGAGG
5	*LINC00607ex3-4*	forward	GGCTTCCCAGGTATCTTGAC
6	*LINC00607ex3-4*	reverse	CCAAGAGGCCAGAGTATGTG
7	*LINC00607ex4-5*	forward	GTGGAGTGGCAGGACTTATG

8	*LINC00607ex4-5*	reverse	AACCCTGCAGTTGGGAATAC
9	*LINC00607ex5annot-6*	reverse	CCACCACCACCATTACTTTC
10	*LINC00607ex5new-6*	forward	CACGAGACAAGCCTCTAAGC
11	*LINC00607ex6-7*	forward	CTGTGACCAGGCAAAGAATC
12	*LINC00607ex6-7*	reverse	CTCAGAGGGTCTTTGTAACG
13	*LINC00607ex4-5new*	reverse	GAGTAGCTTAGAGGCTTGTC
14	*LINC00607ex7.1*	forward	CTGATCTGCTGGAATGATGG
15	*LINC00607ex7.1*	reverse	GCTGGGTTTGATCTTGTCTG
16	*LINC00607ex7.2*	forward	TGTAGGTACGCAGCTCATTG
17	*LINC00607ex7.2*	reverse	CATCTGACACTTGGCGAAAC
18	*LINC00607ex7.3*	forward	GTGTCAGATGCCAAGAAGTG
19	*LINC00607ex7.3*	reverse	TCTCCATGGCCCTTAAAGTC

3.1.8 Small Interfering Ribonucleic Acid (siRNAs)

Table 11. List of siRNAs

Gene	Order No.	Company
LINC00607 (Silencer® Select)	s56342	Thermo Fisher Scientific, Schwerte
BRG1 (Stealth)	HSS110005	Thermo Fisher Scientific, Schwerte
Negative control (Stealth)	12935300	Thermo Fisher Scientific, Schwerte

3.1.9 Antisense oligonucleotides (5’ biotin- or TYE-tagged)

Table 12. List of Antisense oligonucleotides

Name	Sequence	Manufacturer
LINC00607 (5‘-TYE)	AGGAGCTGAGATGCACATACT	Qiagen, Hilden
Scramble control (5‘-TYE)	GTGTAACACGTCTATACGCCCA	Qiagen, Hilden

3.1.10 Plasmids

Table 13. List of plasmids

Name	Origin
pcDNA3.1-*LINC00607*	Biomatic, Wilmington (USA)
psPAX2	Addgene plasmid #12260, Gift from Didier Trono
pVSVG (pMD2.G)	Addgene plasmid #12259, Gift from Didier Trono
lentiCRISPRv2 (puromycin resistance)	Addgene plasmid #52961, Gift from Feng Zhang
lentiCRISPRv2 (hygromycin resistance)	provided by Frank Schnütgen (Department of Haematology, University Clinic Frankfurt/Main)

3.1.11 Antibodies

3.1.11.1 Primary antibodies

Table 14. List of Primary antibodies

Protein	Order No.	Species	Dilution	Company
BRG1	A303-877A-M-1	goat	1:1000	Bethyl, Montgomery (USA)
BRG1	ab110641	rabbit	1:1000	Abcam, Cambridge (USA)
B-Actin	4970S	rabbit	1:1000	Cell Signalling, Danvers (USA)
FLT1 (sFLT1)	36110	rabbit	3 µg/mL	Thermo Fisher Scientific, Schwerte
VWF	ab6994	rabbit	1:1000	Abcam, Cambridge (USA)
PECAM1	sc376764	mouse	1:1000	Santa Cruz Biotechnology, Dallas (USA)
TGFβ2	sc374658	mouse	1:1000	Santa Cruz Biotechnology, Dallas (USA)

3.1.11.2 Secondary antibodies

Table 15. List of secondary antibodies

Reactivity	Order No.	Species	Dilution	Company
Goat IgG; 800CW	926-32214	donkey	1:15000	LI-COR Biosciences, Bad Homburg
Rabbit IgG; 680RD	926-68073	donkey	1:15000	LI-COR Biosciences, Bad Homburg
Mouse IgG; 800CW	926-32212	donkey	1:15000	LI-COR Biosciences, Bad Homburg

3.1.12 Reaction systems

Table 16. Reaction systems

Name	Company
lllumina Tagment DNA Enzyme and Buffer Kit	Illumina, San Diego (USA)
Lenti-X™ GoStix™ Plus kit	Takara, Kusatsu (Japan)
Lenti-X™ GoStix™ Plus kit	Takara, Kusatsu (Japan)
NEBNext® Ultra II Kit	New England Biolabs GmbH, Frankfurt/Main
Neon Transfection System 100 µL Kit	Thermo Fisher Scientific, Schwerte
peqGOLD XChange Plasmid Maxi-EF Kit	PEQLAB Biotechnologie GmbH (USA)

QIAquick Gel Extraction Kit	Qiagen, Hilden
RNA Mini Kit	Bio&Sell, Feucht
RNAscope 2.5 HD Detection Reagents	ACD (USA)
SMARTer Stranded Total RNA Sample Prep Kit - HI Mammalian	Takara, Kusatsu (Japan)
truChIP kit	Covaris, Woburn (USA)

3.1.13 Software

Table 17. List of software

Name	Company
Agilent Aria MX 1.7	Agilent Technologies, California (USA)
GraphPadPrism 9	GraphPad Software, San Diego (USA)
Imaris (Bitplane Version 9.6)	Oxford Instruments, Abingdon (UK)
Image J	National Institutes of Health, Bethesda (USA)
Image studio 5.2	LI-COR, Bad Homburg
Nanodrop, 2000/200c	Thermo Scientific, Waltham (USA)
ImSpectorPro Version_3.1.8	LAVision BioTech GmbH, Bielefeld
R (4.1.2)	https://www.r-project.org
R Studio (2022.02.0+443)	Rstudio Inc., Boston (USA)
Zen blue edition 3.0	Zeiss, Oberkochen
Zotero 6.0.20	Roy Rosenzweig Centers for History and New Media; Mason University Virginia (USA)

Table 18. List of R-packages

Name	Source
DESeq2 (1.32.0)	Bioconductor
ggplot2 (3.3.5)	CRAN
Stats (4.1.1)	RStudio Inc., Boston (USA)

3.1.14 Animals

Table 19. Mouse lines

Genotype	Strain Code	Source
SCID Mouse (CB17/Icr-*Prkdc*^{scid}/IcrIcoCrl)	236	Charles River, Deisenhofen

3.1.15 Publically available datasets

Table 20. Publically available datasets

Dataset	Summary	Source
GSE109696 (NCBI GEO)	RNA-Seq of HUVEC with siKD of ERG	Nagai *et al*. (2019)[115]
GSE124891 (NCBI GEO)	ERG ChIP Seq, CTL and siKD of ERG	Kalna *et al.* (2019)[88]
GSE70330 (NCBI GEO)	RNA-Seq of HUVEC cultured under normoxia or hypoxia	Fiedler *et al.* (2015)[116]
GSE176555 (NCBI GEO)	RNA-Seq of ACF treated HUVECs under normoxia	Seredinski *et al.* (2022)[117]
GSE186297 (NCBI GEO)	RNA-Seq of ACF treated HUVECs under hypoxia	Seredinski *et al.* (2022)[117]
GSE118446 (NCBI GEO)	EndMT treatments of HUVEC and PAEC	Monteiro *et al.* (2021)[118]
	FANTOM5 CAGE and ENCODE expression data	Forrest *et al.* (2014)[119] Lizio *et al.* (2015)[1] Noguchi *et al.* (2017)[120]

3.2 Methods

3.2.1 Cell culture

3.2.1.1 Cell culture conditions of human eukaryotic cells

Pooled human umbilical vein endothelial cells (HUVEC, batches 405Z013, 408Z014, 416Z042) were cultured in a humidified atmosphere of 5% CO_2 at 37 °C on gelatin-coated dishes in enhanced endothelial growth medium (EGM) containing 8% fetal calf serum (FCS). HUVEC, previously frozen and stored at passage two, were thawed and seeded for passage three and immediately used without further passaging.

3.2.1.2 Passaging and cell counting

In order to split HUVEC, medium was discarded, and the cells were washed once with PBS without Ca^{2+} and Mg^{2+}. Per 10 cm dish, 2 mL Trypsin was added, the cells were detached and collected in 6 mL EGM. The cells were centrifuged (4 min, 1,200 xg, RT), the supernatant discarded, and the cells resuspended in 6 mL EGM. The cell count was determined with the CASY®TT. For this, 25 µL of cells

suspension was mixed with 10 mL CASY TON solution and the cells counted. The desired number of cells was calculated and plated onto gelatin-coated dishes.

3.2.1.3 Cell stimulation

The day before stimulation, HUVEC were seeded and cultured as described above. The following chemicals and concentrations were used for stimulation experiments: Human recombinant VEGF-A 165 (30 ng/mL), DMOG (1 mM), acriflavine (10 µM), Propranolol hydrochloride (100 µM), TGFβ2 (10 ng/mL), Interleukin 1β (IL1β; 1 ng/mL) and RNase A (10 mg/mL). Experiments involving hypoxic conditions were performed in a SciTive Workstation. Cells were cultured for 24 h at 1% O_2 and 5% CO_2. For EndMT (endothelial to mesenchymal transition), HUVEC were stimulated in differentiation medium containing IL-1β and TGFβ2 for 5 d. Stimulations were performed in either EGM (containing 12% FCS) or EBM (containing 6% FCS) (e.g. spheroid VEGF-A stimulations). The durations of stimulation varied between experiments and are therefore indicated in the individual figure legends. For each experiment, at least three different batches of HUVEC from passage 3 were used.

3.2.1.4 Overexpression procedure

HUVEC were transfected with plasmids with the NEON electroporation system. For this, confluent HUVEC were harvested and counted and the desired number of cell suspension (450,000 cells per sample) was calculated, and the respective volume was collected in a 2 mL tube. Cells were washed with PBS and resuspended in 110 µL E2-solution and the plasmids added. For the electroporation, the cells were aspirated into a 100 µL Neon® electroporation pipette, pulsed once with 1400 V and 30 ms and immediately plated on gelatin-coated dishes containing EBM (10% FCS). After incubating the cells for 4 h in the incubator, the medium was exchanged to EGM. Depending on the subsequent experiment, the cells were cultured for an additional 24-48 h before use.

3.2.1.5 siRNA-mediated knockdown

The day before transfection, 250,000-300,000 HUVEC were plated on gelatin-coated 3.5 cm dishes. The transfection was performed using the GeneTansII Transfection Reagent. Reagents were prepared by adding 14 µL GeneTransII to 60 µL EBM and diluting 80 nM siRNA in 70 µL GeneTransII Diluent. Both solutions were incubated separately for 10 minutes before adding 72 µL of the GeneTransII

solution to the siRNA mixture. The solution was incubated for 20 min at RT while the EGM on HUVEC was exchanged with 1 mL EBM. 120 µL siRNA mixture was added to each dish and the cells were incubated for 4 h in the incubator before exchanging the medium with 1.5 mL EGM. Depending on the following experiments, cells were incubated for 24-48 h after transfection and then harvested.

3.2.2 CRISPR/Cas9 knockout

3.2.2.1 CRISPR/Cas9 strategy and Golden Gate target guide cloning

The individual guide RNAs (gRNAs) (**Table 8**) were cloned into the lentiCRISPRv2 (LCV2) vector backbone with either a puromycin or hygromycin resistance gene (**Table 13**). For this, sense and antisense oligos were annealed to form a double-stranded DNA insert. A mixture of both 10 mM oligos was incubated at 98 °C for 5 min and cooled down to RT. The annealed oligos were inserted into the LCV2 vector using the Golden Gate PCR approach. A mixture of 150 ng LCV2, 5 µL annealed oligos, 2 µL 10x T4 ligase buffer, 1 µL *Esp*3I Fast Digest enzyme, 1 µL T4 ligase and ddH_2O were incubated using the following PCR program: 10 cycles of 37 °C for 5 min, 16 °C for 10 min and 37 °C for 15 min, followed by 80 °C for 5 min and cooling the sample. The PCR product was transformed into competent E.coli, insertion of the gRNA validated by Sanger sequencing and plasmids prepared by Maxi Prep as described in section **3.2.7.2**.

In order to achieve a successful CRISPR/Cas9 mediated KO, the CRISPR strategy is crucial. In case of the *LINC00607* KO, a dual gRNA system was used with two gRNAs positioned upstream and downstream of the identified TSS. One gRNA was cloned into the puromycin, the other in the hygromycin selection LCV2 vector. This way transduced HUVEC could be selected for both gRNA-containing viruses simultaneously. For BRG1 KO, a single gRNA was designed, targeting the 3′ splice site of exon 2. This way a nonsense transcript was generated leading to a complete KO of BRG1.

3.2.2.2 Generation of pseudotyped lentivirus

Pseudotyped lentiviruses were produced by LentiX HEK293T cells as described by Chen *et al.* (2016)[121]. For this, 80% confluent LentiX HEK293T cells were transfected using polyethyleneimine (PEI; DNA:PEI ratio 1:5) with 4.1 µg of the corresponding lentiviral overexpression plasmid together with lentiviral packaging plasmids psPAX2 (3.8 µg) and VSV-G (2.1 µg). After incubating PEI and plasmids

for 20 min at RT, the mixture was added dropwise to the cells. The first day after transfection the medium was exchanged to fresh medium. On the second and third day after transfection, viral supernatants were collected, pooled and sterile filtered. The viral titer was determined using the Lenti-X™ GoStix™ Plus kit (Takara). Virus aliquots were snap-frozen, documented according to the biosafety rules (S2) and stored at -80 °C until viral transduction of cells.

3.2.2.3 Lentiviral transduction

Transduction was performed on HUVEC, previously seeded on gelatin-coated 6 cm dishes at 70% confluency. 1 mL of virus was added to 2 mL fresh EGM, supplemented with 1 µg/µL polybrene solution and the cells were incubated over night. 24 h after adding virus to the cells, virus-containing EGM was replaced with fresh EGM. On the second day after viral transduction, selection was started by the addition of puromycin (1 µg/mL) or hygromycin (100 µg/mL). After selecting for 7 days, cells were cultured as described previously (**3.2.1.1**).

3.2.2.4 Validation of CRISPR/Cas9 knockout

Genomic DNA was isolated after selection. Cells were washed, collected and incubated with 500 µL Genomic DNA lysis buffer. After removing cell fragments (1 min, 12000 xg, 4 °C), DNA was precipitated by adding the equal volume 100% isopropanol followed by centrifugation for 10 min at 12000 xg and 4 °C. The DNA was washed with 70% EtOH for 10 min at 12000 xg and 4 °C, air-dried and dissolved in TE-Buffer. CRISPR/Cas9 target sites were amplified by PCR with PCR Mastermix, containing forward and reverse primers (10 µM) and 100–500 ng DNA followed by agarose gel electrophoresis and ethidium bromide staining. The primers used are listed in **Table 9**. Additionally, for BRG1 CRISPR/Cas9-mediated KO was confirmed by protein isolation followed by Western blotting (**3.2.6.1**& **3.2.6.2**).

3.2.3 Molecular biology assays

3.2.3.1 RNA isolation, reverse transcription and quantitative real-time PCR

Total RNA was isolated from human cells using the RNA Mini Kit (BIO&SELL) according to the manufacturer's instructions. The RNA concentration was determined using the NanoDrop 1000.

In order to generate complement DNA (cDNA), isolated RNA (1,000 ng, with H_2O up to 29.5 µL) was mixed with 4 µL Random Primer mix (50 µg/mL), 2.5 µL dNTPs

(10 mM of each dNTP) and 1 µL oligo(dT)^{23} anchored (70 mM). The primers were annealed by incubation at 65 °C for 5 min, followed by 4 °C for 5 min. After adding 10 µL 5X First Strand Buffer, 2.5 µL DTT (0.1 M) and 0.5 µL SuperScript III polymerase, the mixture was incubated for 5 min at 25 °C. Reverse transcription was done for 1 h at 50 °C followed by an inactivation step for 20 min at 70 °C. The cDNA was diluted 1:1 with ddH_2O and stored at -20 °C until further use.

For reverse transcription, quantitative PCR (RT-qPCR) 10 µL 2X iTaq Universal SYBR® Green Supermix, 8 µL ddH_2O, 0.5 µL of forward and reverse Primer (10 µM) and 1 µL cDNA were mixed. The samples were incubated using the following program (**Table 21**).

Table 21. PCR-program for RT-qPCR

Cycles	Temperature	Duration	Description
1x	95 °C	3:15 min	initial denaturation
45x	95 °C	15 sec	amplification
	55 °C	20 sec	
	72 °C	20 sec	
1x	95 °C	30 sec	melting curve
	65 °C	30 sec	
	95 °C	30 sec	

The results, retrieved from the Agilent Aria MX 1.7 software, were analyzed statistically by comparing the variance between relative RNA-levels ($\Delta\Delta C_t$-method) by one-way ANOVA and Bonferroni's multiple comparison as a post hoc test. As a reference gene, *β-Actin* was used. Primers used for RT-qPCR are listed in **Table 7**.

3.2.3.2 Splicing analysis of the endothelial *LINC00607* transcript

In order to identify the endothelial predominant *LINC00607* transcript, a PCR based splicing analysis was conducted. For this, HUVEC cDNA was used as a template for a series of PCR reactions (**Table 22**). The PCR reaction comprised of 4 µL Phusion Polymerase Buffer, 0.4 µL 10 mM dNTPs, 0.5 µL of the respective forward and reverse primer (**Table 10**), 25 ng cDNA, 13 µL ddH_2O, 0.6 µL DMSO and 0.2 µL Phusion Polymerase. The fragments were amplified by an initial denaturation at 98 °C for 30 sec, followed by 35 cycles of 98 °C for 10 sec, 61-66 °C for 30 sec and

72 °C for 20 sec. The final elongation was performed at 72 °C for 5 min and samples stored at 4 °C. The fragments were analyzed by agarose gel electrophoresis. In brief, samples were mixed 1:6 with DNA loading dye and loaded onto an 1.5% TBA-agarose gel and run at 120 V for 25 min. Using the Intas UV-Gel Imager fragment size was evaluated. Fragments of the expected size were excised and the DNA purified using the QIAquick Gel Extraction Kit (Qiagen) according to the manufacturer's instructions. The sequence of the purified DNA fragments was evaluated by Sanger sequencing by Mycrosynth Seqlab.

Table 22. List of PCR amplification reactions of *LINC00607* from HUVEC cDNA; Primer No. from Table 10 (E = exon)

No.	Description	Forward Primer No.	Reverse Primer No.	PCR-Product Size (nt)
1	E1-2	1	2	160
2	E1-3	1	4	287
3	E1-4	1	6	432
4	E1-5	1	13	679
5	E1-6	1	8	1085
6	E1-7	1	9	1206
7	E2-3	3	4	145
8	E2-4	3	6	293
9	E2-5	3	13	540
10	E2-6	3	8	945
11	E2-7	3	9	1067
12	E3-4	5	6	159
13	E3-5	5	13	406
14	E3-6	5	8	811
15	E3-7	5	9	933
16	E4-5	7	13	333
17	E4-6	7	8	738
18	E4-7	7	9	860
19	E5-6	10	8	430
20	E5-7.1	10	9	552
21	E5-7.2	10	12	647
22	E5-7.1	10	15	1491
23	E6-7	11	12	169
24	E7.1-7.1	14	15	324

25	E7.1-E7.2	14	17	1057
26	E7.1-7.3	14	19	1391
27	E7.2-7.2	16	17	464
28	E7.2-7.3	16	19	799
29	E7.3-7.3	18	19	345

3.2.4 Physiological assays

3.2.4.1 Proliferation assay

To analyze the proliferative capacity of HUVEC, 5,000 cells were seeded on 96-well plates. Nuclei were stained with Incucyte® Nuclight Rapid Red Dye (1:2,000 in EGM). The cells were imaged every three hours in an Incucyte imaging system, using “phase” and “red” image channels and 10x magnification. Cells were monitored and analyzed using the Proliferation Module of the Incucyte S3 Live Cell Analysis System.

3.2.4.2 Apoptosis assay

7,500 HUVEC were seeded on 96-well plates, 16 h after siRNA transfection. Incucyte® Annexin V Green Dye was used to stain nuclei with a 1:500 dilution in EGM. Cells were imaged every 3 h in an Incucyte imaging system, using the image channels “phase” and “green” with a 10x magnification. The Apoptosis Module of the Incucyte S3 Live Cell Analysis System was used to monitor and analyze the cells.

3.2.4.3 Scratch-wound migration assay

Migratory capacity of cells was determined using the scratch-wound assay. 30,000 HUVEC were seeded on gelatin-coated ImageLock 96-well plates. The formed monolayer was scratched with a 96-pin WoundMaker tool (Essen BioScience) the following day. Dead and scraped cells were removed by medium exchange. Following this, the cells were imaged in an Incucyte imaging system for 11 h (one image every one hour, with the “phase” image channel and 10x magnification). The Scratch Wound Cell Migration Module of the Incucyte S3 Live Cell Analysis System was used to monitor and analyze the cells.

3.2.4.4 Spheroid outgrowth assay

Spheroid outgrowth assays in HUVEC were performed as described in Korff and Augustin 1998[122]. In brief, spheroids containing 400 HUVEC were created in

hanging drops over night (EGM, 20% methocel). Spheroids were harvested and embedded in a collagen-methocel mixture (1:1, 10% FCS). Stimulation of embedded spheroids was performed with VEGF-A_{165} for 16 h. Spheroids were imaged with an Evos XL Core microscope. The cumulative sprout length and spheroid diameter were quantified by analysis with ImageJ.

3.2.5 Cellular imaging methods

3.2.5.1 Immunofluorescence

Cells were grown on gelatin-coated 8-well µ-slides, fixed in 4% paraformaldehyde for 10 min at RT, washed twice with PBS and 10 min at RT with 2% glycine. Cells were permeabilized with 0.05% TritonX-100 in PBS for 10 min at RT. After blocking with 3% BSA in PBS, the first antibody was added (1:100 in 3% BSA) and incubated over night at 4 °C. Cells were washed 3 times with 0.3% Tween20 in PBS and once with PBS before adding the secondary antibody (1:500 in 3% BSA) for 30 min at RT. This was followed by nuclear staining using DAPI (1:200 in 0.3% Tween20) for 10 min at RT and washing twice with 0.3% Tween20 and PBS. Images were taken with a laser scanning confocal microscope (LSM800) using the Zen Blue 3.0 software.

3.2.5.2 RNA fluorescence in-situ hybridisation (RNA-FISH)

Cells, grown on gelatin-coated 8-well µ-slides were fixed in 4% paraformaldehyde for 10 min at RT and washed 3 times with PBS. Cells were permeabilized using 0.5% TritonX-100 in PBS (40 U/µL SUPERase-In™ RNase Inhibitor, 5 mM Vanadyl Complex) for 10 min on ice. After washing 3 times in PBS and once with 2x SSC buffer, the Hybridization buffer supplemented with the RNA-FISH probe was added to the cells and incubated for 37 °C over night. Cells were washed four times with 2x SSC buffer containing 50% formamide for 20 min each at 37 °C. Nuclei were stained with DAPI, diluted 1:200 in PBS, for 10 min at RT. Images were taken with a laser scanning confocal microscope (LSM800) and fluorescent intensities were quantified with ImageJ.

3.2.5.3 RNAscope

RNA in situ hybridization was performed on tissue sections using RNAscope 2.5 HD Detection Reagents and the HybEZ system (ACD). The single-plex chromogenic brown assay was used according to manufacturer's instructions with minor changes. Paraffin-embedded, formalin-fixed sections were deparaffinized prior to staining.

Optimal cutting temperature compound (OCT-compound) was removed from unfixed, cryopreserved tissue-sections in PBS for 5 min, baked for 30 min at 60 °C and post-fixed in 4% PFA. Sections were treated with hydrogen peroxide before incubation in boiling target retrieval buffer for 20 min using a Braun steamer and dried. Sections were incubated with protease plus reagent for 30 min in a HybEZ oven at 40 °C in a humidified atmosphere. After washing twice in 1x wash buffer, RNAscope probes were added and the sections incubated in the HybEZ oven for 2 h. The probe signal was amplified in a series of amplification and washing steps. Amplification steps 1 to 4 were performed in the HybEZ oven at 40 °C and steps 5 and 6 at RT. The first and third step were incubated for 30 min, whereas the second, fourth and sixth step were 15 min. Amplification step five was incubated 45 min. After the last amplification step, signals were detected by incubating DAB for 20 min at RT. The sections were dehydrated and mounted using EcoMount. Images were acquired using a light microscope.

3.2.6 Protein biochemical methods

3.2.6.1 Protein isolation and Bradford assay

Cells were harvested using RIPA lysis buffer. After washing with Hanks' buffer, 100 µL RIPA lysis buffer was added per 10 cm dish of HUVEC. The cells were scratched on ice, collected in a tube and centrifuged for 10 min at 4 °C with 17,000 g). The supernatant was collected and the protein concentration measured using a Bradford assay. For the Bradford assay, the Roti®Quant Kit was used. The samples were diluted 1:100 in ddH_2O and 80 µL of sample or BSA standard (0 µg/µL, 2.5 µg/µL, 5 µg/µL, 10 µg/µL, 20 µg/µL, 30 µg/µL, 40 µg/µL, 50 µg/µL) was added onto a 96-well plate in duplicates. After the addition of 200 µL Roti-Bradford reagent, the absorbance at 595 nm was measured and the protein amount calculated.

3.2.6.2 SDS-PAGE and Western blotting

30 µg of the isolated proteins were analysed using SDS-PAGE followed by Western Blot. For this, the samples were mixed with Laemmli buffer [1:3] and incubated at 95 °C for 5 min followed by centrifugation for 5 min with 17,000 xg at RT. The samples were loaded onto an 8% PAA Gel, embedded in a BioRad chamber and the proteins were separated at 120 V. Proteins were wet-blotted onto a Nitrocellulose membrane with 1x Blotting-buffer at 0.25 A/blot for 90 min. The

membrane was blocked for 45 min at RT with 1x Roti Blocking Solution. After adding the first antibody in 15 mL blocking solution, the blot was incubated over night at 4 °C while gently shaking. Prior to incubating the second antibody, the membrane was washed 3 times with wash buffer containing 0.3% Tween and once with wash buffer without Tween for 15 min, respectively. The second antibody (diluted 1:15,000 in 1:3 blocking reagent and wash buffer without Tween), directed against the first antibody, was incubated for 1 h and the membrane was washed afterwards 3 times with wash buffer containing 0.3% Tween and once with wash buffer without Tween for 15 min, respectively. The membrane was scanned with the LICOR Odyssey western blot scanner. The band-density was quantified using Image Studio 5.2.

3.2.6.3 RNA-Immunoprecipitation (RIP)

To identify RNAs bound to a protein of interest, specific antibodies and Pierce™ Protein G Magnetic Beads were used to immunoprecipitate RNAs together with the target protein. Cells were grown to 80% confluence on a 10 cm plate (ca. 3 million cells) and washed once with Hanks' buffer. 6 mL Hanks' buffer was added to the cells on ice and irradiated with 0.150 J/cm^2 254 nm UV light (BIO-LINK, BLX-254). Cells were scraped twice in 500 µL Hanks' buffer and centrifuged at 1,000 xg at 4 °C for 4 min. For nuclear protein isolation, cells were resuspended in buffer A and incubated on ice for 15 min. Nonidet was added to a final concentration of 0.75 % and cells were centrifuged (1 min, 4 °C, 16,000 xg). The nuclear-pellet was washed twice in RIP Buffer A, lysed in buffer C and centrifuged (5 min, 4 °C, 16,000 xg). 10 % of the nuclear lysate was taken as input. 4 µg of antibody was pre-coupled to 30 µL protein G magnetic beads in bead wash buffer for 1 h at RT, then washed once with RIP Buffer C and twice with bead wash buffer. The antibody-coupled beads were added to the nuclear lysate and rotated for 1 h at 4 °C. Samples were placed on a magnetic bar and the lysate discarded. The beads were washed three times in high salt buffer at 4 °C for 10 min per wash. Beads were then washed twice in RIP Bead Wash Buffer 2. For RNase A treatment, beads were placed in RIP RNaseA digestion buffer for 30 min at 37 °C and then washed again in bead wash buffer. For elution of RNA, the remaining wash buffer was removed and 1 mL QIAzol was added to the beads and incubated at RT for 10 min. 400 µL chloroform was added to the samples and vortexed for 10 sec followed by incubation for a further 10 min at RT. Samples were then centrifuged at 12,000 xg for 15 min at 4 °C. 500 µL

of the upper aqueous phase was transferred to a new tube and 2 µL glycogen (20 mg/ml) and 500 µL isopropanol added. Samples were inverted multiple times and incubated at RT for 10 min before being centrifuged at 12,000 xg for 10 min. The supernatant was removed and the pellet washed with 1 mL 75 % ethanol by vortexing. The pellet was centrifuged at 7,500 xg for 5 min at 4 °C, dried and resuspended in 30 µL nuclease-free water. RNA samples were reverse transcribed for qPCR as described above.

3.2.6.4 Cleavage Under Targets & Release Using Nuclease (CUT&RUN)

CUT&RUN is a method to identify DNA binding sites of the protein of interest as reported by Skene and Henikoff in 2017[123]. CUT&RUN for BRG1 was performed as described in Boos *et al.* (2023)[124]. The protocol essentially follows the EpiCypher CUT&RUN Protocol v2.0, with minor modifications for the cell type and antibody used. 500,000 NTC or *BRG1* KO HUVEC were washed with CUT&RUN wash buffer at RT. Cells were resuspended in CUT&RUN wash buffer and 10 µL BioMag®Plus Concanavalin A (ConA) beads were added for 10 min at RT. Beads were separated on a magnetic rack and washed once before being resuspended in 100 µL antibody buffer (CUT&RUN wash buffer, 0.25 % Digitonin and 2 mM EDTA) and 1 µL BRG1 antibody (Abcam). Beads were rotated with the antibody over night at 4 °C. The next day, beads were washed twice with 200 µL 0.25 % Digitonin wash buffer and resuspended in Digitonin wash buffer containing 2 µL CUTANA™ pAG-MNase and incubated on ice for 30 min. After two washing steps, the beads were resuspended in 100 µL Digitonin wash buffer containing $CaCl_2$ (final concentration 100 mM) and incubated for 2 h at 4 °C with gentle shaking. 33 µL of 2x “stop solution” was added to the beads and incubated at 37 °C for 10 min. Samples were placed on a magnetic rack and the supernatant removed and kept for DNA purification. Briefly, 5x volume of binding buffer was added to the samples and the pH adjusted with sodium acetate before being transferred to a purification column and centrifuged at 11,000 xg for 30 sec. The column was then washed with 750 µL CUT&RUN wash buffer and dried by centrifugation for 2 min. DNA was eluted with 25 µL elution buffer and the DNA concentration measured with a Qubit 3.0 Fluorometer.

3.2.7 Plasmid generation

3.2.7.1 Transformation of competent *E.coli* cells by heat shock

Competent cells of the *E.coli* strands DH5α or XL10-gold, were thawed on ice for 5 min, before adding 10 ng of plasmid DNA and incubating the mixture on ice for 30 min. Subsequently, a heat shock was performed at 42 °C for 45 s followed by a second incubation on ice for 5 min. Then, 500 µL of 2YT bacterial growth media, without antibiotics, was added and the cells were incubated at 37 °C for 45 min on a shaker (650 rpm). Samples were centrifuged for 5 min with 6,000 xg at RT, the supernatant (approx. 450 µL) was removed, and the samples were resuspended in 50 µL 2YT and plated out on pre-warmed 2YT-agar plates supplemented with the appropriate antibiotics for selection and incubated over night at 37 °C.

3.2.7.2 Preparation of plasmid DNA

A single bacterial colony was inoculated into 2YT-medium (5 mL for MiniPrep/ 200 mL for MaxiPrep) supplemented with the corresponding antibiotic. The bacterial culture was incubated at 37 °C overnight on a shaker at 220 rpm and harvested the next morning by centrifugation (2,400 xg for 10 min, 4 °C). Purification of plasmid DNA from pelleted cells was either performed using the GeneJET Plasmid Miniprep Kit (Thermo Fisher Scientific) or the peqGOLD XChange Plasmid Maxi EF Kit (Peqlab) according to the manufacturer's instructions. The DNA concentration was determined by measuring the absorption at 260 nm using a NanoDrop 100 spectrophotometer. The DNA sequence was validated by Sanger sequencing at Microsynth Seqlab (Göttingen, Germany).

3.2.8 In vivo experiments

3.2.8.1 Mouse breeding and housing

The animal experiment in mice was approved by the University´s Animal Care Committee and the Federal Authorities for Animal Research (Regierungspräsidium Darmstadt; approval number: FU_K6571). Groups of up to five mice were housed in a pathogen-free facility with a 12 h day/ 12 h night cycle. They had free access to water and chow. Severe combined immunodeficient (SCID) mice (CB17/Icr-Prkdc^{scid}/IcrIcoCrl, Strain Code 236) were obtained from Charles River. The experiment was carried out with 8 week old mice.

3.2.8.2 In vivo Matigel Plug Assay

The Matrigel Plug Assay is an *in vivo* experiment evaluating the capacity of modified cells to integrate into a newly formed vascular network. The assay was carried out following the experimental scheme depicted in **Figure 13**. Performed in SCID mice, human cells and cell lines can be implanted as a xenograft. *LINC00607* KO and NTC-control HUVEC were used for the Matrigel Plug Assay. For each plug, 150,000 cells were stained with Vybrant Dil, diluted 1:200 in 1 mL EBM for 45 min at 37 °C and 5 min at 4 °C. Cells were washed with EGM and resuspended in 25 mL EGM containing 20 % methocel per plug. Stained cells were cultured in 25 µL hanging drops on non-adherent square cell-culture dishes (QNAP) overnight. Harvesting of spheroids and injection of matrigel containing spheroids into SCID mice (Charles River Laboratories) was performed as described previously[125]. In brief, spheroids were harvested in PBS, centrifuged (5 min, 1,000 xg, no break) and resuspended in 300 µL mixture containing equal parts EBM, methocel and Fibrinogen (1 µg/mL VEGF-A 165 and 1 µg/mL bFGF). 1,000 spheroids were harvested per plug. Next, the resuspended spheroids were mixed with 300 µL liquid matrigel and 4 µL Thrombin and immediately injected into the inner thigh of anesthetized mice. 21 d after injection, Isolectin GS-IB4 from *Griffonia simplicifolia*, Alexa Fluor® 647 Conjugate was administered intravenously to stain the endothelial glycocalyx and was allowed to circulate for 20 min. After transcardial perfusion of the animals, the plugs were dissected, cleaned and fixed in 4% PFA.

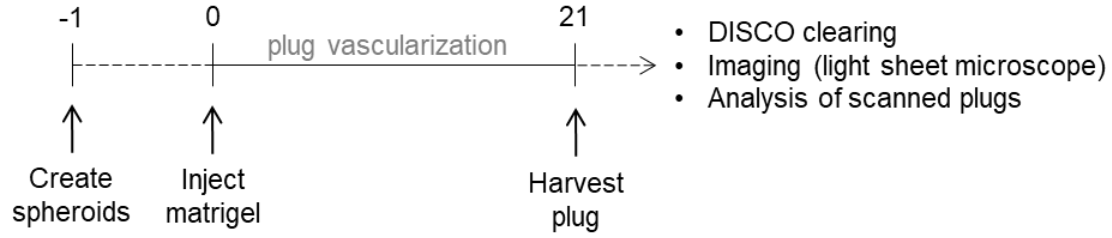

Figure 13 Workflow of the in vivo Matrigel plug assay

Samples were cleared and dehydrated with the 3DISCO clearing protocol[126]. The samples were dehydrated in a serial dilution of Tetrahydrofuran (THF). First, samples were incubated in 50% THF overnight at 4 °C, followed by 70% THF, 80% THF and 100% THF for 2 h each at RT. Next, samples were incubated in 100% THF overnight at 4 °C and 100% Dichloromethane until samples sunk to the bottom to the vial and transferred to Dibenzyl ether (DBE) overnight at RT. Until imaging, samples were kept in DBE at RT, in the dark.

3.2.8.3 Visualization of Matrigel plugs by light sheet microscopy

Imaging was carried out with the Ultramicroscope II at 16X magnification (10 Zoom body + 2 × Objective). Pictures were taken with a Neo 5.5 (3-tap) sCOMs Camera using ImSpectorPro. Quantification of 3D Images was performed with Imaris. Auto fluorescence signals and artefacts were manually removed using the surface function. Baseline subtraction was used removing signal background. Cells were detected and counted with the Spots-Algorithm (estimated diameter = 10.0 µm; background subtraction = true; “intensity center Ch = 3" above 395; Region Growing Type = Local Contrast). Lower threshold was chosen depending to the background signal. Cells were considered incorporated in the vascular network with the threshold of the “intensity Max. channel = 2” above 575.

3.2.8.4 Non-human primate tissue samples

Experiments on adult male Cynomolgus monkeys (*Macaca fascicularis*) were approved by the Institutional Care and Use Committee of the University of Iowa [127] and vessels were kindly provided by Francis J. Miller Jr (Vanderbilt University, Nashville, USA). The vessels originated from a previous study Hathaway *et al*. (2002)[127], in which *Macacae fascicularis* were fed with three different diets. They either received a normal diet, an atherosclerotic diet for 47±10 (mean ± SE) months, or an atherosclerotic diet with an additional 8-month long recovery phase. RNA was isolated from vessels and RT-qPCR was performed for the orthologues of human *GAPDH* and *LINC00607* with *Macacae fascicularis (Mf)* specific primers. Cryopreserved carotid artery tissue sections from *Macaca fascicularis* from the same study Hathaway *et al.* (2002)[127] were subjected to RNAscope to visualize *LINC00607*.

Experimental procedures with common marmosets (*Challitrix jacchus*) were in accordance with regulations of the German Legislative and vessels were kindly provided by Dr. Matthias Mietsch and Prof. Dr. Rabea Hinkel (German Primate Center, Leibnitz Institute für Primatenforschung, Göttingen, Germany). Experiments were approved by the institutional animal welfare committee as well as the Lower Saxony State Office for Consumer Protection and Food Safety (LAVES). Animals were kept at the German Primate Center, Göttingen, Germany. Abdominal aorta sections of two young (473g, 3.6 years and 395g, 2.8 years, respectively) and two old (437g, 12.0 years and 329g, 15.8 years, respectively) male common marmosets were subjected to RNAscope to visualize *LINC00607*.

3.2.8.5 Human arteriovenous malformation samples

Patients with arteriovenous malformation (AVM) evaluated at University Hospital Frankfurt entered into an ongoing prospective registry. The study protocol was approved by the ethical committee of the Goethe University (approval number UCT-63-2020, Frankfurt am Main, Germany). All patients with confirmed unruptured AVMs gave written informed consent to be included. AVM tissue samples were taken for further analysis from patients who underwent microsurgery and were kindly provided by Dr. Sepide Kashefiolasl (Department of Neurosurgery, University Hospital Frankfurt, Germany). Tissue bank cases of unruptured brain AVMs without pre-surgical embolization and without previous history of rupture were selected. AVM tissue (pieces with a diameter of 0.5 cm) was cultured immediately after surgical resection in the presence of 100 µM propranolol or solvent DMSO for 72 h. Afterwards, RNA was isolated and RT-qPCR was performed. Additionally, tissue sections of AVM were subjected to RNAscope to visualize *LINC00607*.

3.2.8.6 Human endothelial cells from plaque-free and plaque-containing arteries

Cells were isolated and cultured as previously described by Bibli *et al.* (2021)[128]. Studies were approved from the scientific and ethic committee of Hipokrateion University Hospital and the Goethe University (extension to SC55/22-2-2018). Samples were kindly provided by Prof. Dr. Sofia-Iris Bibli (Institute for Vascular Signalling, Goethe University, Frankfurt, Germany). For patient characteristics, see **Table 23**. Cultured cells were stained using RNA-FISH.

Table 23. Clinical data from human subjects from Bibli *et al.* 2021 [128]

Characteristics	Plaque free subjects	Plaque subjects
Demographic data		
No.	4	4
Mean age (range)	68 ± 5	71 ± 4
Male/female	4/0	4/0
Clinical data		
Hypertension	0	4
Hyperlipidemia	0	4
Angiographic carotid stenosis < 87%	0	4

3.2.9 Next generation sequencing

3.2.9.1 RNA-sequencing

RNA-sequencing of *LINC00607* KO and BRG1 knockdown and control HUVEC was performed by Dr. Stefan Guenther (Max-Planck-Institut für Herz- und Lungenforschung, Bad Nauheim) as described in Boos *et al.* (2023)[124].

900 ng of total RNA was used as input for SMARTer Stranded Total RNA Sample Prep Kit - HI Mammalian. Sequencing was performed on the NextSeq500 instrument (Illumina) using v2 chemistry, resulting in average of 38M reads per library with 1x75bp single end setup. The resulting raw reads were assessed for quality, adapter content and duplication rates with FastQC[129]. Trimmomatic version 0.39 was employed to trim reads after a quality drop below a mean of Q20 in a window of 10 nucleotides[130]. Only reads between 30 and 150 nucleotides were cleared for further analyses. Trimmed and filtered reads were aligned against the Ensembl human genome version hg38 (release 99) using STAR 2.7.3a with the parameter "--outFilterMismatchNoverLmax 0.1" to increase the maximum ratio of mismatches to mapped length to 10%[131]. The number of reads aligning to genes was counted with featureCounts 1.6.5 tool from the Subread package[132]. Only reads mapping at least partially inside exons were admitted and aggregated per gene. Reads overlapping multiple genes or aligning to multiple regions were excluded. Differentially expressed genes were identified using DESeq2 version 1.26.0[133]. Only genes with a minimum fold change of ± 1.5 (log2 +-0.59), a maximum Benjamini-Hochberg corrected p-value of 0.05, and a minimum combined mean of 5 reads were deemed to be significantly differentially expressed. The Ensemble annotation was enriched with UniProt data (release 06.06.2014) based on Ensembl gene identifiers (Activities at the Universal Protein Resource (UniProt)[134]).

3.2.9.2 ATAC-sequencing

ATAC-sequencing of *LINC00607* KO and control HUVEC was performed by Dr. Stefan Guenther (Max-Planck-Institut für Herz- und Lungenforschung, Bad Nauheim) as described previously[124].

50,000 HUVEC were used for ATAC library preparation using lllumina Tagment DNA Enzyme and Buffer Kit (Illumina). The cell pellet was resuspended in 50 µL of the lysis/transposition reaction mix (25 µL TD-Buffer, 2.5 µL Nextera Tn5 Transposase, 0.5 µL 10 % NP-40 and 32 µL H2O) and incubated at 37 °C for 30

min followed by immediate purification of DNA fragments with the MinElute PCR Purification Kit (Qiagen). Amplification of Library and Indexing was performed as described elsewhere[135]. Libraries were mixed in equimolar ratios and sequenced on NextSeq500 platform using V2 chemistry. Trimmomatic version 0.39 was employed to trim raw reads after a quality drop below a mean of Q20 in a window of 5 nt[130]. Only reads above 15 nt were cleared for further analyses. These were mapped against the hg38 version (emsambl release 101) of the human genome with STAR 2.7.7a[131] using only unique alignments to exclude reads with uncertain arrangement. Reads were further deduplicated with Picard 2.21.7[136] to avoid PCR artefacts leading to multiple copies of the same original fragment. The Macs2 peak caller version 2.1.1 was employed to accommodate for the range of peak widths typically expected for ATAC-Seq[137]. The minimum q-value was set to -4 and FDR was fixed at 0.0001. Peaks overlapping ENCODE blacklisted regions (known misassemblies, satellite repeats) were excluded. In order to be able to compare peaks in different samples, the resulting lists of significant peaks were overlapped and unified to represent identical regions. The counts per unified peak per sample were computed with BigWigAverageOverBed[138]. Raw counts for unified peaks were submitted to DESeq2 (version 1.20.0) for normalization [133]. Peaks were annotated with the promoter of the nearest gene in range (TSS +- 5000 nt) based on reference data of GENCODE vM15. Peaks were deemed to have significantly different counts between conditions at an average score of 20, and a log2 transformed fold change of <-0.59 or >0.59.

3.2.9.3 Differential ATAC-sequencing analysis and intersection with gene-linked regulatory elements

The integration of ATAC-Seq reads with RNA-Seq data from *LINC00607* KO and control HUVEC was performed as described in Boos *et al*. (2023)[124]. Alignment files arising from ATAC-sequencing data analysis detailed above were subjected to replicate-based differential peak calling using THOR (v0.13.1)[139], which employs a hidden Markov model-based approach to identify differentially accessible regions of chromatin between conditions. Differential peaks were those with reported adjusted p-values less than 0.01. Differential peaks were subsequently intersected with regulatory elements from EpiRegio (v1.0.0)[140], a collection of regulatory elements and their associated genes. Genes whose expression was dependent on differentially accessible regulatory elements were subjected to pathway enrichment

analysis using the ReactomePA (v1.36.0)[141] package for R. Subsequently, differential accessibility of regulatory elements linked to genes differentially expressed in RNA-Seq could be quantified for different gene sets, and displayed graphically with ggplot2 (v3.3.5)[142]. Motif enrichment analysis of differential ATAC-sequencing peaks was performed using HOMER (v4.11.1)[143] by providing sequences underlying the peaks, and otherwise the default parameters.

3.2.9.4 CUT&RUN library preparation and sequencing

CUT&RUN sequencing of BRG1 KD and control HUVEC was performed by Dr. Stefan Guenther (Max-Planck-Institut für Herz- und Lungenforschung, Bad Nauheim) as described previously[124].

DNA libraries were prepared using the NEBNext® Ultra II Kit according to the manufacturer's protocol with some minor adjustments for CUT&RUN samples. Briefly, sample volumes were adjusted to 50 µL with 0.1X TE buffer and DNA end preparation performed as instructed (20 °C for 20 min, 58 °C for 45 min). Adaptor ligation was performed with a 1:10 dilution of adaptor. For DNA purification, 0.9X Volume AMPure XP beads was added to the samples and incubated 5 min at RT. Beads were washed twice with 200 µL 80 % ethanol and DNA eluted with 17 µL 0.1X TE buffer for 2 min at RT. PCR amplification of the eluted DNA was performed as described in the manufacturer's protocol but with the addition of 2.5 µL Evagreen (20X) for visualization of the amplification curves on an AriaMx Real-time PCR system (Agilent). The denaturation and annealing/extension steps of the PCR amplification were performed for around 12 cycles and stopped before the curves plateaued. A cleanup of the PCR reaction was performed twice with 1.1X Ampure beads and eluted each time in 33 µL 0.1X TE buffer. DNA concentrations was determined with a Qubit and size distributions measured on a Bioanalyzer.

Sequencing was performed on an Illumina NextSeq1000/2000. The resulting raw reads were assessed for quality, adapter content and duplication rates with FastQC[129]. Trim Galore![144] was used to trim reads before alignment to the Ensembl human genome version hg38 (ensembl release 104) using Bowtie2[145,146]. Duplicate reads were removed with rmdup[147] and coverage tracks were generated with bamCoverage (deepTools Version 3.5.1)[148]. ComputeMatrix[148] and plotHeatmap (deepTools Version 3.5.1) were used on the coverage tracks to generate heatmaps of BRG1 binding across the genome. Peaks were called on the aligned data using

MACS2[137] and annotatePeaks (HOMER)[143] was used to identify the nearest genes to called peaks.

3.2.10 Statistics

Unless otherwise indicated, data are given as means ± standard deviation (SD). n indicates the number of individual experiments or animals. Calculations, tests for normal distribution and similarity of variance were performed with Prism 8.0. and Prism 9.0 or BiAS.10.12. The latter was also used to test for normal distribution (Shapiro-Wilk) and similarity of variance. Individual statistics of unpaired samples was performed by t-test, Mann-Whitney test or ANOVA, according to normal distribution and group number. In case of multiple testing, Bonferroni correction was applied. A p-value of ≤ 0.05 was considered as significant.

4 Results

4.1 Long non-coding RNA *LINC00607* in endothelial homeostasis and angiogenic function

4.1.1 *LINC00607* is a highly endothelial-enriched lncRNA

In order to identify highly expressed lncRNAs in HUVEC, a deep RNA-Seq (150 Mio reads) in HUVEC under basal conditions was performed (provided by PD. Dr. Matthias Leisegang, Vascular Research Center, University Clinic Frankfurt). After sorting for lncRNAs, the screen reported *LINC00607*, which was unstudied in endothelial cells at the time starting this PhD thesis, among the top-expressed lncRNAs (**Table 24**). Nearly 6,000 lncRNAs were detected, with *LINC00607* being the 7th most highly expressed lncRNA.

Table 24. Deep RNA-Seq in HUVEC

Top 15 lncRNAs expressed in a 150 million reads deep HUVEC RNA-sequencing dataset (provided by PD. Dr. Matthias Leisegang, Vascular Research Center, University Clinic Frankfurt). *LINC00607* is the 7th highest expressed lncRNA.

Rank	lncRNAs	Ensembl gene id	Reads
1	*MALAT1*	ENSG00000251562	94587
2	*NEAT1*	ENSG00000245532	23107
3	*NORAD*	ENSG00000260032	21876
4	*FGD5-AS1*	ENSG00000225733	8605
5	*TUG1*	ENSG00000253352	7641
6	*MEG3*	ENSG00000214548	4242
7	***LINC00607***	**ENSG00000235770**	**2885**
8	*KCNQ1OT1*	ENSG00000269821	2738
9	*MIR4435-2HG*	ENSG00000172965	2144
10	*EBLN3*	ENSG00000281649	2053
11	*RP11-736K20.5*	ENSG00000255471	1750
12	*C15orf54*	ENSG00000175746	1679
13	*LINC01197*	ENSG00000248441	1379
14	*HHIP-AS1*	ENSG00000248890	1486
15	*HCG18*	ENSG00000231074	1405

Next, the tissue- and cell type-specific expression of *LINC00607* was investigated, which revealed that *LINC00607* is almost exclusively expressed in endothelial cells (**Figure 14**).

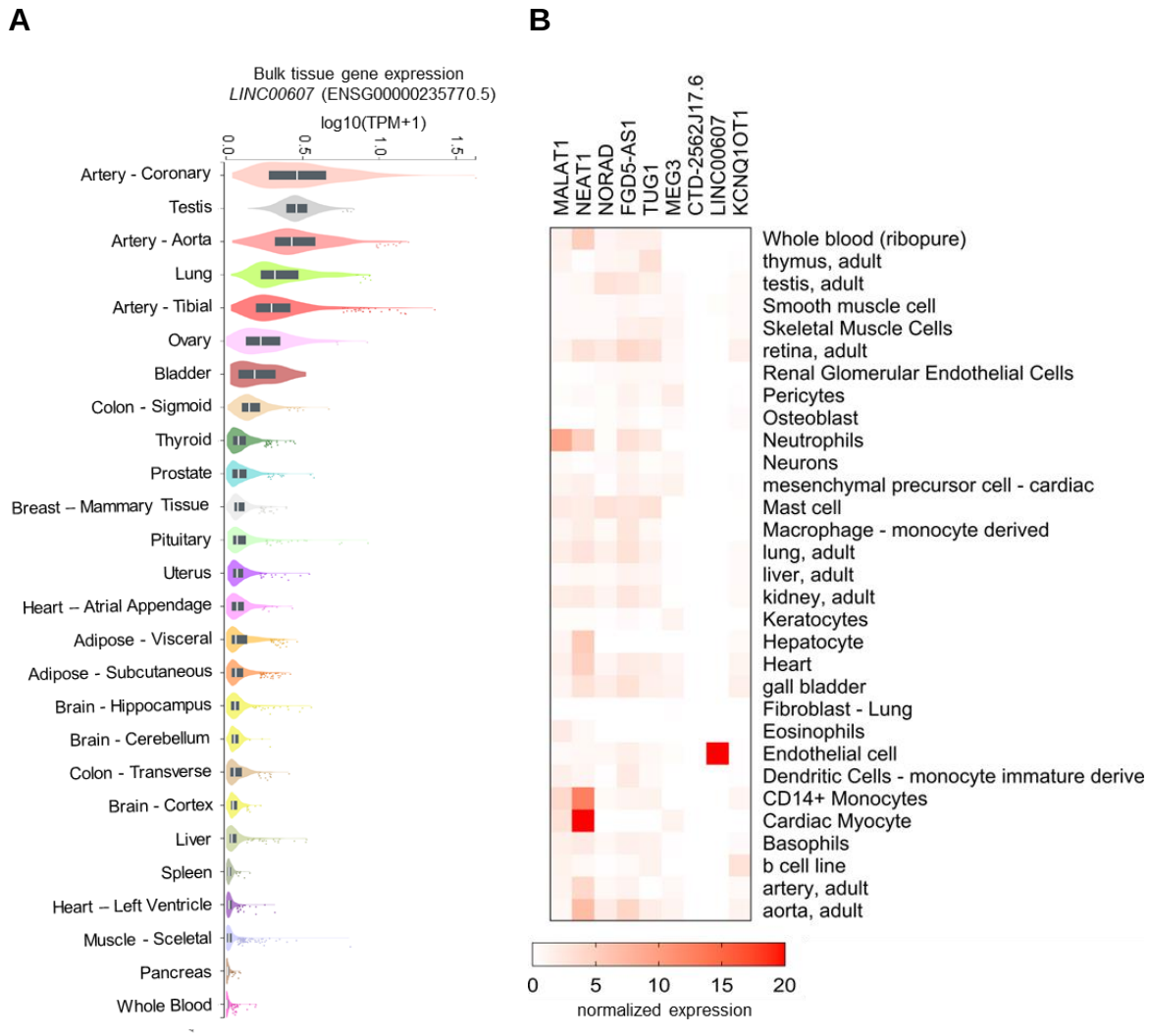

Figure 14 Tissue expression of *LINC00607*
A *LINC00607* expression (log10(TPM+1)) in human tissues from the GTEx Portal (GTEx Analysis Release V8 (dbGaP Accession phs000424.v8.p2). TPM, transcripts per million. **B** FANTOM5 CAGE expression of the 9 highest endothelial expressed lncRNAs across different tissues. Individual values are listed in Table 25. To compare the individual lncRNA expression towards all other cell types, each cell type-specific signal was divided through the mean signal observed in all cell types.

In healthy human tissues from the GTEx Portal (GTEx Analysis Release V8 (dbGaP Accession phs000424.v8.p2) *LINC00607* expression was reported in arteries and highly vascularized tissues, such as lung (**Figure 14A**). Compared to the other top-expressed endothelial lncRNAs, *LINC00607* was among the most endothelial-enriched lncRNAs in the FANTOM5 CAGE (Cap Analysis of Gene Expression) database (**Figure 14B**).

Additionally, expression of *LINC00607* between the different endothelial cell-types was compared (**Figure 15**).

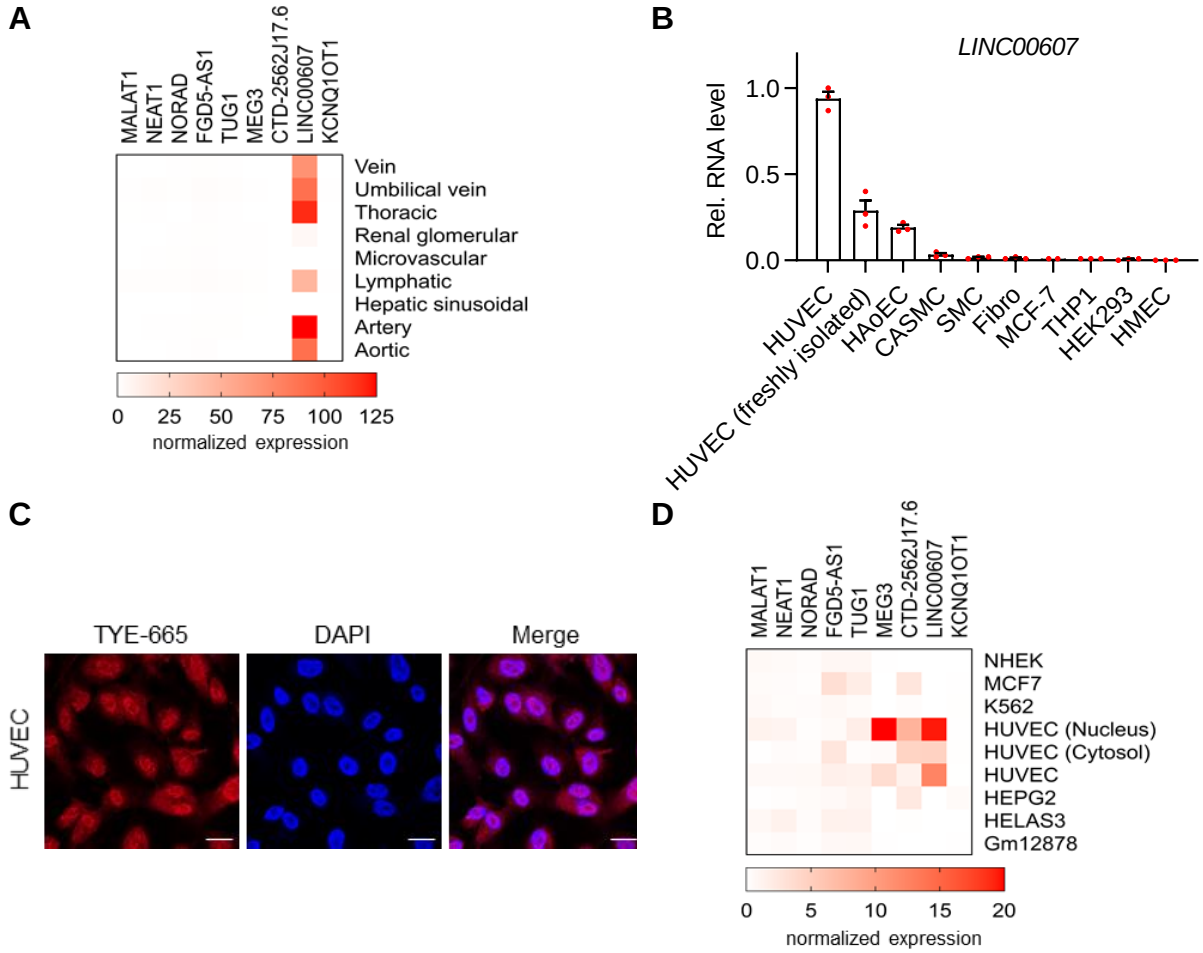

Figure 15 Cell type-specific expression of *LINC00607*
A FANTOM5 CAGE expression of the 9 highest expressed endothelial lncRNAs across different endothelial cell types. Calculation was performed similar as shown in 14B. Individual values are listed in Table 26**. B** Relative RNA-expression of *LINC00607* in different cell types, ordered by expression. n=3. **C** RNA-FISH of *LINC00607* in HUVEC. *LINC00607* is labelled with a 5'TYE-665 probe, DAPI was used to stain the DNA. Scale bar indicates 20 µm. **D** FANTOM5 CAGE expression of the 9 highest expressed endothelial lncRNAs across different endothelial cell types. Calculation was performed as shown in Fig. 14B. Individual values are listed in Table 27.

Among the different endothelial cell types, *LINC00607* was detected at high levels in aortic, venous, lymphatic, thoracic and arterial ECs in FANTOM5 CAGE-ENCODE data (**Figure 15A**). Low expression was observed in microvascular, renal glomerular and hepatic sinusoidal ECs (**Figure 15A**). *LINC00607* expression was highest in HUVEC in a RT-qPCR experiment compared to other culture cell types (**Figure 15B&D**). Within HUVEC, *LINC00607* had both, nuclear and cytosolic localization, as shown by RNA-FISH with TYE-665 labelled *LINC00607* probes and FANTOM5 CAGE-ENCODE HUVEC expression data (**Figure 15C&D**).

4.1.2 *LINC00607* transcription is induced by hypoxia and during EndMT

To identify the gene regulatory mechanisms controlling *LINC00607* expression, a promoter analysis was conducted. For this, the promoter region and transcription start site (TSS) of *LINC00607* was determined (**Figure 16**).

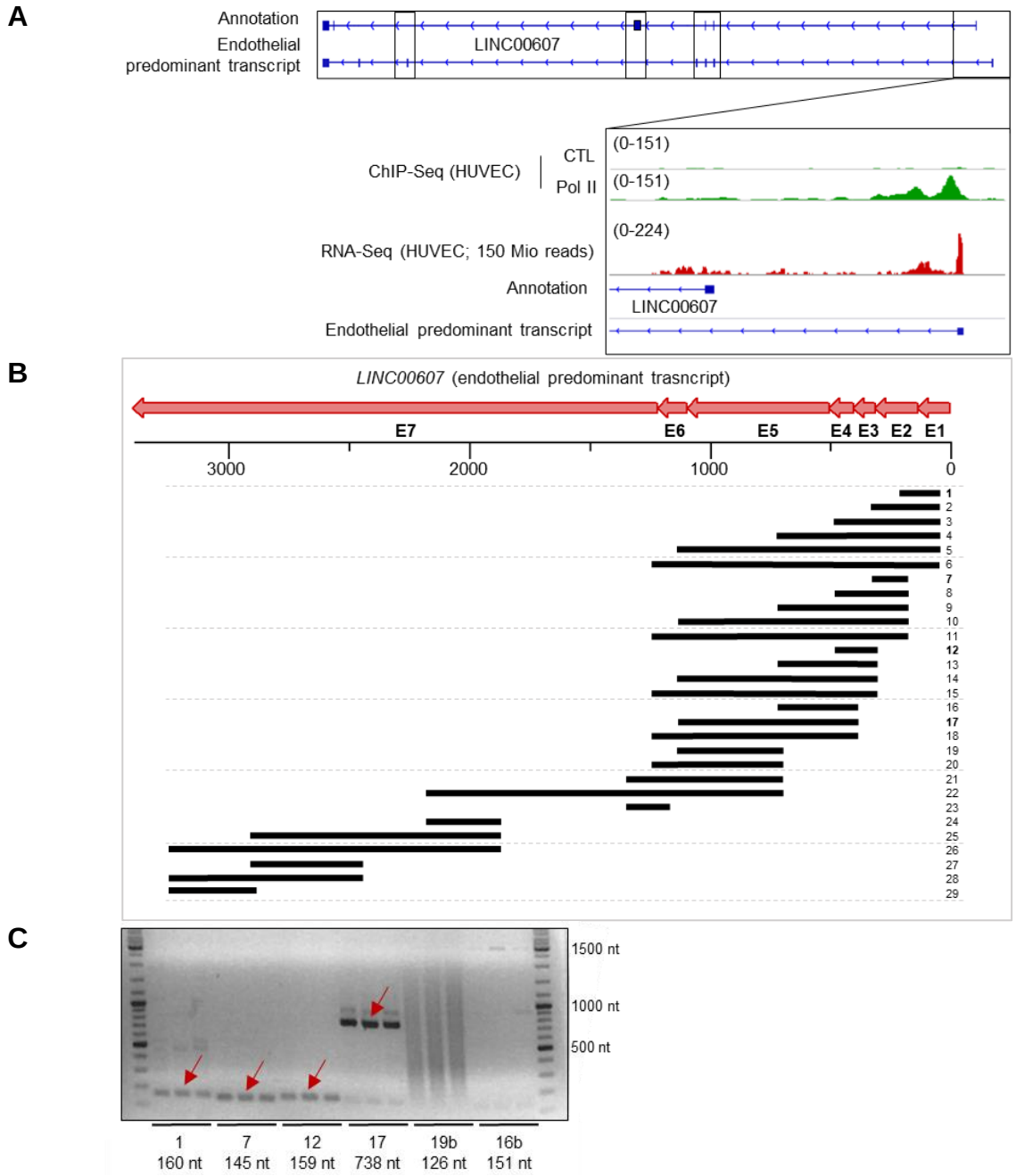

Figure 16 Endothelial transcript of *LINC00607*
A IGV tracks of annotated and experimentally evaluated endothelial transcripts of *LINC00607*. The annotated version is the GeneCode transcript ENST00000445174.5. The endothelial predominant transcript based on HUVEC RNA-Seq reads (150 Mio reads), TSS of *LINC00607* determined by RNA Pol II ChIP-Seq reads and RNA-Seq counts from HUVEC, FANTOM5 CAGE expression data and PCR-based splicing analysis. **B** Scheme of the PCR based splicing analysis. Each number and line represents an exon spanning primer pair (**Table 10, Table 22**) amplifying a certain part of the endothelial predominant transcript of *LINC00607*. **C** Exemplary fragments amplified by PCR on HUVEC cDNA, n=3. Fragments 1 (160 nt), 7 (145 nt), 12 (159 nt) and 17 (738 nt) confirmed the transcript, while fragments 19b (expected size: 126 nt) and 16b (expected size: 151 nt) proved the skipping of the annotated exon 5 (A) as a primer laid within its sequence. Fragments are indicated with a red arrow.

The promoter region is by definition the genomic region upstream of the TSS of a gene[149]. The TSS is determined by a multitude of features but the binding of RNA Polymerase II is a robust indicator for a transcription initiation site[150].

The first exon and TSS of the NCBI-officially annotated *LINC00607* transcript (**Figure 16**, ENST00000445174.5) was not found in the same location as RNA-Seq reads from HUVEC and the endothelial RNA Pol II signature, obtained by ChIP-Seq (**Figure 16A**). To fully uncover the endothelial *LINC00607* transcript, the splicing pattern of the *LINC00607* gene was investigated. For this, a series of *LINC00607* fragments was created by PCR using exon-spanning primers, including those, which correspond to the identified exon1 by RNA-Seq (**Figure 16B**, **Table 10, Table 22**). The generated fragments were initially assessed for size in an agarose gel electrophoresis, as shown by a representative gel (**Figure 16C**) and fragments of the expected size were sequenced by Sanger sequencing. In the example shown, fragments for amplification reactions 1, 7, 12 and 17 were at the expected length, whereas reactions 19b and 16b did not create fragments of the expected size as their forward primers were located in the annotated exon 5 (**Figure 16A**), which is excluded in the endothelial predominant transcript.

Combining the results of the PCR-based splicing analysis with RNA-Seq data (**Figure 16B&C**) and the TSS from FANTOM5 CAGE expression data, the predominant *LINC00607* transcript of endothelial cells was determined. This transcript (named as endothelial predominant transcript) contains an alternative TSS and a slightly different exon-intron structure compared to the annotated transcript (**Figure 16**). On the basis of the predominant *LINC00607* transcript, the promoter analysis was performed, using the MoLoTool[89] (**Figure 17**).

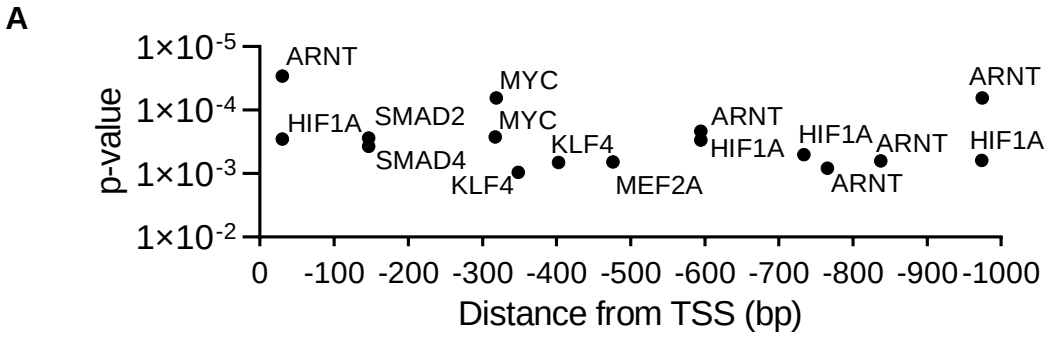

Figure 17 Promoter analysis of *LINC00607*
1000 base pairs (bp) upstream of the *LINC00607* transcriptional start site (TSS) of the endothelial predominant transcript was analyzed with MoLoTool for transcription factor binding sites. Discovered motifs plotted according to p-value.

The analysis retrieved binding motifs of the TFs ARNT (also known as Hypoxia Inducible Factor 1 Beta) and HIF1A (Hypoxia Inducible Factor 1 Alpha), which were identified multiple times within 1 kb upstream of the TSS (**Figure 17**). This may

suggest transcriptional regulation of *LINC00607* by hypoxia. To determine whether *LINC00607* is indeed induced by hypoxia, HUVEC were cultured under normoxia and hypoxia, and expression of *LINC00607* was analyzed by RT-qPCR. In parallel, publicly available RNA-Seq data of EC treated with hypoxia and after stimulation with the DNA topoisomerase and hypoxia-inducible factor(HIF)-repressor acriflavine (ACF)[117] was analyzed (**Figure 18**).

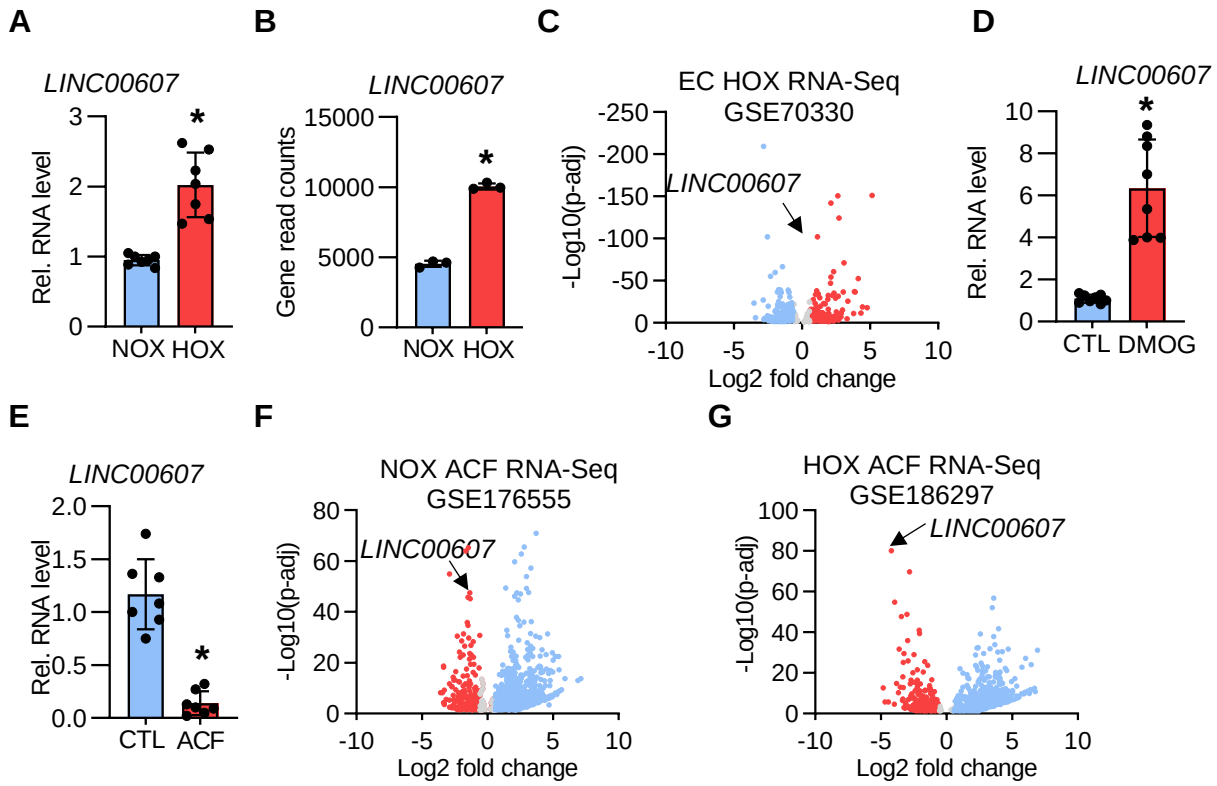

Figure 18 Hypoxia induces *LINC00607* expression
A Relative *LINC00607* expression in HUVEC treated with normoxia (NOX) or hypoxia (HOX), n=7. Mann-Whitney U test. **B** *LINC00607* gene read counts in HUVEC cultured under normoxic and hypoxic conditions, n=3. Unpaired t-test. **C** Volcano plot of log2 fold changes of lncRNAs expressed in hypoxia versus normoxia. **D** Relative expression of *LINC00607* in HUVEC after stimulation with DMOG. DMSO served as control (CTL), n=8, Mann-Whitney U Test. **E** Relative expression of *LINC00607* in HUVEC after stimulation with acriflavine (ACF), n=7, Mann-Whitney U Test. **F-G** Volcano plot of log2 fold changes of lncRNAs in HUVEC treated with acriflavine (ACF) cultured under normoxia (**F**) or hypoxia (**G**). Error bars are defined as mean +/- SD. *p<0.05. p-adj, p-adjusted value.

LINC00607 was highly and significantly upregulated under hypoxia (1% O_2, 24 h), as observed in RT-qPCR experiments, as well as in publicly available RNA-Seq data[116] (**Figure 18A&B**). Induction of *LINC00607* expression furthermore occurred in response to the HIF-stabilizing compound DMOG (1 mM, 16 h). ACF (10 µM, 16 h), which is through to block HIF-induced gene expression (RNA-Seq datasets from Seredinski *et al.*[117]) lead to significantly reduced expression of *LINC00607* (**Figure 18E-G**). The data suggest that the expression of *LINC00607* is controlled by hypoxia.

The promoter analysis yielded also Suppressor of Mothers against Decapentaplegic (SMAD) binding motifs in addition to the HIF binding sites (**Figure 17**). SMADs are involved in the induction of endothelial to mesenchymal transition (EndMT) in HUVEC[151]. Therefore, the relevance of the SMAD binding motifs for *LINC00607* expression control was evaluated in a publicly available dataset[118] of cells with induced EndMT. Indeed, *LINC00607* was upregulated in response to EndMT induction in HUVEC (**Figure 19A**) and pulmonary arterial endothelial cells (PAEC; **Figure 19B**)[118].

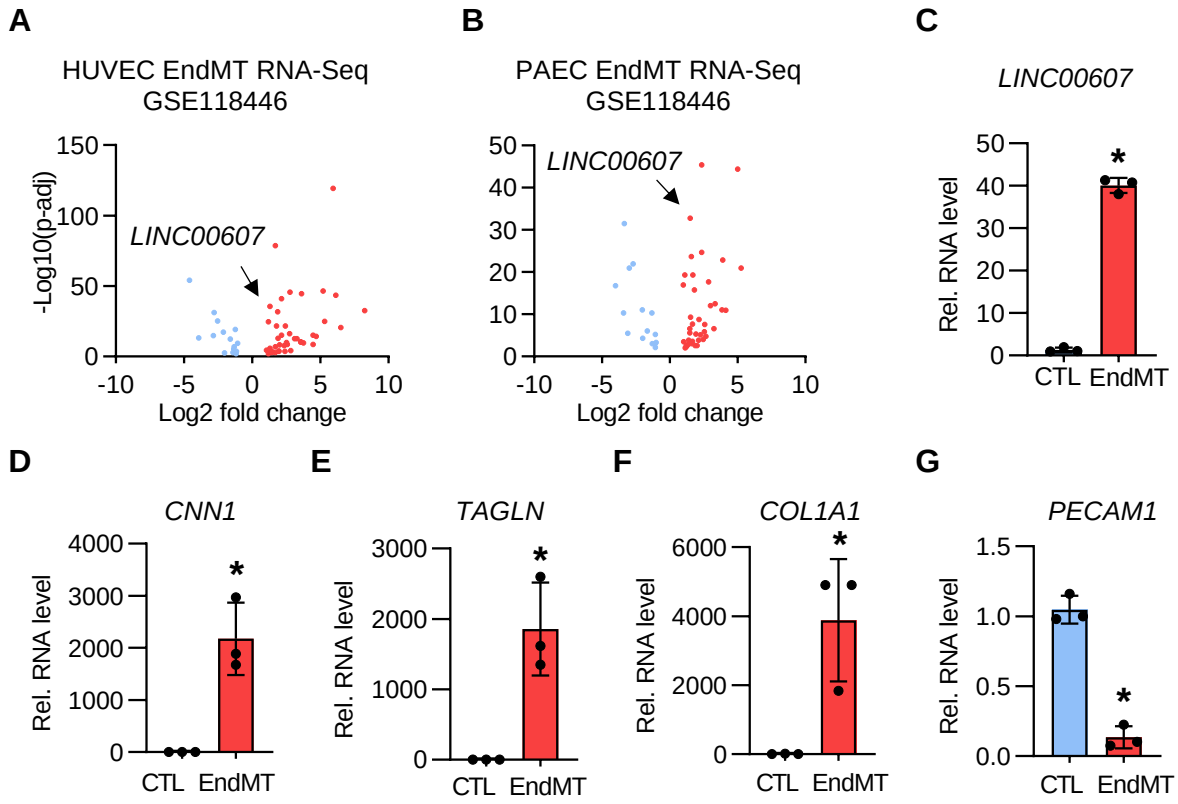

Figure 19 EndMT induces *LINC00607* expression
A-B Volcano plot of log2 fold changes of lncRNAs after EndMT versus unstimulated control in HUVEC (A) or pulmonary arterial endothelial cells (PAEC) (B). Error bars are defined as mean +/- SD. *p<0.05. p-adj, p-adjusted value. **C** Relative expression of *LINC00607* in HUVEC under basal (CTL) or EndMT conditions. Normalized to ubiquitin C (*UBC*). n=3, Unpaired t-test. **C-F** EndMT validation. Relative expression of EndMT control genes Calponin 1 (*CNN1*), Transgelin (*TAGLN*) and Collagen, type I, alpha 1 (*COL1A1*) in HUVEC under basal (CTL) or EndMT conditions. n=3, Unpaired t-test. **G** Relative expression of endothelial control gene Platelet endothelial cell adhesion molecule-1 (*PECAM1*) in HUVEC under basal (CTL) or EndMT conditions. n=3, Unpaired t-test.

Additionally, induction of EndMT through TGFβ2 (10 ng/mL) and IL-1β (1 ng/mL) stimulation of HUVEC for 5 days, strongly induced *LINC00607* expression (**Figure 19C**). EndMT induction was validated with increased expression of mesenchymal markers *Calponin 1* (*CNN1,* **Figure 19D**), *Transgelin* (*TAGLN,* **Figure 19E**) and *Collagen, type I, alpha 1* (*COL1A1,* **Figure 19F**) and decreased expression of the endothelial marker *Platelet endothelial cell adhesion molecule-1* (*PECAM1,* **Figure**

19**G**). These data suggest that *LINC00607* is tightly controlled by TFs involved in hypoxia sensing and TGFβ signalling.

4.1.3 *LINC00607* is required for endothelial angiogenic function

In order to determine the physiological relevance of *LINC00607* in endothelial cells, proliferation, apoptosis and spheroid outgrowth assays were performed after siRNA-mediated depletion (**Figure 20**) or CRISPR/Cas9-mediated KO of *LINC00607* (**Figure 21**).

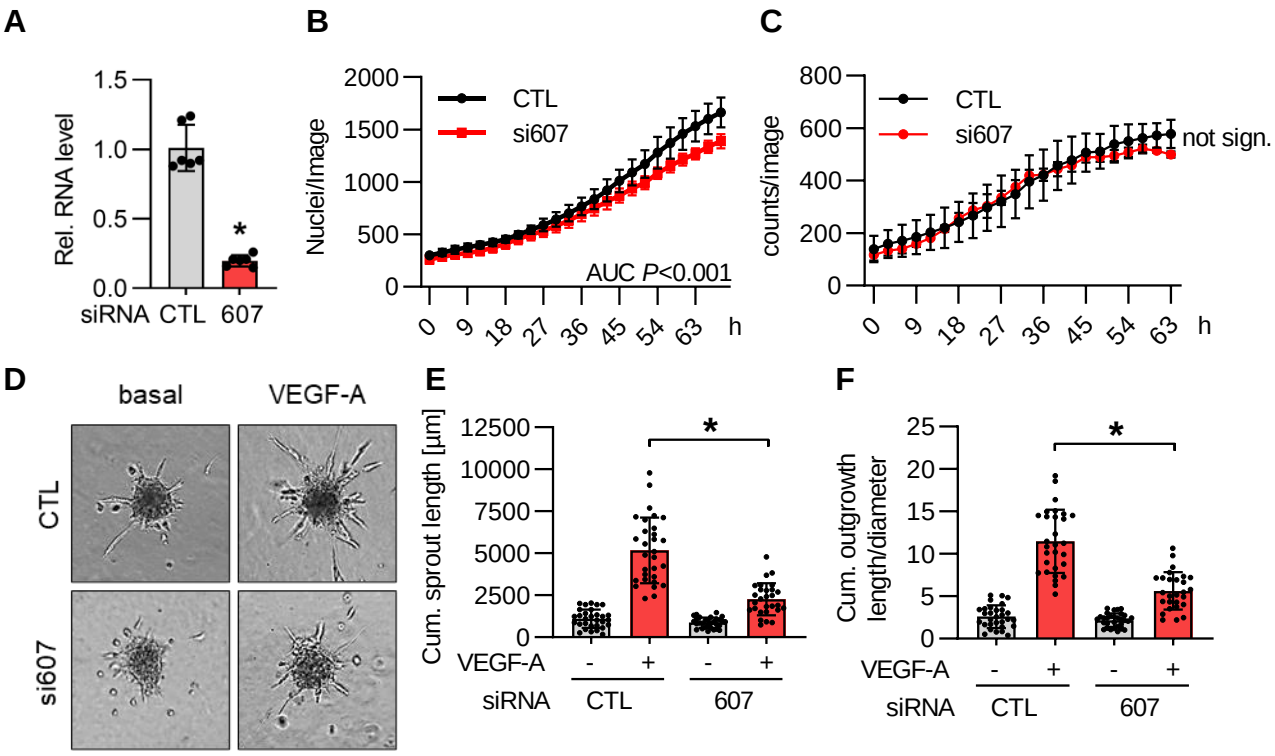

Figure 20 Knockdown of *LINC00607* reduces endothelial cell proliferation and sprouting
A RT-qPCR of *LINC00607* with and without siRNA-based knockdown for 48 h of *LINC00607* (607). Scrambled siRNA served as negative control (CTL). n=6. Mann-Whitney. **B** Proliferation Assay of HUVEC with and without siRNA-mediated *LINC00607* knockdown. Nuclear count per image per well. Seeding density on a 96-well plate: 5000 cells/well. Pictures taken every 3 h. siRNA knockdown 16 h prior to seeding. n=3, Area under the Curve (AUC) and unpaired t-test. **C** Apoptosis Assay of HUVEC with and without siRNA-mediated *LINC00607* knockdown. Apoptotic cell counts per image per well. Seeding density on a 96-well plate: 7500 cells/well. Pictures taken every 3 h. siRNA knockdown 16 h prior to seeding. n=3, Area under the Curve and unpaired t-test. **D** Spheroid outgrowth assay and without siRNA-based knockdown of *LINC00607* (607). Cells treated with or without VEGF-A (16 h) are shown. **E&F** Quantification of cumulative sprout length (E) and the ratio of cumulative outgrowth length and respective spheroid diameter (F) from spheroid outgrowth assay shown in D, n=28-30, two-way ANOVA.

SiRNA-mediated knockdown of *LINC00607* significantly decreased *LINC00607* expression (**Figure 20A**) and proliferative capacity, but did not affect the apoptosis rate of endothelial cells (**Figure 20B&C**). Additionally, knockdown of *LINC00607* reduced endothelial sprouting in response to VEGF-A stimulation (**Figure 20D**). *LINC00607* KD significantly reduced the cumulative sprout length and the ratio of

cumulative outgrowth length to the spheroid diameter upon VEGF-A stimulation (**Figure 20E&F**).

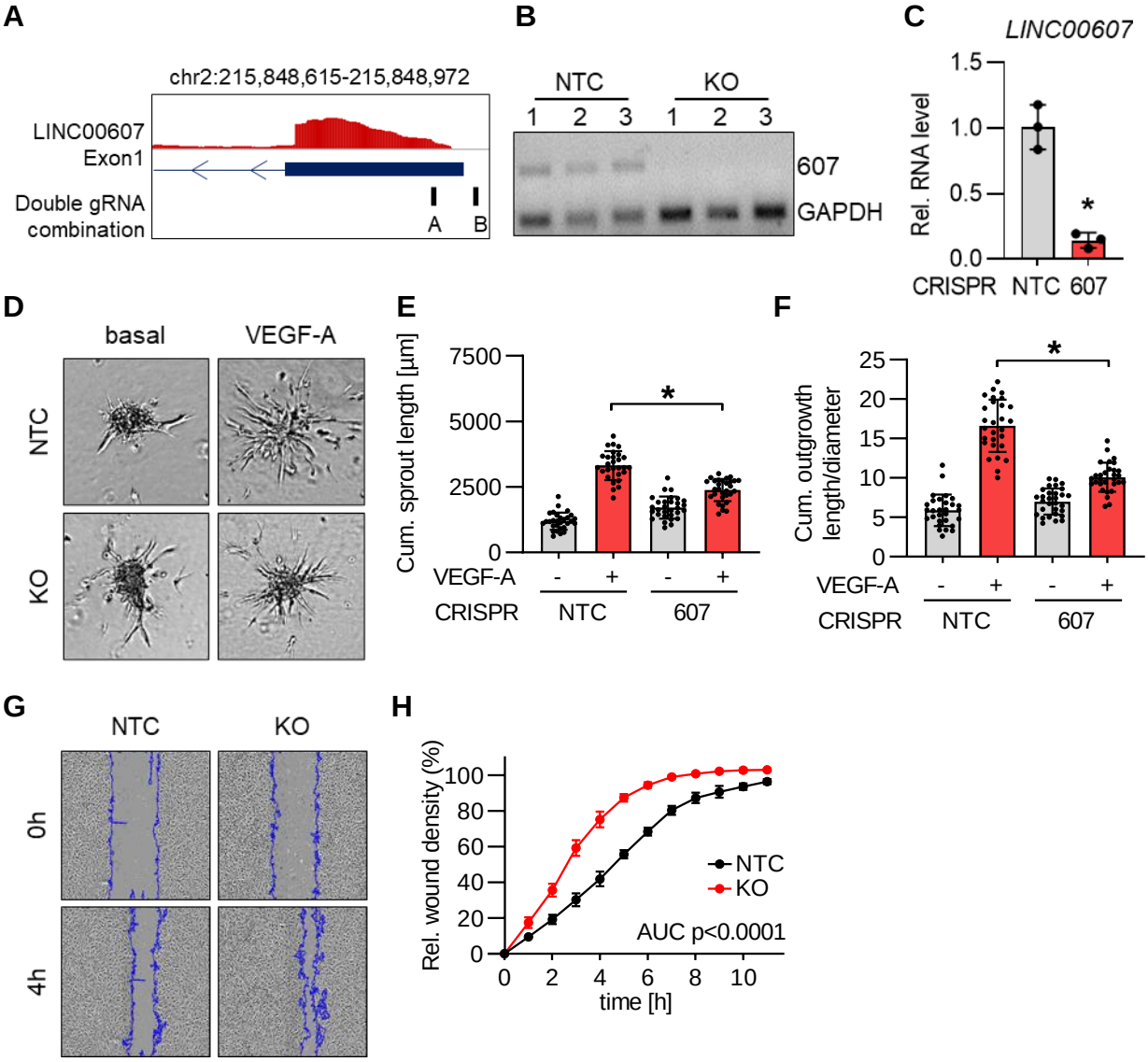

Figure 21 CRISPR/Cas9 knockout of *LINC00607* has profound effects on endothelial angiogenic functions of HUVEC
A Scheme of gRNA target region used for KO of *LINC00607*. **B** Genomic DNA-PCR of HUVEC with *LINC00607* knockout (KO) or non-targeting control (NTC). Three different HUVEC batches (1-3) are shown. GAPDH served as housekeeping gene. **C** RT-qPCR of *LINC00607* after KO and control (NTC). **D** Spheroid outgrowth assay of HUVEC with and without *LINC00607* knockout (KO) or non-targeting control (NTC). **E&F** Quantification of cumulative sprout length (E) and ratio of cumulative outgrowth length and respective spheroid diameter (F) from spheroid outgrowth assay (D), n=28-30, two-way ANOVA. **G** Scratch wound assay of *LINC00607* KO and NTC control cells. Representative images after 0 h and 4 h after scratch (blue line) are shown. **H** Quantification of relative wound closure of migration assay (G) of *LINC00607* KO and NTC control HUVEC. n=3, area under the curve (AUC) p<0.0001 (two-tailed t-test).

Next, a CRISPR/Cas9 knockout (KO) of *LINC00607* was created in HUVEC. Here, a lentiviral, dual-gRNA approach was performed by removing the experimentally determined TSS of *LINC00607* (**Figure 16**, **Figure 21A**), resulting in a significant *LINC00607* knockout on genomic (**Figure 21B**) and RNA level (**Figure 21C**).

Similar as in the knockdown experiments, *LINC00607* KO reduced in sprouting upon VEGF-A stimulation (**Figure 21D-F**). Additionally, HUVEC with *LINC00607* KO displayed enhanced migratory capacity into a scratch wound (**Figure 21G, H**). The effect on sprouting in response to VEGF-A in *LINC00607* KO cells (**Figure 20D-F**, **Figure 21D-F**) was rescued by a transient overexpression of the endothelial predominant *LINC00607* transcript from a pcDNA3.1+*LINC00607* plasmid (**Figure 22A-C**).

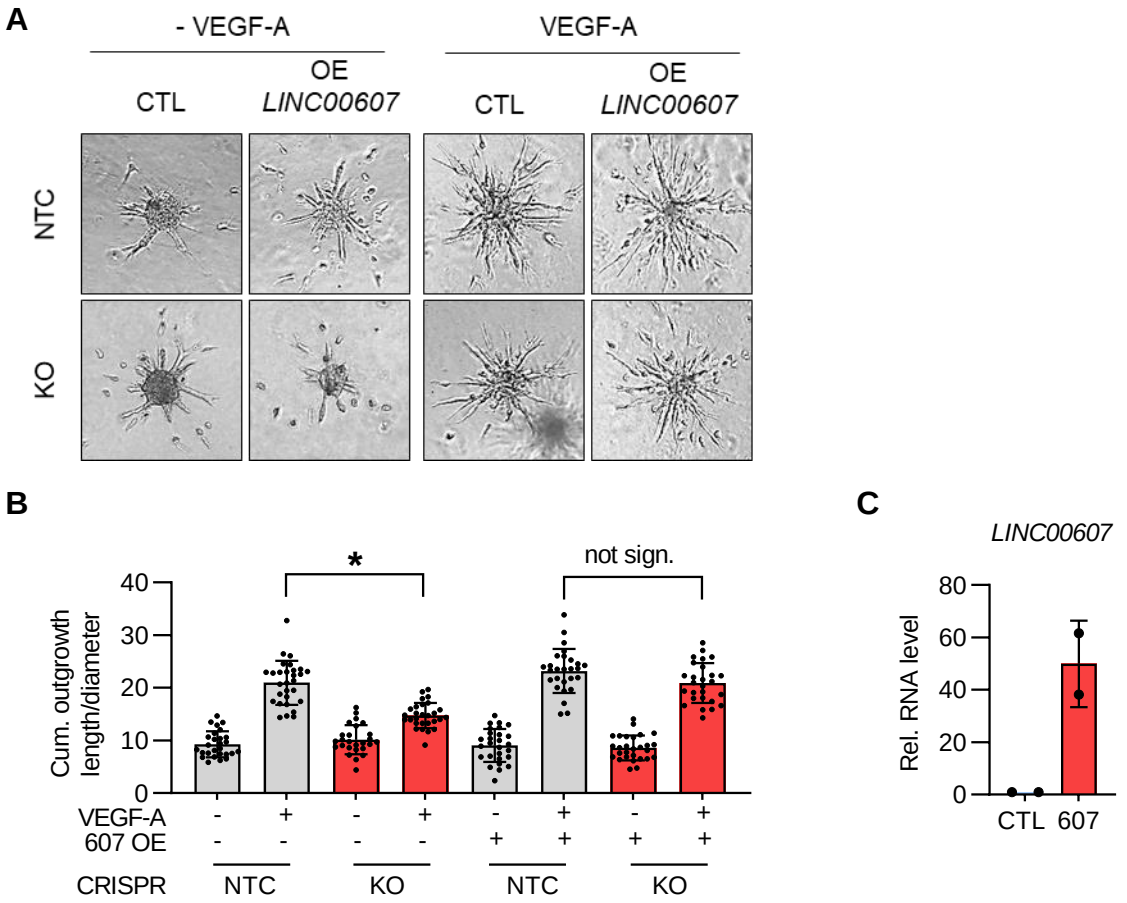

Figure 22 Sprouting deficits of *LINC00607* KO after VEGF-A are rescued by overexpression of *LINC00607*
A Spheroid outgrowth assay of HUVEC after *LINC00607* KO or non-targeting control (NTC). Cells treated with and without VEGF-A for 16 h with/ without *LINC00607* overexpression (OE) are shown. Empty vector transfection served as control (CTL). **B** Quantification of the ratio of cumulative outgrowth length and respective spheroid diameter from spheroid outgrowth assay (A). n=26-29, One-way ANOVA with Bonferroni post hoc test. **C** Relative RNA expression of *LINC00607* after overexpression 48 h in HUVEC. n=2.

This suggests that the *LINC00607* directly mediates the observed functional effects by acting in *trans* and not through *cis* action of the genomic locus of *LINC00607*. Taken together these results demonstrate *in vitro* and *in vivo* that *LINC00607* is highly important lncRNA for endothelial angiogenic function.

4.1.4 *LINC00607* is differentially expressed in vascular diseases and conserved among primates

Considering its high degree of endothelial enrichment and physiological importance, it was further investigated whether the expression of *LINC00607* might be perturbed in vascular diseases. For this, *LINC00607* expression was examined in endothelial cells and tissues derived from different vascular diseases, including atherosclerotic plaques and arteriovenous malformation (AVM) (**Figure 23**).

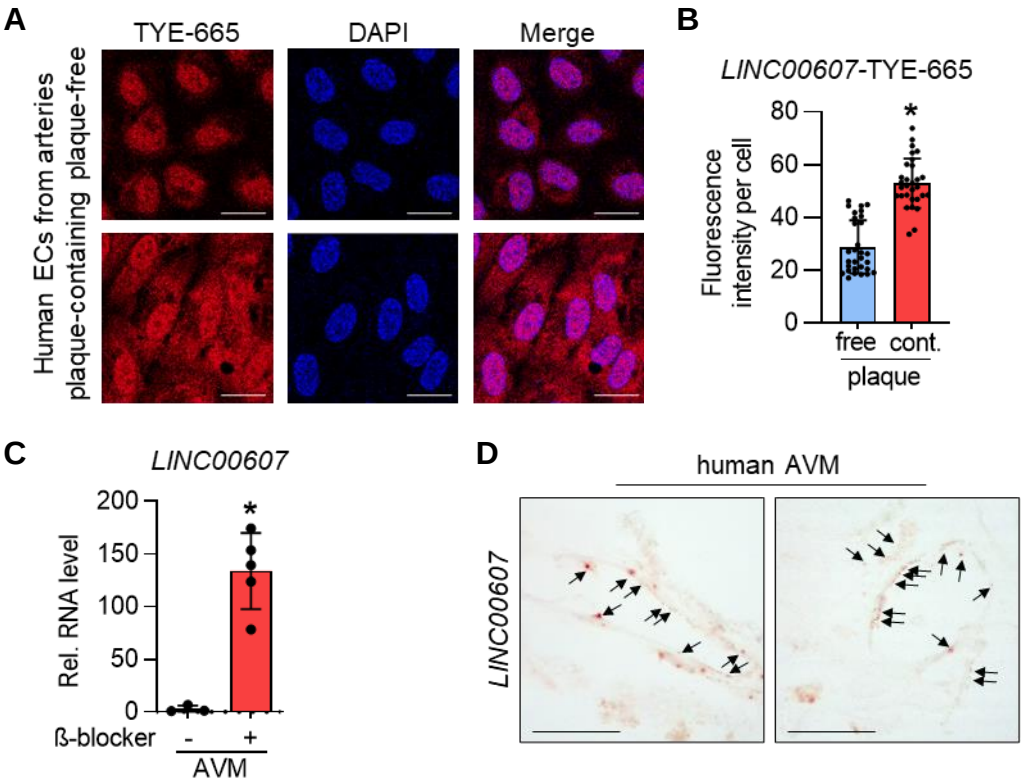

Figure 23 *LINC00607* in human vascular diseases
A RNA-FISH of *LINC00607* in cultured endothelial cells retrieved from human plaque-free and plaque-containing arteries. Scale bar indicates 20 µm. **B** Fluorescence intensity per cell for TYE-665 (*LINC00607*) of RNA-FISH images in A. (Plaque-free arteries: "free"; plaque-containing arteries: "cont."). n=26-30, unpaired t-test. **C** RT-qPCR of *LINC00607* in human arteriovenous malformation (AVM) treated with or without the β-blocker Propranolol for 72 h. n=5, Mann-Whitney U test. **D** RNA *in situ* hybridization of human arteriovenous malformation with RNAscope. Tissue originating from neurosurgical resections of AVM. Arrows point to dots indicating *LINC00607* RNA. Representative images are shown. Scale bar indicates 20 µm.

Firstly, *LINC00607* expression was increased in human endothelial cells isolated and cultured from plaque-containing arteries, regarded as post-atherosclerotic[128], when compared to endothelial cells originated from plaque-free arteries (**Figure** 23**A&B**). Secondly, AVM explants showed a significantly increased *LINC00607* expression after stimulation with the β-blocker propranolol. The explants belonged to a study, identifying whether the β-blockers impact on ECs might be beneficial to AVM disease progression and were kindly provided by Dr. Sepide Kashefiolasl (Department of Neurosurgery, University Hospital Frankfurt, Germany). The

propranolol treatment was based on results observed in hemangioma, were β-blockers lead to regression by directly acting on endothelial cells[152](**Figure 23C**). The bulk RNA RT-qPCR signal for *LINC00607* indeed derived from the endothelial fraction, as shown by a *LINC00607* RNA-scope on tissue sections of AVM after resection (**Figure 23D**).

Next, the conservation across the primate lineage was investigated to potentially observe *LINC00607* expression changes in samples from non-human primate studies (**Figure 24**).

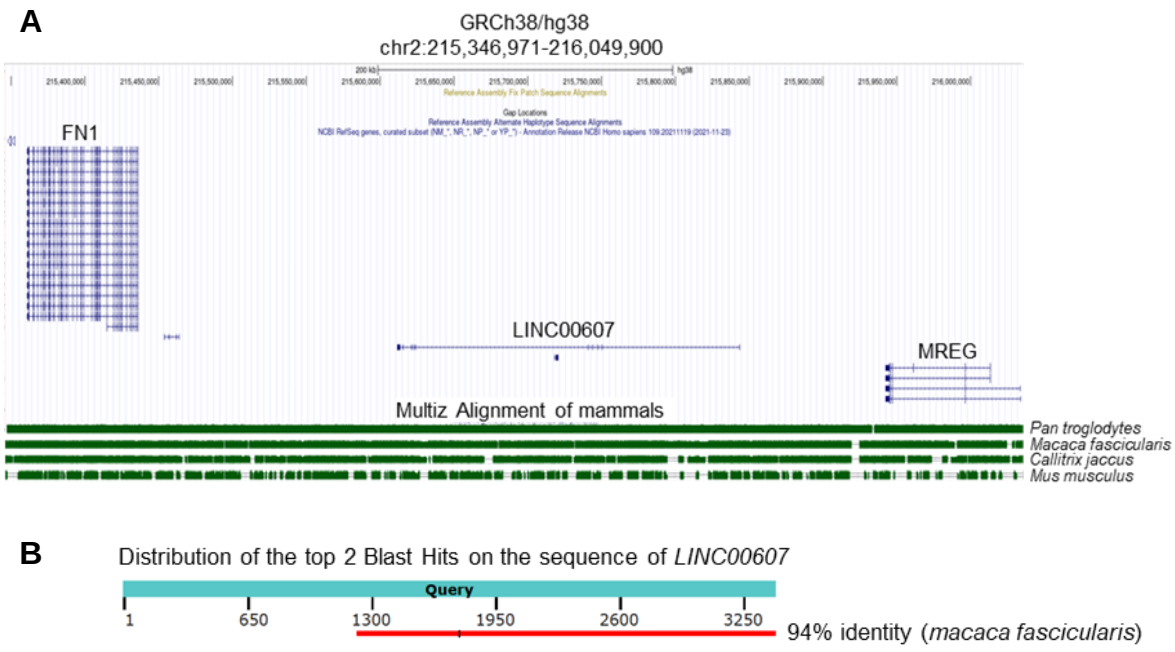

Figure 24 Conservation of the *LINC00607* locus
A UCSC genome browser of human *LINC00607* locus and neighbouring genes Fibronectin1 (FN1) and Melanoregulin (MREG). Below the RefSeq gene annotation[153] is the Multiz Alignment of mammal genomes[154] of *Pan troglodytes* (Pan_tro 3.0/panTro5), *Macaca fascicularis* (Macaca_fascicularis_5.0/macFas5), *Callitrix jaccus* (Callitrix jaccus_calJac4) and Mus musculus (GRCm38/mm10). **B** Results of a nucleotide Blast[155] of the endothelial predominant *LINC00607* RNA sequence against the nucleotide database from *Macaca fascicularis.* A large fraction of *LINC00607* was matched to a nucleotide with a 94% sequence identity.

Indeed, the locus and genes surrounding *LINC00607* was observed as highly conserved in cynomolgus monkey (*Macaca fascicularis),* common marmoset (*Callitrix jaccus*) and mouse (*Mus musculus*) (**Figure 24A**). A nucleotide-BLAST (NCBI) of the endothelial predominant *LINC00607* RNA sequence against the genome of *Macaca fascicularis* revealed matched sequences within the nucleotide database (**Figure 24B**). Primers for *LINC00607* orthologues were designed based on these results and *LINC00607* expression was evaluated.

Although the locus of *LINC00607* was partially conserved in mice, there were no hits retrieved for a murine orthologue of *LINC00607.* This result is common for many

human long-intergenic RNAs (lincRNAs)[156,157]. This limits the utility of mice to study the in vivo relevance of *LINC00607*. To overcome this, a xenograft model based on a modified Matrigel plug assay was performed[125]. To avoid rejection, experiments were conducted in severe combined immunodeficient (SICD) mice. This assay assesses the ability of implanted HUVEC to integrate into a newly formed vascular network. After three weeks, plugs were excised and imaged by light sheet microscopy. Co-localization of fluorescent signals of implanted HUVEC and newly formed vessels was interpreted as an incorporated HUVEC. After three weeks, *LINC00607*-depleted HUVEC were significantly less integrated into the vascular network as compared to the control HUVEC (**Figure 25**).

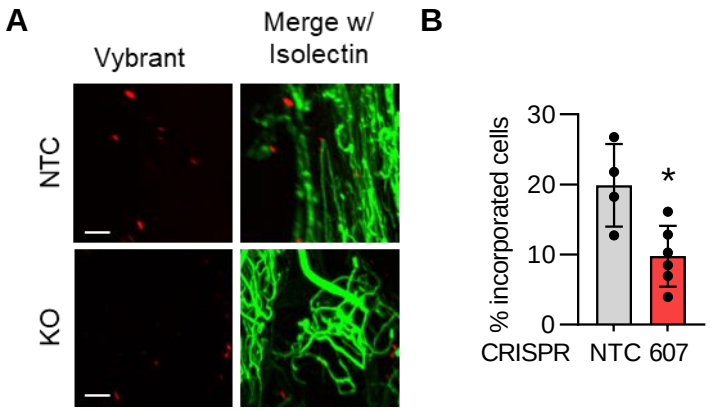

Figure 25 *LINC00607* KO HUVEC display reduced capacity to integrate into a newly formed vascular network
A *LINC00607* KO and control cells (NTC) after *in vivo* Matrigel plug assay in SCID mice. HUVEC stained with Vybrant dil (red); vessels stained with Isolectin GS-b4 Alexa 647 conjugated (green). Images were taken by light sheet microscopy 21 d after injection. Scale bar indicates 100 µm. Representative pictures are shown. **B** Quantification of cells per plug integrated into the newly formed vascular network shown in (A). n=4-6. Mann Whitney U test. *p<0.05.

As *LINC00607* is conserved and expressed in non-human primates, its expression was investigated in carotid arteries of *Macaca fascicularis* with high fat diet induced atherosclerosis from the study by Hathaway *et al.* (2002)[127] and in abdominal aorta from young and aged *Callitrix jaccus* (**Figure 26**).

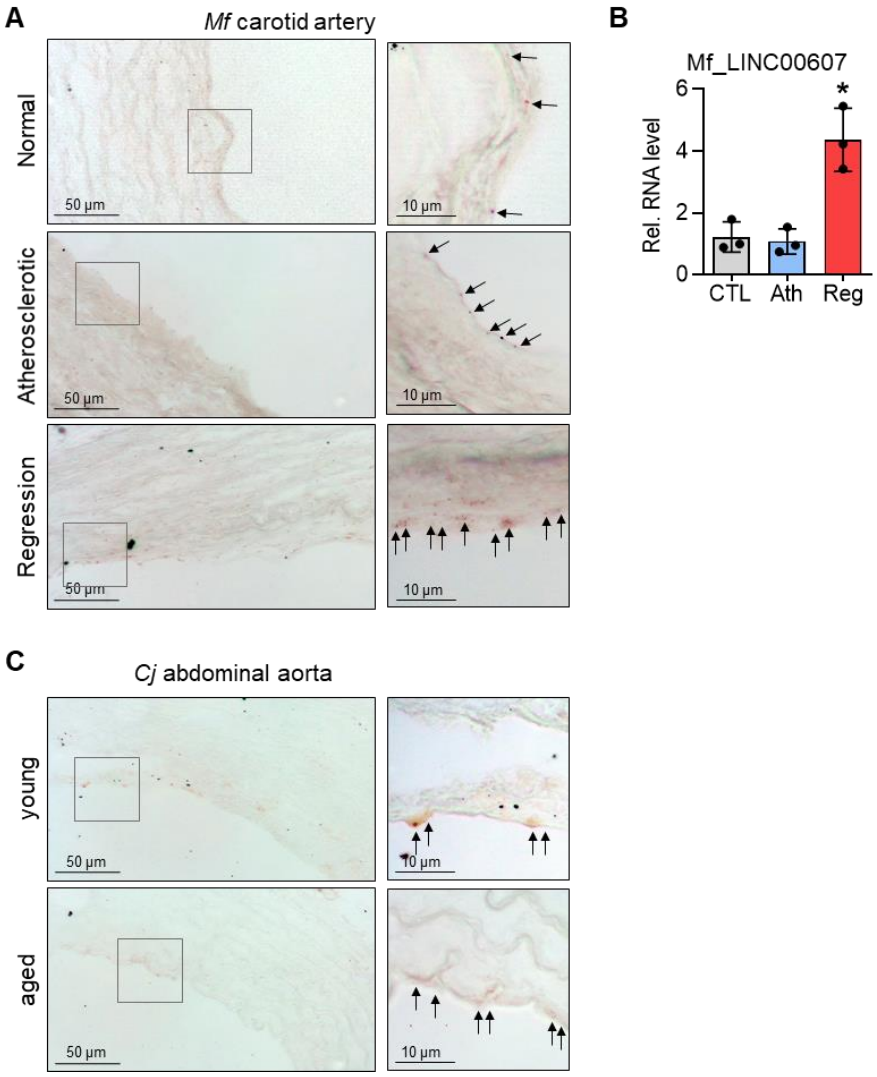

Figure 26 Endothelial localization and regulation of *LINC00607* homologue in non-human primates
A RNA in situ hybridization of carotid artery from *Macaca fascicularis* (Mf) with RNAscope. Vessels originating from *Macaca fascicularis* of the study by Hathaway *et al.* (2002)[127]. *Macaca fascicularis* were treated either with a normal diet (Normal), a high fat diet (Atherosclerotic) or with a high-fat diet and a subsequent recovery phase (Regression). Arrows point to dots indicating *LINC00607* orthologue RNA. Representative images are shown. **B** RT-qPCR of the *LINC00607* orthologue in vessels originating from *Macaca fascicularis* treated either with a normal diet (CTL), a high fat diet (Ath) or with a high-fat diet and a subsequent recovery phase (Reg). n=3. One-way ANOVA with Bonferroni post hoc test. **C** RNA in situ hybridization of *LINC00607* in abdominal aorta from *Callitrix jaccus* (Cj) with RNAscope. Arrows point to endothelial cells with staining of *LINC00607* RNA.

The corresponding orthologue of *LINC00607* was significantly upregulated in the regression phase after atherosclerosis induction (**Figure 26A&B**). As the quantification by RT-qPCR was performed on bulk tissue RNA, endothelial localization of the *LINC00607* RNA was visualized by RNAscope in tissue samples from the same study[127] (**Figure 26A**). Staining *LINC00607* in the endothelium of abdominal aorta from young and aged *Callitrix jaccus* further validated *LINC00607* conservation in non-human primates (**Figure 26C**). These results show that *LINC00607* has potential clinical implications in CVDs related to atherosclerosis.

4.1.5 *LINC00607* maintains transcription of genes involved in many important endothelial pathways

To identify how angiogenic function is mediated by *LINC00607* in endothelial cells, gene expression was compared between RNA-Seq data of *LINC00607* KO and control HUVEC (**Figure 27**).

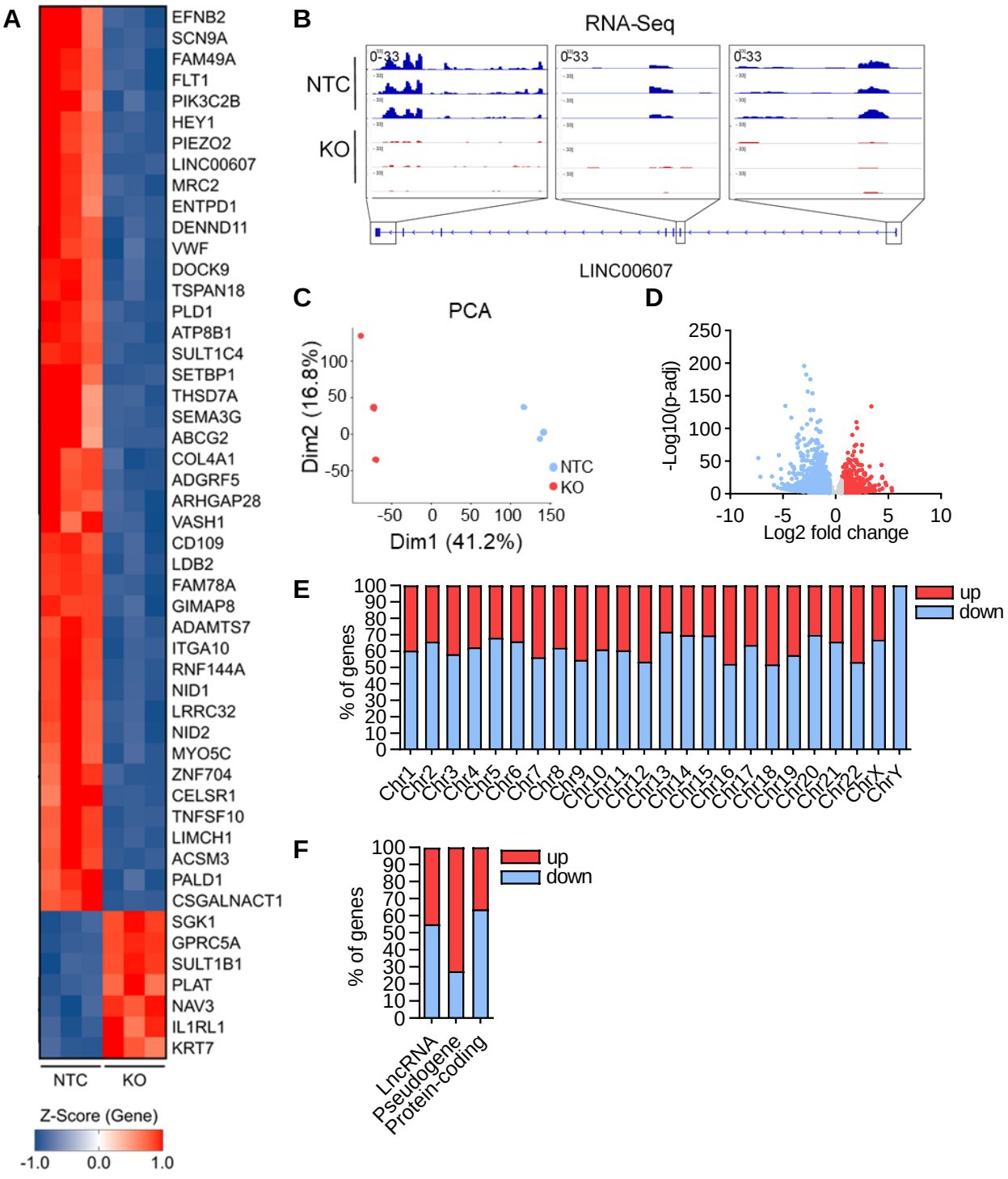

Figure 27 *LINC00607* depletion strongly impacts on gene expression

A Heatmap of the top 50 differentially expressed genes as determined by RNA-Seq of cells with (KO) or without (NTC) CRISPR/Cas9-mediated knockout of *LINC00607*. Three different batches of HUVEC are shown. Genes shown have a padj<0.05, and a log2 fold change greater than ±0.585. Z-score represents up- (red, positive value) or down-regulated (blue, negative values) genes. Individual values are listed in Table 28. **B** IGV tracks of *LINC00607* locus of RNA-Seq reads of *LINC00607* KO and NTC HUVEC. **C** Principal Component Analysis (PCA) plot of the single replicates of RNA-Seq. **D** Volcano plot of RNA-Seq showing the log2 fold changes (KO vs. NTC) of all genes expressed against their p-adjusted value (p-adj). **E&F** Chromosomal distribution and percentage of genes up- or downregulated (DEGs) (E) or percentage of genes belonging to lncRNAs, pseudogenes or protein-coding genes (F) in the RNA-Seq after *LINC00607* KO in HUVEC. Only genes with a log2FC of +/-0.585, a basemean expression of 5 and a p-adj.<0.05 are shown.

The RNA-Seq confirmed the KO of *LINC00607*, as the lncRNA was among the top 50 differentially expressed genes and reads for the lncRNA were almost lacking completely for the complete *LINC00607* gene body (**Figure 27A&B**). A Principal Component Analysis (PCA) showed distinct clustering of the individual samples according to their condition (**Figure 27C**). Loss of *LINC00607* strongly affected gene expression and resulted predominantly in the downregulation of many protein-coding genes (**Figure 27A, D-F**).

Next, the differential expression in response to *LINC00607* KO was validated on RNA and protein level using Western Blotting, RT-qPCR and immunofluorescence staining (**Figure 28**). Among the downregulated genes were many members of important endothelial pathways. Some of them, including TGFβ2 (Transforming growth factor beta 2), RSPO3 (R-Spondin 3), PECAM1 (Platelet endothelial cell adhesion molecule-1), VWF (von Willebrand Factor), FLT1 (Fms Related Receptor Tyrosine Kinase 1), DLL4 (Delta Like Canonical Notch Ligand 4) and GUCY1A1 (Guanylate Cyclase 1 Soluble Subunit Alpha 1) were validated on their expression level changes using immunofluorescence, RT-qPCR and Western blot (**Figure 28**). These examples of genes with known importance to ECs confirmed the importance of *LINC00607* for HUVEC.

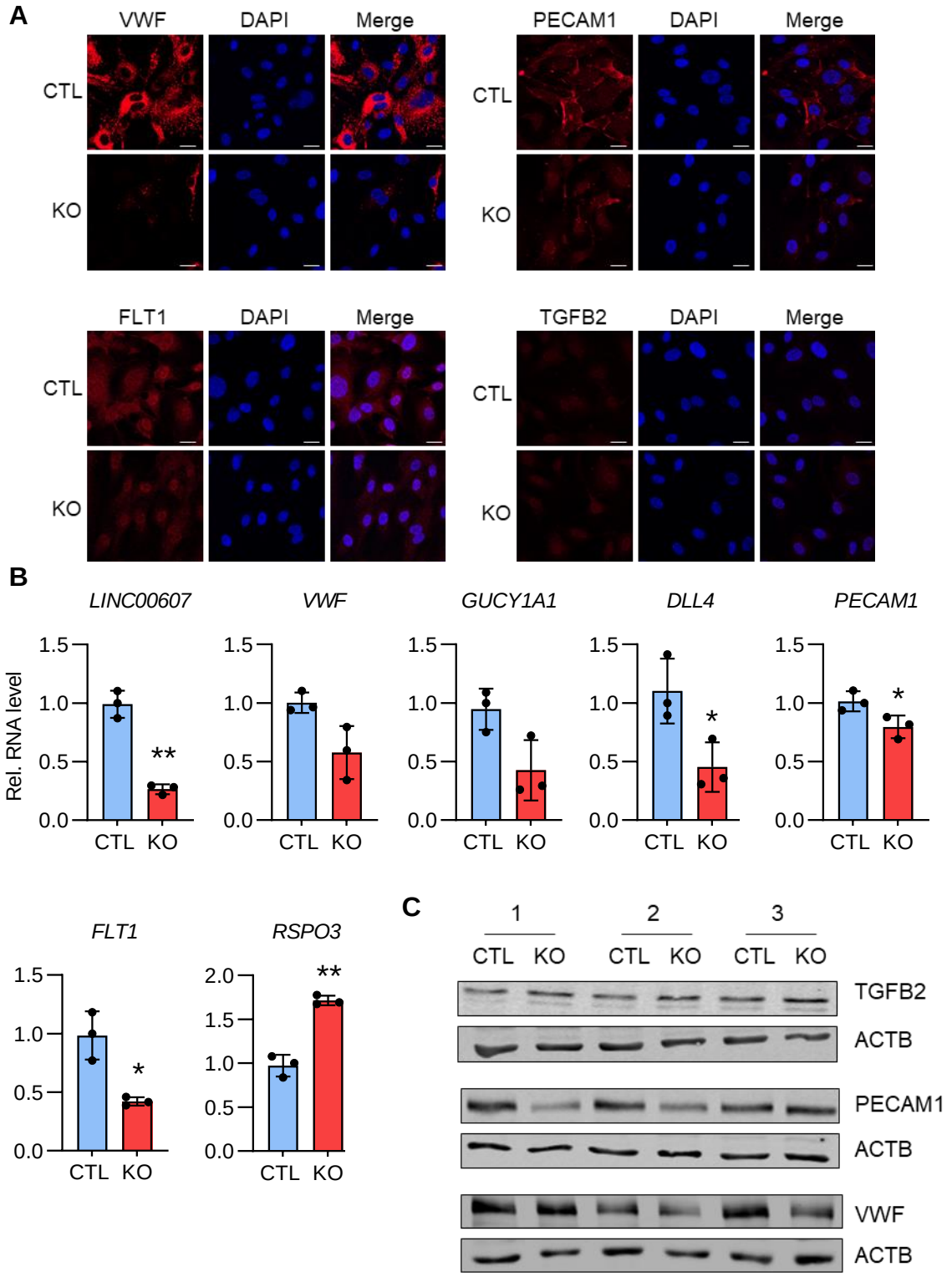

Figure 28 Validation of DEG in response to *LINC00607* KO
A Immunofluorescence with antibodies against von Willebrand Factor (VWF), Platelet endothelial cell adhesion molecule-1 (PECAM1), Fms Related Receptor Tyrosine Kinase 1 (FLT1) and Transforming growth factor beta 2 (TGFβ2) in HUVEC with (607 KO) or without (NTC) CRISPR/Cas9-mediated knockout of *LINC00607*. Nuclei were stained with DAPI. Scale bar indicates 20 µm. **B** RT-qPCR of differentially expressed genes after *LINC00607* KO: *LINC00607*, *VWF*, Guanylate Cyclase 1 Soluble Subunit Alpha 1 (*GUCY1A1*), Delta Like Canonical Notch Ligand 4 (*DLL4*), *PECAM1*, *FLT1*, R-Spondin 3 (*RSPO3*). n=3, Unpaired t-test. *p<0.05, **p<0.01. **C** Western analysis with antibodies against VWF, PECAM1, TGFβ2 and β-Actin of control (NTC) or *LINC00607* KO HUVEC.

4.1.6 Gene transcription of VEGF signalling genes is reduced after *LINC00607* KO

In order to classify the changes observed in the *LINC00607* KO RNA-Seq a reactome-pathway analysis helped allocating the multitude of changes observed[141]. Among the strongly altered pathways were DNA replication, cell adhesion and extracellular matrix organisation, the coagulation cascade and the VEGF signalling pathway (**Figure 29A**).

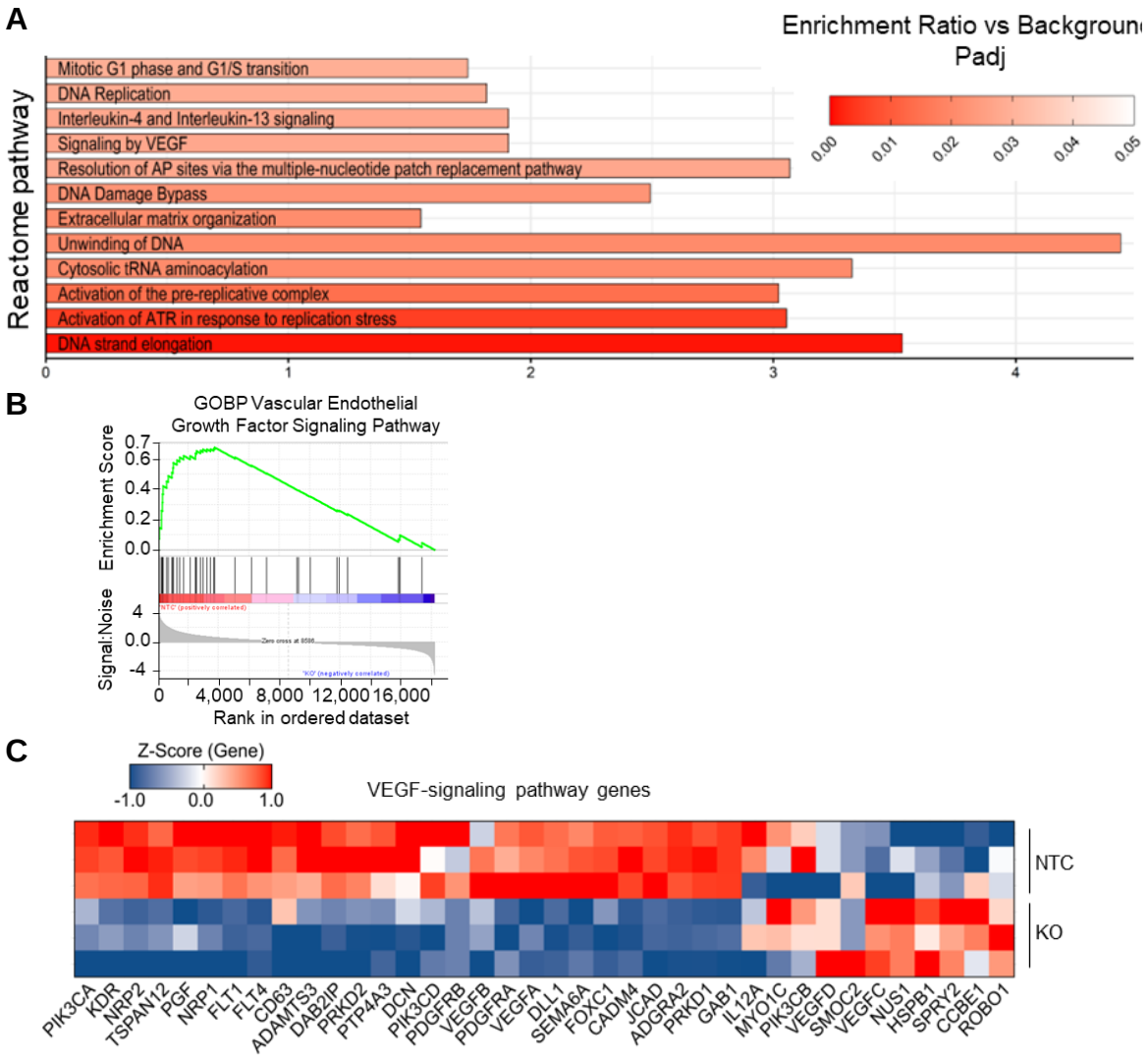

Figure 29 VEGF signalling pathway after *LINC00607* KO
A Reactome pathway analysis of *LINC00607* RNA-Seq and ATAC-Seq overlap. **B** Gene Set Enrichment Analysis (GSEA) of significantly altered genes showing an enrichment score and signal to noise ratio for the Gene Ontology biological process (GOBP) Vascular Endothelial Growth Factor Signalling Pathway. **C** Heatmap of VEGF-signalling pathway genes and their expression differences after *LINC00607* RNA-Seq. Z-score represents up- (red, positive value) or down-regulated (blue, negative values) genes.

As the physiological assays already indicated an altered response to VEGF stimulation, the VEGF signalling pathway was of particular interest. The changes of genes belonging to the VEGF signalling pathway were confirmed by a gene set

enrichment analysis (GSEA)[158,159] performed on all differentially expressed genes after *LINC00607* depletion (**Figure 29B**). The GSEA revealed a strong association of differentially expressed genes within the VEGF signalling pathway in response to *LINC00607* KO. These changes were visualized in a heatmap, showing the majority of VEGF signalling genes to be downregulated (**Figure 29B&C**). As mentioned above, *LINC00607* was important for endothelial angiogenic sprouting under VEGF-A stimulated conditions (**Figure 20, Figure 22**). The data obtained by RNA-Seq, however, suggested a more fundamental role of the *LINC00607* for VEGF signalling and transcription control in EC.

4.1.7 *LINC00607* depletion reduces the accessibility of ETS transcription factor binding sites

Due to the strong effects of *LINC00607* KO on gene expression and its nuclear localization, it can be assumed that loss of *LINC00607* might alter chromatin accessibility and transcription factor binding. To study this, *LINC00607* KO and control HUVEC were subjected to the assay for transposase accessible chromatin by sequencing (ATAC-Seq).

Samples of *LINC00607* KO and control clustered distinctly in the PCA (**Figure 30A**). Analysis of the ATAC-Seq showed that the accessibility of thousands of DNA regions (named as peaks) was changed after *LINC00607* depletion (**Figure 30B**).

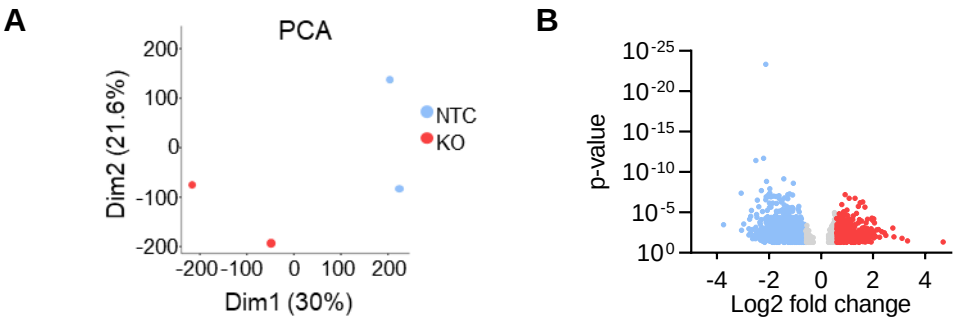

Figure 30 ATAC-Seq of *LINC00607* KO cells
A Principal Component analysis (PCA) of the ATAC-Seq, n=2. **B** Volcano plot of ATAC-Seq showing the log2 fold change (KO vs. NTC) of all peaks against their p-value. Individual values of the most significant peaks are listed in Table 32 and Table 33.

Furthermore, increased as well decreased peaks could be observed, suggesting that the regulation is profound. In order to visualize, classify and comprehend the differential chromatin accessibility, the ATAC-Seq data were integrated with the RNA-Seq data (**Figure 31**).

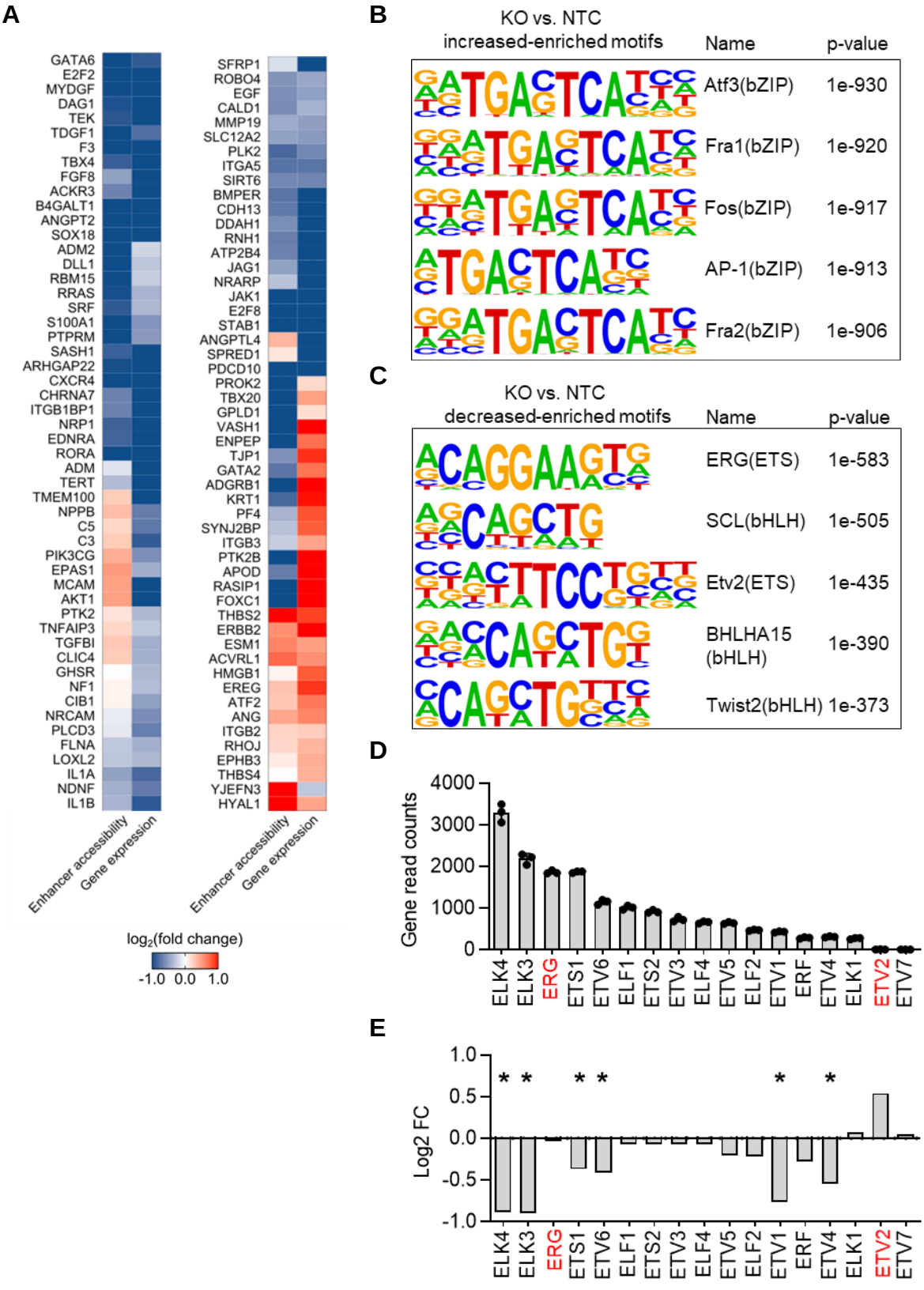

Figure 31 Overlap of ATAC-Seq and RNA-Seq and motif enrichment analysis
A Heatmap of the overlap of ATAC-Seq (enhancer accessibility) and RNA-Seq (gene expression) differential signals in response to knockout of *LINC00607* in HUVEC. Genes shown belong to the angiogenesis pathway (GO:0001525). **B-C** HOMER DNA-motif enrichment analysis of differential accessible peaks (*LINC00607* KO vs. NTC). Five most highly increased-enriched (B) or decreased-enriched (C) transcription factor motifs are shown. **D** Gene expression of ETS transcription factor family members, measured by gene read counts of NTC-treated HUVEC (from RNA-Seq), n=3. **E** Differential gene expression of ETS TFs comparing *LINC00607* KO and NTC control mean log2 fold change (FC) of the RNA-Seq.

To visualize the comparison of both sequencing datasets, the significantly differentially expressed genes of the angiogenesis gene ontology pathway (GO:0001525) were plotted alongside the gene-linked enhancers (as annotated by EpiRegio[140]) (**Figure 31A**). As shown in the heatmap, *LINC00607* KO had similar effects on gene expression and enhancer accessibility of that gene: genes, downregulated after *LINC00607* KO, displayed reduced enhancer accessibility (e.g. *ANGPT2*, *TEK*, *GATA2*; **Figure 31A**) and upregulated genes had increased enhancer accessibility (e.g. *ANG*, *EREG*, *ERBB2*; **Figure 31A**). This indicated that *LINC00607* influences gene expression probably through regulating the accessibility of TF binding sites.

To identify differentially accessible TF-binding motifs, a HOMER DNA-motif enrichment analysis[143] was performed (**Figure 31B&C**). The motifs with a strongly increased accessibility belonged to the class of Basic Leucine Zipper domain motifs (bZIP; **Figure 31B**). Strongly decreased in accessibility were the motifs for the Basic Helix–Loop–Helix (bHLH) and Erythroblast Transformation Specific (ETS) TF motifs (**Figure 31C**). In the absence of *LINC00607*, the ETS motifs of the endothelial TFs ERG (ETS Transcription Factor ERG) and ETV2 (ETS Variant Transcription Factor 2) were identified as less accessible (**Figure 31B**). Both ETS TFs identify the core consensus motif GGA(A/T)[86], which is known to be present in many promoters and/or enhancers important for endothelial cell function[85,160]. Therefore, the motif is highly important for endothelial gene expression.

To rule out that differential gene expression after *LINC00607* KO was not a result of differential expression of the transcription factors themselves, the expression of ERG, ETV2 and other members of the ETS transcription factor family was examined (**Figure 31D&E**). As determined by RNA-Seq under basal conditions, ERG was among the highest expressed ETS family members in HUVEC, whereas ETV2 was lowly expressed (**Figure 31D**). Both TFs were stably expressed after *LINC00607* KO, however, ETV2 expression was slightly upregulated and was therefore excluded from further analyses (**Figure 31E**). Because of its endothelial importance, stably high expression and transcriptional independence of *LINC00607*, ERG was selected as a candidate TF mediating *LINC00607*-dependent transcription.

4.1.8 Many ERG regulated genes are downregulated in *LINC00607* KO

To investigate further if the ERG target-gene expression is controlled by *LINC00607*-dependent chromatin accessibility changes, differential expression from a publicly available RNA-Seq dataset of HUVEC after ERG knockdown (GSE1248[88]) was compared to the expression changes after *LINC00607* KO (**Figure 32**).

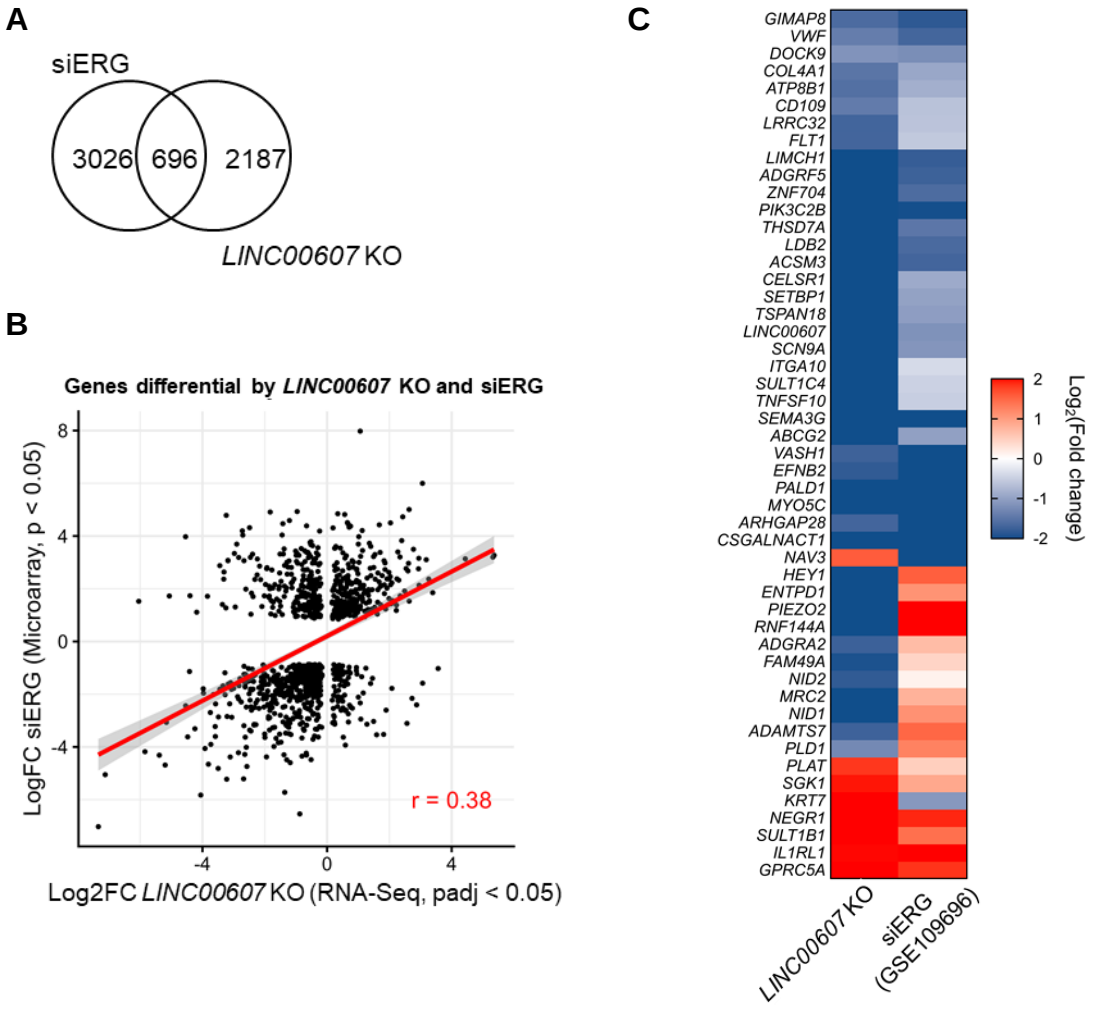

Figure 32 Validation of the association of the changes after *LINC00607* KO and ERG KD
A&B Venn diagram (A) and scatter plot (B) of differentially expressed genes from RNA-Seq of *LINC00607* KO and ChIP-Seq of siRNA knockdown of ERG (siERG; GSE124891[88]) in HUVEC. Scatter plot shows genes by log2 fold change (log2FC) with a p-value cut-off below 0.05. **C** Heatmap of the top 50 DEGs of RNA-Seq from *LINC00607* KO HUVEC and RNA-Seq after ERG knockdown in HUVEC; (padj<0.05); log2 FC shows up- (red, positive value) or down-regulated (blue, negative values) genes. Individual values are listed in Table 29.

From the many differentially expressed genes almost 700 genes were shared between both datasets (**Figure 32A**). These genes displayed similar expression tendencies (**Figure 32B**). Importantly, the majority of the top 50 differentially expressed genes from *LINC00607* KO cells shared a similar expression change after siRNA knockdown of ERG (**Figure 32C**). Taken together, the results indicate that ERG-mediated transcription is dependent on *LINC00607.* How *LINC00607*

controls transcription factor binding site accessibility was investigated in the next chapter.

4.1.9 *LINC00607* alters chromatin states in cooperation with the chromatin remodeling protein BRG1

Usually, lncRNAs do not independently act to control gene transcription and chromatin accessibility; they rather contribute to chromatin remodeling by an interaction with chromatin remodeling proteins and complexes[4]. It is therefore plausible to assume that also *LINC00607* interacts with a chromatin remodeler orchestrating its function. An important and well characterized chromatin remodeling protein in ECs is Brahma related gene 1 (BRG1), which serves as the catalytic subunit of the SWI/SNF chromatin remodeling complex[61,161]. BRG1 is also known to interact with lncRNAs which alter its control of gene transcription in ECs, e g. *MANTIS*[60] or *Mhrt*[162]. By performing RNA-immunoprecipitation of BRG1 followed by RT-qPCR for *LINC00607*, a significant interaction of BRG1 with *LINC00607* was detected (**Figure 33A**). The binding of *LINC00607* to BRG1 was proven to be specific: *LINC00607* was not pulled down by the non-primary antibody control IgG, whereas the mRNA of *β-Actin* was precipitated to a similar extend with both antibodies (**Figure 33B**). RNase A treatment abolished the signal of *LINC00607* and of *ß-Actin*, indicating that indeed RNA was retrieved. BRG1 expression was also not affected by *LINC00607* KO, suggesting that the function -and not the expression- of BRG1 is controlled by *LINC00607* (**Figure 33C**).

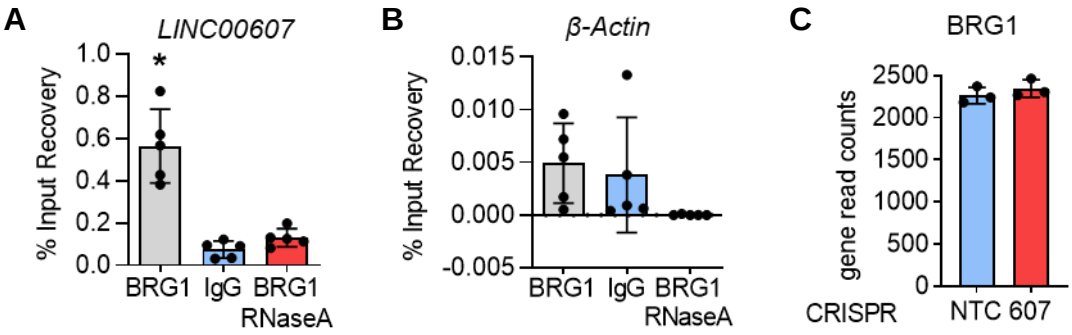

Figure 33 *LINC00607* is associated to BRG1
A-B RNA-immunoprecipitation with BRG1 antibody, with and without RNase A digestion, followed by RT-qPCR of *LINC00607* (A) and β-*Actin* (B). IgG is the non-primary antibody control. n=5. One-Way ANOVA with Bonferroni post hoc test. **C** Gene read counts of BRG1 from *LINC00607* KO RNA-Seq, n=3.

These data indicate that *LINC00607* might influence BRG1 binding to DNA.

This hypothesis was tested by performing Cleavage Under Targets & Release Using Nuclease (CUT&RUN)[123] sequencing of BRG1 in HUVEC, mapping DNA binding sites in high resolution (**Figure 34**).

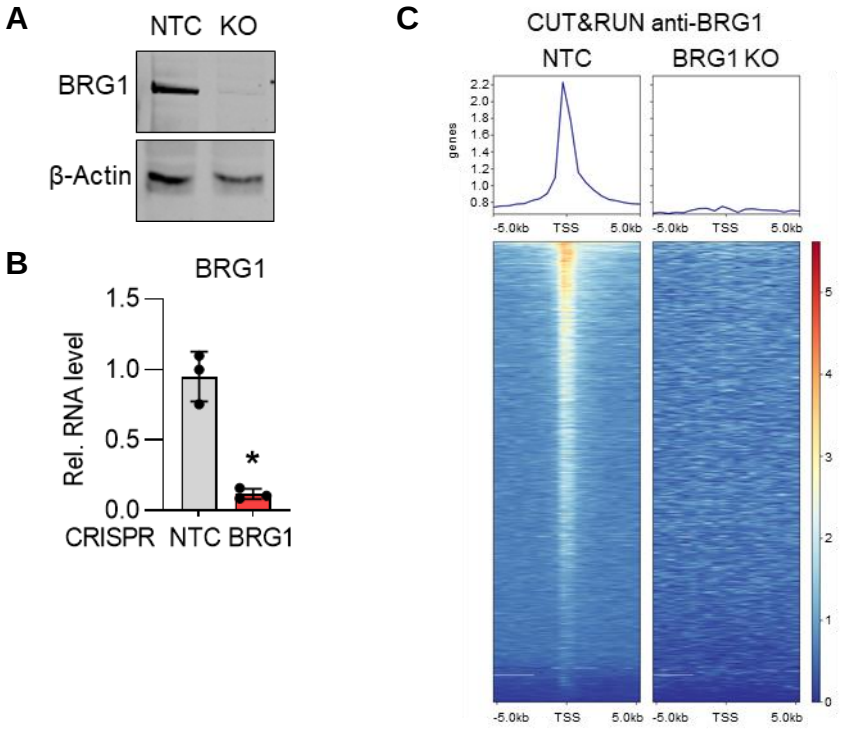

Figure 34 BRG1 genome-binding site detection by CUN&RUN sequencing of BRG1 KO and control HUVEC
A Validation of CRISPR/Cas9-mediated knockout (KO) of BRG1 in HUVEC on Western Blot with antibodies against BRG1 and β-Actin. NTC served as negative control. **B** RT-qPCR of NTC and BRG1 KO HUVEC, n=3, paired t-test. **C** Chromatin accessibility matrix of differential peaks from BRG1 CUT&RUN of control (NTC) and *BRG1* knockout (KO) HUVEC. Binding regions center-aligned to the transcription start sites (TSS) +/- 0.5 kb are shown.

A CRISPR/Cas9 KO of BRG1 in HUVEC served as a negative control. BRG1 predominantly bound DNA at the transcriptional start sites of genes and the binding was lost in BRG1 KO HUVEC (**Figure 34C**).

4.1.10 *LINC00607* maintains chromatin states of ERG target genes through interaction with BRG1

Next, it was determined whether BRG1 binding occurs around the TSS of ERG target genes. For this, an overlap was created between ERG-associated genes identified using ERG ChIP-Seq data (GSE124891)[88], genes with a BRG1 binding signature and genes, with differential expression and ATAC peak in response to *LINC00607* knockout (**Figure 35A**).

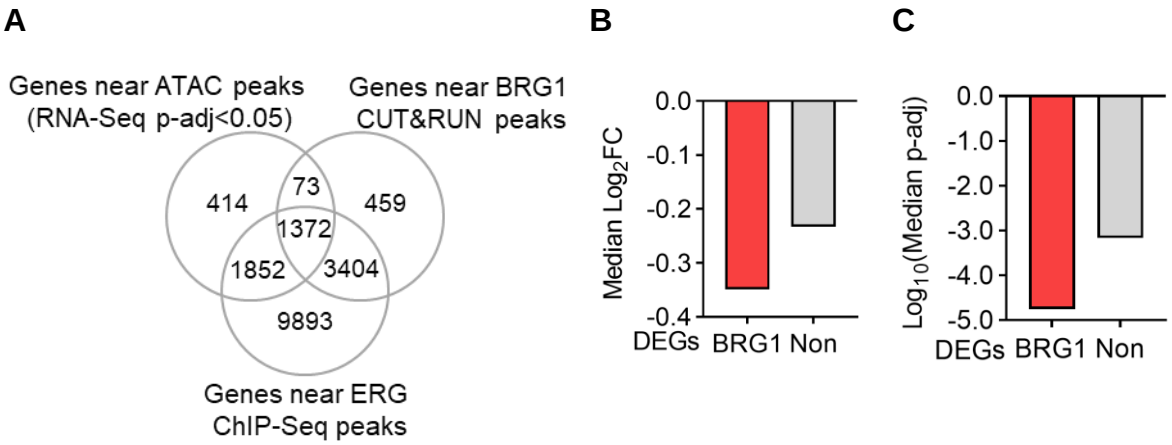

Figure 35 Overlap of three datasets: BRG1 target genes, ERG target genes and genes with differential expression and altered chromatin states after *LINC00607* KO
A Venn diagram showing the overlap of genes located near a differential ATAC-Seq peak of *LINC00607* knockout, genes near a BRG1 CUT&RUN peak and genes near a ERG ChIP-Seq peak. **B** Median log2 fold change (FC) of differentially expressed genes from *LINC00607* KO that are located near a differential ATAC-Seq peak of *LINC00607* knockout and also found near a BRG1 CUT&RUN peak (BRG1) or not (Non). **C** Median p-adjusted value of differentially expressed genes from *LINC00607* KO that are located near a differential ATAC-Seq peak of *LINC00607* knockout and also found near a BRG1 CUT&RUN peak (BRG1) or not (Non).

Interestingly, there was a strong overlap between BRG1 target genes and *LINC00607* differentially expressed genes (1,445 genes) (**Figure 35A**). Almost all (1,372 out of 1,445) genes, with a BRG1 signature and differential accessibility after *LINC00607* KO, were shared with genes, with ERG binding present at their promoter or TSS (**Figure 35A**).

Additionally, BRG1-associated genes displayed significantly stronger decreased expression after *LINC00607* KO, compared to genes without a BRG1 signature (**Figure 35B&C**). As the majority of differentially expressed genes after *LINC00607* depletion, with a BRG1 signature, were downregulated and had the ERG TF-motif strongly enriched, the described geneset was further overlapped with a dataset of ERG ChIP-Seq[88] (**Figure 35A**).

By visual inspection, a handful of genes with importance to endothelial cells were checked manually for differential expression and chromatin accessibility after *LINC00607* KO, CUT&RUN of BRG1 and ChIP-Seq of ERG (**Figure 36**). These were von Willebrand factor (VWF), Serum/Glucocorticoid Regulated Kinase 1 (SGK1), Angiopoietin Like 5 (ANGPTL5), Tetraspanin 12 (TSPAN12), Kinase Insert Domain Receptor (KDR) and Gap Junction Protein Alpha 5 (GJA5). All of these genes shared a strong ERG ChIP-Seq peak and a BRG1 CUT&RUN peak, both at their TSS, which is lost in the BRG1 KO control, differential expression upon *LINC00607* KO and slightly altered chromatin accessibility (**Figure 36**). These data

show the importance of *LINC00607* for endothelial gene expression. *LINC00607* is needed for stable transcription of ERG-target genes in endothelial cells.

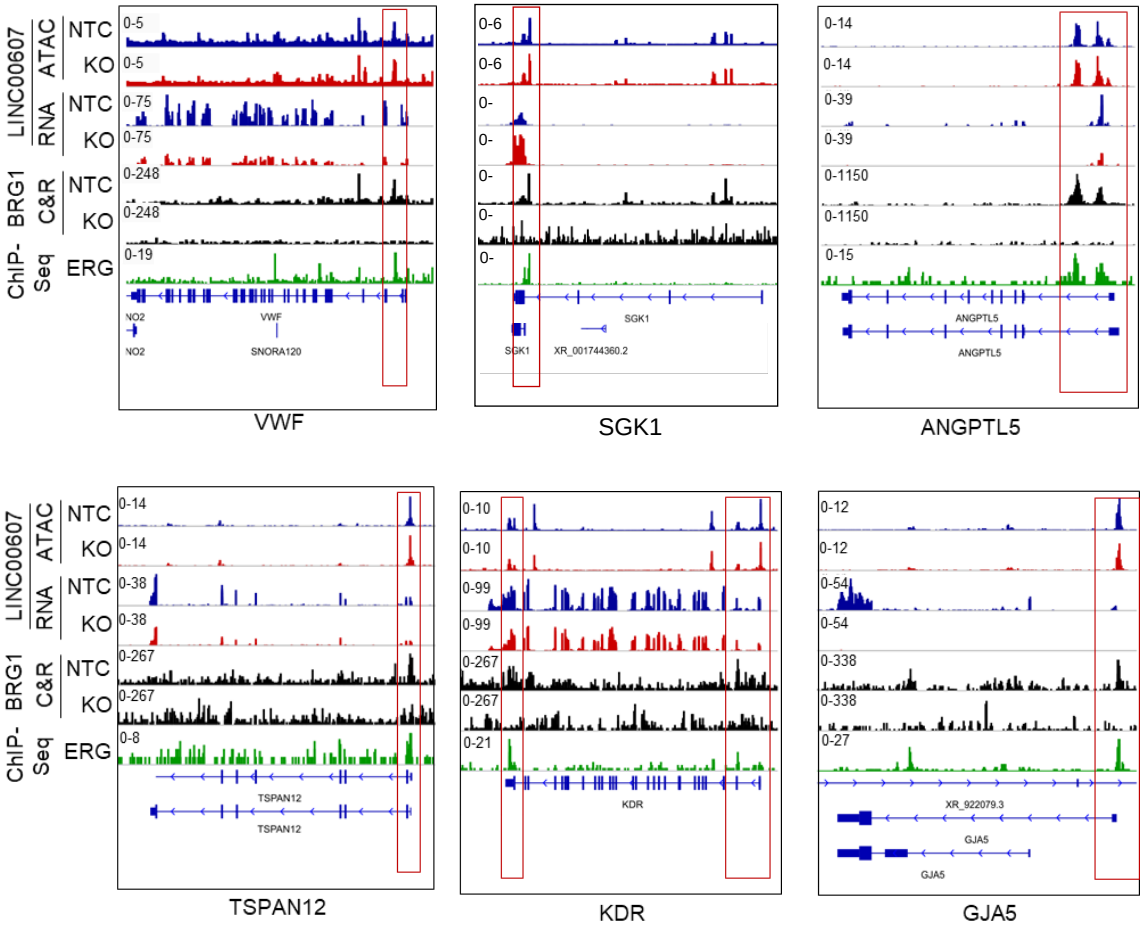

Figure 36 Exemplary genome tracks of genes with confirmed dependency of expression on *LINC00607* recruitment of BRG1 to ensure ERG TF binding and expression
Genome tracks of ATAC-Seq, RNA-Seq, BRG1 CUT&RUN and ERG ChIP-Seq. Loci of von Willebrand factor (VWF), Serum/Glucocorticoid Regulated Kinase 1 (SGK1), Angiopoietin Like 5 (ANGPTL5), Tetraspanin 12 (TSPAN12), Kinase Insert Domain Receptor (KDR) and Gap Junction Protein Alpha 5 (GJA5) are shown. ATAC-Seq and RNA-Seq of *LINC00607* KO (red) and NTC (blue) are shown. Tracks of replicates were overlaid. CUT&RUN with anti-BRG1 antibodies of NTC or *BRG1* KO HUVEC are shown in black. ChIP-Seq of ERG is shown in green.

These results suggest a mechanism of action for the endothelial lncRNA *LINC00607*: under healthy conditions, *LINC00607* navigates the chromatin remodelling protein BRG1 to genomic sites of the ERG-binding motif, ensuring a stably accessible chromatin state for ERG binding. Upon loss of *LINC00607*, BRG1 is no longer recruited to ERG target genes leading to decreased expression of ERG target genes.

4.2 *LINC00607* and its role in alternative splicing

In the first part of the results, it was reported that *LINC00607* is important for the maintenance of the endothelial phenotype, the regulation of gene expression and chromatin accessibility. In the second part, another pathway in which *LINC00607* appears to contribute will be presented: splicing regulation.

4.2.1 Knockout of *LINC00607* alters the splicing patterns of FLT1

As mentioned, VEGF signalling is strongly affected after depletion of *LINC00607*. VEGF signalling is not only regulated by differential expression of pathway members but also by alternative splicing of key factors, such as VEGF and FLT1 to either pro- or anti-angiogenic isoforms[100]. Therefore, a Junction sequencing splicing analysis (JunctionSeq)[163] was carried out comparing the RNA-Seq data with and without *LINC00607* KO to uncover potential splicing events affecting VEGF signalling (**Figure 37**). The analysis revealed many alternative splicing (AS) events, with skipped exons and retained introns most frequently observed (**Figure 37A**). AS occurred in genes, regardless of their expression changes after *LINC00607* KO. Among the differentially expressed genes, most alternative splicing events were observed in downregulated genes (**Figure 37B**). One of the most highly significant alternatively spliced transcripts was FLT1 (**Figure 37C&D**). As one of the major targets of *LINC00607*, FLT1 was therefore selected as an interesting candidate for further investigation as it is known to be strongly affected by AS and essential for VEGF signalling.

A

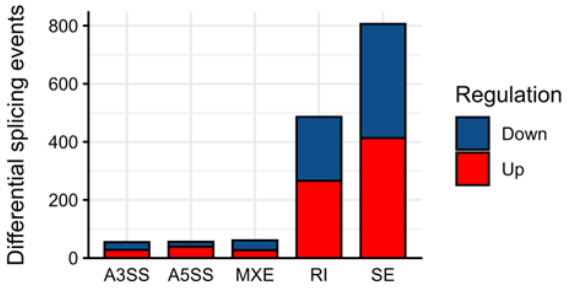

B

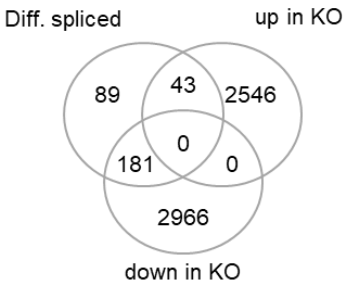

C

Rank	Gene name	Exon No.	chr	start	end	strand	p-val	Log2FC (whole gene)
1	MAP4	E011	chr3	47909267	47910388	-	4,97E-70	0,21
2	MAP4	E010	chr3	47910388	47912421	-	3,07E-43	0,21
3	SYNPO	E003	chr5	150650303	150652334	+	2,86E-37	NA
4	FLT1	E013	chr13	28385566	28389632	-	5,40E-32	-1,70
5	TRIP12	E041	chr2	229763837	229767440	-	2,69E-30	NA
6	SLC44A2	E001	chr19	10625593	10625670	+	5,42E-29	-0,80
7	DHX36	E025	chr3	154272545	154275667	-	1,66E-28	NA
8	CCDC50	E011	chr3	191392175	191398670	+	3,28E-28	-0,29
9	FLT1	E015	chr13	28368095	28368663	-	5,17E-28	-1,70
10	ATF6	E016	chr1	161958445	161964070	+	5,60E-27	-0,55

D

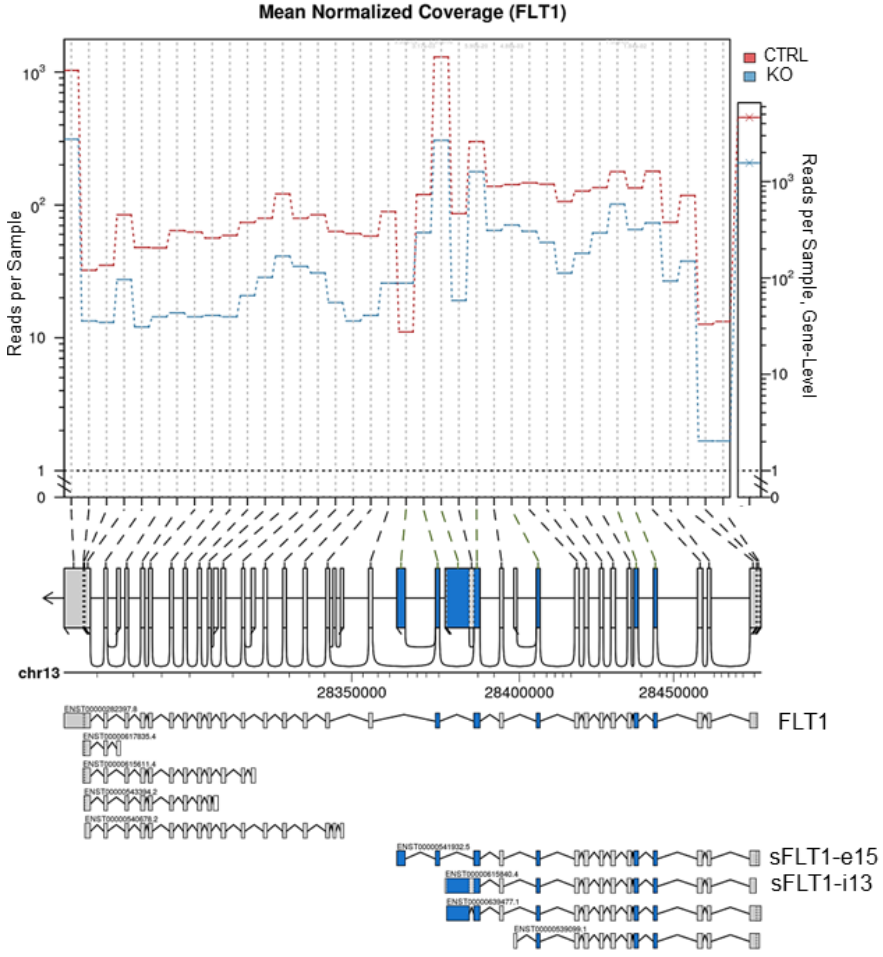

Figure 37 Splicing analysis of differentially expressed genes in response to *LINC00607* KO

A Number of AS events in the *LINC00607* KO. A3SS, Alternative 3' splice site; A5SS, Alternative 5' splice site; MXE, mutually exclusive exon; RI, retained intron; SE, Skipped exon. **B** Venn diagram of the overlap of significantly up- and down-regulated genes of the RNA-Seq in response to *LINC00607* KO in HUVEC and the differential spliced genes identified through JunctionSeq Analysis. **C** Top 10 AS events in *LINC00607* KO versus non-target control (NTC), ranked by p-value. The log2 fold changes (log2FC) shown for whole gene expression changes after *LINC00607* KO. **D** Gene plot profile of FLT1 from JunctionSeq analysis. Upper central plotting area displays mean normalized read counts of each FLT1 exon in *LINC00607* KO (blue) and non-target control (CTRL, red) and the gene-level normalized read counts on the right. Displayed below is the genomic locus of FLT1, its exon-intron structure and a representation of FLT1 isoforms. Indicated in blue are exons and introns overrepresented in *LINC00607* KO reads.

The JunctionSeq reported AS of FLT1 exons 13 and 15 (**Figure 37**). AS of exon 13 refers to the partial inclusion of intron 14, resulting in an elongated exon 13 (sFLT1-i13; **Figure 37D**). Overall, this isoform seemed to be expressed to a similar extend as membrane bound FLT1 (mFLT1). Strikingly, JunctionSeq genome tracks, RNA-Seq read overlappings, as well as Sashimi plots revealed not only that FLT1 was strongly downregulated, but that alternative exon 15 was upregulated after *LINC00607* KO (sFLT1-e15; **Figure 37D**). The observed splicing events were validated by sashimi blot and RT-qPCR (**Figure 38**).

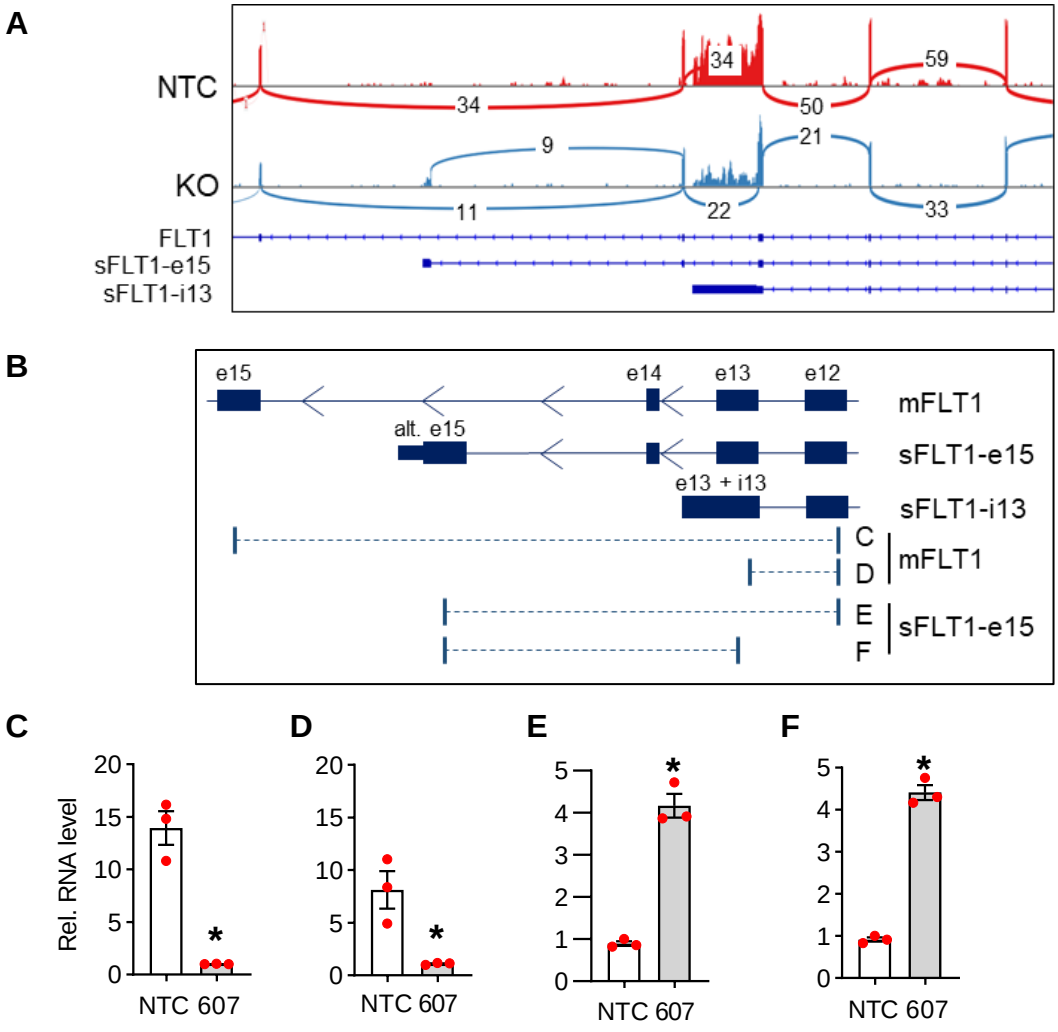

Figure 38 Alternative splicing of FLT1 after *LINC00607* KO

A Sashimi plot of the RNA-Seq indicating FLT1 exons 11-15 in control (NTC) and *LINC00607* KO (KO). Numbers indicate mean reads per exon of n=3 RNA-Seq. **B** Location of primer pairs used for RT-qPCR splicing analysis shown in C-F. e, Exon; i, Intron; alt e15, alternative exon 15. **C-F** RT-qPCR splicing analysis of FLT1 alternative splicing displayed by the relative RNA expression of the individual FLT1 isoforms in *LINC00607* KO and NTC. **C** Relative expression of the long isoform of FLT1. **D** Relative expression of the sFLT1-e15b isoform. **E** Relative expression of FLT1 exons 13-15. **F** Relative expression FLT1 exons 14-15. Unpaired t-test. *p<0.05.

The isoform sFLT1-e15, has normal slicing of exons 13 and 14, but is characterized by the inclusion of alternative exon 15. Alternative exon 15 is encoded within intron 14, leading to a premature stop-codon and intronic poly(A) signal sequences[164] and thereby to a shortened soluble isoform of FLT1 (sFLT1) (**Figure 38**). To confirm these findings, RT-qPCR with primers specific for mFLT1 and the sFLT1-e15 was performed (**Figure 38B-F**). KO of *LINC00607* strongly decreased the expression of mFLT1, whereas sFLT1-e15 was significantly increased (**Figure 38E&F**).

4.2.2 Perturbed angiogenic response after *LINC00607* KO can be restored by neutralizing soluble FLT1

Through AS after *LINC00607* KO, the sFLT1-e15 and sFLT1-i13 isoforms of FLT1 were generated. These isoforms lack the transmembrane and intracellular domains, resulting in receptor secretion of the soluble FLT1 isoforms (sFLT1) (**Figure 39**)[101,165].

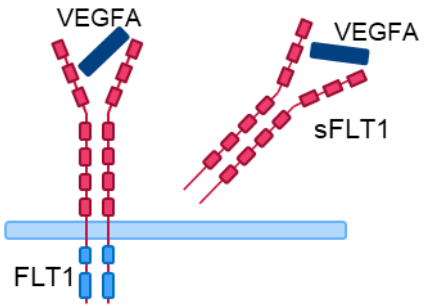

Figure 39 Domain structure of FLT1 and soluble FLT1 (sFLT1)
FLT1 and sFLT1 can bind VEGF, but only binding to FLT1 triggers downstream signalling, as the sFLT1 isoform is missing the transmembrane- and intracellular domains (blue).

Soluble FLT1 acts as scavenging receptor for VEGF. It binds and sequesters VEGF, preventing it from binding to its membrane receptor, leading to attenuated VEGF signalling[165]. To an extend this regulation of VEGF signalling is important but excessive inhibition of angiogenesis by sFLT1 can be dangerous[101,166].

In order to test whether the reduced sprouting in response to VEGF-A after *LINC00607* depletion was a result of sFLT AS, a rescue experiment was conducted (**Figure 40**).

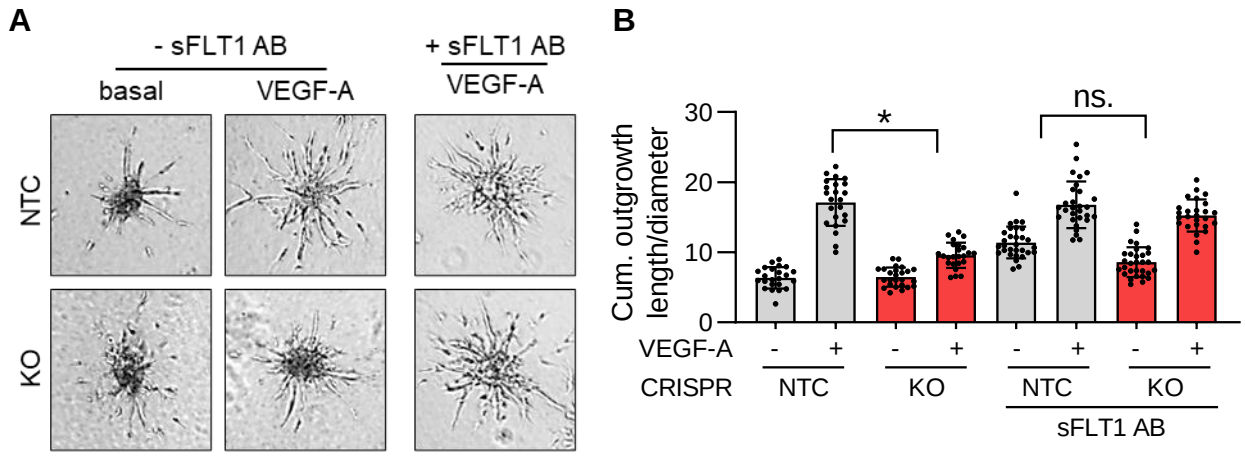

Figure 40 Antibodies against sFLT1 rescue *LINC00607* knockout-derived endothelial dysfunction
A Spheroid outgrowth assay of HUVEC after CRISPR/Cas9-mediated *LINC00607* KO or NTC treated with or without sFLT1 neutralizing antibody (sFLT1 AB). Cells also treated with or without VEGF-A (16h). **B** Quantification of the quotient of cumulative outgrowth length and respective spheroid diameter from spheroid outgrowth assay shown in c. n=28-30, One-way ANOVA with Bonferroni post hoc test. Error bars are defined as mean +/- SD. *p<0.05.

For this, a neutralizing antibody against sFLT1 was added to the spheroid outgrowth assay of *LINC00607* KO and control HUVEC. This restored angiogenic sprouting in *LINC00607* KO cells to the same level as of the control cells (**Figure 40A&B**). Thus, *LINC00607* dependent AS of FLT1 is also functionally important.

4.2.3 AS of FLT1 after *LINC00607* depletion might be linked to BRG1

As in the case of chromatin accessibility changes, *LINC00607* is unlikely to alter or maintain AS alone. Since chromatin accessibility was not changed by *LINC00607* KO in the FLT1 locus, the changes should not be attributed to epigenetic rearrangements (**Figure 41**).

A

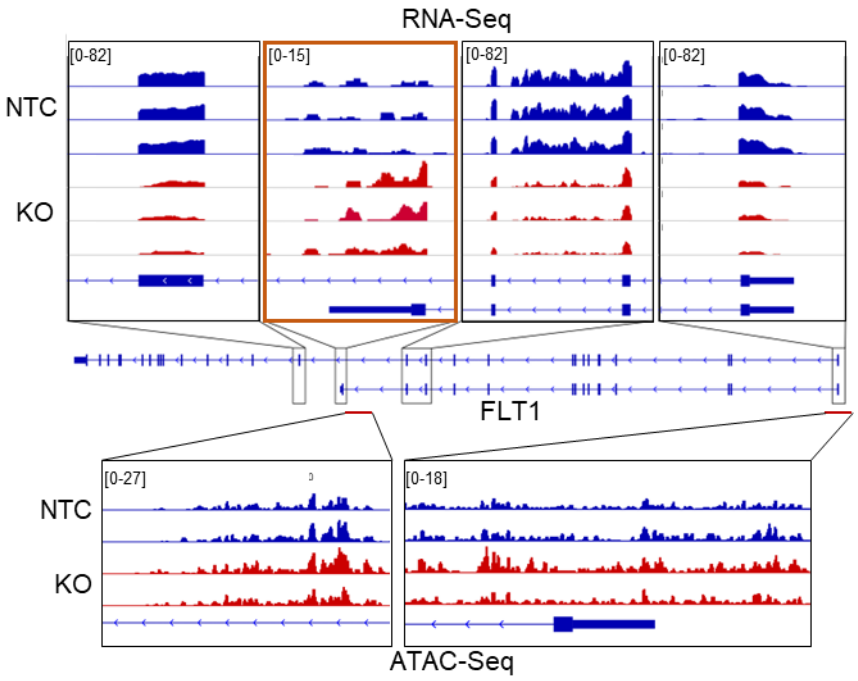

Figure 41 RNA- and ATAC-Seq reads after *LINC00607* KO at the FLT1 locus
A IGV genome tracks of the FLT1 locus. Upper tracks: RNA-Seq reads of different parts of FLT1 in *LINC00607* KO and NTC. Circled in orange is the locus of alternative exon 15. Lower IGV tracks: ATAC-Seq reads of FLT1 TSS and an intronic region upstream of alternative exon 15.

LINC00607 is functionally associated to BRG1, which has been reported recently to also contribute to AS[56]. In order to test whether BRG1 is involved in AS of FLT1, RNA-Seq of HUVEC treated with siRNA against BRG1 were subjected to JunctionSeq analysis. The JunctionSeq yielded over 100 differentially spliced genes (**Figure 42A**).

When comparing the differentially spliced genes after BRG1 knockdown (KD) with the results from *LINC00607* KO JunctionSeq, a substantial overlap was observed (**Figure 42A**). Among the shared genes was FLT1 (**Figure 42A&C**). More interestingly, 25 out of the 53 differentially spliced genes after *LINC00607* KO or BRG1 KD were alternatively spliced at the same exon, including FLT1, SYNPO (Synaptopodin), SUGT1 (SGT1 Homolog, MIS12 Kinetochore Complex Assembly Cochaperone), RTN3 (Reticulon 3) and MAP4K4 (Mitogen-Activated Protein Kinase Kinase Kinase Kinase 4; **Figure 42A&C**).

A

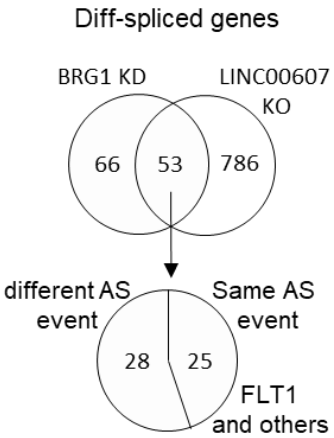

B

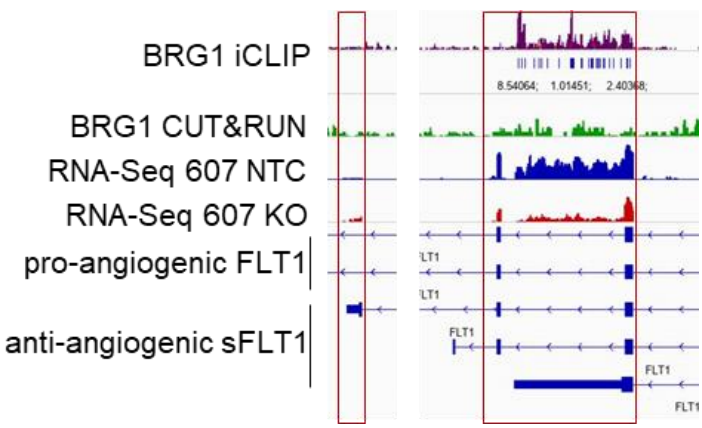

C

Rank	Gene name	Exon No.	chr	start	end	strand	pvalue 607	pvalue BRG1
1	SYNPO	E003	chr5	150650303	150652334	+	2,86E-37	5,40E-08
2	FLT1	E013	chr13	28385566	28389632	-	5,40E-32	7,71E-09
3	SUGT1	E014	chr13	52689945	52700909	+	3,12E-21	1,83E-12
4	RTN3	E003	chr11	63719197	63721032	+	1,89E-15	1,33E-05
5	MAP4K4	E031	chr2	101891987	101894687	+	6,22E-14	3,10E-27
6	PCDH9	E002	chr13	67201014	67225404	-	7,45E-14	1,19E-06
7	CEP68	E006	chr2	65083638	65087004	+	1,09E-13	1,38E-08
8	CLCN3	E012	chr4	169720545	169723183	+	5,76E-11	9,08E-06
9	SESTD1	E018	chr2	179101691	179109321	-	2,24E-10	3,82E-09
10	RTN4	E004	chr2	55025085	55027206	-	4,94E-10	3,59E-09

D

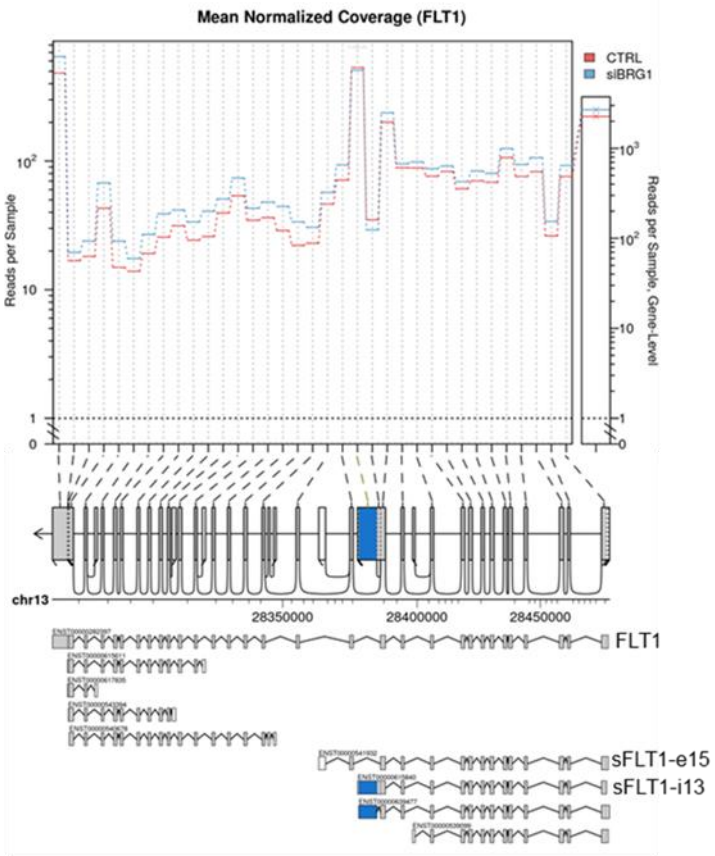

Figure 42 Knockdown of BRG1 shows similar AS like *LINC00607* KO

A Upper: Venn diagram of AS events identified by JunctionSeq after *LINC00607* KO and siRNA mediated BRG1 siKD. Lower: Shared genes from both JunctionSeq analyses; 25 genes have the same AS event and 28 genes are spliced in a different location. **B** IGV genome tracks of BRG1 iCLIP (kindly provided by Dr. James Oo), and CUT&RUN, *LINC00607* RNA-Seq after KO and control (NTC) in the FLT1 locus. Circled in red: right: alternative exon 13; left: alternative exon 15. **C** Top 10 splicing events occurring in both JunctionSeq analyses of BRG1 KD and in *LINC00607* KO, ranked by p-value of AS event in *LINC00607* KO (pvalue *607*), shown also are the p-values of the splicing events from BRG1 KO (pvalue BRG1). **D** Gene plot profile of FLT1 from JunctionSeq analysis. Upper central plotting area displays mean normalized read counts of each FLT1 exon in BRG1 knockdown (siBRG1; blue) and siRNA-control (CTRL, red) and the gene-level normalized read counts on the right. Displayed below is the genomic locus of FLT1, its exon-intron structure and a representation of FLT1 isoforms. Indicated in blue are exons and introns overrepresented in BRG1 KD reads.

The AS for FLT1 was reported in both datasets for exon 13, especially the retained intron of sFLT1-i13 (**Figure 42C&D**). Importantly, iCLIP (individual-nucleotide resolution Cross-Linking and Immunoprecipitation sequencing; kindly provided by Dr. James Oo) data of BRG1 showed BRG1 binding to FLT1 mRNA at the sequence of the sFLT1-i13 retained intron (**Figure 42B**). These results show that *LINC00607* and BRG1 might be cooperatively involved in the maintenance of FLT1 splicing to prevent the creation of soluble FLT1.

4.2.3.1 Trophoblast cells express *LINC00607* to a high extent

Within recent years, sFLT1 was identified as a clinical marker for preeclampsia during pregnancy[167]. Due to the generation of sFLT1 in *LINC00607* KO HUVECs, a potential relevance of *LINC00607* in the AS of FLT1 during preeclampsia can be inferred. To study a potential link between *LINC00607* and pregnancy and fetal development, its expression in publicly available single cell RNA-Seq data[168] was checked (**Figure 43A**).

Analysis of *LINC00607* levels in placenta of both fetal and maternal sites showed higher expression in the fetus as compared to the maternal cell populations, especially in cells characterized as extravillous trophoblasts and fetal placenta syncytiotrophoblasts. Importantly, these cell types are known to be a major source of sFLT1 during the clinical onset of preeclampsia[169] and also showed the strongest expression signature for the sFLT1-i13 isoform intron 13 (**Figure 43B**).

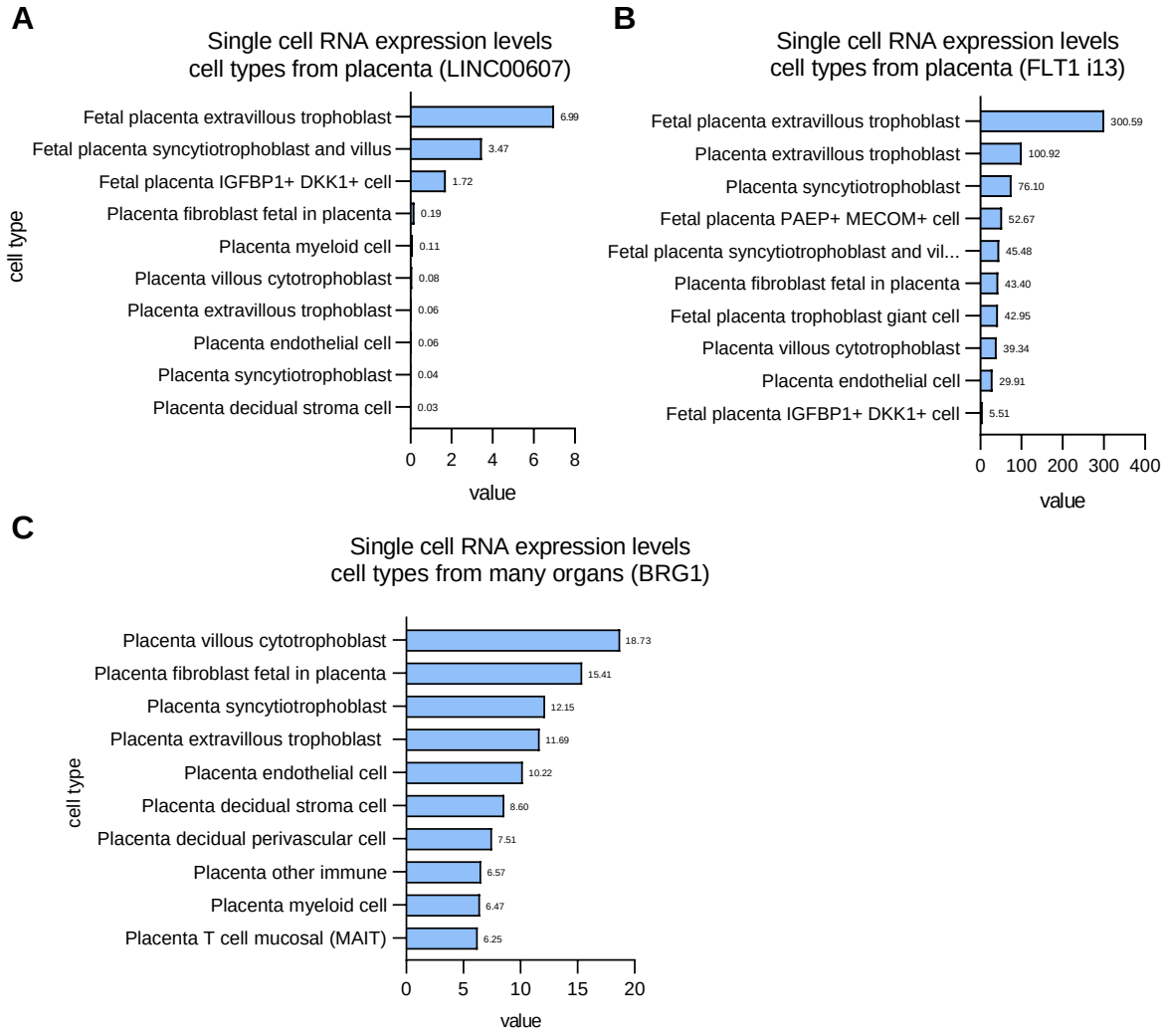

Figure 43 Single cell RNA-Seq of *LINC00607,* FLT1 and BRG1 in adult and fetal placenta
A-C Single cell RNA-Seq expression levels of *LINC00607* (A) and FLT1 (B) and BRG1 (C) in adult and fetal placenta taken from the UCSC browser[170]. Values shown from the human fetal cell atlas[171] and the early maternal–fetal interface reconstruction in humans[168] were normalized to be in parts per million using the matrixNormalize command available from UCSC genome browser.

As of now, the involvement of BRG1 in AS of FLT1 is unclear. It might be, however, an additional factor in the clinical manifestation of preeclampsia. An initial indication is the high expression of BRG1 in the extravillous trophoblast cells and other cell types of the placenta (**Figure 43C**)[168].

Further experiments will be needed to determine the role of *LINC00607* in the placenta and its potential contribution to preeclampsia.

5 Discussion

5.1 Summary and significance of this work

The role of lncRNAs in the CVS and the endothelium is highly diverse and has been subject to a substantial amount of research over the last decade. The identification of lncRNAs as clinically relevant biomarkers and as co-regulatory molecules let to the appreciation of the functional relevance of lncRNAs.

In the present study, *LINC00607* was identified as an endothelial-enriched, human-specific lncRNA. With its distinct functions, *LINC00607* maintains and supports the endothelial homeostasis especially in response to VEGF-A signalling.

In the first part of this study, *LINC00607* was functionally characterized in human endothelial cells. *LINC00607* is highly and specifically expressed in endothelial cells and is differentially regulated in CVDs. Depletion of *LINC00607* resulted in decreased angiogenic sprouting, reduced integration of ECs in a newly formed vascular network *in vivo*, enhanced endothelial migration and differential expression of many important genes for endothelial cell homeostasis. Functionally, *LINC00607* maintains ERG-driven endothelial gene expression programs through BRG1. BRG1 secures stably accessible enhancer regions as well as TSS of ERG target genes, thus enabling transcription of endothelial gene programs.

The second part of this study proposes an additional mode of action for *LINC00607*. The strongly impaired response to VEGF-A after *LINC00607* KO can only be partially explained by its' expression control of ERG target genes. It rather appears that *LINC00607* is involved in the control of alternative splicing of VEGF receptor FLT1. The differential splicing of FLT1 produces the anti-angiogenic soluble isoform of FLT1. Even though further validation is needed to uncover the underlying mechanism, there is the potential of a more general role of *LINC00607* in splicing control through BRG1. As AS of FLT1 is a clinical marker in preeclampsia, *LINC00607* might qualify to be an additional marker for the onset and manifestation of the pregnancy disorder.

Taken together, *LINC00607* is a target in future for molecular therapy in CVD to restore a healthy endothelial phenotype and has the potential to serve as a biomarker in preeclampsia.

5.2 EC phenotype control by *LINC00607*

This study revealed *LINC00607* to be of special importance for endothelial phenotype control and homeostasis. Essentially, *LINC00607* safeguards EC maintenance and angiogenic response to various stimuli, in particular to VEGF-A.

5.2.1 *LINC00607* in the endothelium

LINC00607 was initially selected to be characterized in ECs as it is specifically enriched in ECs. This enrichment was notably pronounced in comparison to other lncRNAs with similar or higher expression in HUVEC. Especially *MALAT1*, the lncRNA with the highest detected expression, is not exclusively expressed in ECs and has been extensively characterized in many different cell types, tissues and in disease contexts[172]. For the majority of lncRNAs, cell type specificity is a common trait, which is the reason they are mainly said to provide tissue specificity to protein function[3,4].

LINC00607 is not conserved beyond the primate lineage. Lack of conservation is not uncommon for lncRNAs but creates an additional challenge in their investigation using translational models [156,157]. In the search for a murine and non-human primate orthologue of *LINC00607,* a general conservation of the locus surrounding *LINC00607* was observed. The flanking genes encoding for Fibronectin (FN1) and Melanoregulin (MREG) are locally conserved. Even though a locus-conserved orthologue of *LINC00607* was found in non-human primates, there were no indications for the existence of a murine lncRNA transcribed from this locus in endothelial cells. This does not exclude the potential existence of a lncRNA with similar function to *LINC00607* in mice. In contrast to protein coding genes, lncRNAs can be not only conserved by the sequence and position on the genome but also by other features including splice sites, secondary structure or short DNA motifs within lncRNA sequences[173–175]. An example is the lncRNA *MALAT1*, which has functional and sequence conservation in other mammals and vertebrates for parts of its secondary structure. The helices present in the human *MALAT1* are conserved, enabling binding of proteins bound by human *MALAT1,* in other species[176]. Another example is the lncRNA *Chaserr*, which influences the CHD2 CRC activity across species. Despite having no notable sequence conservation beyond the vertebrate lineage, its intron-exon structure is conserved to zebrafish (*Danio rerio*) and western clawed frog (*Xenopus tropicalis*)[177].

As a consequence of *LINC00607* locus conservation to the primate but not the murine lineage, *LINC00607's* functional relevance has to be restricted to HUVEC as a cell culture model of the endothelium, to data and tissue from studies in non-human primates and to human disease tissue and to a xenograft mouse model. These experiments uncovered the functional importance of *LINC00607* in ECs.

5.2.2 *LINC00607* in EC dysfunction and endothelial regeneration

LINC00607 is upregulated in ECs from human AVM treated with a β-blocker *ex vivo*, as well as in ECs from *Macaca fascicularis* in regression after high fat induced atherosclerosis and cultured ECs from plaque-containing arteries. All ECs from these tissues share the trait of vascular regeneration, the recovery from EC dysfunction.

AVM is a congenital fast-flow vascular malformation with directly connects arteries and veins, sparing the capillary bed (**Figure 44**)[178]. B-blockers do not specifically treat the AVM and the precise mechanisms by which β-blockers impact on ECs in AVM are not fully understood. Research on hemangioma-derived ECs showed that β-blockers also act on cultured ECs[179,180]. As endothelial β-adrenergic receptors increase cAMP and promote proliferation[181], β-blocker treatment strongly impacted molecular functions in hemangioma-derived ECs[152,179]. These include local vasoconstriction, reduced secretion of angiogenic growth factors and matrix metalloproteinases, as well as decreased proliferation and increased apoptosis of endothelial cells[152].

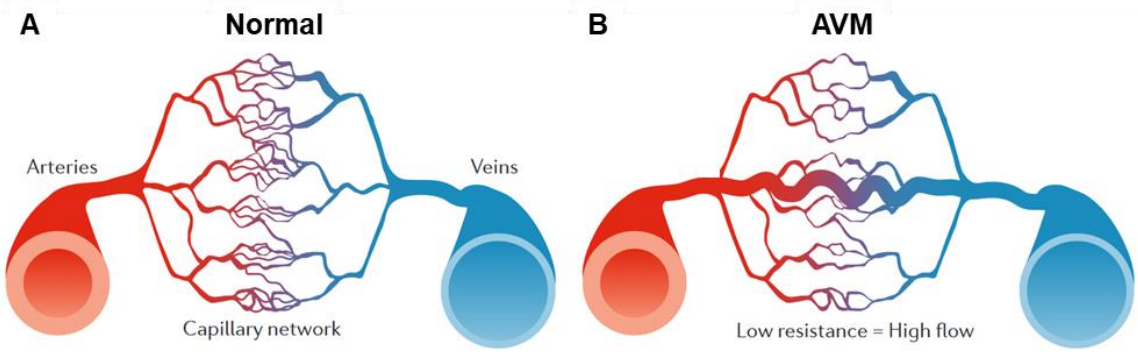

Figure 44 Schematic comparison of a healthy vasculature and AVM
In a normal vasculature, the capillary network connects arteries and veins ensuring optimal oxygen supply to the surrounding tissue. In AVM the capillaries are circumvented by the malformed vessels, resulting in a high blood follow to the venous system and reduced oxygen supply to the tissue. Figure adapted from Lawton *et al*. (2015)[178].

In ECs from *Macaca fascicularis*[127], *LINC00607* was only upregulated in the regression phase after a high fat diet induced atherosclerosis. The same was true for ECs isolated and cultured from plaque containing arteries, which are considered post-atherosclerotic[128]. This indicates the relevance of *LINC00607* for EC phenotype control. *LINC00607* might serve as a factor in vascular regeneration, restoring endothelial homeostasis after atherosclerosis-induced EC dysfunction. A similar expression pattern was previously reported for the atheroprotective lncRNA *MANTIS. MANTIS* depletion results in decreased expression of angiogenesis related genes and it is upregulated in ECs undergoing vascular regeneration[60]. Like *LINC00607*, *MANTIS* regulates endothelial gene expression by interaction with BRG1[60,61]. Collectively, *LINC00607* serves an important atheroprotective function in vascular regeneration, upholding and restoring the endothelial phenotype from EC dysfunction.

5.2.3 Expression control of *LINC00607* by hypoxia and EndMT

The promoter analysis was performed to identify ques for transcriptional regulation of *LINC00607* to get an indication of pathways potentially requiring *LINC00607* function[182]. The promoter analysis identified several important TF binding motifs: e.g. HIF1α/ARNT and SMADs. The experimental evaluation revealed increased endothelial expression of *LINC00607* during EndMT and hypoxia. Additionally, *LINC00607* expression can be induced by TNFα and high glucose in ECs[183].

Hypoxia is an important trigger for angiogenesis and its signalling is, among others, carried out by VEGF-A[90]. Hypoxia is a key feature and significant contributor to acute and chronic cardiovascular diseases[92]. Therefore, hypoxia-mediated induction of *LINC00607* might have evolved in order to maintain the pro-angiogenic endothelial phenotype by strengthening its interaction with BRG1. The close connection between hypoxia signalling, *LINC00607* and angiogenesis was documented in the present work by the upregulation of *LINC00607* in response to DMOG and the decrease in expression after Topoisomerase repression by Acriflavine.

Surprisingly, TGFβ2 and IL1-β-mediated induction of EndMT also resulted in increased expression of *LINC00607*. EndMT is a type of cellular transdifferentiation in which ECs adopt a mesenchymal phenotype[151]. These ECs acquire a migratory and proliferative phenotype and display an altered transcriptome. Expression of EC

marker genes, including PECAM1, VWF and VE-Cadherin is lost during EndMT, while mesenchymal-specific genes, like α-Smooth Muscle Actin, N-Cadherin and type III collagens are induced[184]. The induction of *LINC00607* during EndMT might be a direct result of expression control by the TFs SMAD and MYC (MYC Proto-Oncogene, BHLH Transcription Factor). Binding motifs for both TF were identified in the promoter of *LINC00607*.

SMAD TFs have been reported to actively participate in EndMT[151,185]. MYC, which usually is mutually antagonistic to TGFβ2, cooperatively drives gene expression in epithelial-to-mesenchymal transition (EMT)[186]. EMT similarly relies on TGFβ2 signalling as in EndMT and occurs during tumor invasion and metastasis[187]. In an RNA-Seq dataset after EndMT induction in HUVEC, increased MYC expression was observed (unpulished work of PD Dr. Matthias Leisegang). The high levels of MYC might be a reason for increased *LINC00607* expression during EndMT. Increased *LINC00607* expression under EndMT may point towards additional functions of *LINC00607* beyond the endothelial phenotype.

Indeed, there are reports of *LINC00607* expression in malignant cells. In osteosarcoma cells, *LINC00607* promoted tumor proliferation[188] and *LINC00607* upregulation was reported in doxorubicin-resistant thyroid cancer cells[189]. In lung adenocarcinoma, *LINC00607* expression was decreased[190]. It is possible that under basal conditions *LINC00607* guides BRG1 to ERG target genes to maintain chromatin accessibility and secure the EC phenotype. In case of endothelial dysfunction, *LINC00607* might recruit BRG1 to pro-angiogenic ERG target genes. The role of *LINC00607* during EndMT and in cellular malignancies, however, requires further investigation.

5.2.4 *LINC00607* plays an important role in securing ERG target gene expression in the endothelium

The depletion of *LINC00607* revealed its crucial importance for normal endothelial function, and loss of *LINC00607* disrupted the normal endothelial phenotype. For example, *LINC00607* KO cells integrate less into the newly formed vascular network *in vivo* and displayed reduced angiogenic sprouting and proliferation but enhanced migration. In the RNA-Seq, the expression of typical endothelial pathway genes, such as VEGF receptors, was decreased. Additionally, KO of *LINC00607* reduced

the chromatin accessibility of enhancer and promoter regions of many typical endothelial signature genes, most of which are regulated by the TF ERG.

ERG is highly expressed in mature ECs and an important driver of endothelial gene expression[160]. The ERG core consensus binding motif GGA(A/T) is present in every endothelial promoter and enhancer[85,88,160]. Among the ERG-activated pathways are angiogenesis, blood vessel morphogenesis, platelet activation and blood coagulation[160]. Prominent examples of ERG-regulated genes[88], include von Willebrand factor (VWF), Delta-like protein 4 (DLL4), Claudin 5 (CLDN5), genes of related to VEGF signaling. Interestingly, all these were strongly downregulated after *LINC00607* KO. In *LINC00607* depleted HUVEC, the ETS motif of ERG was identified as less accessible, indicating that *LINC00607* secures ERG motif accessibility in ECs. Importantly, *LINC00607* KO did not affect ERG expression. Differential expression of TF target genes can be deregulated either by differential expression of the TF itself or differential accessibility of the specific TF DNA-binding motif[191]. Because of stable expression of ERG after *LINC00607* KO, the most likely cause for differential expression of ERG target genes is differential accessibility of the ERG binding motif. *LINC00607* might contribute to this by recruiting the chromatin remodeler BRG1 to ERG target sites (**Figure 45**). Recruitment of BRG1 and the SWI/SNF complex, in fact, is a known and reported function of lncRNAs.

LINC00607 is not the first lncRNA reported to impact on ERG transcription programs. *MEG3*, for example, maintains expression of the ERG target gene VEGFR2[192]. Another example is the lncRNA *SENCR* (Smooth Muscle And Endothelial Cell Enriched Migration/Differentiation-Associated LncRNA), which is needed for maintained expression of ERG target genes related to EC migration and angiogenesis[193]. These examples demonstrate that ERG target gene expression control through lncRNAs is a relevant mechanism.

5.2.5 *LINC00607* interaction with BRG1

LINC00607 directed the chromatin remodeling protein BRG1 to promoter regions of ERG target genes in ECs, subsequently ensuring accessible chromatin around the ERG TF binding motif. Changing the accessibility of binding motifs of pioneering TFs and cell specific gene programs is a known function of BRG1 and the SWI/SNF complex[53]. In different cell types, BRG1 exhibits distinct and cell type-specific binding signatures to chromatin as shown by ChIP sequencing[194]. In addition, the

binding signature of BRG1 changes over the course of differentiation. This was shown in venous specification during mouse embryonic development where BRG1 secures the expression of the venous pioneering TF COUP-TFII[195].

BRG1 recruitment to specific genomic loci can be modulated by lncRNAs[3,4]. For example in hepatocytes, the lncRNA *MALAT1* recruits BRG1 to the locus of Interleucin 6 (IL-6) and C-X-C Motif Chemokine Ligand 8 (CXCL8), promoting their expression and thus driving NFκB-dependent inflammation and proliferation[196]. *MALAT1* is as a potential therapeutic target, as silencing of *MALAT1 in vivo* reduced inflammation, proliferation and invasion in hepatocellular carcinoma[196]. Another example is the lncRNA *MANTIS*, which guides BRG1 to activate expression of angiogenesis-related genes and to repress ICAM-1 in ECs[60,61]. These cases show that lncRNAs are able to recruit BRG1 and the SWI/SNF complex to genomic loci to alter the expression of cell type-specific gene programs. Based on the presented results we postulate that *LINC00607* provides BRG1 with an endothelium-specific binding signature to guide it to ERG target genes (**Figure 45**).

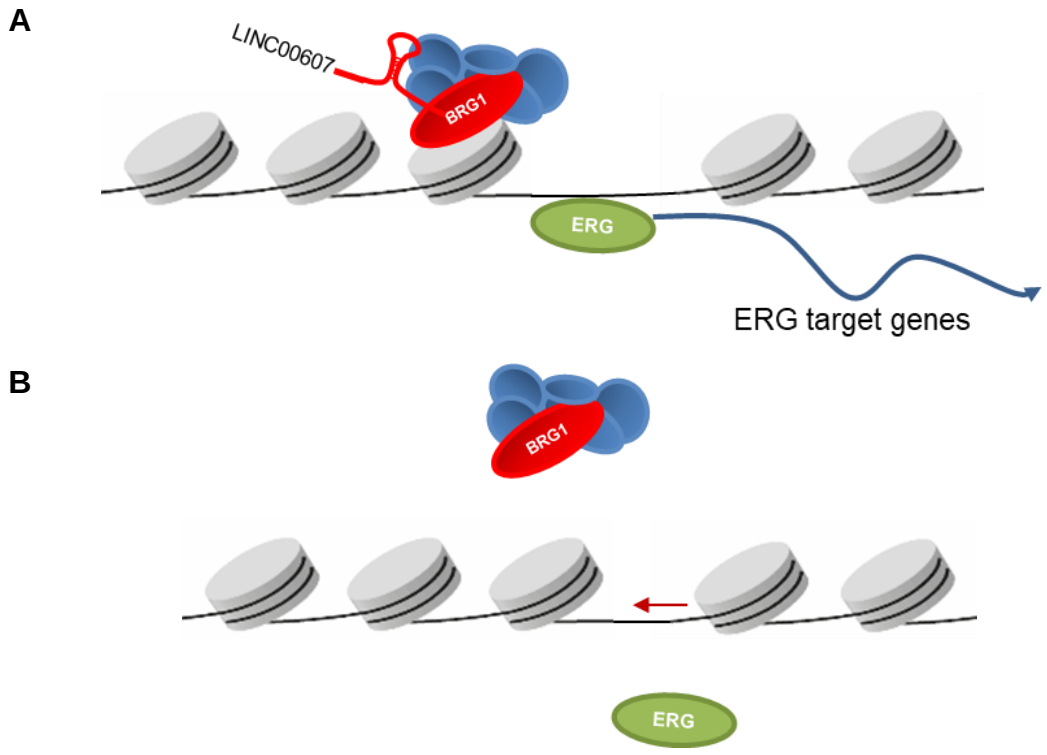

Figure 45 Proposed gene-regulatory mechanism of *LINC00607* in endothelial cells
A-B, Chromatin state in presence (A) and absence (B) of *LINC00607* in HUVEC around ERG binding sites.

5.3 Alternative splicing control by *LINC00607*

In addition to controlling ERG, we also observed an involvement of *LINC00607* in AS. Depletion of *LINC00607* resulted in many AS events as detected by JunctionSeq analysis. AS increases protein diversity from a single gene, which is postulated to facilitate a better adaptation to the microenvironment[66,67]. AS is, however, also implicated in the pathogenesis of many diseases[67,197].

5.3.1 *LINC00607* regulating AS

LINC00607 is not the first lncRNA associated with AS. LncRNAs affect splicing either by binding to the chromatin or pre-mRNA of the gene being transcribed and by binding to splicing factors or chromatin remodeling proteins[79]. A direct binding to pre-mRNA or chromatin is usually reported for *cis*-acting lncRNAs, impacting on their host gene[78]. For *LINC00607,* an intergenic *trans*-acting lncRNA, this mode of action is therefore not common. Given its interaction with BRG1, it is tempting to speculate that also BRG1 may impact on splicing.

5.3.2 AS might be impacted by BRG1 through *LINC00607*

Indeed, a relevance of BRG1 and the SWI/SNF complex for splicing regulation does exist[56,76]. In *Drosophila,* BRG1 binds nascent pre-mRNA, controlling the transcription speed, modulating binding of mRNA with components of the splicing machinery and splicing of certain transcripts[55]. The human BRG1 modulates alternative cleavage site selection by degrading the 3' end Cleavage stimulation factor (CstF)[198]. Mechanistically, BRG1 and the SWI/SNF complex are involved in the early stages of pre-mRNA recognition and formation of the pre-B complex by recruitment of the U2 snRNP[56,76]. The detains, how *LINC00607* together with BRG1 impacts on AS in the endothelium, however, still remain to be identified.

5.3.3 AS of FLT1 in the endothelium and its significance in angiogenic response

We focused our splicing analysis on the VEGF receptor 1 (FLT1). FLT1 AS fits with the observed physiological changes after *LINC00607* KO with a reduced angiogenic response to VEGF. In addition, *LINC00607* is functionally linked to ERG-target gene expression. ERG is a known driver of VEGF inducible genes, but is itself functionally dependent on VEGF signalling[199]. VEGF signalling through the VEGF receptor 2 (VEGFR2) leads to ERK-dependent phosphorylation of ERG, activating it to its maximal functional capacity[199]. Therefore, ERG activity is not only actively driving

angiogenesis gene expression but is also enhanced in its activity by angiogenic signalling[199]. A Reactome Pathway analysis of the *LINC00607* KO RNA-Seq showed strongly decreased expression of VEGF signalling related genes after KO. This decreased expression does not fully explain the strong anti-angiogenic phenotype of *LINC00607* KO ECs. Additionally, FLT1 AS is among the most significant AS events and its AS variants are well studied. Indeed, the soluble isoforms are well characterized on a molecular level and sFLT1 serves as clinical markers in preeclampsia[165,167,169].

The soluble isoform of FLT1 is created by either an inclusion of an alternative exon 15, located within intron 14 or by inclusion of the intron 13. In both cases, inclusion is followed by a premature stop-codon and an intronic poly(A) signal sequences[165]. As a consequence, these transcripts lack the transmembrane and intracellular kinase domain of FLT1 and are therefore secreted as soluble receptors. A mechanism described by Boeckel *et al*. (2011)[165] singled out the splicing proteins Jumonji domain-containing protein 6 (JMJD6) and U2 Small Nuclear RNA Auxiliary Factor 2 (U2AF2) as required for the AS of FLT1[165]. It remains unclear whether *LINC00607* also binds to these proteins to facilitate AS of FLT1.

In terms of pro-angiogenic signalling, membrane-bound FLT1 is not as important as KDR, the VEGFR-2. Although, VEGF-A has a higher binding affinity to FLT1 than KDR, the tyrosine kinase activity of KDR is 10-fold higher than of FLT1 (**Figure 46**)[98,200].

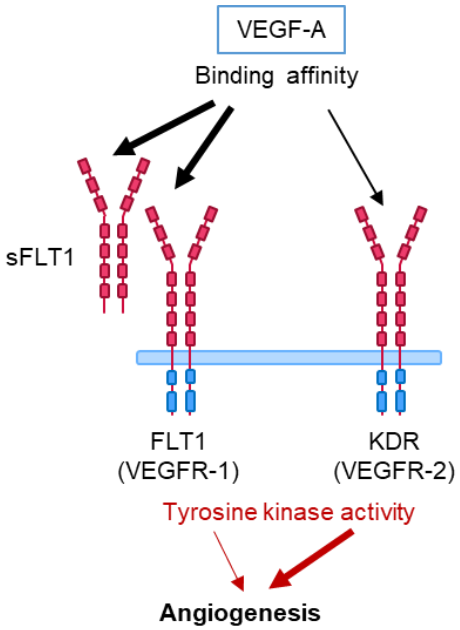

Figure 46 Binding affinity of VEGF-A to FLT1 and KDR and the intensity of resulting downstream signalling
FLT1 and sFLT1 have a stronger affinity for VEGF-A binding compared to KDR but KDR is responsible for the majority of VEGF signalling upon VEGF binding. Therefore, FLT1 is mainly a regulator for VEGF-A accessibility to KDR[200].

Accordingly, FLT1 functions as a regulator of VEGF-A availability to KDR. This mechanism prevents an overshooting response to VEGF-A in ECs and therefore maintains the integrity of the endothelial barrier[84]. This was shown by the embryonic lethality of homozygous FLT1 KO mice at day E8.5 due to a disorganized vascular network and overgrowth of ECs[201]. Like FLT1, KDR was strongly downregulated after *LINC00607* KO, contributing to the low angiogenic response to VEGF stimulation. In contrast to membrane-bound FLT1, soluble FLT1 (sFLT1) has the ability to completely capture VEGF-A in the extracellular space, completely inhibiting the response to VEGF-A[101].

5.3.4 *LINC00607* might be involved in FLT1 AS in preeclampsia

Interestingly, sFLT1 serves as an important mediator of angiogenesis during embryogenesis. By acting on the barrier between maternal and fetal circulation, sFLT1 prevents vascular overgrowth in the placenta[98]. Abnormal overexpression of sFLT1 can lead to manifestation of preeclampsia, one of the most prevalent and serious pregnancy diseases[167]. Additionally, sFLT1 serum concentration correlate with the severity of preeclampsia[166]. As a consequence, sFLT1 is a clinical preeclamsia-marker in maternal serum[167]. This makes the understanding of underlying mechanism of AS of FLT1 in the creation of sFLT1 even more important

as preeclampsia is the cause of up to 8% of maternal deaths and approximately 40% of fetal mortality[167].

In the first stage of preeclampsia, vascularization of the placenta is disturbed and, if left untreated, manifests in maternal hypertension and proteinuria, as well as death of fetus and/or mother[167]. The AS of sFLT1 mainly occurs in the extravillous trophoblasts and fetal placenta syncytiotrophoblas, cell types which strongly express *LINC00607*[168,169]. The high expression of *LINC00607* in fetal cell types was unexpected, given the past focus on adult cells and the exclusive endothelial expression in the adult organs. Interestingly, BRG1, functionally linked to *LINC00607* in adult ECs, is expressed in the cell types responsible for sFLT1 production during preeclampsia[168]. This further links the mechanistic regulation of AS of FLT1 to *LINC00607*. Additionally, BRG1 was shown to be bound to the intron 13, included in the sFLT1-i13 soluble isoform by iCLIP-Seq. In the process of splicing, BRG1 is involved in the early assembly of the spliceosome[56,76] and therefore is bound to the site of co-transcriptional splicing reactions. BRG1 might be associated to FLT1 AS but needs to be validated further.

Further analysis is needed to functionally link *LINC00607*, BRG1 and AS of FLT1 but the preliminary results hint to an important and impactful role in the onset and manifestation of preeclampsia.

5.4 Outlook and future perspectives

Endothelial lncRNAs have diverse functions, impacting on numerous aspects ranging from homeostasis to differentiation. Expanding the knowledge of endothelial-specific lncRNAs and their contribution to CVDs may allow for the developement of novel treatment modalities.

We could show an association and functional dependence of ERG-driven endothelial gene programs to *LINC00607*-guided BRG1 chromatin remodeling. *LINC00607* expression was increased in ECs recovering from dysfunction such as atherosclerosis. Therefore, it will be interesting to study the dependence of the BRG1-chromatin association on *LINC00607*.

In addition, it is still unclear how *LINC00607* facilitates binding to BRG1 and how BRG1 is being recruited to specific chromatin sites. To determine this, investigation into whether *LINC00607* has a specific BRG1 binding motif and where *LINC00607*

binds the protein should be carried out. Interestingly, the binding specificity of RNA to unconventional RNA binding proteins, lacking a canonical RNA binding domain, has been challenged recently[202]. BRG1 has a reported RNA binding domain, the AT-hook[203] but lncRNA binding has been observed also to the non-RNA binding motifs of BRG1. *Evf2* binds the HSA and BRK domains, known for protein interaction and helicase activity of BRG1[65]. *Mhrt* has been shown to bind the HELICc domain, a domain involved in binding and unwinding chromatinized DNA[204]. A more systematic approach to this aspect is needed, which could involve binding experiments, such as RIP (RNA Immunoprecipitation)-Seq using BRG1- and *LINC00607* deletion mutants.

We also found evidence of an involvement of *LINC00607* in AS. This function also appears to require BRG1, and affects important genes, like FLT1. The fact that there were many more transcripts identified as alternatively spliced upon either *LINC00607* or BRG1 depletion hints to a general role of the two molecules in AS. Examples include SYNPO (Synaptopodin), which is crucial for laminar flow induced wound healing[205] and MAP4K4 (Mitogen-Activated Protein Kinase Kinase Kinase Kinase 4), which promotes recruitment of immune cells in atherosclerosis[206]. Both proteins are crucial for normal endothelial function and their response to injury. The investigation of other alternatively spliced transcripts will provide insights into the mechanism by which AS is regulated by BRG1 and *LINC00607* and their implication in endothelial function.

For such studies, understanding the binding specifications of *LINC00607* to BRG1 is valuable. The association of *LINC00607* to splicing factors was not investigated but will provide crucial information in this regard. To identify *LINC00607*-associated splicing factors, a mass spectrometry analysis after *LINC00607* antisense-oligo pulldown could be performed.

An importation functional connection linking *LINC00607* to sFLT1 is the unexpectedly high expression of *LINC00607* and BRG1 in the extravillous trophoblast and fetal placenta syncytiotrophoblast, tissues giving rise to sFLT1 during pregnancy and preeclampsia. If the results of our cell-based models can be confirmed in clinical samples, such as umbilical blood, blood of preeclampsia patients or scRNA-Seq (single cell RNA-Sequencing) data of placenta tissue, *LINC00607* may have the potential as a clinical marker for preeclampsia.

6 Deutsche Zusammenfassung

Einleitung

Lange nicht-kodierende RNAs (lncRNAs) sind definiert als Transkripte mit einer Länge von mehr als 200 Nukleotiden, die nicht in Proteine übersetzt werden. Als biologisch aktive Moleküle interagieren lncRNAs mit Proteinen, DNA und RNA und spielen eine Rolle in der Genomorganisation, Genexpression und Zellstruktur. Im Zellkern beeinflussen lncRNAs die Transkription, indem sie die Bindung von Transkriptionsfaktoren (TFs) an das Chromatin modulieren, oder die Rekrutierung von Komplexen zur Umgestaltung des Chromatins verändern. Chromatin-Remodelling Komplexe (CRC) verändern die Zugänglichkeit des Chromatins u.a. durch Verschieben oder Entfernen von Nukleosomen. Einer dieser CRCs ist der SWI/SNF Komplex, dessen Aktivität von der zentralen ATPase BRG1 abhängt und durch lncRNAs beeinflusst werden kann. Ein anderer wichtiger zellulärer Prozess, der von lncRNAs mitgesteuert wird ist alternatives Splicing (AS). Splicing beschreibt den Prozess der Bearbeitung von prä-mRNA zu reifer mRNA. Dabei werden Introns entfernt und kodierende Exons vereint.

Diese Prozesse sind besonders wichtig in Endothelzellen. Sie bilden die innere einzellige Schicht der Blutgefäße, die als semipermeable Barriere dient, um die Gefäßwand vom zirkulierenden Blut zu trennen. Das Endothel ist entscheidend für eine angemessene Anpassung an verschiedene physiologische und pathologische Reize, wie zum Beispiel Gewebehypoxie, die Angiogenese in umliegenden Gefäßen auslöst. Fehlgeleitete Reaktionen auf diese Reize, in Form von Chromatin Umgestaltung und alternativem Splicing, können zur Entwicklung von endothelialer Dysfunktion führen, die eine Grundlage für viele Herz-Kreislauf-Erkrankungen darstellt.

Die vielfältigen Funktionen und Expression von lncRNAs sind meist zelltypspezifisch. Der Fokus dieser Arbeit liegt auf der lncRNA *LINC00607*. Diese lncRNA weist eine starke endothelzellspezifische Expression auf und reguliert die Aktivität des Chromatin-Remodellers BRG1 sowie AS des VEGF Rezeptors FLT1.

LINC00607 spielt eine wichtige Rolle in der Aufrechterhaltung des endothelspezifischen Geno- und Phänotypen

LINC00607 wurde als eine lange nicht-kodierende intergene RNA identifiziert, die eine hohe Expression in Endothelzellen hat und in fast keinem anderen Zelltyp exprimiert wird. *LINC00607* weist auch eine veränderte Expression in Herz-Kreislauf-Erkrankungen auf: in postatherosklerotischen Endothelzellen und in Propranolol behandelten Atheriovenösen Missbildungen war die *LINC00607* Expression weiter gesteigert. Eine Promoteranalyse identifizierte DNA-Bindestellen für die Transkriptionsfaktoren HIF1A, ARNT und SMADs. Die Expressionsregulation durch diese TFs konnte durch Inkubation von HUVEC (humane Nabelschnurvenen-Endothelzellen) in Hypoxie und mit der Induktion von EndMT (Endothelial-Mesenchymale Transition) validiert werden. In beiden Fällen kam es zu einer erhöhten *LINC00607* Expression.

Um die Rolle von *LINC00607* in Endothelzellen besser zu verstehen, wurden Knockdown- und Deletionsversuche mittels siRNA und CRISPR/Cas9 durchgeführt. Physiologische Assays wurden verwendet, um die Auswirkungen auf die Funktion der Zellen zu bewerten. Die Deletion von *LINC00607* führte zu einer geringeren Integration von Endothelzellen in ein neu-gebildetes vaskuläres Netzwerk *in vivo* und einer verstärkten Migration der Endothelzellen. Zudem kam es zu einer verminderten angiogenen Sprossung nach VEGF Stimulation in einem Spheroid-Auswuchs Assay, die jedoch durch die Überexpression von *LINC00607* wiederhergestellt werden konnte. RNA-Sequenzierung (RNA-Seq) wurde durchgeführt, um die molekularen Veränderungen der Genexpression in *LINC00607* KO- und Kontrollzellen zu untersuchen. Dabei wurde festgestellt, dass die Expression mehrerer endothelialer Genprogramme stark abnahm, einschließlich der Signalwege des vaskulären endothelialen Wachstumsfaktors (VEGF), der extrazellulären Matrixorganisation und der Zelladhäsionsmoleküle wie ITGA10 und PECAM1. Auf der anderen Seite wurden Gene, die mit DNA-Replikation und dem Zellzyklus in Verbindung stehen, verstärkt exprimiert. Diese Ergebnisse deuten darauf hin, dass Endothelzellen ohne *LINC00607* ihren Endothelzellcharakter verlieren und scheinbar den sonst starren Zellverband verlassen, um zu migrieren und zu proliferieren. Diese vielfältigen Veränderungen der Genexpressionen können nur partiell durch die Deletion von *LINC00607* erklärt werden, weshalb eine ATAC Sequenzierung (ATAC-Seq) durchgeführt wurde. Auf diese Weise können

Veränderungen der Zugänglichkeit des Chromatins festgestellt werden. Die ATAC-Seq wurde einer DNA Motif Anreicherungsanalyse unterzogen, die differentiell zugängliche TF-Erkennungsmotife der DNA nach *LINC00607* KO identifizierte. Unter den Motifen, mit dem stärksten Rückgang der Zugänglichkeit befand sich das Erkennungsmotif für den TF ERG (ETS Transkriptions Faktor). Dieser TF ist Teil der Gruppe der ETS TFs, die eine der wichtigsten TF Gruppen in Endothelzellen ist. Sie kontrolliert die Differenzierung der Endothelvorläuferzellen zu Endothelzellen und vor allem ERG reguliert die Expression aller wichtigen Gene, die in der endothelialen Homöostase benötigt werden. Dies ist bekannt, da das ERG-DNA-Bindemotif in jedem Promoter der endothelspezifischen Gene zu finden ist. Die verminderte Zugänglichkeit des ERG-Bindemotifs in Endothelzellen nach *LINC00607* KO könnte die vielfältigen Veränderungen der Genexpression erklären.

Es ist unwahrscheinlich, dass *LINC00607* diese Veränderungen direkt vermittelt. Neben vielen anderen Funktionen interagieren lncRNAs mit CRCs, die für Veränderungen der Chromatin-Zugänglichkeit bewirken. Experimentell konnte in der vorliegenden Studie eine Interaktion von *LINC00607* mit der ATPase BRG1 nachgewiesen werden. Aufgrund der signifikanten Überlappung der von BRG1 kontrollierten Gene, der Gene mit ERG-Bindestelle und der Gene, bei denen nach Deletion von *LINC00607* eine signifikante Veränderung der Expression festgestellt wurde, wurde der folgende Mechanismus postuliert: *LINC00607* rekrutiert BRG1 zu den von ERG kontrollierten Genen, um dort eine stabile und offene Chromatinkonformation zu ermöglichen. Als Folge erhält *LINC00607* die Expression endothelspezifischer Geneprogramme in Endothelzellen. Auf der Grundlage der vorgestellten Ergebnisse postulieren wir, dass *LINC00607* BRG1 mit einer endothelspezifischen Bindungssignatur ausstattet, die es erlaubt BRG1 zu ERG-Zielgenen zu leiten. Weitere Erforschung der Interaktion von *LINC00607* und BRG1 könnte ein tiefergehendes Verständnis für die Entstehung und den Verlauf verschiedener Herz-Kreislauf-Erkrankungen bringen. Diese könnte dazu beitragen neue diagnostische Verfahren und Therapien dieser Erkrankungen zu entwickeln. In der Tat, wurden bereits zahlreiche andere lncRNAs als klinisch relevante Biomarker identifiziert: Die lncRNA *ANRIL* wird als Biomarker für Atherosklerose genutzt, während *MIAT* und *HOTAIR* Biomarker für Myokardinfarkt und *LIPCAR* für Herzinsuffizienz sind. Darüber hinaus wurde einer Reihe verschiedener lncRNAs eine Rolle bei der Entstehung und dem Fortschreiten von Herz-Kreislauf-

Erkrankungen nachgewiesen. Eine geänderte lncRNA Expression kann dabei den Krankheitsverlauf beeinflussen. In diesem Kontext konnte auch die Rekrutierung von BRG1 zur gezielten Expressionskontrolle zelltypspezifischer Genprogrammen durch die lncRNA *MALAT1* gezeigt werden. In Leberzellen rekrutiert *MALAT1* BRG1 an den Lokus von Interleucin 6 (IL-6) und C-X-C-Motiv-Chemokin-Ligand 8 (CXCL8), fördert deren Expression und treibt so die NFκB-abhängige Entzündung und Proliferation an. *MALAT1* Knockout führte zu einer reduzierten Entzündung, Proliferation und Invasion von Leberzellkarzinomzellen, weshalb *MALAT1* ein potenzieller therapeutischer Angriffspunkt in der Therapie von Leberkrebs ist. Im Kontext der vorliegenden Arbeit wurde für *LINC00607* die funktionelle Bedeutung im Endothel aufgedeckt. In einem nächsten Schritt könnte die Rolle von *LINC00607* im Kontext kardiovaskulärer Erkrankungen erforscht werden.

LINC00607 ist am alternativem Splicing (AS) des VEGF Rezeptors FLT1 beteiligt

Der Knockout von *LINC00607* führte zu einer Vielzahl von Veränderungen in Endothelzellen. Eine weiterführende Analyse der Expressionsdaten nach *LINC00607*-KO zeigte auch eine umfangreiche Veränderung des Splicings verschiedener mRNAs. Besonders interessant war, dass der VEGF-Rezeptor FLT1 zu den am stärksten alternativ gesplicten mRNAs gehörte. Diese Splicing-Analyse zeigte, dass durch das Splicing eine Verschiebung in den Häufigkeiten der Rezeptorisoformen stattfand. Neben der funktionell wichtigsten membrangebundenen Isoform FLT1 wurde auch die lösliche Isoform (sFLT1) des Rezeptors gebildet. Diese lösliche Isoform, der die intrazelluläre und Transmembrandomäne fehlt, wird sezerniert und bindet VEGF im Sinne eines Decoy-Rezeptors, was die VEGF-induzierte Angiogenese hemmt. Die Anwesenheit der löslichen FLT1-Isoform wurde experimentell bestätigt. Durch Neutralisierung der sFLT1-Isoform mittels eines Antikörpers konnte die beeinträchtigte endotheliale Sprossung nach *LINC00607*-Knockout wiederhergestellt werden.

Nach der Validierung des AS blieb die Frage, wie die lncRNA *LINC00607* Einfluss auf Splicing nehmen kann. BRG1, der Interaktionspartner von *LINC00607*, wurde bereits mit AS in Verbindung gebracht. Deshalb wurden RNA-Seq Daten nach BRG1 Knockdown mittels siRNA in HUVEC ebenfalls einer Splicing Analyse unterzogen. Auch nach dem Knockdown von BRG1 wurde eine Veränderung des

FLT1-Splicings beobachtet, wobei die Bildung der löslichen Isoform bevorzugt war. Darüber hinaus konnten auch andere alternativ gesplicte mRNAs in beiden Sequenzierungen nachgewiesen werden. Dies legt nahe, dass sowohl BRG1 als auch *LINC00607* möglicherweise eine grundsätzliche Funktion bei der Regulation von Splicing haben.

sFLT1 ist vor allem als klinischer Marker der hypertensiven Schwangerschaftserkrankung Präeklampsie bekannt. Dies legt eine potentielle Rolle von *LINC00607* bei Präeklampsie nahe. Um erste Erkenntnisse darüber zu gewinnen, ob *LINC00607* während der Schwangerschaft und fötalen Entwicklung eine Wirkung entfalten kann, wurde die Expression von *LINC00607* in öffentlich verfügbaren Einzelzell-RNA-Sequenzierungsdaten untersucht. Tatsächlich war *LINC00607* in extravillösen Trophoblastenzellen stark exprimiert, in denen während der klinischen Manifestierung von Präeklampsie sFLT1 Splicing hauptsächlich gebildet wird. Im Falle der FLT1-AS sind weitere Analysen erforderlich, um *LINC00607*, BRG1 und die AS von FLT1 funktionell zu verknüpfen. Ein wichtiger Zusammenhang zwischen *LINC00607* und sFLT1 ist die unerwartet hohe Expression von *LINC00607* im extravillösen Trophoblasten. Wenn sich die in unseren zellbasierten Modellen gewonnenen Ergebnisse in klinischen Proben, wie Nabelschnurblut, Blut von Präeklampsie-Patientinnen oder Plazentagewebe, bestätigen, hat *LINC00607* das Potenzial, zusätzlich zu sFLT1 als klinischer Marker für Präeklampsie eingeführt zu werden. Dies könnte eine verbesserte Diagnose und/oder Behandlung von Präeklampsie nach sich ziehen.

7 References

1. Lizio, M., Harshbarger, J., Shimoji, H., Severin, J., Kasukawa, T., Sahin, S., Abugessaisa, I., Fukuda, S., Hori, F., Ishikawa-Kato, S., et al. (2015). Gateways to the FANTOM5 promoter level mammalian expression atlas. Genome Biol *16*, 22. 10.1186/s13059-014-0560-6.

2. Uchida, S., and Dimmeler, S. (2015). Long Noncoding RNAs in Cardiovascular Diseases. Circ Res *116*, 737–750. 10.1161/CIRCRESAHA.116.302521.

3. Oo, J.A., Brandes, R.P., and Leisegang, M.S. (2022). Long non-coding RNAs: novel regulators of cellular physiology and function. Pflugers Arch *474*, 191–204. 10.1007/s00424-021-02641-z.

4. Statello, L., Guo, C.-J., Chen, L.-L., and Huarte, M. (2021). Gene regulation by long non-coding RNAs and its biological functions. Nat Rev Mol Cell Biol *22*, 96–118. 10.1038/s41580-020-00315-9.

5. Mattick, J.S., Amaral, P.P., Carninci, P., Carpenter, S., Chang, H.Y., Chen, L.-L., Chen, R., Dean, C., Dinger, M.E., Fitzgerald, K.A., et al. (2023). Long non-coding RNAs: definitions, functions, challenges and recommendations. Nat Rev Mol Cell Biol. 10.1038/s41580-022-00566-8.

6. Wu, H., Yang, L., and Chen, L.-L. (2017). The Diversity of Long Noncoding RNAs and Their Generation. Trends in Genetics *33*, 540–552. 10.1016/j.tig.2017.05.004.

7. Derrien, T., Johnson, R., Bussotti, G., Tanzer, A., Djebali, S., Tilgner, H., Guernec, G., Martin, D., Merkel, A., Knowles, D.G., et al. (2012). The GENCODE v7 catalog of human long noncoding RNAs: Analysis of their gene structure, evolution, and expression. Genome Res. *22*, 1775–1789. 10.1101/gr.132159.111.

8. Di Agostino, S., Vahabi, M., Turco, C., and Fontemaggi, G. (2022). Secreted Non-Coding RNAs: Functional Impact on the Tumor Microenvironment and Clinical Relevance in Triple-Negative Breast Cancer. ncRNA *8*, 5. 10.3390/ncrna8010005.

9. Graf, J., and Kretz, M. (2020). From structure to function: Route to understanding lncRNA mechanism. BioEssays *42*, 2000027. 10.1002/bies.202000027.

10. Pheasant, M., and Mattick, J.S. (2007). Raising the estimate of functional human sequences. Genome Res. *17*, 1245–1253. 10.1101/gr.6406307.

11. Necsulea, A., Soumillon, M., Warnefors, M., Liechti, A., Daish, T., Zeller, U., Baker, J.C., Grützner, F., and Kaessmann, H. (2014). The evolution of lncRNA repertoires and expression patterns in tetrapods. Nature *505*, 635–640. 10.1038/nature12943.

12. Huarte, M., and Marín-Béjar, O. (2015). Long noncoding RNAs: from identification to functions and mechanisms. AGG, 257. 10.2147/AGG.S61842.

13. de Koning, A.P.J., Gu, W., Castoe, T.A., Batzer, M.A., and Pollock, D.D. (2011). Repetitive Elements May Comprise Over Two-Thirds of the Human Genome. PLoS Genet *7*, e1002384. 10.1371/journal.pgen.1002384.

14. Kelley, D., and Rinn, J. (2012). Transposable elements reveal a stem cell-specific class of long noncoding RNAs. Genome Biol *13*, R107. 10.1186/gb-2012-13-11-r107.

15. Johnson, R., and Guigó, R. (2014). The RIDL hypothesis: transposable elements as functional domains of long noncoding RNAs. RNA *20*, 959–976. 10.1261/rna.044560.114.

16. Morlando, M., Ballarino, M., and Fatica, A. (2015). Long Non-Coding RNAs: New Players in Hematopoiesis and Leukemia. Front. Med. *2*. 10.3389/fmed.2015.00023.

17. van Heesch, S., Witte, F., Schneider-Lunitz, V., Schulz, J.F., Adami, E., Faber, A.B., Kirchner, M., Maatz, H., Blachut, S., Sandmann, C.-L., et al. (2019). The Translational Landscape of the Human Heart. Cell *178*, 242-260.e29. 10.1016/j.cell.2019.05.010.

18. Olins, D.E., and Olins, A.L. (2003). Chromatin history: our view from the bridge. Nat Rev Mol Cell Biol *4*, 809–814. 10.1038/nrm1225.

19. Felsenfeld, G., and Groudine, M. (2003). Controlling the double helix. Nature *421*, 448–453. 10.1038/nature01411.

20. Khorasanizadeh, S. (2004). The Nucleosome. Cell *116*, 259–272. 10.1016/S0092-8674(04)00044-3.

21. Bannister, A.J., and Kouzarides, T. (2011). Regulation of chromatin by histone modifications. Cell Res *21*, 381–395. 10.1038/cr.2011.22.

22. Mersfelder, E.L., and Parthun, M.R. (2006). The tale beyond the tail: histone core domain modifications and the regulation of chromatin structure. Nucleic Acids Research *34*, 2653–2662. 10.1093/nar/gkl338.

23. Tan, M., Luo, H., Lee, S., Jin, F., Yang, J.S., Montellier, E., Buchou, T., Cheng, Z., Rousseaux, S., Rajagopal, N., et al. (2011). Identification of 67 Histone Marks and Histone Lysine Crotonylation as a New Type of Histone Modification. Cell *146*, 1016–1028. 10.1016/j.cell.2011.08.008.

24. Allis, C.D., and Jenuwein, T. (2016). The molecular hallmarks of epigenetic control. Nat Rev Genet *17*, 487–500. 10.1038/nrg.2016.59.

25. Hyun, K., Jeon, J., Park, K., and Kim, J. (2017). Writing, erasing and reading histone lysine methylations. Exp Mol Med *49*, e324–e324. 10.1038/emm.2017.11.

26. Margueron, R., and Reinberg, D. (2011). The Polycomb complex PRC2 and its mark in life. Nature *469*, 343–349. 10.1038/nature09784.

27. Brockdorff, N. (2017). Polycomb complexes in X chromosome inactivation. Phil. Trans. R. Soc. B *372*, 20170021. 10.1098/rstb.2017.0021.

28. Tu, S., Yuan, G.-C., and Shao, Z. (2017). The PRC2-binding long non-coding RNAs in human and mouse genomes are associated with predictive sequence features. Sci Rep *7*, 41669. 10.1038/srep41669.

29. Maclary, E., Hinten, M., Harris, C., Sethuraman, S., Gayen, S., and Kalantry, S. (2017). PRC2 represses transcribed genes on the imprinted inactive X chromosome in mice. Genome Biol *18*, 82. 10.1186/s13059-017-1211-5.

30. Wu, C.-S., Yu, C.-Y., Chuang, C.-Y., Hsiao, M., Kao, C.-F., Kuo, H.-C., and Chuang, T.-J. (2014). Integrative transcriptome sequencing identifies *trans* -splicing events with important roles in human embryonic stem cell pluripotency. Genome Res. *24*, 25–36. 10.1101/gr.159483.113.

31. Yap, K.L., Li, S., Muñoz-Cabello, A.M., Raguz, S., Zeng, L., Mujtaba, S., Gil, J., Walsh, M.J., and Zhou, M.-M. (2010). Molecular Interplay of the Noncoding RNA ANRIL and Methylated Histone H3 Lysine 27 by Polycomb CBX7 in Transcriptional Silencing of INK4a. Molecular Cell *38*, 662–674. 10.1016/j.molcel.2010.03.021.

32. Holdt, L.M., Hoffmann, S., Sass, K., Langenberger, D., Scholz, M., Krohn, K., Finstermeier, K., Stahringer, A., Wilfert, W., Beutner, F., et al. (2013). Alu Elements in ANRIL Non-Coding RNA at Chromosome 9p21 Modulate Atherogenic Cell Functions through Trans-Regulation of Gene Networks. PLoS Genet *9*, e1003588. 10.1371/journal.pgen.1003588.

33. Blanco, M.R., and Guttman, M. (2017). Re-evaluating the foundations of lncRNA-Polycomb function. EMBO J *36*, 964–966. 10.15252/embj.201796796.

34. Cairns, B.R. (2007). Chromatin remodeling: insights and intrigue from single-molecule studies. Nat Struct Mol Biol *14*, 989–996. 10.1038/nsmb1333.

35. Clapier, C.R., and Cairns, B.R. (2009). The Biology of Chromatin Remodeling Complexes. Annu. Rev. Biochem. *78*, 273–304. 10.1146/annurev.biochem.77.062706.153223.

36. Becker, P.B., and Workman, J.L. (2013). Nucleosome Remodeling and Epigenetics. Cold Spring Harbor Perspectives in Biology *5*, a017905–a017905. 10.1101/cshperspect.a017905.

37. Clapier, C.R., Iwasa, J., Cairns, B.R., and Peterson, C.L. (2017). Mechanisms of action and regulation of ATP-dependent chromatin-remodelling complexes. Nat Rev Mol Cell Biol *18*, 407–422. 10.1038/nrm.2017.26.

38. Dutta, A., Sardiu, M., Gogol, M., Gilmore, J., Zhang, D., Florens, L., Abmayr, S.M., Washburn, M.P., and Workman, J.L. (2017). Composition and Function of Mutant Swi/Snf Complexes. Cell Reports *18*, 2124–2134. 10.1016/j.celrep.2017.01.058.

39. Kasten, M.M., Clapier, C.R., and Cairns, B.R. (2011). SnapShot: Chromatin Remodeling:SWI/SNF. Cell *144*, 310-310.e1. 10.1016/j.cell.2011.01.007.

40. Bevilacqua, A., Willis, M.S., and Bultman, S.J. (2014). SWI/SNF chromatin-remodeling complexes in cardiovascular development and disease. Cardiovascular Pathology *23*, 85–91. 10.1016/j.carpath.2013.09.003.

41. Sokpor, G., Xie, Y., Rosenbusch, J., and Tuoc, T. (2017). Chromatin Remodeling BAF (SWI/SNF) Complexes in Neural Development and Disorders. Front. Mol. Neurosci. *10*, 243. 10.3389/fnmol.2017.00243.

42. Doroshevskiĭ, I.L. (1979). ["Isolated" volvulus of the small intestine in newborn infants and its surgical treatment]. Vestn Khir Im I I Grek *122*, 91–96.

43. Stern, M., Jensen, R., and Herskowitz, I. (1984). Five SWI genes are required for expression of the HO gene in yeast. Journal of Molecular Biology *178*, 853–868. 10.1016/0022-2836(84)90315-2.

44. Mohrmann, L., and Verrijzer, C.P. (2005). Composition and functional specificity of SWI2/SNF2 class chromatin remodeling complexes. Biochimica et Biophysica Acta (BBA) - Gene Structure and Expression *1681*, 59–73. 10.1016/j.bbaexp.2004.10.005.

45. Romero, O.A., and Sanchez-Cespedes, M. (2014). The SWI/SNF genetic blockade: effects in cell differentiation, cancer and developmental diseases. Oncogene *33*, 2681–2689. 10.1038/onc.2013.227.

46. Lu, C., and Allis, C.D. (2017). SWI/SNF complex in cancer. Nat Genet *49*, 178–179. 10.1038/ng.3779.

47. Centore, R.C., Sandoval, G.J., Soares, L.M.M., Kadoch, C., and Chan, H.M. (2020). Mammalian SWI/SNF Chromatin Remodeling Complexes: Emerging Mechanisms and Therapeutic Strategies. Trends in Genetics *36*, 936–950. 10.1016/j.tig.2020.07.011.

48. Karasaki, T., Moore, D.A., Veeriah, S., Naceur-Lombardelli, C., Toncheva, A., Magno, N., Ward, S., Bakir, M.A., Watkins, T.B.K., Grigoriadis, K., et al. (2023). Evolutionary characterization of lung adenocarcinoma morphology in TRACERx. Nat Med *29*, 833–845. 10.1038/s41591-023-02230-w.

49. Negrao, M.V., Araujo, H.A., Lamberti, G., Cooper, A.J., Akhave, N.S., Zhou, T., Delasos, L., Hicks, J.Kevin., Aldea, M., Minuti, G., et al. (2023). Co-mutations and KRAS G12C inhibitor efficacy in advanced NSCLC. Cancer Discovery, CD-22-1420. 10.1158/2159-8290.CD-22-1420.

50. Stanton, B.Z., Hodges, C., Calarco, J.P., Braun, S.M.G., Ku, W.L., Kadoch, C., Zhao, K., and Crabtree, G.R. (2017). Smarca4 ATPase mutations disrupt direct eviction of PRC1 from chromatin. Nat Genet *49*, 282–288. 10.1038/ng.3735.

51. Kadam, S., and Emerson, B.M. (2003). Transcriptional Specificity of Human SWI/SNF BRG1 and BRM Chromatin Remodeling Complexes. Mol Cell *11*, 377–389. 10.1016/S1097-2765(03)00034-0.

52. Wu, Q., Lian, J.B., Stein, J.L., Stein, G.S., Nickerson, J.A., and Imbalzano, A.N. (2017). The BRG1 ATPase of human SWI/SNF chromatin remodeling enzymes as a driver of cancer. Epigenomics *9*, 919–931. 10.2217/epi-2017-0034.

53. Bieluszewski, T., Prakash, S., Roulé, T., and Wagner, D. (2023). The Role and Activity of SWI/SNF Chromatin Remodelers. Annu. Rev. Plant Biol. *74*, annurev-arplant-102820-093218. 10.1146/annurev-arplant-102820-093218.

54. Banine, F., Bartlett, C., Gunawardena, R., Muchardt, C., Yaniv, M., Knudsen, E.S., Weissman, B.E., and Sherman, L.S. (2005). SWI/SNF Chromatin-Remodeling Factors Induce Changes in DNA Methylation to Promote Transcriptional Activation. Cancer Research *65*, 3542–3547. 10.1158/0008-5472.CAN-04-3554.

55. Tyagi, A., Ryme, J., Brodin, D., Östlund Farrants, A.K., and Visa, N. (2009). SWI/SNF Associates with Nascent Pre-mRNPs and Regulates Alternative Pre-mRNA Processing. PLoS Genet *5*, e1000470. 10.1371/journal.pgen.1000470.

56. Gañez-Zapater, A., Mackowiak, S.D., Guo, Y., Tarbier, M., Jordán-Pla, A., Friedländer, M.R., Visa, N., and Östlund Farrants, A.-K. (2022). The SWI/SNF subunit BRG1 affects alternative splicing by changing RNA binding factor interactions with nascent RNA. Mol Genet Genomics *297*, 463–484. 10.1007/s00438-022-01863-9.

57. Bultman, S., Gebuhr, T., Della Yee, La Mantia, C., Nicholson, J., Gilliam, A., Randazzo, F., Metzger, D., Chambon, P., Crabtree, G., et al. (2000). A Brg1 Null Mutation in the Mouse Reveals Functional Differences among Mammalian SWI/SNF Complexes. Mol Cell *6*, 1287–1295. 10.1016/s1097-2765(00)00127-1.

58. Reisman, D., Glaros, S., and Thompson, E.A. (2009). The SWI/SNF complex and cancer. Oncogene *28*, 1653–1668. 10.1038/onc.2009.4.

59. Trotter, K.W., and Archer, T.K. (2008). The BRG1 transcriptional coregulator. Nucl Recept Signal *6*, nrs.06004. 10.1621/nrs.06004.

60. Leisegang, M.S., Fork, C., Josipovic, I., Richter, F.M., Preussner, J., Hu, J., Miller, M.J., Epah, J., Hofmann, P., Günther, S., et al. (2017). Long Noncoding RNA MANTIS Facilitates Endothelial Angiogenic Function. Circulation *136*, 65–79. 10.1161/CIRCULATIONAHA.116.026991.

61. Leisegang, M.S., Bibli, S.-I., Günther, S., Pflüger-Müller, B., Oo, J.A., Höper, C., Seredinski, S., Yekelchyk, M., Schmitz-Rixen, T., Schürmann, C., et al. (2019). Pleiotropic effects of laminar flow and statins depend on the Krüppel-like factor-induced lncRNA MANTIS. Eur Heart J *40*, 2523–2533. 10.1093/eurheartj/ehz393.

62. Kawaguchi, T., Tanigawa, A., Naganuma, T., Ohkawa, Y., Souquere, S., Pierron, G., and Hirose, T. (2015). SWI/SNF chromatin-remodeling complexes function in noncoding RNA-dependent assembly of nuclear bodies. Proc. Natl. Acad. Sci. U.S.A. *112*, 4304–4309. 10.1073/pnas.1423819112.

63. Ma, P., Pan, Y., Yang, F., Fang, Y., Liu, W., Zhao, C., Yu, T., Xie, M., Jing, X., Wu, X., et al. (2020). KLF5-Modulated lncRNA NEAT1 Contributes to Tumorigenesis by Acting as a Scaffold for BRG1 to Silence GADD45A in Gastric Cancer. Molecular Therapy - Nucleic Acids *22*, 382–395. 10.1016/j.omtn.2020.09.003.

64. Wang, X., Gong, Y., Jin, B., Wu, C., Yang, J., Wang, L., Zhang, Z., and Mao, Z. (2014). Long non-coding RNA urothelial carcinoma associated 1 induces cell replication by inhibiting BRG1 in 5637 cells. Oncology Reports *32*, 1281–1290. 10.3892/or.2014.3309.

65. Cajigas, I., Leib, D.E., Cochrane, J., Luo, H., Swyter, K.R., Chen, S., Clark, B.S., Thompson, J., Yates, J.R., Kingston, R.E., et al. (2015). Evf2 lncRNA/BRG1/DLX1 interactions reveal RNA-dependent inhibition of chromatin remodeling. Development *142*, 2641–2652. 10.1242/dev.126318.

66. Wang, E.T., Sandberg, R., Luo, S., Khrebtukova, I., Zhang, L., Mayr, C., Kingsmore, S.F., Schroth, G.P., and Burge, C.B. (2008). Alternative isoform regulation in human tissue transcriptomes. Nature *456*, 470–476. 10.1038/nature07509.

67. Baralle, F.E., and Giudice, J. (2017). Alternative splicing as a regulator of development and tissue identity. Nat Rev Mol Cell Biol *18*, 437–451. 10.1038/nrm.2017.27.

68. Liu, S., and Cheng, C. (2013). Alternative RNA splicing and cancer. Wiley Interdiscip Rev RNA *4*, 547–566. 10.1002/wrna.1178.

69. Will, C.L., and Luhrmann, R. (2011). Spliceosome Structure and Function. Cold Spring Harbor Perspectives in Biology *3*, a003707–a003707. 10.1101/cshperspect.a003707.

70. Moore, M.J., and Sharp, P.A. (1993). Evidence for two active sites in the spliceosome provided by stereochemistry of pre-mRNA splicing. Nature *365*, 364–368. 10.1038/365364a0.

71. Yan, C., Wan, R., and Shi, Y. (2019). Molecular Mechanisms of pre-mRNA Splicing through Structural Biology of the Spliceosome. Cold Spring Harb Perspect Biol *11*, a032409. 10.1101/cshperspect.a032409.

72. Lerner, M.R., Boyle, J.A., Mount, S.M., Wolin, S.L., and Steitz, J.A. (1980). Are snRNPs involved in splicing? Nature *283*, 220–224. 10.1038/283220a0.

73. Boesler, C., Rigo, N., Anokhina, M.M., Tauchert, M.J., Agafonov, D.E., Kastner, B., Urlaub, H., Ficner, R., Will, C.L., and Lührmann, R. (2016). A spliceosome intermediate with loosely associated tri-snRNP accumulates in the absence of Prp28 ATPase activity. Nat Commun *7*, 11997. 10.1038/ncomms11997.

74. Wilkinson, M.E., Lin, P.-C., Plaschka, C., and Nagai, K. (2018). Cryo-EM Studies of Pre-mRNA Splicing: From Sample Preparation to Model Visualization. Annu. Rev. Biophys. *47*, 175–199. 10.1146/annurev-biophys-070317-033410.

75. Herzel, L., Ottoz, D.S.M., Alpert, T., and Neugebauer, K.M. (2017). Splicing and transcription touch base: co-transcriptional spliceosome assembly and function. Nat Rev Mol Cell Biol *18*, 637–650. 10.1038/nrm.2017.63.

76. Makarov, E.M., Owen, N., Bottrill, A., and Makarova, O.V. (2012). Functional mammalian spliceosomal complex E contains SMN complex proteins in

addition to U1 and U2 snRNPs. Nucleic Acids Research *40*, 2639–2652. 10.1093/nar/gkr1056.

77. Montañés-Agudo, P., and Pinto, Y.M. (2022). Triadin-Antisense: An lncRNA in the Backstage of Cardiac Alternative Splicing. Circulation *146*, 715–717. 10.1161/CIRCULATIONAHA.122.061232.

78. Ouyang, J., Zhong, Y., Zhang, Y., Yang, L., Wu, P., Hou, X., Xiong, F., Li, X., Zhang, S., Gong, Z., et al. (2022). Long non-coding RNAs are involved in alternative splicing and promote cancer progression. Br J Cancer *126*, 1113–1124. 10.1038/s41416-021-01600-w.

79. Pisignano, G., and Ladomery, M. (2021). Epigenetic Regulation of Alternative Splicing: How LncRNAs Tailor the Message. ncRNA *7*, 21. 10.3390/ncrna7010021.

80. Gonzalez, I., Munita, R., Agirre, E., Dittmer, T.A., Gysling, K., Misteli, T., and Luco, R.F. (2015). A lncRNA regulates alternative splicing via establishment of a splicing-specific chromatin signature. Nat Struct Mol Biol *22*, 370–376. 10.1038/nsmb.3005.

81. Villamizar, O., Chambers, C.B., Riberdy, J.M., Persons, D.A., and Wilber, A. (2016). Long noncoding RNA Saf and splicing factor 45 increase soluble Fas and resistance to apoptosis. Oncotarget *7*, 13810–13826. 10.18632/oncotarget.7329.

82. Tripathi, V., Ellis, J.D., Shen, Z., Song, D.Y., Pan, Q., Watt, A.T., Freier, S.M., Bennett, C.F., Sharma, A., Bubulya, P.A., et al. (2010). The nuclear-retained noncoding RNA MALAT1 regulates alternative splicing by modulating SR splicing factor phosphorylation. Mol Cell *39*, 925–938. 10.1016/j.molcel.2010.08.011.

83. Deanfield, J.E., Halcox, J.P., and Rabelink, T.J. (2007). Endothelial function and dysfunction: testing and clinical relevance. Circulation *115*, 1285–1295. 10.1161/CIRCULATIONAHA.106.652859.

84. Rahimi, N. (2017). Defenders and Challengers of Endothelial Barrier Function. Front. Immunol. *8*, 1847. 10.3389/fimmu.2017.01847.

85. Val, S., and Black, B.L. (2009). Transcriptional control of endothelial cell development. Dev Cell *16*, 180–195. 10.1016/j.devcel.2009.01.014.

86. Wei, G.-H., Badis, G., Berger, M.F., Kivioja, T., Palin, K., Enge, M., Bonke, M., Jolma, A., Varjosalo, M., Gehrke, A.R., et al. (2010). Genome-wide analysis of ETS-family DNA-binding in vitro and in vivo. EMBO J *29*, 2147–2160. 10.1038/emboj.2010.106.

87. Randi, A.M., Sperone, A., Dryden, N.H., and Birdsey, G.M. (2009). Regulation of angiogenesis by ETS transcription factors. Biochemical Society Transactions *37*, 1248–1253. 10.1042/BST0371248.

88. Kalna, V., Yang, Y., Peghaire, C.R., Frudd, K., Hannah, R., Shah, A.V., Osuna Almagro, L., Boyle, J.J., Göttgens, B., Ferrer, J., et al. (2019). The Transcription

Factor ERG Regulates Super-Enhancers Associated With an Endothelial-Specific Gene Expression Program. Circ Res *124*, 1337–1349. 10.1161/CIRCRESAHA.118.313788.

89. Kulakovskiy, I.V., Vorontsov, I.E., Yevshin, I.S., Sharipov, R.N., Fedorova, A.D., Rumynskiy, E.I., Medvedeva, Y.A., Magana-Mora, A., Bajic, V.B., Papatsenko, D.A., et al. (2018). HOCOMOCO: towards a complete collection of transcription factor binding models for human and mouse via large-scale ChIP-Seq analysis. Nucleic Acids Res *46*, 252–259. 10.1093/nar/gkx1106.

90. Krüger-Genge, Blocki, Franke, and Jung (2019). Vascular Endothelial Cell Biology: An Update. IJMS *20*, 4411. 10.3390/ijms20184411.

91. Fukumura, D., and Jain, R.K. (2007). Tumor microenvironment abnormalities: Causes, consequences, and strategies to normalize. J. Cell. Biochem. *101*, 937–949. 10.1002/jcb.21187.

92. Lee, J.W., Ko, J., Ju, C., and Eltzschig, H.K. (2019). Hypoxia signaling in human diseases and therapeutic targets. Exp Mol Med *51*, 1–13. 10.1038/s12276-019-0235-1.

93. Vito, A., El-Sayes, N., and Mossman, K. (2020). Hypoxia-Driven Immune Escape in the Tumor Microenvironment. Cells *9*, 992. 10.3390/cells9040992.

94. Das, B., Yeger, H., Tsuchida, R., Torkin, R., Gee, M.F.W., Thorner, P.S., Shibuya, M., Malkin, D., and Baruchel, S. (2005). A hypoxia-driven vascular endothelial growth factor/Flt1 autocrine loop interacts with hypoxia-inducible factor-1alpha through mitogen-activated protein kinase/extracellular signal-regulated kinase 1/2 pathway in neuroblastoma. Cancer Res *65*, 7267–7275. 10.1158/0008-5472.CAN-04-4575.

95. Rosenfeld, P.J., Brown, D.M., Heier, J.S., Boyer, D.S., Kaiser, P.K., Chung, C.Y., and Kim, R.Y. (2006). Ranibizumab for Neovascular Age-Related Macular Degeneration. N Engl J Med *355*, 1419–1431. 10.1056/NEJMoa054481.

96. Ferrara, N., Mass, R.D., Campa, C., and Kim, R. (2007). Targeting VEGF-A to treat cancer and age-related macular degeneration. Annu Rev Med *58*, 491–504. 10.1146/annurev.med.58.061705.145635.

97. Laschke, M.W., Gu, Y., and Menger, M.D. (2022). Replacement in angiogenesis research: Studying mechanisms of blood vessel development by animal-free in vitro, in vivo and in silico approaches. Front. Physiol. *13*, 981161. 10.3389/fphys.2022.981161.

98. Shibuya, M. (2011). Vascular Endothelial Growth Factor (VEGF) and Its Receptor (VEGFR) Signaling in Angiogenesis: A Crucial Target for Anti- and Pro-Angiogenic Therapies. Genes & Cancer *2*, 1097–1105. 10.1177/1947601911423031.

99. Peach, C., Mignone, V., Arruda, M., Alcobia, D., Hill, S., Kilpatrick, L., and Woolard, J. (2018). Molecular Pharmacology of VEGF-A Isoforms: Binding and Signalling at VEGFR2. IJMS *19*, 1264. 10.3390/ijms19041264.

100. Bowler, E., and Oltean, S. (2019). Alternative Splicing in Angiogenesis. IJMS *20*, 2067. 10.3390/ijms20092067.

101. Di Matteo, A., Belloni, E., Pradella, D., Cappelletto, A., Volf, N., Zacchigna, S., and Ghigna, C. (2020). Alternative splicing in endothelial cells: novel therapeutic opportunities in cancer angiogenesis. J Exp Clin Cancer Res *39*, 275. 10.1186/s13046-020-01753-1.

102. Lee, K.-H. (2004). Non-hypoxic transcriptional activation of the aryl hydrocarbon receptor nuclear translocator in concert with a novel hypoxia-inducible factor-1alpha isoform. Nucleic Acids Research *32*, 5499–5511. 10.1093/nar/gkh880.

103. Falk, T., Gonzalez, R.T., and Sherman, S.J. (2010). The Yin and Yang of VEGF and PEDF: Multifaceted Neurotrophic Factors and Their Potential in the Treatment of Parkinson's Disease. IJMS *11*, 2875–2900. 10.3390/ijms11082875.

104. Tsuji-Tamura, K., and Ogawa, M. (2018). Morphology regulation in vascular endothelial cells. Inflamm Regener *38*, 25. 10.1186/s41232-018-0083-8.

105. Bui, K., and Hong, Y.-K. (2020). Ras Pathways on Prox1 and Lymphangiogenesis: Insights for Therapeutics. Front. Cardiovasc. Med. *7*, 597374. 10.3389/fcvm.2020.597374.

106. Nakayama, K. (2013). cAMP-response Element-binding Protein (CREB) and NF-κB Transcription Factors Are Activated during Prolonged Hypoxia and Cooperatively Regulate the Induction of Matrix Metalloproteinase MMP1. Journal of Biological Chemistry *288*, 22584–22595. 10.1074/jbc.M112.421636.

107. Zhang, Z., Yao, L., Yang, J., Wang, Z., and Du, G. (2018). PI3K/Akt and HIF-1 signaling pathway in hypoxia-ischemia (Review). Mol Med Report. 10.3892/mmr.2018.9375.

108. Fang, Y., Xu, Y., Wang, R., Hu, L., Guo, D., Xue, F., Guo, W., Zhang, D., Hu, J., Li, Y., et al. (2020). Recent advances on the roles of LncRNAs in cardiovascular disease. J. Cell. Mol. Med. *24*, 12246–12257. 10.1111/jcmm.15880.

109. Vausort, M., Wagner, D.R., and Devaux, Y. (2014). Long Noncoding RNAs in Patients With Acute Myocardial Infarction. Circ Res *115*, 668–677. 10.1161/CIRCRESAHA.115.303836.

110. Gao, L., Liu, Y., Guo, S., Yao, R., Wu, L., Xiao, L., Wang, Z., Liu, Y., and Zhang, Y. (2017). Circulating Long Noncoding RNA HOTAIR is an Essential Mediator of Acute Myocardial Infarction. Cell Physiol Biochem *44*, 1497–1508. 10.1159/000485588.

111. Kumarswamy, R., Bauters, C., Volkmann, I., Maury, F., Fetisch, J., Holzmann, A., Lemesle, G., de Groote, P., Pinet, F., and Thum, T. (2014). Circulating Long Noncoding RNA, LIPCAR, Predicts Survival in Patients With Heart Failure. Circ Res *114*, 1569–1575. 10.1161/CIRCRESAHA.114.303915.

112. Viereck, J., Bührke, A., Foinquinos, A., Chatterjee, S., Kleeberger, J.A., Xiao, K., Janssen-Peters, H., Batkai, S., Ramanujam, D., Kraft, T., et al. (2020). Targeting muscle-enriched long non-coding RNA H19 reverses pathological cardiac hypertrophy. European Heart Journal *41*, 3462–3474. 10.1093/eurheartj/ehaa519.

113. Michalik, K.M., You, X., Manavski, Y., Doddaballapur, A., Zörnig, M., Braun, T., John, D., Ponomareva, Y., Chen, W., Uchida, S., et al. (2014). Long noncoding RNA MALAT1 regulates endothelial cell function and vessel growth. Circ Res *114*, 1389–1397. 10.1161/CIRCRESAHA.114.303265.

114. Man, H.S.J., Sukumar, A.N., Lam, G.C., Turgeon, P.J., Yan, M.S., Ku, K.H., Dubinsky, M.K., Ho, J.J.D., Wang, J.J., Das, S., et al. (2018). Angiogenic patterning by STEEL, an endothelial-enriched long noncoding RNA. Proc Natl Acad Sci U S A *115*, 2401–2406. 10.1073/pnas.1715182115.

115. Nagai, N., Ohguchi, H., Nakaki, R., Matsumura, Y., Kanki, Y., Sakai, J., Aburatani, H., and Minami, T. (2018). Downregulation of ERG and FLI1 expression in endothelial cells triggers endothelial-to-mesenchymal transition. PLoS Genet *14*, e1007826. 10.1371/journal.pgen.1007826.

116. Fiedler, J., Breckwoldt, K., Remmele, C.W., Hartmann, D., Dittrich, M., Pfanne, A., Just, A., Xiao, K., Kunz, M., Müller, T., et al. (2015). Development of Long Noncoding RNA-Based Strategies to Modulate Tissue Vascularization. J Am Coll Cardiol *66*, 2005–2015. 10.1016/j.jacc.2015.07.081.

117. Seredinski, S., Boos, F., Günther, S., Oo, J.A., Warwick, T., Izquierdo Ponce, J., Lillich, F.F., Proschak, E., Knapp, S., Gilsbach, R., et al. (2022). DNA topoisomerase inhibition with the HIF inhibitor acriflavine promotes transcription of lncRNAs in endothelial cells. Mol Ther Nucleic Acids *27*, 1023–1035. 10.1016/j.omtn.2022.01.016.

118. Monteiro, J.P., Rodor, J., Caudrillier, A., Scanlon, J.P., Spiroski, A.-M., Dudnakova, T., Pflüger-Müller, B., Shmakova, A., Kriegsheim, A., Deng, L., et al. (2021). MIR503HG Loss Promotes Endothelial-to-Mesenchymal Transition in Vascular Disease. Circ Res *128*, 1173–1190. 10.1161/CIRCRESAHA.120.318124.

119. Forrest, A.R.R., Kawaji, H., Rehli, M., Baillie, J.K., Hoon, M.J.L., Haberle, V., Lassmann, T., Kulakovskiy, I.V., Lizio, M., Itoh, M., et al. (2014). A promoter-level mammalian expression atlas. Nature *507*, 462–470. 10.1038/nature13182.

120. Noguchi, S., Arakawa, T., Fukuda, S., Furuno, M., Hasegawa, A., Hori, F., Ishikawa-Kato, S., Kaida, K., Kaiho, A., Kanamori-Katayama, M., et al. (2017). FANTOM5 CAGE profiles of human and mouse samples. Sci Data *4*, 170112. 10.1038/sdata.2017.112.

121. Chen, X., Rinsma, M., Janssen, J.M., Liu, J., Maggio, I., and Gonçalves, M.A.F.V. (2016). Probing the impact of chromatin conformation on genome editing tools. Nucleic Acids Res *44*, 6482–6492. 10.1093/nar/gkw524.

122. Korff, T., and Augustin, H.G. (1998). Integration of endothelial cells in multicellular spheroids prevents apoptosis and induces differentiation. J Cell Biol *143*, 1341–1352. 10.1083/jcb.143.5.1341.

123. Skene, P.J., and Henikoff, S. (2017). An efficient targeted nuclease strategy for high-resolution mapping of DNA binding sites. Elife *6*. 10.7554/eLife.21856.

124. Boos, F., Oo, J.A., Warwick, T., Günther, S., Izquierdo Ponce, J., Lopez, M., Rafii, D., Buchmann, G., Pham, M.D., Msheik, Z.S., et al. (2023). The endothelial-enriched lncRNA LINC00607 mediates angiogenic function. Basic Res Cardiol *118*, 5. 10.1007/s00395-023-00978-3.

125. Laib, A.M., Bartol, A., Alajati, A., Korff, T., Weber, H., and Augustin, H.G. (2009). Spheroid-based human endothelial cell microvessel formation in vivo. Nat Protoc *4*, 1202–1215. 10.1038/nprot.2009.96.

126. Ertürk, A., Becker, K., Jährling, N., Mauch, C.P., Hojer, C.D., Egen, J.G., Hellal, F., Bradke, F., Sheng, M., and Dodt, H.-U. (2012). Three-dimensional imaging of solvent-cleared organs using 3DISCO. Nat Protoc *7*, 1983–1995. 10.1038/nprot.2012.119.

127. Hathaway, C.A., Heistad, D.D., Piegors, D.J., and Miller, F.J. (2002). Regression of atherosclerosis in monkeys reduces vascular superoxide levels. Circ Res *90*, 277–283. 10.1161/hh0302.104724.

128. Bibli, S.-I., Hu, J., Looso, M., Weigert, A., Ratiu, C., Wittig, J., Drekolia, M.K., Tombor, L., Randriamboavonjy, V., Leisegang, M.S., et al. (2021). Mapping the Endothelial Cell S-Sulfhydrome Highlights the Crucial Role of Integrin Sulfhydration in Vascular Function. Circulation *143*, 935–948. 10.1161/CIRCULATIONAHA.120.051877.

129. Andrews S. (2010). FastQC: a quality control tool for high throughput sequence data.

130. Bolger, A.M., Lohse, M., and Usadel, B. (2014). Trimmomatic: a flexible trimmer for Illumina sequence data. Bioinformatics *30*, 2114–2120. 10.1093/bioinformatics/btu170.

131. Dobin, A., Davis, C.A., Schlesinger, F., Drenkow, J., Zaleski, C., Jha, S., Batut, P., Chaisson, M., and Gingeras, T.R. (2013). STAR: ultrafast universal RNA-seq aligner. Bioinformatics *29*, 15–21. 10.1093/bioinformatics/bts635.

132. Liao, Y., Smyth, G.K., and Shi, W. (2014). featureCounts: an efficient general purpose program for assigning sequence reads to genomic features. Bioinformatics *30*, 923–930. 10.1093/bioinformatics/btt656.

133. Love, M.I., Huber, W., and Anders, S. (2014). Moderated estimation of fold change and dispersion for RNA-seq data with DESeq2. Genome Biol *15*, 550. 10.1186/s13059-014-0550-8.

134. UniProt: a worldwide hub of protein knowledge (2019). Nucleic Acids Res *47*, 506–515. 10.1093/nar/gky1049.

135. Buenrostro, J.D., Wu, B., Chang, H.Y., and Greenleaf, W.J. (2015). ATAC-seq: A Method for Assaying Chromatin Accessibility Genome-Wide. Curr Protoc Mol Biol *109*, 21291–21299. 10.1002/0471142727.mb2129s109.

136. Broad Institute (2019). Picard Toolkit.

137. Zhang, Y., Liu, T., Meyer, C.A., Eeckhoute, J., Johnson, D.S., Bernstein, B.E., Nusbaum, C., Myers, R.M., Brown, M., Li, W., et al. (2008). Model-based analysis of ChIP-Seq (MACS). Genome Biol *9*, 137. 10.1186/gb-2008-9-9-r137.

138. Kent, W.J., Zweig, A.S., Barber, G., Hinrichs, A.S., and Karolchik, D. (2010). BigWig and BigBed: enabling browsing of large distributed datasets. Bioinformatics *26*, 2204–2207. 10.1093/bioinformatics/btq351.

139. Allhoff, M., Seré, K., F Pires, J., Zenke, M., and G Costa, I. (2016). Differential peak calling of ChIP-seq signals with replicates with THOR. Nucleic Acids Res *44*, 153. 10.1093/nar/gkw680.

140. Baumgarten, N., Hecker, D., Karunanithi, S., Schmidt, F., List, M., and Schulz, M.H. (2020). EpiRegio: analysis and retrieval of regulatory elements linked to genes. Nucleic Acids Res *48*, 193–199. 10.1093/nar/gkaa382.

141. Yu, G., and He, Q.-Y. (2016). ReactomePA: an R/Bioconductor package for reactome pathway analysis and visualization. Mol Biosyst *12*, 477–479. 10.1039/C5MB00663E.

142. Wickham, H. (2009). Ggplot2: Elegant graphics for data analysis (Springer).

143. Heinz, S., Benner, C., Spann, N., Bertolino, E., Lin, Y.C., Laslo, P., Cheng, J.X., Murre, C., Singh, H., and Glass, C.K. (2010). Simple combinations of lineage-determining transcription factors prime cis-regulatory elements required for macrophage and B cell identities. Mol Cell *38*, 576–589. 10.1016/j.molcel.2010.05.004.

144. Felix Krueger, Frankie James, Phil Ewels, Ebrahim Afyounian, and Benjamin Schuster-Boeckler (2021). FelixKrueger/TrimGalore: v0.6.7 - DOI via Zenodo. 10.5281/zenodo.5127899.

145. Langmead, B., Trapnell, C., Pop, M., and Salzberg, S.L. (2009). Ultrafast and memory-efficient alignment of short DNA sequences to the human genome. Genome Biol *10*, 25. 10.1186/gb-2009-10-3-r25.

146. Langmead, B., and Salzberg, S.L. (2012). Fast gapped-read alignment with Bowtie 2. Nat Methods *9*, 357–359. 10.1038/nmeth.1923.

147. Li, H., Handsaker, B., Wysoker, A., Fennell, T., Ruan, J., Homer, N., Marth, G., Abecasis, G., and Durbin, R. (2009). The Sequence Alignment/Map format and SAMtools. Bioinformatics *25*, 2078–2079. 10.1093/bioinformatics/btp352.

148. Ramírez, F., Ryan, D.P., Grüning, B., Bhardwaj, V., Kilpert, F., Richter, A.S., Heyne, S., Dündar, F., and Manke, T. (2016). deepTools2: a next generation

web server for deep-sequencing data analysis. Nucleic Acids Res *44*, 160–165. 10.1093/nar/gkw257.

149. Haberle, V., and Stark, A. (2018). Eukaryotic core promoters and the functional basis of transcription initiation. Nat Rev Mol Cell Biol *19*, 621–637. 10.1038/s41580-018-0028-8.

150. Guenther, M.G., Levine, S.S., Boyer, L.A., Jaenisch, R., and Young, R.A. (2007). A chromatin landmark and transcription initiation at most promoters in human cells. Cell *130*, 77–88. 10.1016/j.cell.2007.05.042.

151. Kovacic, J.C., Dimmeler, S., Harvey, R.P., Finkel, T., Aikawa, E., Krenning, G., and Baker, A.H. (2019). Endothelial to Mesenchymal Transition in Cardiovascular Disease: JACC State-of-the-Art Review. J Am Coll Cardiol *73*, 190–209. 10.1016/j.jacc.2018.09.089.

152. Lorusso, B., Cerasoli, G., Falco, A., Frati, C., Graiani, G., Madeddu, D., Nogara, A., Corradini, E., Roti, G., Cerretani, E., et al. (2022). B-blockers activate autophagy on infantile hemangioma-derived endothelial cells in vitro. Vascular Pharmacology *146*, 107110. 10.1016/j.vph.2022.107110.

153. Pruitt, K.D., Brown, G.R., Hiatt, S.M., Thibaud-Nissen, F., Astashyn, A., Ermolaeva, O., Farrell, C.M., Hart, J., Landrum, M.J., McGarvey, K.M., et al. (2014). RefSeq: an update on mammalian reference sequences. Nucl. Acids Res. *42*, D756–D763. 10.1093/nar/gkt1114.

154. Blanchette, M., Kent, W.J., Riemer, C., Elnitski, L., Smit, A.F.A., Roskin, K.M., Baertsch, R., Rosenbloom, K., Clawson, H., Green, E.D., et al. (2004). Aligning Multiple Genomic Sequences With the Threaded Blockset Aligner. Genome Res. *14*, 708–715. 10.1101/gr.1933104.

155. Altschul, S.F., Gish, W., Miller, W., Myers, E.W., and Lipman, D.J. (1990). Basic local alignment search tool. Journal of Molecular Biology *215*, 403–410. 10.1016/S0022-2836(05)80360-2.

156. Hezroni, H., Koppstein, D., Schwartz, M.G., Avrutin, A., Bartel, D.P., and Ulitsky, I. (2015). Principles of Long Noncoding RNA Evolution Derived from Direct Comparison of Transcriptomes in 17 Species. Cell Reports *11*, 1110–1122. 10.1016/j.celrep.2015.04.023.

157. Palazzo, A.F., and Koonin, E.V. (2020). Functional Long Non-coding RNAs Evolve from Junk Transcripts. Cell *183*, 1151–1161. 10.1016/j.cell.2020.09.047.

158. Subramanian, A., Tamayo, P., Mootha, V.K., Mukherjee, S., Ebert, B.L., Gillette, M.A., Paulovich, A., Pomeroy, S.L., Golub, T.R., Lander, E.S., et al. (2005). Gene set enrichment analysis: a knowledge-based approach for interpreting genome-wide expression profiles. Proc Natl Acad Sci U S A *102*, 15545–15550. 10.1073/pnas.0506580102.

159. Li, L., Chen, Z., Scheidt, M., Li, S., Steiner, A., Güldener, U., Koplev, S., Ma, A., Hao, K., Pan, C., et al. (2022). Transcriptome-wide association study of

coronary artery disease identifies novel susceptibility genes. Basic Res Cardiol *117*, 6. 10.1007/s00395-022-00917-8.

160. Meadows, S.M., Myers, C.T., and Krieg, P.A. (2011). Regulation of endothelial cell development by ETS transcription factors. Semin Cell Dev Biol *22*, 976–984. 10.1016/j.semcdb.2011.09.009.

161. Li, Z., Kong, X., Zhang, Y., Zhang, Y., Yu, L., Guo, J., and Xu, Y. (2020). Dual roles of chromatin remodeling protein BRG1 in angiotensin II-induced endothelial–mesenchymal transition. Cell Death Dis *11*, 549. 10.1038/s41419-020-02744-y.

162. Han, P., Li, W., Lin, C.-H., Yang, J., Shang, C., Nuernberg, S.T., Jin, K.K., Xu, W., Lin, C.-Y., Lin, C.-J., et al. (2014). A long noncoding RNA protects the heart from pathological hypertrophy. Nature *514*, 102–106. 10.1038/nature13596.

163. Hartley, S.W., and Mullikin, J.C. (2016). Detection and visualization of differential splicing in RNA-Seq data with JunctionSeq. Nucleic Acids Res *44*, 127. 10.1093/nar/gkw501.

164. Thomas, C.P., Raikwar, N.S., Kelley, E.A., and Liu, K.Z. (2010). Alternate processing of Flt1 transcripts is directed by conserved cis -elements within an intronic region of FLT1 that reciprocally regulates splicing and polyadenylation. Nucleic Acids Research *38*, 5130–5140. 10.1093/nar/gkq198.

165. Boeckel, J.-N., Guarani, V., Koyanagi, M., Roexe, T., Lengeling, A., Schermuly, R.T., Gellert, P., Braun, T., Zeiher, A., and Dimmeler, S. (2011). Jumonji domain-containing protein 6 (Jmjd6) is required for angiogenic sprouting and regulates splicing of VEGF-receptor 1. Proc. Natl. Acad. Sci. U.S.A. *108*, 3276–3281. 10.1073/pnas.1008098108.

166. Koga, K., Osuga, Y., Yoshino, O., Hirota, Y., Ruimeng, X., Hirata, T., Takeda, S., Yano, T., Tsutsumi, O., and Taketani, Y. (2003). Elevated Serum Soluble Vascular Endothelial Growth Factor Receptor 1 (sVEGFR-1) Levels in Women with Preeclampsia. The Journal of Clinical Endocrinology & Metabolism *88*, 2348–2351. 10.1210/jc.2002-021942.

167. Anderson, U.D., Olsson, M.G., Kristensen, K.H., Åkerström, B., and Hansson, S.R. (2012). Review: Biochemical markers to predict preeclampsia. Placenta *33*, S42–S47. 10.1016/j.placenta.2011.11.021.

168. Vento-Tormo, R., Efremova, M., Botting, R.A., Turco, M.Y., Vento-Tormo, M., Meyer, K.B., Park, J.-E., Stephenson, E., Polański, K., Goncalves, A., et al. (2018). Single-cell reconstruction of the early maternal–fetal interface in humans. Nature *563*, 347–353. 10.1038/s41586-018-0698-6.

169. Huang, Q.T., Zhang, M., Zhong, M., Yu, Y.H., Liang, W.Z., Hang, L.L., Gao, Y.F., Huang, L.P., and Wang, Z.J. (2013). Advanced glycation end products as an upstream molecule triggers ROS-induced sFlt-1 production in extravillous trophoblasts: a novel bridge between oxidative stress and preeclampsia. Placenta *34*, 1177–1182. 10.1016/j.placenta.2013.09.017.

170. Nassar, L.R., Barber, G.P., Benet-Pagès, A., Casper, J., Clawson, H., Diekhans, M., Fischer, C., Gonzalez, J.N., Hinrichs, A.S., Lee, B.T., et al. (2023). The UCSC Genome Browser database: 2023 update. Nucleic Acids Research *51*, D1188–D1195. 10.1093/nar/gkac1072.

171. Cao, J., O'Day, D.R., Pliner, H.A., Kingsley, P.D., Deng, M., Daza, R.M., Zager, M.A., Aldinger, K.A., Blecher-Gonen, R., Zhang, F., et al. (2020). A human cell atlas of fetal gene expression. Science *370*, eaba7721. 10.1126/science.aba7721.

172. Zhang, X., Hamblin, M.H., and Yin, K.-J. (2017). The long noncoding RNA Malat1: Its physiological and pathophysiological functions. RNA Biology *14*, 1705–1714. 10.1080/15476286.2017.1358347.

173. Ulitsky, I. (2016). Evolution to the rescue: using comparative genomics to understand long non-coding RNAs. Nat Rev Genet *17*, 601–614. 10.1038/nrg.2016.85.

174. Szcześniak, M.W., Kubiak, M.R., Wanowska, E., and Makałowska, I. (2021). Comparative genomics in the search for conserved long noncoding RNAs. Essays in Biochemistry *65*, 741–749. 10.1042/EBC20200069.

175. Camilleri-Robles, C., Amador, R., Klein, C.C., Guigó, R., Corominas, M., and Ruiz-Romero, M. (2022). Genomic and functional conservation of lncRNAs: lessons from flies. Mamm Genome *33*, 328–342. 10.1007/s00335-021-09939-4.

176. McCown, P.J., Wang, M.C., Jaeger, L., and Brown, J.A. (2019). Secondary Structural Model of Human MALAT1 Reveals Multiple Structure–Function Relationships. IJMS *20*, 5610. 10.3390/ijms20225610.

177. Rom, A., Melamed, L., Gil, N., Goldrich, M.J., Kadir, R., Golan, M., Biton, I., Perry, R.B.-T., and Ulitsky, I. (2019). Regulation of CHD2 expression by the Chaserr long noncoding RNA gene is essential for viability. Nat Commun *10*, 5092. 10.1038/s41467-019-13075-8.

178. Lawton, M.T., Rutledge, W.C., Kim, H., Stapf, C., Whitehead, K.J., Li, D.Y., Krings, T., terBrugge, K., Kondziolka, D., Morgan, M.K., et al. (2015). Brain arteriovenous malformations. Nat Rev Dis Primers *1*, 15008. 10.1038/nrdp.2015.8.

179. Stiles, J., Amaya, C., Pham, R., Rowntree, R.K., Lacaze, M., Mulne, A., Bischoff, J., Kokta, V., Boucheron, L.E., Mitchell, D.C., et al. (2012). Propranolol treatment of infantile hemangioma endothelial cells: A molecular analysis. Experimental and Therapeutic Medicine *4*, 594–604. 10.3892/etm.2012.654.

180. Spindler, V., and Waschke, J. (2011). Beta-Adrenergic Stimulation Contributes to Maintenance of Endothelial Barrier Functions Under Baseline Conditions: Beta Adrenoceptors and Endothelial Barrier. Microcirculation *18*, 118–127. 10.1111/j.1549-8719.2010.00072.x.

181. Ji, Y., Chen, S., Li, K., Xiao, X., Zheng, S., and Xu, T. (2013). The role of β-adrenergic receptor signaling in the proliferation of hemangioma-derived endothelial cells. Cell Div *8*, 1. 10.1186/1747-1028-8-1.

182. Wu, Z., Liu, X., Liu, L., Deng, H., Zhang, J., Xu, Q., Cen, B., and Ji, A. (2014). Regulation of lncRNA expression. Cellular and Molecular Biology Letters *19*. 10.2478/s11658-014-0212-6.

183. Calandrelli, R., Xu, L., Luo, Y., Wu, W., Fan, X., Nguyen, T., Chen, C.-J., Sriram, K., Tang, X., Burns, A.B., et al. (2020). Stress-induced RNA-chromatin interactions promote endothelial dysfunction. Nat Commun *11*, 5211. 10.1038/s41467-020-18957-w.

184. Piera-Velazquez, S., and Jimenez, S.A. (2019). Endothelial to Mesenchymal Transition: Role in Physiology and in the Pathogenesis of Human Diseases. Physiological Reviews *99*, 1281–1324. 10.1152/physrev.00021.2018.

185. Ma, J., Sanchez-Duffhues, G., Goumans, M.-J., and Dijke, P. (2020). TGF-β-Induced Endothelial to Mesenchymal Transition in Disease and Tissue Engineering. Front Cell Dev Biol *8*, 260. 10.3389/fcell.2020.00260.

186. Smith, A.P., Verrecchia, A., Fagà, G., Doni, M., Perna, D., Martinato, F., Guccione, E., and Amati, B. (2009). A positive role for Myc in TGFβ-induced Snail transcription and epithelial-to-mesenchymal transition. Oncogene *28*, 422–430. 10.1038/onc.2008.395.

187. Saito, A. (2013). EMT and EndMT: regulated in similar ways? The Journal of Biochemistry *153*, 493–495. 10.1093/jb/mvt032.

188. Zheng, Y., Chen, Z., Zhou, Z., Xu, X., and Yang, H. (2020). Silencing of Long Non-Coding RNA LINC00607 Prevents Tumor Proliferation of Osteosarcoma by Acting as a Sponge of miR-607 to Downregulate E2F6. Front Oncol *10*, 584452. 10.3389/fonc.2020.584452.

189. Li, L., Gao, Z., Zhao, L., Ren, P., and Shen, H. (2021). Long non-coding RNA LINC00607 silencing exerts antioncogenic effects on thyroid cancer through the CASP9 Promoter methylation. J Cell Mol Med *25*, 7608–7620. 10.1111/jcmm.16265.

190. Zhao, B., Xu, H., Ai, X., Adalat, Y., Tong, Y., Zhang, J., and Yang, S. (2018). Expression profiles of long noncoding RNAs in lung adenocarcinoma. Onco Targets Ther *11*, 5383–5390. 10.2147/OTT.S167633.

191. Zhu, F., Farnung, L., Kaasinen, E., Sahu, B., Yin, Y., Wei, B., Dodonova, S.O., Nitta, K.R., Morgunova, E., Taipale, M., et al. (2018). The interaction landscape between transcription factors and the nucleosome. Nature *562*, 76–81. 10.1038/s41586-018-0549-5.

192. Ruan, W., Zhao, F., Zhao, S., Zhang, L., Shi, L., and Pang, T. (2018). Knockdown of long noncoding RNA MEG3 impairs VEGF-stimulated endothelial sprouting angiogenesis via modulating VEGFR2 expression in human umbilical vein endothelial cells. Gene *649*, 32–39. 10.1016/j.gene.2018.01.072.

193. Boulberdaa, M., Scott, E., Ballantyne, M., Garcia, R., Descamps, B., Angelini, G.D., Brittan, M., Hunter, A., McBride, M., McClure, J., et al. (2016). A Role for the Long Noncoding RNA SENCR in Commitment and Function of Endothelial Cells. Molecular Therapy *24*, 978–990. 10.1038/mt.2016.41.

194. Ho, P.J., Lloyd, S.M., and Bao, X. (2019). Unwinding chromatin at the right places: how BAF is targeted to specific genomic locations during development. Development *146*, dev178780. 10.1242/dev.178780.

195. Davis, R.B., Curtis, C.D., and Griffin, C.T. (2013). BRG1 promotes *COUP-TFII* expression and venous specification during embryonic vascular development. Development *140*, 1272–1281. 10.1242/dev.087379.

196. Huang, M., Wang, H., Hu, X., and Cao, X. (2019). lncRNA MALAT1 binds chromatin remodeling subunit BRG1 to epigenetically promote inflammation-related hepatocellular carcinoma progression. OncoImmunology *8*, e1518628. 10.1080/2162402X.2018.1518628.

197. El Marabti, E., and Younis, I. (2018). The Cancer Spliceome: Reprograming of Alternative Splicing in Cancer. Front Mol Biosci *5*, 80. 10.3389/fmolb.2018.00080.

198. Fontana, G.A., Rigamonti, A., Lenzken, S.C., Filosa, G., Alvarez, R., Calogero, R., Bianchi, M.E., and Barabino, S.M.L. (2017). Oxidative stress controls the choice of alternative last exons via a Brahma–BRCA1–CstF pathway. Nucleic Acids Res *45*, 902–914. 10.1093/nar/gkw780.

199. Fish, J.E., Gutierrez, M.C., Dang, L.T., Khyzha, N., Chen, Z., Veitch, S., Cheng, H.S., Khor, M., Antounians, L., Njock, M.-S., et al. (2017). Dynamic regulation of VEGF-inducible genes by an ERK-ERG-p300 transcriptional network. Development, dev.146050. 10.1242/dev.146050.

200. Sawano, A., Takahashi, T., Yamaguchi, S., Aonuma, M., and Shibuya, M. (1996). Flt-1 but not KDR/Flk-1 tyrosine kinase is a receptor for placenta growth factor, which is related to vascular endothelial growth factor. Cell Growth Differ *7*, 213–221.

201. Fong, G.-H., Rossant, J., Gertsenstein, M., and Breitman, M.L. (1995). Role of the Flt-1 receptor tyrosine kinase in regulating the assembly of vascular endothelium. Nature *376*, 66–70. 10.1038/376066a0.

202. Ray, D., Laverty, K.U., Jolma, A., Nie, K., Samson, R., Pour, S.E., Tam, C.L., von Krosigk, N., Nabeel-Shah, S., Albu, M., et al. (2023). RNA-binding proteins that lack canonical RNA-binding domains are rarely sequence-specific. Sci Rep *13*, 5238. 10.1038/s41598-023-32245-9.

203. Filarsky, M., Zillner, K., Araya, I., Villar-Garea, A., Merkl, R., Längst, G., and Németh, A. (2015). The extended AT-hook is a novel RNA binding motif. RNA Biology *12*, 864–876. 10.1080/15476286.2015.1060394.

204. Han, P., and Chang, C.-P. (2015). Long non-coding RNA and chromatin remodeling. RNA Biology *12*, 1094–1098. 10.1080/15476286.2015.1063770.

205. Mun, G.I., Park, S., Kremerskothen, J., and Boo, Y.C. (2014). Expression of synaptopodin in endothelial cells exposed to laminar shear stress and its role in endothelial wound healing. FEBS Letters *588*, 1024–1030. 10.1016/j.febslet.2014.02.012.

206. Roth Flach, R.J., Skoura, A., Matevossian, A., Danai, L.V., Zheng, W., Cortes, C., Bhattacharya, S.K., Aouadi, M., Hagan, N., Yawe, J.C., et al. (2015). Endothelial protein kinase MAP4K4 promotes vascular inflammation and atherosclerosis. Nat Commun *6*, 8995. 10.1038/ncomms9995.

8 Abbreviations

%	Percentage
°C	Degree Celsius
18S	18S ribosomal RNA
2−ΔΔCT	2(-Delta Delta C(T))
3’-poly-A tail	Three-prime polyadenylation tail
3′ss	3′ splice site
5’-Cap	Five-prime cap
5’UTR	Five-prime untranslated region
5′ss	5′ splice site
ANOVA	Analysis of variance
AS	alternative splicning
ATAC-Seq	Assay for Transposase-Accessible Chromatin using sequencing
BRG1	Brahma-Related Gene 1
BSA	Bovine serum albumin
cDNA	Complementary DNA
ChIP	Chromatin immunoprecipitation
cj	*Callitrix jaccus*
CO_2	Carbon dioxide
CRC	chromatin remodeling complex
CRISPR/Cas9	Clustered regularly interspaced short palindromic repeats/ associated protein 9-system
CTL or C	Control
CUT&RUN	Cleavage Under Targets & Release Using Nuclease
CVD	cardiovascular diseases
ddH_2O	Bi-distilled water
DEG	Differentially expressed gene
DMEM	Dulbecco's modified eagle medium
DNA	Deoxyribonucleic acid
DPBS	Dulbecco's phosphate-buffered saline
E.coli	Escherichia coli
EC	endothelial cell
EGM	Endothelial growth medium
eRNA	enhancer RNA
FC	Fold change
FCS	Fetal calf serum
FLT1	fms related receptor tyrosine kinase 1, VEGFR1
g	gravitational -force
gRNAs	Guide RNA
GSEA	Gene Set Enrichment Analysis
hBRM	human Brahma
hox	hypoxia
HUVEC	human umbilical vein endothelial cell

IgG	Immunglobulin G
kb	Kilo base
KD	knockdown
KO	knockout
LINC00607	long intergenic non-coding RNA 607
lincRNA	long intergenic noncoding RNA
lncRNA	long non-coding RNA
mA	Milli ampere
mf	*Macaca fascicularis*
mFLT1	membrane bound isoform of FLT1
miRNA	micro RNA
mRNA	messenger RNA
ncRNAs	Noncoding RNAs
nox	normoxia
nt	nucleotide
NTC	non-targeting control
oligo(dT)$_{23}$	Anchored primers
p	p-value or probability value
PFA	Paraformaldehyde
RNA Pol II	RNA polymerase II
PRC1	Polycomb repressive complex 1
PRC2	Polycomb repressive complex 2
pre-mRNA	precursor messenger RNA
RT-qPCR	Quantitative real-time polymerase chain reaction
RIP	RNA immunoprecipitation
RNA	ribonucleic acid
RNA-Seq	RNA-Sequencing
rpm	Rounds per minute
RT	room temperature
SCID	Severe combined immunodeficiency
Scr	scrambled control
sFLT1	soluble isoform of FLT1
sgRNA	Single guide RNA
siControl	SiRNAs control
siRNAs	small interfering RNAs
snRNP	small nuclear ribonucleoprotein
SWI/SNF	switch/sucrose non-fermentable complex
TE	transposable element
TF	transcription factors
TSS	transcription start site
V	Voltage
VEGF-A 165	vascular endothelial growth factor A

9 List of Figures

10 List of Tables

11 Appendix

11.1 Supplementary data

11.1.1 Experimentally evaluated sequence of *LINC00607* (5'-3'), and chromatin coordinates on GRCh38/hg38

Exon1 (chr2: 215848758-215848892)
GGGCTGCGTGCTGAGGCCCTTCAACAAAGGGGGCACATGCAGATGAGACTCCGTCC
ACCCCAGGCAGCTTTCCTGAGCCCTGGAGGACAGGCTTGAAATGACTCCTAGGCTT
CTGGTGACCCTTGTCACCTATCTAATGCGTGACCTATC

Exon2 (chr2: 215750243-215750402)
CAATCCTTCCTCTCATGGAAACACCAACTCATCCATGCCCTCTGTGCTGAAACTTCGT
CTCAGCCTGCTGGAATCACCTGCACCCCATGGGAACTGTAGCCATATCTTCAGTCCT
GTGAGCCCCCGTCATGGCCTGTCACAGGAGTAAATGAGGAGTAAG

Exon3 (chr2: 215747305-215747394)
GCCCAGAATACTCAGTACCTCTCAATGACCCTCAGACGCTGTAGGAAGAGGATTGGT
TCACCTTTTAACCCAGAATTTCTCACATTGAAT

Exon4 (chr2: 215743814-215743915)
GGACAGGATGCATTCCAAGAGGCCAGAGTATGTGCATCTCAGCTCCTGATGGTTTCC
ACCACCACCATTACTTTCTCTATGTCAAGATACCTGGGAAGCCGG

Exon5 (chr2: 215641231-215641819)
TGTTTCATTTGCATTCTTGGAGCCCAGGAACTGTCTTCTACAAACTTTTCTTCCTAGTA
CCATGTAAACGTACACAGGAAACGTTCAGAAAACATCAGCCAAATAGAAGAATAAGG
AAATTCCTTCACTGACTAGATATTGGTGTTTGATTCTGTCCTGCTTTGTACTCAATGGC
TATTTCGGGGTTTCCATTGCGGAAAACTATTTGGAAAATTGCAAGCCACGAGACAAG
CCTCTAAGCTACTCCAGGATCATTGAGGACTCTCCATGGGTTCTTATTGTTAAAGATC
TTAACTCCTCAAGCCACTGCATTTTTACTATATGCCTTGAACTACAAGATGTGTTAAGA
TTTATAGGATAAGGTTCTCATCTCTAAAAACTCATGGTCTCGATGGAGAAGCAGTATT
TACACACATGGAGAAGTTGAGAGTACTTGAATGTGGAGTATAAAGTGTGCGATATTG
ACAAGAAGCTCTACGAAAGTTCAGGAAGAGGAGGAGCAAGTGAGGATGGAGATGGA
CTTTGCAGAATGGAGGAGAGGCAAAGAAACGGTTAGAAACAATCTACATAATGAAAA
GTCACTTTTGGG

Exon6 (chr2: 215624113-215624235)
AGTTGTTTTAAGGCAGAGTATCATATCGCATCAAAACCGCTCCATAAGTCCTGCCACT
CCACGTGCAATGCCATGAACTTGAAGAAACTGCTGGTAAGAGAAAGCAAATGCTGTG
ACCAGGCA

Exon7 (chr2: 215611563-215613738)
AAGAATCTTGGTCGTCCAGAAAGCTTGCTATAGCTGCCCAGCATTTGCCTCCTCCAC
AAAGAAGGACCAAAAGAACAAGTAGACAATCACATGCCAAATAAAATGTCTAAAGGA
GAGCACTGAAGCTCAGCAAAAACGTTACAAAGACCCTCTGAGGTGCAGAAACTCGG
GATGGCAGCACAAAGAGGAAAGCAAAGCAGCCGGTCAGGATCAGCTCACAGTCAAG
GGCGCCCCGCCTTGAGTAGGAAATGTAAGCAGGAGATGCCCTGCAGGCAACATTCC
CACCACAAATGCCTGCAAGCCTAGCTGTAGGAGAGCCTCGCAGTGTTGAGCCCAGT
GCGGGAGCTGCCTGGAGTCTCTGTGACTACATTACTCCAGAGAGGCCACTGGGTCC
CTCCTTAGTCCCTGGGACCCAAGCCGCTGCAGCACAGTATCATTTTGAGGACAGAGC
CACTGCCAGAATGCTTCCTGTCCTGGGGCCCGGTAACCCCTGCATGTCCTCATCACT
GGAGCCCCAATATCATTCCACAGTTGTATGAGGAGTAAAAATAACTATAAATAAAGAT
AACTCAAGAATTCTATAAGCAAGCATACACATGAAATTCATTTTATAAGAGGAAAGCTA
ACTCCATCTCTCTTGAAATATGGAATAGGTTCTTGAAGCAATTCTAAATGCTGATCTG
CTGGAATGATGGCTTCATTGCACAAGAATTCTGCTTAGTTCATTGAAGTCTCCTTGAA

GAAGTCAGTCTGAGAATGGGGGAATTCCGTTGTTGGTCAGAAGAATTCTTTGGTCAC
TATTGGAAGTGGGTTCAGTTTAGGGTGACTATTGATCAACAGGGTTCATGGGTTTGC
TAAAACTCATTTCAGGCAAGCTTTGGAAGTGCAGTTCGCTTGGTGCTTATGGGGTTAA
AAACAGGAGGAAGAGAATTTCACATTATTGGAGGGCCTGAAAGGAAACTGATTCCCG
CAAGATGCTCAGACAAGATCAAACCCAGCCCCTTTTCTGGTTTGGAATTTCTCTGGG
CTATAAAGGTAGAAGAAAAGGCCCTGCATGGGCCCACTCTAAGTGCTTGGAGGTTTT
AGATAATTTTATTAAATTGTAGAATCTTAAACAGAACTACAAGGTTGCTTTTAAAACCA
GATCTCAGATTTCTTTGAGCTAACAAATGGTAAAATGTATCTTTAGTATTAGAGTGAGA
TAAAGGTAGTTATAACTTTTTTTTTTACTTATTTTATGTTAACGTATGCAACAAAGGGTA
CAAATTGTAGGTACGCAGCTCATTGAACTTTTATGTCTGCACATGCCTATGAAACCAA
CACCCAGAGTAAGATGCGGATAATTTTCTGCTCCCCTGAAAATTCCCTTGTGCCTTTT
CCTCATCAGTACCTCCAAAGGTAACCACTATTTTGATTTCCATTACCATAGATGAGTTA
TACTTGTTTTTGAAAAGATTATTTGAAATGTGTAATATAAATAATAGCGGTTGCTTATCT
TACAGAAATATCACTGAGAATTCATTTCTTCTCTCCTTCATTTATTCATTTGTTCAAAAC
ACTGTCTAGTACCAACATTGTCCACCGGGCGTTGAGAATACAATATTGAAGAAGAGT
CACTGCCTGCCCTCTGGAAAAATCAGAGTATTTGAAAGAATACACACAAGTAAACAG
GCAGCTATGGCAAAGTGGGTAAAAGCTGCAAAACAGGGAAGTTTCGCCAAGTGTCA
GATGCCAAGAAGTGTCAGATGCCAAGAAGAAAGGGTGCATGACATAGACTTGGGGG
GGTCAGTAGTGGTTTCTGGAACGAGTGACATTTAGACTGAAACTGGAAGGATATGAG
TAAGGGCTAATCGGACCAAGATGAAGAGATACAGAAGCAGAAGGAACAGTAGGAAC
AAATGCTCAGAGGCAAAAGAAAGCTTTGAATATTTGAGGAACTGAAAAGCAAAACAAC
AAAAAATAGCCATCCCTTGACTAGACAAGTGACCTGGGGTCAGATCCTGAAGGGCTT
TGCAGATCACTTTTCCGCTTGTAGACTTTGTACTTGACTTTAAGGGCCATGGAGAGCC
ACTGAAGCATTTTCAGCAAGGGACTGTCATCAGCAGATTGGTATTTGTTTTGAAGTAG
CACATGTAAGAGAAAATAACAATATGGACAAATAAAGAGTTTGAAAAAC

11.1.2 Data displayed in this study

Table 25. Expression of 9 highest expressed lncRNAs from HUVEC in different human tissues and cell types from FANTOM5 CAGE; Data shown in Figure 14B

Human Tissues	MALAT1	NEAT1	NORAD	FGD5-AS1	TUG1	MEG3	CTD-2562J17.	LINC00607	KCNQ1OT1
aorta, adult	0,581	6,867	1,849	4,164	1,711	0,980	0,000	0,000	1,136
artery, adult	1,057	3,845	0,681	1,119	0,000	0,618	0,000	0,000	0,559
b cell line	1,198	0,663	0,107	0,466	1,131	0,005	0,000	0,000	2,808
Basophils	1,532	1,871	0,685	1,372	1,130	0,083	0,000	0,000	0,265
Cardiac Myocyte	2,834	26,879	0,000	0,000	0,000	1,000	0,000	0,000	0,000
CD14+ Monocytes	3,821	12,684	0,577	1,049	1,285	0,015	0,000	0,000	0,869
Dendritic Cells	1,341	0,909	0,113	2,043	0,530	0,000	0,000	0,000	0,139
EC	0,419	0,669	0,752	1,537	0,768	0,213	0,000	69,71	0,131
Eosinophils	1,903	0,767	0,000	0,000	0,000	0,000	0,000	0,000	0,000
Fibro Lung	0,017	0,000	0,000	0,000	0,000	0,169	0,000	0,000	0,000
gall bladder	0,895	2,926	1,629	2,974	1,522	1,151	0,000	0,000	1,491
Heart	1,459	4,636	0,853	1,907	1,649	0,860	0,000	0,000	1,058
Hepatocyte	0,922	5,220	0,000	0,000	0,000	0,000	0,000	0,000	0,542

Keratocytes	0,217	0,234	0,113	0,418	0,168	1,043	0,000	0,000	0,000
kidney, adult	1,792	2,017	1,066	2,523	1,516	0,044	0,000	0,000	0,517
liver, adult	0,300	0,726	0,572	1,119	0,906	0,072	0,000	0,000	0,355
lung, adult	1,689	2,730	1,426	2,780	1,504	0,094	0,000	0,000	0,518
Macrophage	0,842	1,822	0,577	2,618	0,592	0,000	0,000	0,000	0,000
Mast cell	1,987	1,639	2,925	2,550	2,980	0,049	0,000	0,000	0,050
mesenchymal precursor cell	1,085	1,561	0,179	1,370	0,884	1,281	0,000	0,000	0,098
Neurons	0,486	0,130	0,402	1,181	0,199	0,724	0,000	0,000	0,000
Neutrophils	8,922	4,755	0,195	3,112	1,994	0,000	0,000	0,000	0,000
Osteoblast	0,018	0,029	0,218	0,726	0,000	0,281	0,000	0,000	0,326
Pericytes	0,193	0,367	0,204	1,161	0,471	1,714	0,000	0,000	0,112
Renal Glomerular EC	0,048	0,173	0,296	0,695	0,684	0,416	0,000	0,000	0,000
retina, adult	1,003	2,952	2,108	3,922	3,008	0,591	0,000	0,000	1,570
Skeletal Muscle Cells	0,564	0,306	0,444	1,388	1,744	1,025	0,000	0,000	0,551
SMCs	0,263	0,476	0,339	0,849	0,350	0,731	0,000	0,247	0,395
testis, adult	0,413	0,665	2,819	2,477	1,582	0,379	0,000	0,000	0,551
thymus, adult	1,130	0,157	0,868	1,085	3,018	0,013	0,000	0,000	0,111
Whole blood (ribopure)	1,341	4,912	0,790	1,358	1,517	0,000	0,000	0,000	0,000

Table 26. Expression of 8 highest expressed lncRNAs from HUVEC in different endothelial cell types; Data shown in Figure 15A

EC cell types	MALAT1	NEAT1	NORAD	FGD5-AS1	TUG1	MEG3	CTD-2562J17.6	LINC00607
Aortic	0,084	0,203	0,497	1,101	0,216	0,022	0,000	89,359
Artery	0,106	0,422	0,517	0,880	0,866	0,062	0,000	124,980
Lymphatic	1,589	1,335	1,321	1,796	1,314	0,826	0,000	47,659
Microvascular	0,214	0,690	0,881	0,999	0,703	0,332	0,000	0,000
Thoracic	0,279	0,678	0,159	1,101	0,610	0,112	0,000	118,301
Umbilical vein	0,663	1,497	0,851	2,118	1,538	0,554	0,000	89,162
Vein	0,041	0,197	0,392	0,721	0,461	0,123	0,000	69,876

Table 27. Tissue expression of the 9 highest expressed lncRNAs from HUVEC in different cultured human cell lines; Data shown in Figure 15D

Cell lines	MALAT1	NEAT1	NORAD	FGD5-AS1	TUG1	MEG3	CTD-2562J17.	LINC00607	KCNQ1OT1	MIR4435-2HG
Gm12878	0,306	0,476	0,221	0,695	0,776	0,073	0,000	0,000	0,102	0,132
Helas3	0,732	1,387	0,403	1,402	1,318	0,003	0,153	0,000	0,000	0,000
Hepg2	0,092	0,223	0,450	0,639	1,038	0,014	2,340	0,007	0,531	0,019
Huvec	0,631	0,603	0,670	1,542	1,379	3,551	1,353	12,48	0,042	0,020
Huvec Cytosol	0,060	0,387	0,290	2,631	0,340	0,489	4,543	4,726	0,125	0,072
Huvec Nucleus	1,282	1,107	0,209	0,554	1,753	27,47	7,874	19,54	0,099	0,055
K562	0,582	0,357	0,416	0,777	0,458	0,000	0,319	0,000	0,125	0,006
Mcf7	0,431	0,414	0,218	3,302	1,941	0,019	2,604	0,006	0,093	0,032
Nhek	0,667	0,545	0,326	0,845	0,811	0,074	0,000	0,000	0,035	0,005

Table 28. Top 50 DEGs after *LINC00607* KO in HUVEC, Data shown in Figure 27A

Ensembl gene id	Ensembl gene	baseMean CTL	baseMean 607-KO	log2FC 607-KO/CTL	padj
ENSG00000154864	PIEZO2	2256	286	-2,97562	3,94E-192
ENSG00000152217	SETBP1	1590	229	-2,79313	3,94E-179
ENSG00000116962	NID1	2410	458	-2,39300	3,04E-172
ENSG00000147408	CSGALNACT1	1332	213	-2,64158	1,05E-153
ENSG00000069122	ADGRF5	2045	447	-2,18948	7,53E-151
ENSG00000118777	ABCG2	968	34	-4,77159	4,55E-132
ENSG00000013588	GPRC5A	78	826	3,39045	2,41E-131
ENSG00000064042	LIMCH1	1620	378	-2,09495	1,41E-125
ENSG00000157570	TSPAN18	1661	313	-2,40200	1,91E-125
ENSG00000138185	ENTPD1	737	40	-4,18465	5,87E-114
ENSG00000169744	LDB2	1207	241	-2,32199	1,57E-111
ENSG00000156535	CD109	3595	1321	-1,44385	6,39E-110
ENSG00000102755	FLT1	4745	1455	-1,70486	2,24E-107
ENSG00000115602	IL1RL1	517	2058	1,99093	2,89E-107
ENSG00000151692	RNF144A	813	124	-2,70567	4,27E-104
ENSG00000173597	SULT1B1	381	1590	2,05909	1,68E-98
ENSG00000169432	SCN9A	728	80	-3,16633	4,25E-98
ENSG00000125266	EFNB2	2469	691	-1,83542	5,00E-97

ENSG00000081923	ATP8B1	1907	640	-1,57317	8,02E-94
ENSG00000110799	VWF	5258	1962	-1,42144	3,91E-93
ENSG00000187498	COL4A1	3540	1236	-1,51664	1,09E-92
ENSG00000198075	SULT1C4	522	45	-3,50506	1,19E-88
ENSG00000067798	NAV3	662	1994	1,59027	6,97E-88
ENSG00000010319	SEMA3G	594	46	-3,65005	8,48E-85
ENSG00000121858	TNFSF10	535	66	-3,00642	5,22E-82
ENSG00000005108	THSD7A	1370	287	-2,25314	4,67E-81
ENSG00000071246	VASH1	1753	522	-1,74477	1,58E-80
ENSG00000133056	PIK3C2B	1462	311	-2,23111	3,08E-80
ENSG00000128833	MYO5C	1047	214	-2,28487	1,37E-79
ENSG00000235770	LINC00607	483	44	-3,44098	1,37E-79
ENSG00000126882	FAM78A	982	260	-1,91527	2,20E-79
ENSG00000088756	ARHGAP28	1503	460	-1,70467	2,81E-77
ENSG00000107719	PALD1	939	167	-2,48406	1,33E-76
ENSG00000087303	NID2	1205	337	-1,83608	9,55E-76
ENSG00000171115	GIMAP8	1656	534	-1,63008	2,68E-75
ENSG00000164683	HEY1	438	35	-3,61707	5,83E-75
ENSG00000118515	SGK1	223	875	1,96616	1,96E-73
ENSG00000005187	ACSM3	529	82	-2,68028	3,98E-73
ENSG00000135480	KRT7	137	791	2,51834	8,70E-73
ENSG00000075275	CELSR1	522	70	-2,87498	2,65E-72
ENSG00000088387	DOCK9	2949	1315	-1,16427	1,87E-71
ENSG00000104368	PLAT	368	1314	1,83480	2,42E-71
ENSG00000075651	PLD1	2029	833	-1,28249	6,62E-71
ENSG00000143127	ITGA10	409	33	-3,57888	5,74E-69
ENSG00000257093	DENND11	1129	362	-1,63909	1,79E-68
ENSG00000137507	LRRC32	1090	333	-1,70828	8,56E-67
ENSG00000164684	ZNF704	778	190	-2,03184	1,40E-66
ENSG00000136378	ADAMTS7	900	268	-1,74343	3,41E-66
ENSG00000011028	MRC2	742	155	-2,25367	1,08E-65
ENSG00000197872	FAM49A	931	240	-1,95304	2,36E-65

Table 29. Fold changes of genes significantly differentially expressed after *LINC00607* KO and siRNA mediated ERG KD[88]; Data shown in Figure 32C

Gene	LogFC_LINC00607 KO	LogFC_siERG KD
PIEZO2	-2,97561609	2,24401184
SETBP1	-2,79312652	-0,99717693
NID1	-2,39300227	1,12256038
CSGALNACT1	-2,64157995	-4,2829076

ADGRF5	-2,18947946	-1,75006261
ABCG2	-4,77158696	-1,01466699
GPRC5A	3,3904494	1,85168344
LIMCH1	-2,09495488	-1,80266671
TSPAN18	-2,40199686	-1,04721473
ENTPD1	-4,18464908	1,11079749
LDB2	-2,32198866	-1,64697034
CD109	-1,44385459	-0,64276006
FLT1	-1,70485933	-0,57056215
IL1RL1	1,99092534	2,3727519
RNF144A	-2,70566514	4,0336817
SULT1B1	2,05908918	1,43225053
SCN9A	-3,16633093	-1,13633331
EFNB2	-1,83541802	-2,61957049
ATP8B1	-1,57317297	-0,84490552
VWF	-1,42143637	-1,69445022
COL4A1	-1,51663871	-0,94091062
SULT1C4	-3,50505523	-0,47612343
NAV3	1,59026933	-3,53917612
SEMA3G	-3,65005166	-2,0122969
TNFSF10	-3,00642125	-0,51303526
THSD7A	-2,25314195	-1,49778051
VASH1	-1,74476845	-3,26896748
PIK3C2B	-2,23111267	-1,98423716
MYO5C	-2,284873	-3,15432591
LINC00607	-3,44097507	-1,17841923
ARHGAP28	-1,70467085	-3,98290944
PALD1	-2,4840612	-3,36138889
NID2	-1,83607577	0,14070272
GIMAP8	-1,63007615	-1,85485194
HEY1	-3,61707001	1,57186739
SGK1	1,96615924	0,9033945
ACSM3	-2,68028072	-1,70689673
KRT7	2,5183376	-1,10803563
CELSR1	-2,87498341	-0,90514372
DOCK9	-1,16427073	-1,22593598
PLAT	1,83479799	0,5058744
PLD1	-1,28248547	1,27055651
ITGA10	-3,57887932	-0,38102973
LRRC32	-1,70828105	-0,62637345

ZNF704	-2,03184085	-1,62637475
ADAMTS7	-1,74343266	1,50648861
MRC2	-2,2536682	0,79513937
FAM49A	-1,95303646	0,44543139
ADGRA2	-1,7572953	0,7021197
NEGR1	2,42972725	1,91452374

11.1.3 Differentially expressed genes in HUVEC after *LINC00607* KO identified by RNA-Sequencing

Table 30. Top 50 down regulated genes after *LINC00607* KO in HUVEC

Ensembl gene id	Ensembl gene	log2FoldChange 607-KO/CTL	pvalue	padj
ENSG00000265107	GJA5	-7,34278	2,12E-55	4,71E-53
ENSG00000240583	AQP1	-7,12200	9,17E-27	4,88E-25
ENSG00000152207	CYSLTR2	-6,04510	1,62E-27	8,93E-26
ENSG00000169129	AFAP1L2	-5,84661	5,89E-14	1,23E-12
ENSG00000132514	CLEC10A	-5,50089	2,67E-10	3,84E-09
ENSG00000187513	GJA4	-5,38519	4,64E-60	1,23E-57
ENSG00000163083	INHBB	-5,19750	1,48E-38	1,52E-36
ENSG00000171864	PRND	-5,15790	5,95E-24	2,65E-22
ENSG00000174600	CMKLR1	-5,14988	1,62E-08	1,83E-07
ENSG00000164929	BAALC	-5,06331	3,46E-16	8,69E-15
ENSG00000135914	HTR2B	-4,89003	1,46E-08	1,66E-07
ENSG00000233321	LINC02669	-4,83139	2,75E-14	5,92E-13
ENSG00000253177	AC104211.2	-4,81523	2,46E-08	2,71E-07
ENSG00000118777	ABCG2	-4,77159	1,55E-135	4,55E-132
ENSG00000187151	ANGPTL5	-4,68651	6,47E-08	6,77E-07
ENSG00000088882	CPXM1	-4,54323	4,56E-16	1,13E-14
ENSG00000136011	STAB2	-4,53997	2,82E-07	2,68E-06
ENSG00000254810	AP001189.3	-4,47855	2,08E-07	2,02E-06
ENSG00000103528	SYT17	-4,47445	3,62E-12	6,43E-11
ENSG00000204136	GGTA1P	-4,41658	1,19E-08	1,37E-07
ENSG00000136842	TMOD1	-4,40002	1,48E-32	1,10E-30
ENSG00000260244	AC104083.1	-4,39352	1,39E-06	1,17E-05
ENSG00000129521	EGLN3	-4,38717	1,38E-11	2,32E-10
ENSG00000277013	AC008556.1	-4,35879	3,20E-14	6,82E-13
ENSG00000120328	PCDHB12	-4,27957	2,43E-06	1,96E-05
ENSG00000108947	EFNB3	-4,24497	4,98E-11	7,85E-10
ENSG00000170323	FABP4	-4,24313	2,75E-46	4,21E-44

ENSG00000138185	ENTPD1	-4,18465	3,34E-117	5,87E-114
ENSG00000102575	ACP5	-4,17584	1,26E-12	2,33E-11
ENSG00000286320	AC108053.1	-4,13861	1,69E-23	7,30E-22
ENSG00000112936	C7	-4,13294	1,96E-10	2,86E-09
ENSG00000184611	KCNH7	-4,10970	1,83E-06	1,51E-05
ENSG00000172348	RCAN2	-4,10468	3,39E-11	5,45E-10
ENSG00000137726	FXYD6	-4,09081	1,50E-13	3,07E-12
ENSG00000178175	ZNF366	-4,05574	2,75E-42	3,40E-40
ENSG00000164116	GUCY1A1	-4,00098	6,56E-33	4,99E-31
ENSG00000167037	SGSM1	-3,97588	2,23E-13	4,50E-12
ENSG00000128917	DLL4	-3,96721	7,16E-42	8,68E-40
ENSG00000178538	CA8	-3,95421	2,10E-08	2,32E-07
ENSG00000113389	NPR3	-3,94496	7,80E-12	1,34E-10
ENSG00000137809	ITGA11	-3,93732	8,90E-39	9,25E-37
ENSG00000185477	GPRIN3	-3,91962	9,29E-38	9,22E-36
ENSG00000287527	AC005753.3	-3,89948	1,73E-05	1,19E-04
ENSG00000260400	AL513534.3	-3,89387	1,68E-05	1,16E-04
ENSG00000114654	EFCC1	-3,88753	8,07E-06	5,90E-05
ENSG00000155011	DKK2	-3,87504	1,19E-06	1,02E-05
ENSG00000169418	NPR1	-3,85843	8,86E-30	5,56E-28
ENSG00000179855	GIPC3	-3,84047	5,25E-09	6,37E-08
ENSG00000186907	RTN4RL2	-3,82257	1,24E-09	1,64E-08
ENSG00000113212	PCDHB7	-3,80977	8,53E-08	8,78E-07

Table 31. Top 50 upregulated genes after *LINC00607* KO in HUVEC

Ensembl gene id	**Ensembl gene**	**log2FoldChange 607-KO/CTL**	**pvalue**	**padj**
ENSG00000075223	SEMA3C	5,36027	1,53E-05	1,06E-04
ENSG00000251011	TMEM108-AS1	5,32129	8,37E-10	1,13E-08
ENSG00000185860	CCDC190	4,83032	3,21E-14	6,84E-13
ENSG00000128510	CPA4	4,71837	1,12E-17	3,12E-16
ENSG00000286215	AL356534.1	4,46316	1,00E-26	5,33E-25
ENSG00000138134	STAMBPL1	4,43570	6,85E-09	8,19E-08
ENSG00000138356	AOX1	4,41533	2,85E-25	1,41E-23
ENSG00000092969	TGFB2	4,37648	2,88E-45	4,25E-43
ENSG00000164532	TBX20	4,17593	1,74E-06	1,44E-05
ENSG00000123689	G0S2	4,13633	3,97E-16	9,87E-15
ENSG00000169933	FRMPD4	4,10320	1,75E-14	3,82E-13
ENSG00000088053	GP6	3,79937	1,13E-11	1,91E-10
ENSG00000136167	LCP1	3,78351	2,02E-05	1,37E-04

ENSG00000253500	AF121898.1	3,75210	4,63E-13	9,10E-12
ENSG00000123496	IL13RA2	3,66889	6,91E-09	8,26E-08
ENSG00000258667	HIF1A-AS3	3,59934	2,37E-11	3,88E-10
ENSG00000145242	EPHA5	3,56454	1,39E-11	2,32E-10
ENSG00000255281	AC090124.2	3,52761	4,52E-05	2,83E-04
ENSG00000135114	OASL	3,42279	1,21E-09	1,60E-08
ENSG00000285106	AC016831.6	3,40769	1,23E-12	2,29E-11
ENSG00000214244	SETP21	3,40371	1,77E-08	1,99E-07
ENSG00000101311	FERMT1	3,39306	4,89E-27	2,67E-25
ENSG00000013588	GPRC5A	3,39045	9,61E-135	2,41E-131
ENSG00000141198	TOM1L1	3,27526	2,90E-08	3,17E-07
ENSG00000258791	LINC00520	3,26222	2,10E-24	9,81E-23
ENSG00000253161	LINC01605	3,23489	1,71E-11	2,84E-10
ENSG00000249867	LINC02742	3,22784	1,50E-42	1,92E-40
ENSG00000253746	AC091182.2	3,22636	3,74E-05	2,38E-04
ENSG00000226935	LINC00161	3,22513	1,85E-05	1,26E-04
ENSG00000120658	ENOX1	3,22324	5,20E-16	1,27E-14
ENSG00000127324	TSPAN8	3,20923	5,97E-16	1,45E-14
ENSG00000226562	CYP4F26P	3,18884	9,82E-08	9,99E-07
ENSG00000134363	FST	3,18279	1,10E-03	4,90E-03
ENSG00000237523	LINC00857	3,18019	1,53E-05	1,06E-04
ENSG00000163053	SLC16A14	3,16661	4,28E-06	3,30E-05
ENSG00000267316	AC090409.2	3,16067	5,07E-07	4,62E-06
ENSG00000267175	AC105094.2	3,15257	1,83E-05	1,25E-04
ENSG00000189410	SH2D5	3,14684	3,56E-09	4,40E-08
ENSG00000105929	ATP6V0A4	3,06620	7,13E-04	3,35E-03
ENSG00000228536	LYPLAL1-AS1	3,06305	3,80E-05	2,42E-04
ENSG00000124875	CXCL6	3,06179	4,62E-04	2,29E-03
ENSG00000285108	AC103718.1	3,06082	2,73E-22	1,08E-20
ENSG00000227972	THAP12P3	3,03797	8,18E-04	3,77E-03
ENSG00000176697	BDNF	2,97408	3,13E-21	1,15E-19
ENSG00000133101	CCNA1	2,95292	4,52E-09	5,50E-08
ENSG00000146374	RSPO3	2,94443	2,96E-09	3,71E-08
ENSG00000107779	BMPR1A	2,93469	1,05E-07	1,07E-06
ENSG00000211448	DIO2	2,89542	5,25E-06	3,98E-05
ENSG00000113361	CDH6	2,87331	6,05E-03	2,16E-02
ENSG00000236081	ELFN1-AS1	2,85185	1,28E-03	5,60E-03

11.1.4 Differentially accessible chromatin sites in HUVEC after *LINC00607* KO identified by ATAC-Sequencing

Table 32. Differential peaks with lost accessibility in HUVEC after *LINC00607* KO

Upeak id	Peak chromosome	Peak start	Peak stop	log2FoldChange 607-KO/CTL	pvalue
upeak-32547	chr5	168085318	168085794	-3,07	4,19E-08
upeak-33691	chr6	13248115	13248378	-2,74	7,28E-05
upeak-7822	chr1	218765825	218766125	-2,71	3,09E-05
upeak-69573	chr14	66804263	66804622	-2,68	5,83E-06
upeak-86636	chr20	57999476	58000031	-2,51	3,55E-12
upeak-66728	chr13	49596161	49596521	-2,51	6,98E-04
upeak-10641	chr2	49265479	49265832	-2,48	1,73E-05
upeak-43771	chr8	788793	789172	-2,47	4,20E-05
upeak-81702	chr18	61748000	61748442	-2,45	3,04E-07
upeak-44344	chr8	21179255	21179801	-2,40	1,97E-06
upeak-56479	chr10	129426644	129427006	-2,35	1,68E-04
upeak-10283	chr2	40814651	40814942	-2,34	2,72E-04
upeak-44488	chr8	23881120	23881482	-2,34	8,20E-05
upeak-81907	chr18	71603858	71604118	-2,32	1,17E-03
upeak-35252	chr6	47247336	47247767	-2,29	1,95E-08
upeak-47971	chr8	142028972	142029357	-2,29	7,43E-05
upeak-47692	chr8	132045724	132046027	-2,29	7,18E-04
upeak-67252	chr13	76813022	76813205	-2,27	1,36E-03
upeak-60879	chr11	127733578	127733931	-2,26	7,89E-06
upeak-71160	chr15	32005094	32005504	-2,23	1,13E-03
upeak-12459	chr2	121483166	121483392	-2,21	1,62E-03
upeak-40966	chr7	72292607	72293588	-2,21	1,98E-12
upeak-35959	chr6	82823495	82823837	-2,19	4,70E-03
upeak-18625	chr3	65268457	65268678	-2,18	1,63E-03
upeak-14565	chr2	192007692	192008163	-2,16	5,02E-05
upeak-15949	chr2	233673903	233674269	-2,15	2,29E-03
upeak-16244	chr2	239858108	239858696	-2,13	2,79E-07
upeak-3237	chr1	67590250	67590723	-2,13	5,09E-05
upeak-40954	chr7	70614718	70615025	-2,13	3,42E-03
upeak-88478	chr22	32248556	32249073	-2,13	1,07E-03
upeak-27617	chr4	184293590	184293848	-2,12	8,43E-04
upeak-16243	chr2	239830399	239831845	-2,12	4,68E-24
upeak-20376	chr3	132555441	132555686	-2,12	1,24E-03
upeak-10058	chr2	36013027	36013645	-2,11	1,14E-07

upeak-55785	chr10	110944915	110945288	-2,11	1,72E-04
upeak-67347	chr13	79724362	79724942	-2,10	1,37E-09
upeak-23440	chr4	16514000	16514410	-2,10	1,18E-04
upeak-77127	chr17	9446654	9446986	-2,10	2,13E-03
upeak-14432	chr2	189528578	189528945	-2,09	1,14E-04
upeak-51152	chr9	121171327	121171641	-2,09	2,70E-05
upeak-53271	chr10	33858323	33858677	-2,08	2,81E-04
upeak-81182	chr18	44761652	44762077	-2,08	1,96E-04
upeak-56420	chr10	127587862	127588302	-2,07	5,56E-06
upeak-60424	chr11	118216682	118217122	-2,07	3,31E-04
upeak-61115	chr11	133520840	133521321	-2,06	3,40E-05
upeak-53924	chr10	60258286	60258605	-2,06	2,34E-03
upeak-30150	chr5	96371021	96371345	-2,06	1,65E-03
upeak-38293	chr6	156279376	156279704	-2,06	3,61E-03
upeak-66695	chr13	48636400	48636820	-2,04	1,83E-04
upeak-66693	chr13	48600841	48601395	-2,02	7,22E-08

Table 33. Differential peaks with gained accessibility in HUVEC after *LINC00607* KO

Upeak id	**Peak chromosome**	**Peak start**	**Peak stop**	**log2FoldChange 607-KO/CTL**	**pvalue**
upeak-56727	chr11	2355030	2355493	3,32	3,37E-02
upeak-54836	chr10	86410481	86410732	2,75	8,74E-04
upeak-84912	chr20	6960050	6960344	2,34	2,49E-03
upeak-87602	chr21	40845738	40846145	2,21	1,36E-03
upeak-49620	chr9	73613306	73613615	2,13	1,42E-03
upeak-69910	chr14	74574750	74574970	2,10	9,80E-03
upeak-12490	chr2	124081227	124081665	2,06	1,96E-04
upeak-26999	chr4	155007698	155008168	2,03	6,24E-05
upeak-45532	chr8	59617270	59617510	2,02	3,11E-03
upeak-91460	chrX	136214576	136215081	1,98	9,50E-05
upeak-63959	chr12	83880340	83880907	1,95	5,18E-05
upeak-66465	chr13	42025938	42026319	1,95	2,99E-03
upeak-25200	chr4	93719651	93719912	1,93	1,47E-03
upeak-66976	chr13	61665314	61665685	1,93	1,08E-03
upeak-15189	chr2	214311884	214312631	1,91	6,54E-05
upeak-46078	chr8	83808288	83808759	1,91	8,59E-03
upeak-48872	chr9	23073230	23073474	1,83	3,24E-03
upeak-6014	chr1	170175048	170175602	1,79	7,00E-05
upeak-23375	chr4	14726978	14727457	1,77	2,66E-03

upeak-50837	chr9	111052745	111053152	1,77	9,79E-04
upeak-63701	chr12	74862751	74863135	1,75	6,68E-03
upeak-46074	chr8	82870995	82871400	1,74	3,28E-03
upeak-11472	chr2	81835406	81835883	1,74	1,94E-04
upeak-41976	chr7	103818249	103818629	1,70	9,14E-03
upeak-78138	chr17	41099693	41100227	1,69	2,29E-06
upeak-49623	chr9	73714178	73714572	1,69	2,88E-03
upeak-90371	chrX	52852816	52853129	1,66	8,42E-03
upeak-12284	chr2	113078441	113078889	1,66	7,53E-04
upeak-27924	chr5	9148249	9148492	1,64	1,82E-02
upeak-75358	chr16	57667528	57667994	1,63	8,26E-03
upeak-77286	chr17	16864809	16865433	1,62	1,31E-02
upeak-49619	chr9	73583666	73584188	1,60	5,09E-07
upeak-37044	chr6	125713647	125714089	1,60	4,33E-03
upeak-41920	chr7	102490674	102490922	1,60	4,86E-03
upeak-19434	chr3	106765320	106765695	1,60	8,29E-04
upeak-31063	chr5	128579008	128579599	1,58	1,15E-03
upeak-4929	chr1	125174012	125174265	1,57	1,03E-02
upeak-16981	chr3	20546169	20546875	1,56	1,15E-04
upeak-38437	chr6	158655060	158655300	1,55	3,76E-02
upeak-46924	chr8	112616508	112616881	1,54	7,21E-03
upeak-19675	chr3	113847634	113847962	1,52	2,64E-02
upeak-14177	chr2	180990299	180990691	1,51	2,87E-03
upeak-46975	chr8	116201823	116202375	1,51	2,99E-03
upeak-67058	chr13	68850964	68851362	1,51	2,53E-02
upeak-70824	chr14	102923475	102923748	1,50	2,95E-02
upeak-40151	chr7	35249395	35249903	1,50	6,55E-07
upeak-52946	chr10	24865100	24865563	1,50	8,98E-03
upeak-83503	chr19	38256388	38256697	1,50	1,17E-02
upeak-51050	chr9	115605213	115605469	1,49	2,52E-02
upeak-54667	chr10	79923454	79923775	1,49	1,01E-02

11.2 Publications and conference presentations

11.2.1 Publications

Boos F, Oo JA, Warwick T, Günther S, Izquierdo Ponce J, Lopez M, Rafii D, Buchmann G, Pham MD, Msheik ZS, Li T, Seredinski S, Haydar S, Kashefiolasl S, Plate KH, Behr R, Mietsch M, Krishnan J, Pullamsetti SS, Bibli S-I, Hinkel R, Baker AH, Boon RA, Schulz MH, Wittig I, Miller FJ, Brandes RP, Leisegang MS.
The endothelial-enriched lncRNA LINC00607 mediates angiogenic function.
Basic Res Cardiol. 2023;118:5. PMID: 36700983. doi: 10.1007/s00395-023-00978-3
Impact: 12.41

Leisegang MS, Bains JK, Seredinski S, Oo JA, Krause NM, Kuo C-C, Günther S, Sentürk Cetin N, Warwick T, Cao C, **Boos F**, Izquierdo Ponce J, Haydar S, Bednarz R, Valasarajan C, Fuhrmann DC, Preussner J, Looso M, Pullamsetti SS, Schulz MH, Jonker HRA, Richter C, Rezende F, Gilsbach R, Pflüger-Müller B, Wittig I, Grummt I, Ribarska T, Costa IG, Schwalbe H, Brandes RP.
HIF1α-AS1 is a DNA:DNA:RNA triplex-forming lncRNA interacting with the HUSH complex.
Nat Commun. 2022;13:6563. PMID: 36323673.doi: 10.1038/s41467-022-34252-2
Impact: 17.69

Oo JA, Pálfi K, Warwick T, Wittig I, Prieto-Garcia C, Matkovic V, Tomašković I, **Boos F**, Izquierdo Ponce J, Teichmann T, Petriukov K, Haydar S, Maegdefessel L, Wu Z, Pham MD, Krishnan J, Baker AH, Günther S, Ulrich HD, Dikic I, Leisegang MS, Brandes RP.
Long non-coding RNA PCAT19 safeguards DNA in quiescent endothelial cells by preventing uncontrolled phosphorylation of RPA2.
Cell Rep. 2022;41:111670. PMID: 36384122. doi: 10.1016/j.celrep.2022.111670
Impact: 9.99

Seredinski S, **Boos F**, Günther S, Oo JA, Warwick T, Izquierdo Ponce J, Lillich FF, Proschak E, Knapp S, Gilsbach R, Pflüger-Müller B, Brandes RP, Leisegang MS.
DNA topoisomerase inhibition with the HIF inhibitor acriflavine promotes transcription of lncRNAs in endothelial cells.
Mol Ther Nucleic Acids. 2022;27:1023–1035. PMID: 35228897. doi: 10.1016/j.omtn.2022.01.016
Impact: 10.18

11.2.2 Conference presentations

Deutsche Gesellschaft für Kardiologie Conference, Virtual, 7 – 10 April 2021
Poster presentation – “LINC00607: An endothelial-specific highly expressed long non-coding RNA which governs the endothelial phenotype”

Cardio Pulmonary Institute Retreat 2021 – Day of Science in the CPI, Frankfurt am Main, 9 September 2021
Poster presentation – “Governing of the endothelial cell phenotype by the highly endothelial-specific long non-coding RNA *LINC00607*”

Deutsche Gesellschaft für Kardiologie Conference, Frankfurt am Main, 30 September – 2 October 2021
Poster presentation – “Governing of the endothelial cell phenotype by the highly endothelial-specific long non-coding RNA *LINC00607*”

TRR267 PhD Retreat, Alpbach 10-11 November 2021
Project presentation – “Vascular lncRNAs in the control of the BRG1 remodelling complex”

Deutsche Gesellschaft für Kardiologie Conference, Mannheim, 11 May 2022
Poster presentation – “Governing of the endothelial cell phenotype by the highly endothelial-specific long non-coding RNA *LINC00607*”

RNA Society Conference (27th Annual Meeting), Boulder (Co) USA, 31 May – 5 June 2022
Poster presentation; winner of a Poster Prize – “Governing of the endothelial cell phenotype by the highly endothelial-specific long non-coding RNA *ENDOPHY*”

Europhysiology 2022, Copenhagen, 16 – 18 September 2022
Poster presentation; winner of a Poster Prize – “The endothelial-specific *LINC00607* mediates endothelial angiogenic function”

Merz Symposium of the CPI and the Fierdrich Merz Professorship, Frankfurt am Main, 11 October 2022
Poster presentation – “The endothelial-specific *LINC00607* mediates endothelial angiogenic function”

Deutsche Gesellschaft für Kardiologie Conference, Mannheim, 13 – 15 April 2023
Invited speaker at the Basic Science Box – “The endothelial-specific *LINC00607* mediates endothelial angiogenic function”

11.3 Declaration

Except if stated otherwise by reference or acknowledgement, the work presented was generated by myself under the supervision of my supervisors PD. Dr. Matthias Leisegang and Prof. Dr. Ralf P. Brandes during my doctoral studies.

RNA-, ATAC- and CUT&RUN sequencing was carried out by Dr. Stefan Günther (Max-Planck-Institute for Heart and Lung Research, Bad Nauheim, Germany). *Macaca fascicularis* vessels were kindly provided by Francis J. Miller Jr. (Vanderbilt University, Nashville, USA) and vessels originated from a previous study published by Hathaway *et al*. (2002)[127]. *Challitrix jacchus* vessels were kindly provided by Dr. Matthias Mietsch and Prof. Dr. Rabea Hinkel (German Primate Center, Leibnitz Institute für Primatenforschung, Göttingen, Germany). AVM tissue samples were kindly provided by Dr. Sepide Kashefiolasl (Department of Neurosurgery, University Hospital Frankfurt, Germany). ECs isolated from plaque-free and plaque-containing arteries[128] were kindly provided by Prof. Dr. Sofia Iris Bibli (Institute for Vascular Signalling, Goethe University, Frankfurt, Germany). The integration of ATAC-Seq reads with RNA-Seq data from *LINC00607* KO HUVEC was performed by Dr. Timothy Warwick (Vascular Research Center, University Clinic, Frankfurt).

All contributions from colleagues are explicitly referenced in the thesis.

The following parts of this thesis have been previously published:

Chapter	Published in
1.1	partially in Boos *et al.* (2023)[124]
1.2	partially in Boos *et al.* (2023)[124]
1.4	partially in Boos *et al.* (2023)[124]
2	in a modified version in Boos *et al.* (2023)[124]
3	Boos *et al.* (2023)[124]
4.1	Boos *et al.* (2023)[124]
5.1	Boos *et al.* (2023)[124]
5.2	Boos *et al.* (2023)[124]

Figure	Published in
14 B	in a modified version in Boos *et al.* (2023)[124]
15 A, C, D	Boos *et al.* (2023)[124]
17-23	Boos *et al.* (2023)[124]
25	Boos *et al.* (2023)[124]
26 A, B	Boos *et al.* (2023)[124]
27-29	Boos *et al.* (2023)[124]
30 B	Boos *et al.* (2023)[124]
31	in a modified version in Boos *et al.* (2023)[124]
32-36	Boos *et al.* (2023)[124]

Table	Published in
24-28	Boos *et al.* (2023)[124]
30-33	Boos *et al.* (2023)[124]

11.4 Selbstständigkeitserklärung

Ich erkläre hiermit, dass ich die im Fachbereich Biochemie, Chemie und Pharmazie der Goethe-Universität Frankfurt am Main zur Promotionsprüfung eingereichte Arbeit mit dem Titel:

„The endothelial-specific highly expressed long non-coding RNA *LINC00607* governs the endothelial phenotype“

im Institut für Kardiovaskuläre Physiologie unter Betreuung und Anleitung von Herrn Prof. Dr. Ralf P. Brandes ohne sonstige Hilfe selbst durchgeführt und bei der Abfassung der Arbeit keine anderen als die in der Dissertation angeführten Hilfsmittel benutzt habe.

Ich versichere, die Grundsätze der guten wissenschaftlichen Praxis beachtet, und nicht die Hilfe einer kommerziellen Promotionsvermittlung in Anspruch genommen zu haben.

Ich habe bisher an keiner in- oder ausländischen Universität ein Gesuch um Zulassung zur Promotion eingereicht. Die vorliegende Arbeit wurde bisher nicht als Dissertation eingereicht.

Vorliegende Ergebnisse der Arbeit sind zum Teil veröffentlicht in:

Boos F, Oo JA, Warwick T, Günther S, Izquierdo Ponce J, Lopez M, Rafii D, Buchmann G, Pham MD, Msheik ZS, Li T, Seredinski S, Haydar S, Kashefiolasl S, Plate KH, Behr R, Mietsch M, Krishnan J, Pullamsetti SS, Bibli S-I, Hinkel R, Baker AH, Boon RA, Schulz MH, Wittig I, Miller FJ, Brandes RP, Leisegang MS (2023) The endothelial-enriched lncRNA LINC00607 mediates angiogenic function. *Basic Res Cardiol* **118**: 5, doi:10.1007/s00395-023-00978-3.

Frankfurt am Main, den

_____

(Frederike Margarete Boos)